THE UNIVERSITY OF TEXAS AT AUSTIN
CENTER FOR TRANSPORTATION RESEARCH

TECHNICAL REPORT 0-7016-1
TxDOT PROJECT NUMBER 0-7016

Guidance for Structural Behavior of Design and Detailing of Tall Haunches in Steel and Concrete Composite Girders

Nidhi Khare
Zhenghao Zhang
Shay Rutenberg
Jun Wang
Eric Williamson (RS)
Todd Helwig (RS).

May 2023

http://library.ctr.utexas.edu/ctr-publications/0-7016-1.pdf

Technical Report Documentation Page

1. Report No. FHWA/TX-23/0-7016-1	2. Government Accession No.	3. Recipient's Catalog No.
4. Title and Subtitle Guidance for Structural Behavior of Tall Haunches in Steel and Concrete Composite Girders		5. Report Date Submitted: May 2023
		6. Performing Organization Code
7. Author(s) Nidhi Khare, Zhenghao Zhang, Shay Rutenberg, Jun Wang, Eric Williamson (RS), and Todd Helwig (RS)		8. Performing Organization Report No. 0-7016-1
9. Performing Organization Name and Address Center for Transportation Research The University of Texas at Austin 3925 W. Braker Lane, 4th Floor Austin, TX 78759		10. Work Unit No. (TRAIS)
		11. Contract or Grant No. 0-7016
12. Sponsoring Agency Name and Address Texas Department of Transportation Research and Technology Implementation Division 125 E. 11th Street Austin, TX 78701		13. Type of Report and Period Covered Technical Report August 2019 – May 2023
		14. Sponsoring Agency Code

15. Supplementary Notes

Project performed in cooperation with the Texas Department of Transportation and the Federal Highway Administration.

16. Abstract

This study aimed to investigate the behavior of steel and concrete girder bridges with tall haunches and develop corresponding design guidelines. The research involved conducting push-out tests to assess the capacity and limit states that arise in the composite connection between bridge girders and concrete decks with tall haunches. Additionally, three-dimensional finite element models were developed to facilitate parametric studies, extending the range of scenarios.

The results obtained from the experimental testing and parametric finite element analyses were used to identify the factors that influence the shear strength of bridge girders characterized by tall concrete haunches. For steel girder cases, the most influential parameters affecting shear capacity were found to be stud penetration, stud pitch, and haunch reinforcement detailing. For PSC girder cases, the maximum portion of the shear capacity was controlled by the cohesive resistance between the concrete interfaces. These findings have informed the development of design guidelines for bridges with tall haunches.

17. Key Words	18. Distribution Statement
haunch, shear connector, steel girder, prestressed concrete girder	No restrictions. This document is available to the public through the National Technical Information Service, Alexandria, Virginia 22312; www.ntis.gov.

19. Security Classif. (of report)	20. Security Classif. (of this page)	21. No. of pages	22. Price
Unclassified	Unclassified	TBD [Total count excl. cover]	

Form DOT F 1700.7 (8-72) Reproduction of completed page authorized

THE UNIVERSITY OF TEXAS AT AUSTIN
CENTER FOR TRANSPORTATION RESEARCH

Guidance for Structural Behavior of Tall Haunches in Steel and Concrete Composite Girders

Nidhi Khare

Zhenghao Zhang

Shay Rutenberg

Jun Wang

Eric Williamson

Todd Helwig

CTR Technical Report:	0-7016-1
Report Date:	Submitted: May 2023
Project:	0-7016
Project Title:	Develop Guidance for Structural Behavior of Tall Haunches in TxDOT Beam and Girder Bridges
Sponsoring Agency:	Texas Department of Transportation
Performing Agency:	Center for Transportation Research at The University of Texas at Austin

Project performed in cooperation with the Texas Department of Transportation and the Federal Highway Administration.

Center for Transportation Research

The University of Texas at Austin

3925 W. Braker Lane, 4th floor

Austin, TX 78759

http://ctr.utexas.edu/

Disclaimers

Author's Disclaimer: The contents of this report reflect the views of the authors, who are responsible for the facts and the accuracy of the data presented herein. The contents do not necessarily reflect the official view or policies of the Federal Highway Administration or the Texas Department of Transportation (TxDOT). This report does not constitute a standard, specification, or regulation.

Patent Disclaimer: There was no invention or discovery conceived or first actually reduced to practice in the course of or under this contract, including any art, method, process, machine manufacture, design or composition of matter, or any new useful improvement thereof, or any variety of plant, which is or may be patentable under the patent laws of the United States of America or any foreign country.

Engineering Disclaimer

NOT INTENDED FOR CONSTRUCTION, BIDDING, OR PERMIT PURPOSES.

Project Engineer: Todd Helwig

Professional Engineer License State and Number: Texas No. 94280

P.E. Designation: Research Supervisor

Acknowledgments

The authors gratefully acknowledge the financial support provided for this project by the Texas Department of Transportation. The authors express appreciation to the following TxDOT personnel for their assistance and support on this study: Martin Dassi, Taya Retterer, David Fish, Seth Cole, Yongqian Lin, and Zoran Umicevic. Special thanks are extended to the numerous students and staff members at Ferguson Structural Engineering Laboratory for ensuring the successful completion of the experimental program

Products

Product P1, *Design recommendations for steel and concrete girder bridges with tall haunches*, is included in Chapter 7 of this report.

Table of Contents

List of Figures

List of Tables

Chapter 1. Introduction

Nearly all modern girder bridges make use of composite action between the concrete deck and the primary girder system. Most girder bridges have either structural steel girders or prestressed concrete girders (PSC) that support a cast-in-place (CIP) concrete deck and use a variety of stay-in-place forming systems. Depending on the forming system, the design thickness of the deck may consist of the total thickness of the CIP concrete or may also make use of partial-depth precast concrete deck panels (PCPs). In addition to the thickness of the concrete deck, an additional region of CIP concrete immediately above the top of a girder is often necessary, which is referred to as the "haunch." Haunches generally consist of the CIP concrete between the top surface of the girder and the bottom of the deck (Figure 1.1). The scale of the haunch depicted in Figure 1.1 would generally fall under the category as a "tall" haunch as opposed to a "standard" haunch outlined below. The haunch is necessary in steel girder systems to accommodate changes in flange thickness along the girder length and in both steel and concrete girders to account for differential camber between adjacent girders and other tolerances in the bridge. As a result, the actual depth of the haunch in practice may include a portion that is planned by the designer as well as a modification that is necessary to account for the as-constructed geometry of the bridge. The designer will specify girder camber to account for deflections from the CIP concrete so as to achieve a uniform thickness in the finished concrete bridge deck. However, variations almost always exist between the specified and actual camber due to tolerances on fabrication and/or construction, which therefore necessitate some adjustment of the haunch depth in the field. TxDOT (2022) identifies a minimum haunch height of 0.5 in. for most cases to allow for bedding strips. The maximum haunch height permitted by TxDOT (2022) without any special detailing in the haunch is 3 in. for steel girders and 3.5 in. for PSC girders. Significant errors in construction or unique design requirements can, however, sometimes lead to haunches as large as 15-in. deep.

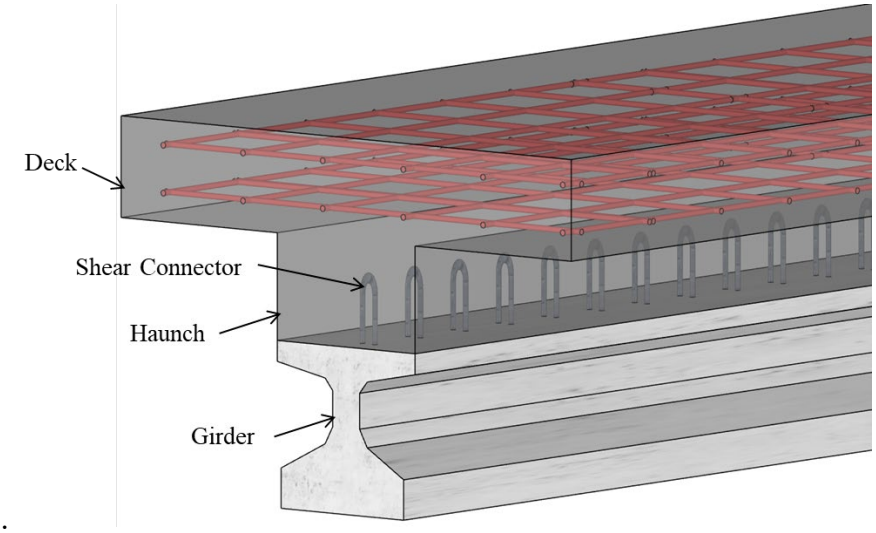

Figure 1.1 Haunch in a PSC Girder

Limited information exists concerning how tall haunches (≥3.5 in.) affect overall bridge structural performance, especially for extreme cases where haunch depths exceed 5 in. The important link between the concrete bridge deck and the steel or PSC girders are the shear connectors that maintain composite action between the deck and girders. For steel girders, the shear connectors often consist of welded shear studs, while concrete girder systems usually include bars R (shown in Figure 1.1). AASHTO LRFD (2020) indicates shear studs on steel girders are required to penetrate at least 2 in. into the concrete deck. With only a 2-in. penetration requirement, there exist instances where studs may not directly interact with longitudinal reinforcement, reducing their effectiveness and overall ductility. The shear transfer from the deck to the girder is questionable in such cases.

TxDOT (2022) requires steel girder haunches taller than 3 in. to be reinforced with transverse steel. For PSC girders, the TxDOT (2022) specifies haunches taller than 3.5 in. require transverse steel reinforcement. Nonetheless, information about shear connector spacing, transverse reinforcement size, and haunch geometry are not described in detail in any of the current TxDOT guidelines (2022, 2023a, and 2023b). Additionally, the available detailing guidelines for tall haunches are not experimentally or analytically verified.

For the current study, project researchers have developed experimental procedures to evaluate the behavior of steel and PSC girder bridges with tall haunches and variable reinforcement detailing. The experimental procedure utilized is based on push-out tests (Figure 1.2) and has been a common practice in structural engineering research over the past century. Essentially, reinforced concrete slabs are cast and connected to steel sections using shear connectors. Forces are then applied either mechanically or hydraulically until specimen failure. The experimental program for this study involves a modified version of a typical push-out test by including haunches (illustrated in Chapters 3 and 4). The push-out tests are performed at the Ferguson Structural Engineering Laboratory (FSEL).

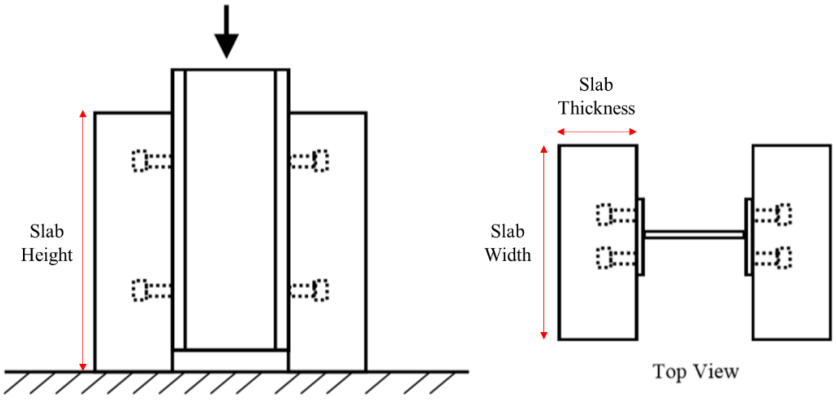

Figure 1.2 Common Push-out Test Setup (Topkaya 2004)

Complimenting the experimental research, finite element (FE) models are developed and validated with the test results. FE model validation is followed by a parametric study to broaden the understanding of how changes in design parameters affect the response of tall haunch specimens. Thus, the objective of this study was to determine how haunch geometry and structural detailing affect the ultimate shear strength of steel and PSC girder specimens through

full-scale testing and computational simulation. Based on the results obtained, analysis and design guidelines are recommended to account for tall haunch behavior on the overall response of a bridge.

This report is organized into six Chapters. The details of each chapter are as follows:

- Chapter 2–Literature Review: A general overview of past studies and existing guidelines related to horizontal shear transfer in steel and PSC girder specimens.
- Chapter 3– Steel Girder Testing: Push-out test layout, fabrication, and setup details are considered for steel girder specimens. The test results for steel girder specimens are also provided.
- Chapter 4– PSC Girder Testing: Push-out test layout, fabrication, and setup details are considered for PSC girder specimens. The test results for PSC girder specimens are also provided.
- Chapter 5– Finite Element Model Validation: Computational model development and validation for both steel and PSC girder specimens are described.
- Chapter 6– Finite Element Parametric Study: A wide range of parameters that can affect the ultimate shear capacity of haunches in steel and PSC girder specimens are evaluated using the validated FE model.
- Chapter 7– Conclusion and Design Recommendations: The main conclusions from the experimental and computational study are outlined. Design recommendations are provided to account for haunch behavior.

Chapter 2. Literature Review

This chapter provides an overview of past research and relevant design specifications and guidelines addressing the composite behavior of both steel and concrete girder systems. Project researchers focus on identifying the variables that most strongly influence the shear capacity of composite connections, the limitations of current design specifications and guidelines, and the experimental techniques used to study the behavior of composite systems. Computational methods used to study composite behavior are also evaluated. Because push-out tests are the most common technique for studying the behavior of composite systems, this chapter includes a description of these types of tests, how they have been used in past research, and how they are used in the current study.

2.1. Push-out Testing in Steel Girders

The literature review presented in this chapter includes peer-reviewed journal and conference papers, theses and dissertations, technical reports, and design specifications or guidelines pertinent to shear connectors with the headed shear studs. The design specifications and guidelines include AASHTO LRFD (2020), ACI318 (2019), Eurocode 4 (CEN 2004a), and TxDOT standard practices.

2.1.1. Existing Design Specifications and Guidelines

2.1.1.1. AASHTO LRFD (2020)

In Chapter 6 of the AASHTO LRFD (2020), design requirements for headed shear studs are provided along with an equation for the nominal shear resistance. As per Section 6.10.10, the minimum aspect ratio (height-to-diameter ratio) of headed shear studs is 4.0. The center-to-center pitch can be no larger than 48 in. for girder web depths greater or equal to 24 in., no larger than 24 in. for webs not exceeding 24 in., and no less than six times the stud diameter. The stud transverse spacing can be no less than four times the stud diameter. A minimum 2-in. penetration into the concrete slab is required.

Chapter 6 of the AASHTO LRFD (2020) provides an equation to predict the nominal strength of headed shear studs. The equation includes a resistance factor of 0.85 and computes ultimate strength as follows:

$$Q_u = 0.5 A_{sc} \sqrt{f'_c E_c} \le A_{sc} F_u \qquad \text{Equation 2.1.1.1}$$

where: Q_u = ultimate strength of shear stud (kips),

A_{sc} = cross-sectional area of shear stud (in.^{2}),

F_u = minimum specified tensile strength of stud steel (ksi),

f_c' = compressive strength of concrete (ksi),

E_c = elastic modulus of concrete (ksi).

2.1.1.2. TxDOT Guidelines

TxDOT guidelines, such as the Bridge Design Manual (2023a), the Bridge Design Guide – LRFD (2023b), the Bridge Detailing Guide (2022) and standard drawings, have been developed with a focus on design efficiency and safety. For shear connectors, the stud size, arrangement, reinforcement detailing, haunch dimensions, and so on, are provided in standard drawings (e.g., see Figure 2.1.1.1). As shown in the standard drawing "Steel Girder Miscellaneous Details" (TxDOT 2019a), 7/8 in. headed shear studs should be used with a minimum height of 5 in. so that ample deck penetration is achieved. The minimum spacing in the longitudinal and transverse directions is four times the stud diameter. The top cover to the studs should be at least 2.5 in., and the studs are required to penetrate at least 2 in. into the deck. Three shear studs are needed in a row parallel to the transverse direction. When prestressed concrete panels (PCP) are used for deck construction, two studs per row should be designed with a pitch reduction of one third to maintain the total number of shear studs. The minimum clear distance between the studs and the panels is 5/8 in.

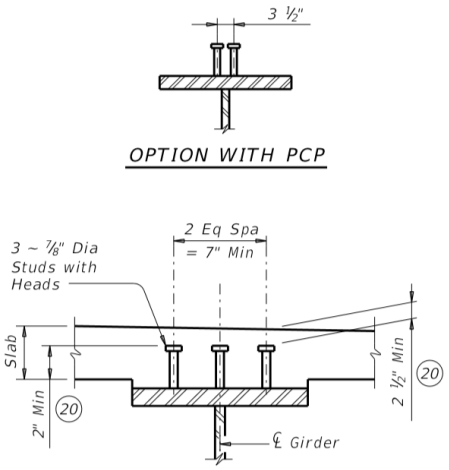

Figure 2.1.1.1 Standard Drawing - Steel Girder Miscellaneous Details (TxDOT 2019a)

The TxDOT Bridge Design Manual (2023a) states that haunches should not be included when calculating composite section properties. As per the TxDOT Bridge Detailing Guide (2022), transverse reinforcement is needed in the beam region when the haunch depth exceeds 3 in. The maximum spacing of the transverse reinforcement is 12 in.

2.1.1.3. Eurocode 4: Design of Composite Steel and Concrete Structures

- Part 1.1 (CEN 2004a): "General Rules and Rules for Buildings," and Part 2 (CEN 2005a): "General Rules and Rules for Bridges"

CEN (2004a) provides general guidelines for both buildings and bridges, and additional design guidance specifically for bridges is presented in CEN (2005a). According to CEN (2005a), the design resistance of headed studs with diameters between 16 mm (0.6 in.) and 25 mm (1 in.) can be calculated using Equation 2.1.1.2.

$$P_{Rd} = \frac{0.8 f_u \pi d^2 / 4}{\gamma_v} \text{ or } \frac{0.29 \alpha d^2 \sqrt{f'_c E_c}}{\gamma_v}$$

Equation 2.1.1.2

whichever is smaller, with

$$\alpha = 0.2(h_{sc} / d + 1) \quad \text{for } 3 \le h_{sc} / d \le 4$$

$$\alpha = 1 \quad \text{for } h_{sc} / d > 4$$

where P_{Rd} = design shear resistance of stud (kips),

d = shank diameter of stud (in.),

f_u = ultimate tensile strength of stud steel (ksi), not greater than 500 N/mm^2 (72.5 ksi),

f_c' = compressive strength of concrete (ksi),

E_c = elastic modulus of concrete (ksi),

γ_v = 1.25 is the partial factor.

The partial factor γ_v is similar to a safety factor and is derived using a reliability-based analysis. The value can vary based on the requirements of National Annexes (NA). NA are national standardized documents that provide guidelines for each European Union (EU) country so that different local policies may be set as needed to accommodate local conditions, climate, and other factors. Generally, γ_v = 1.25 is recommended by Eurocode 4 (CEN 2005a).

CEN (2004a) and CEN (2005a) specify a minimum stud aspect ratio of 3.0. The minimum penetration requirement is defined such that the bottom of the stud head should extend beyond the bottom reinforcement by at least 30 mm (1.2 in.) without a haunch. The minimum longitudinal and transverse spacing for studs should be, respectively, five times and four times the stud diameter. Following are the guidelines for a solid slab haunch:

A. the distance between the bottom of a stud head and the transverse reinforcing bars in a haunch should not be less than 40 mm (1.6 in.),
B. the cover from the side of a haunch to the connector should not be less than 50 mm (2 in.).
C. the side of a haunch should lie outside a line drawn at 45° from the outside edge of a connector.

CEN (2004a) also includes a standard push-out test methodology for assessing composite connection behavior. This methodology is extensively discussed in the push-out test section (Section 2.1.2.1).

2.1.1.4. ACI318 2019

Chapter 17 of ACI318 (2019) presents the design methods for concrete anchors in tension, shear, or combined tension and shear. The shear capacity design requirements are of greatest interest for this research project. There are three different failure modes for shear connectors: 1) shear stud rupture, 2) concrete pryout failure, and 3) concrete breakout, as shown in Figure 2.1.1.2.

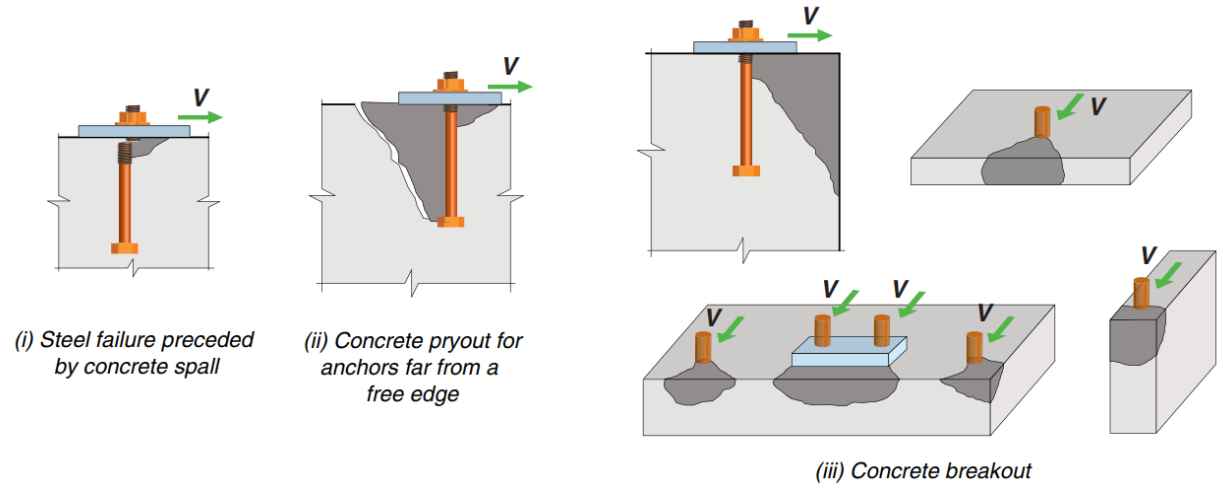

Figure 2.1.1.2 Shear Connector Failure Mode Illustration (ACI318 2019)

Section 17.7.1.2 provides an equation to calculate the ultimate capacity of headed shear studs cast in concrete:

$$V_{sa} = A_{se,V} f_{uta} \qquad \text{Equation 2.1.1.3}$$

where: $A_{se,V}$ = effective cross-sectional area of an anchor in shear (in.^{2}),

f_{uta} = ultimate strength of an anchor (ksi)

Compared with the other design guidelines or specifications, ACI 318 (2019) has more detailed provisions concerning different concrete failure modes. Section 17.7.2 provides equations to predict the concrete breakout capacity of single anchors and anchor groups. The equations are given below:

(a) For shear perpendicular to the edge on a single anchor:

$$V_{cb} = \frac{A_{Vc}}{A_{Vco}} \Psi_{ed,V} \Psi_{c,V} \Psi_{h,V} V_b \qquad \text{Equation 2.1.1.4}$$

(b) For shear perpendicular to the edge on an anchor group:

$$V_{cbg} = \frac{A_{Vc}}{A_{Vco}} \Psi_{ec,V} \Psi_{ed,V} \Psi_{c,V} \Psi_{h,V} V_b \qquad \text{Equation 2.1.1.5}$$

where: A_{Vc} = the projected area of the failure surface on the side of the concrete member at its edge for a single anchor or an anchor group,

A_{Vco} = the maximum projected area for a single anchor that approximates the surface area of the full breakout volume for an anchor unaffected by edge distance, spacing, or depth of member,

$\Psi_{ec,V}$ = breakout eccentricity factor,

$\Psi_{ed,V}$ = breakout edge effect factor,

$\Psi_{c,V}$ = breakout cracking factor,

$\Psi_{h,V}$ = breakout thickness factor,

V_b = basic single anchor breakout strength.

Concrete pryout failure has not been extensively investigated by the research team as it rarely occurs in bridge girders. The push-out test specimens have been designed to have sufficient edge distance to avoid this failure mode from occurring.

2.1.2. Push-out Test Details

Push-out tests have been widely used to investigate the composite behavior of headed shear studs. These types of tests are popular because they effectively and efficiently simulate the longitudinal shear demand on a shear connector by isolating a section of a composite girder. Due to its efficiency, push-out tests are adopted by the research team as the primary method to study the performance of the shear connectors in both steel and concrete girder cases. the latter is discussed in Section 2.2.

A typical double-sided push-out test setup is shown in Figure 2.1.2.1. Concrete slabs are cast on both sides of an I-beam section with or without precast panels. Headed shear studs are welded on the flanges of the I-beam section and embedded in the concrete. The test load is applied on the top of the I-beam section through hydraulic devices, such as MTS actuators. Depending on the nature of the research project, different lateral restraints and supports may be applied to the test setup. Details of the testing procedure used in this project are provided subsequently in this chapter.

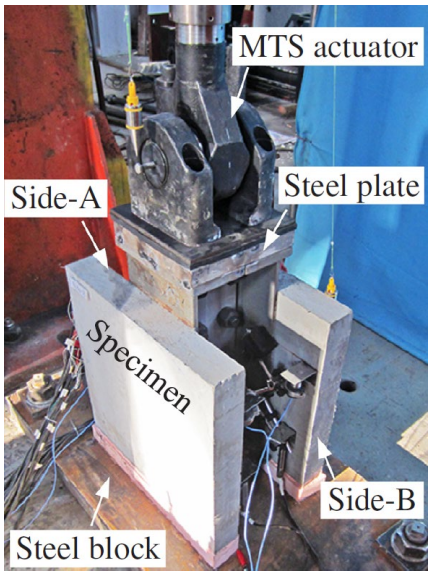

Figure 2.1.2.1 Push-out Test Setup (Liu et al. 2019)

2.1.2.1. Standard Push-out Test Method in Eurocode 4

CEN (2004a) includes a standard push-out test (shown in Figure 2.1.2.2) for assessing composite connection behavior. Many research studies refer to this standard push-out test as described in additional detail below. As shown in Figure 2.1.2.2 key point 2, the base of the concrete slab is embedded in gypsum or mortar and placed on the testing floor. The concrete specimens for the push-out tests are required to be air-cured, horizontally cast, and have grease applied at the concrete-steel interface. Key point 3 in Figure 2.1.2.2 refers to a concrete recess being optional. A concrete recess is a gap introduced at the bottom of the concrete slab to distribute the compressive forces transversely across the entire width (Ernst 2006). This test setup applies to both building and bridge applications. The test is also applicable to haunch specimens provided they are designed using the CEN (2004a) and CEN (2005a) guidelines. Specific tests are required where the haunch does not comply with the CEN (2004a) and CEN (2005a) requirements. These specific tests (CEN (2004a)) require the height of each concrete slab to be related to the longitudinal spacing of the connectors in the composite structure. Additionally, the width of each slab should not exceed the effective width of the composite beam, and the thickness should not exceed the minimum thickness of the slab in the beam under consideration. The haunch size and the haunch reinforcement in the specific tests should be the same as that provided in the composite beam for the specific structure being studied. The testing procedure involves loading the specimen up to 40% of the expected failure load followed by 25 cycles between 5% and 40% of the expected failure load. Subsequent loading increments should be such that failure does not occur in 15 minutes. The specimen loading rate is not provided in CEN (2004a). Slip and transverse separation should be measured at each increment until 20% of the maximum load. Testing consistency requires that there should not be more than a 10% deviation in three identical specimens. If the deviation is greater than 10%, additional testing is required.

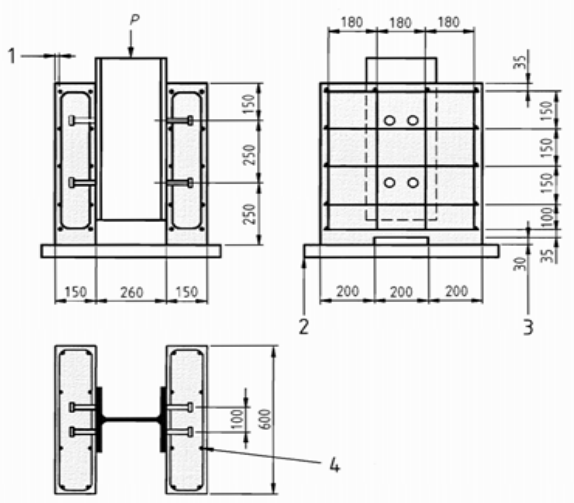

Key

1 cover 15 mm

2 bedded in mortar or gypsum

3 recess optional

4 reinforcement: ribbed bars ϕ 10 mm resulting in a high bond with $450 \leq f_{sk} \leq 550$ N/mm^2
steel section: HE 260 B or 254 x 254 x 89 kg. UC

Figure 2.1.2.2 Standard Push-out Test Diagram as Specified by CEN (2004a)

2.1.2.2. Push-out Test Results

Typically, test data are plotted using load-slip curves, where the load corresponds to that applied by the actuator, and the slip is the relative displacement between the steel and concrete components. Often, the reported results are normalized by dividing the measured load by the total number of shear connectors. Slip is measured at the concrete-steel interface using a variety of techniques. The load-slip behavior is nonlinear, and a typical response is shown in Figure 2.1.2.3. Unloading of the specimen does not affect the envelope of the curve, and reloading is linear until the maximum load prior to unloading is reached (Topkaya 2004).

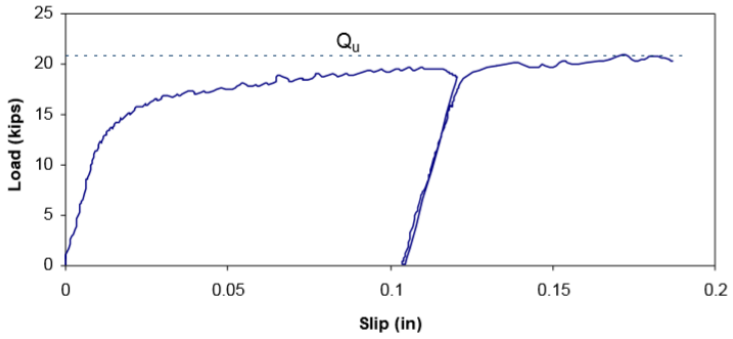

Figure 2.1.2.3 Typical Load-Slip Curve of a Headed Shear Stud (Topkaya 2004)

Among the previous investigations referenced by researchers conducting push-out tests, the study documented in Ollgard et al. (1971) is generally the most frequently cited. The authors of this study aimed to understand the behavior of shear stud connectors embedded in normal-weight

and light-weight concrete. They prepared forty-eight two-sided push-out specimens and considered several geometric variables as well as different material characteristics. The concrete slab dimensions and reinforcement detailing were kept constant. The specimens were cast vertically and in an inverted position to assure no voids were formed under the studs on their bearing side.

Ollgard et al. (1971) observed that the failure modes in the test specimens were either stud shearing or concrete breakout. Based on the measured test results and a regression analysis, the authors determined the parameters affecting composite connection capacity and derived the ultimate strength equation now used in AISC (2016) and AASHTO LRFD (2020). The authors also gave Equation 2.1.2.2 for load-slip curves when the specimens are continuously loaded:

$$Q = Q_u(1 - e^{-18\Delta})^{2/5} \qquad \text{Equation 2.1.2.1}$$

or when the specimens are unloaded after reaching the working load and then reloaded again:

$$Q = Q_u \frac{80\Delta}{1 + 80\Delta} \qquad \text{Equation 2.1.2.2}$$

where: Q = applied load per connector (kips),

Q_u = ultimate strength of shear stud (kips),

Δ = relative slip between steel and concrete (in.).

2.1.2.3. Single-Sided vs. Double-Sided Push-out Tests

Although one-sided vertical push-out tests offer several advantages, the vast majority of tests reported in the research literature use a two-sided vertical setup. Ollgard (1970) conducted tests on both one-sided and two-sided push-out specimens. The two-sided push-out specimens had approximately 20% higher ultimate strength per connector compared to one-sided push-out specimens. As per Ollgard (1970), the reduction in strength for the one-sided specimens was due to load eccentricity causing more severe combined tension and shear on the studs. Based on Slutter and Driscoll (1961), Ollgard (1970) also proposed that the two-sided specimens provide a lower bound to shear stud strength in actual beams; therefore, one-sided specimens reducing the strength further should not be considered. Ernst (2006) developed one-sided vertical tests (Figure 2.1.2.4), which were prone to large eccentric forces that created challenges in interpreting the results. The author then successfully developed another horizontal one-sided push-out test setup (Figure 2.1.2.5) that avoided many of the problems of the initial one-sided vertical test. Nonetheless, the load frame and actuators needed for this test setup are much more elaborate and costly than those used in typical two-sided tests. For the current study, researchers used a two-sided vertical test setup so that experimental results can be readily compared to the majority of past studies reported in the research literature. Details of the testing program are discussed in Chapters 3 and 4.

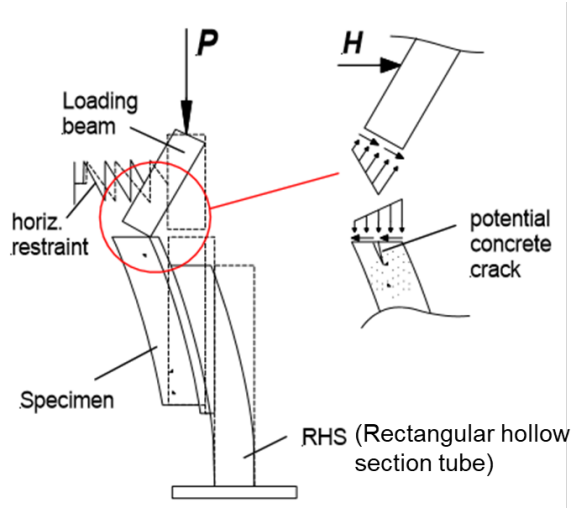

Figure 2.1.2.4 One-sided Vertical Push-out Test Setup (Ernst 2006)

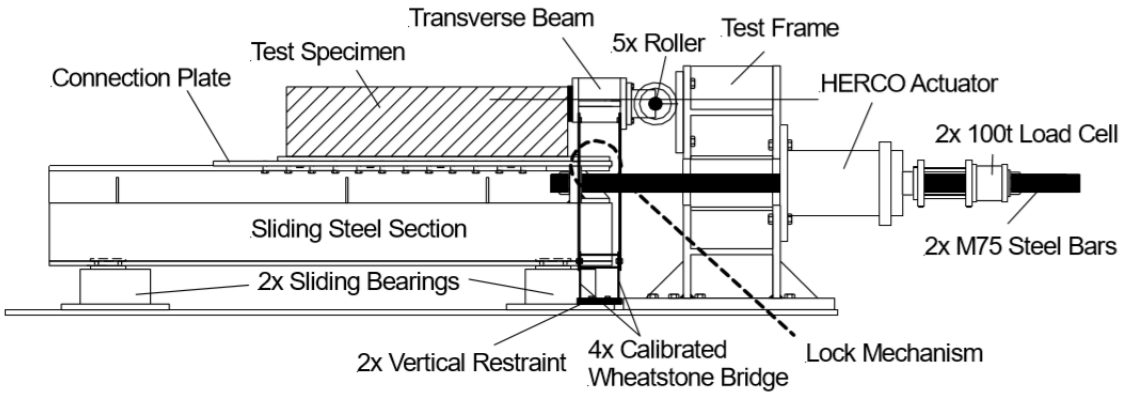

Figure 2.1.2.5 One-sided Horizontal Push-out Test Setup (Ernst 2006)

2.1.2.4. Lateral Restraints

Past research has shown that lateral restraint conditions influence the measured strength of push-out test specimens. Rambo-Roddenberry (2002) tested welded shear connectors and found that the application of lateral restraint (with an actuator that applied a force that was 10% of the vertical actuator's applied force) increased the measured strength of the specimens due to increased friction at the interface between the steel flange and concrete surface. The lateral restraint employed by Rambo-Roddenberry (2002) is depicted in Fig. 2.1.2.6.

Taylor et al. (1970) also experimented with the effects of lateral restraint on one-sided test specimens (an unspecified point load was applied to the concrete slab to prevent separation). Taylor et al. (1970) found that the presence of lateral restraint increased the measured strength of push-out test specimens compared to unrestrained specimens.

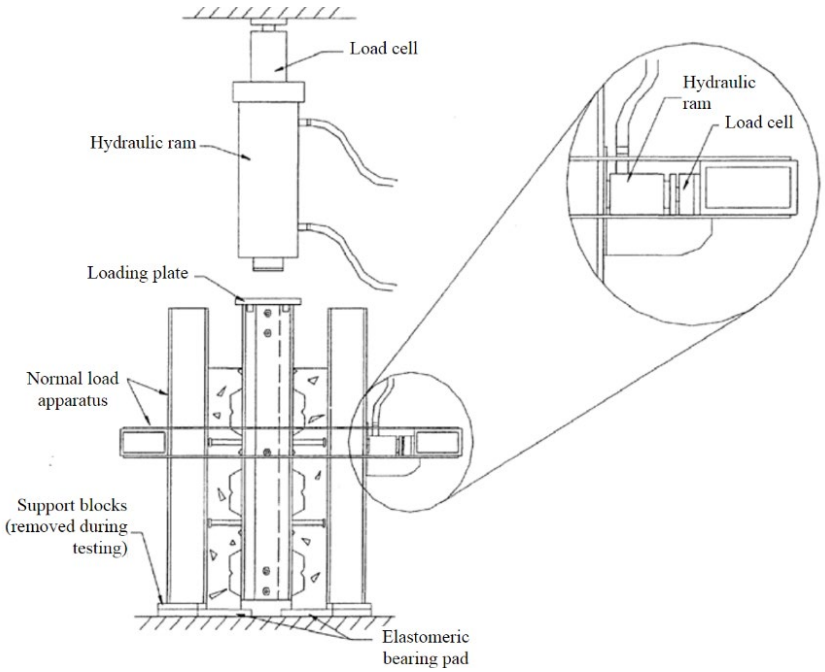

Figure 2.1.2.6 Horizontal Restraint in Two-Sided Push-Out Test (Rambo-Roddenberry 2002)

The findings from Taylor et al. (1970) and Rambo-Roddenberry (2002) indicate the importance of considering the effects of lateral restraint when push-out tests are performed. Under actual field conditions, separation is unlikely to occur as in a vertical push-out test due to the orientation of a bridge girder relative to the direction of gravity or applied load. Lateral restraint in a vertical test setup can eliminate the separation of the slab from the steel section, but it may artificially increase the measured capacity of the composite structure. Thus, measured results could possibly overestimate the strength available under actual field conditions.

2.1.2.5. Concrete Support

Even if a two-sided push-out test setup is geometrically symmetric, slight eccentricities are likely to exist due to small imperfections in the test setup. In most studies, the concrete slabs are placed directly on the testing floor (or on other test structure surfaces) using gypsum or mortar as a leveling agent for the ends of the concrete slabs as shown in Figure 2.1.2.7. This type of base connection has some frictional resistance. If a roller support is provided for the concrete slabs, it will have no horizontal restraint at the base. The overturning moment resulting from load eccentricity will then be solely resisted through the composite connection, leading to its failure at a smaller applied load than when the base of the concrete slabs is restrained. Therefore, measured specimen capacity depends on the base support conditions. Figure 2.1.2.8 shows the relationship between strength and the type of base connection (Ernst 2006).

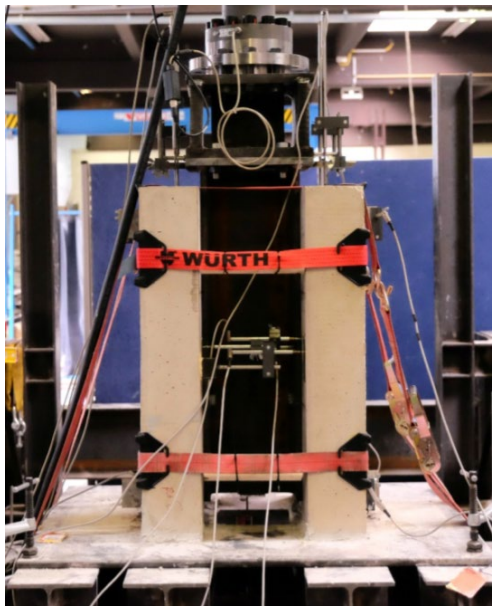

Figure 2.1.2.7 Push-out Test Setup by Kozma et al. (2019)

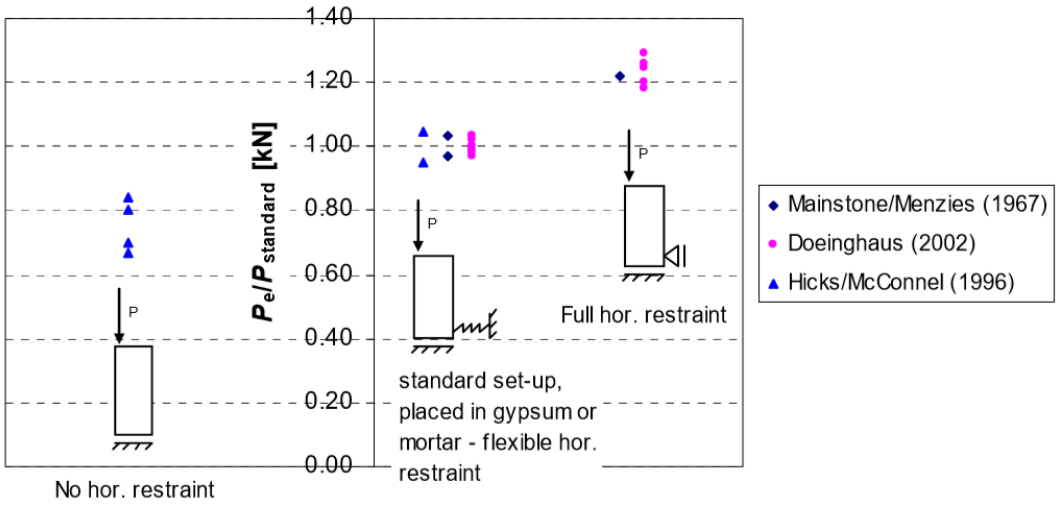

Figure 2.1.2.8 Influence of Support on Connection Strength (Ernst 2006)

2.1.2.6. Friction at the Steel/Concrete Interface

Rambo-Roddenberry (2002) observed the effects of friction at the composite interface in a push-out test specimen. A compressive normal load was applied to the specimen, which increased the friction at the composite interface. The results of this study are summarized in Table 2.1.2.1. The stud capacity ratio represents the ratio of measured-to-predicted ultimate strength as per CEN (2004a). The results show that the increase in normal force at the composite interface increased the capacity ratio. Rambo-Roddenberry (2002) proposed that this increase is due to an increase in frictional resistance at the steel and concrete interface, which increases the apparent strength of the specimen. The results also show that application of grease at the composite interface leads

to a slightly lower recorded ultimate strength relative to the specimens with no grease or applied normal force. The difference, however, is small and indicates that application of grease had a negligible effect. Ernst (2006) reached similar conclusions, where the inclusion of a Teflon layer to reduce the frictional forces at the composite interface had no significant effect on the shear connection behavior. Souza et al. (2017) observed that the application of a cohesive layer only affected the initial stiffness and had no effect on the ultimate capacity of a specimen. For the current study, the specimens did not include any methods for reducing the friction between the steel girders and concrete deck. The specimens reflect expected field conditions expected in practice.

Table 2.1.2.1 Influence of Friction at Composite Interface (Rambo-Roddenberry 2002)

Push-tests Configuration	Normal Force (% of Shear Force)	Stud Capacity Ratio
Steel-concrete interface (3 tests)	0	1.00
Steel-concrete interface (3 tests)	10	1.14
Greased sheet steel at interface	10	0.97

2.1.3. Push-out Test Specimen

As mentioned in Section 2.1.2, different push-out test setups may affect the test results. Additionally, the performance of headed shear studs may also be controlled by the specimen designs, such as rebar detailing, stud spacing, edge distance, haunch geometries, and other parameters. This section summarizes the parameters potentially affecting the composite behavior of shear connectors in tall haunches based on a review of the relevant research literature.

2.1.3.1. Haunch Rebar Detailing

Bridge et al. (2006) tested five push-out specimens. One of the five specimens was well detailed by hoop and ladder reinforcement in the haunch region. This specimen failed in a ductile manner and had a capacity that exceeded the predicted strength. The other four specimens were poorly detailed. They failed in a brittle manner and did not reach the predicted strength. Taylor et al. (1970) reached similar conclusions concerning how well detailed haunch reinforcement improves specimen behavior.

A study by Johnson (1972) intended to derive equations for the design of shear connectors and transverse reinforcement detailing in haunches. As per Johnson (1972), the transverse reinforcement in a haunched specimen reinforces the concrete against longitudinal shear failures and prevents local splitting or bursting in the vicinity of a shear connector. Johnson's research indicates that the critical surfaces for shear failure in a deep haunch are AB and CDEF in Figure 2.1.3.1. The shorter of the two distances governs the transverse reinforcement design. Based on his previous study for zero-haunch specimens (Johnson 1972), Johnson proposed Equation 2.1.3.1 for calculating the required amount of transverse reinforcement. Johnson (1972)

compared the reinforcement obtained from this equation with the transverse reinforcement specified by Taylor et al. (1970) and obtained comparable results from both. This observation led to the conclusion that the equation should be valid for haunched specimens as well. Because the data from Taylor et al. (1970) were obtained from vertical one-sided push-out tests, which some researchers have shown to be problematic (Ollgard 1970, Ernst 2006), the conclusion from Johnson (1972) should be used with caution.

$$pf_y \geq (1.26v_u - 0.28u^{0.5}) \text{ or } 0.55\frac{\text{N}}{\text{mm}^2}(0.08\text{ksi})$$

Equation 2.1.3.1

whichever is greater, where:

p = amount of transverse reinforcement per unit area of the shear plane,

f_y = yield strength of steel (N/mm2),

v_u = mean ultimate shear stress in the specimen (N/mm2),

u = design cube strength (N/mm2).

Note: 1 N/mm^2 is equal to 0.145 ksi.

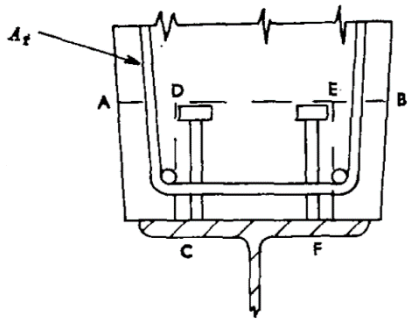

Figure 2.1.3.1 Haunch Reinforcement Illustration (Johnson 1972)

2.1.3.2. Spacing between Headed Shear Studs

Current design guidelines place limits on how closely studs can be placed to one another to reduce the reduction in capacity associated with group effects. The standard drawing "Steel Girder Miscellaneous Details" (2019) indicates both transverse and longitudinal spacings should be no less than four times the stud diameter. AASHTO LRFD (2020) specifies the minimum longitudinal and transverse spacing to be six and four times the stud diameter, respectively. These provisions are well supported by several previous research studies. Jayas and Hosain (1988) tested specimens with various stud longitudinal spacings and observed different failure modes. For specimens with stud spacings of 20*d* and 10*d*, shear stud failure occurred (where *d* is the shear stud diameter). Conversely, a stud spacing of 6.4*d* resulted in concrete failure for the other specimens. The effect of stud spacing on the behavior of tall haunch composite girders remains unclear and requires further study.

2.1.3.3. Haunch Geometry

Taylor et al. (1970) stated the average demand each stud could resist increased proportionally with the haunch width from 3.5-in. to 6.5-in. Oehlers and Park (1994) demonstrated that haunch slope affects the ultimate capacity of specimens. This observation was demonstrated through two-sided push-out test data analysis. The data showed that the specimen strength increased as the angle from the vertical increased (between zero and ninety degrees). A diagram of the varying haunch geometries is provided in Figure 2.1.3.2. According to the test data, haunched specimens have less strength than specimens without a haunch. Although this observation is not new, data from this study provide quantifiable evidence of this behavior. It is important to note that the specimens did not contain transverse reinforcement and failed due to concrete cracking.

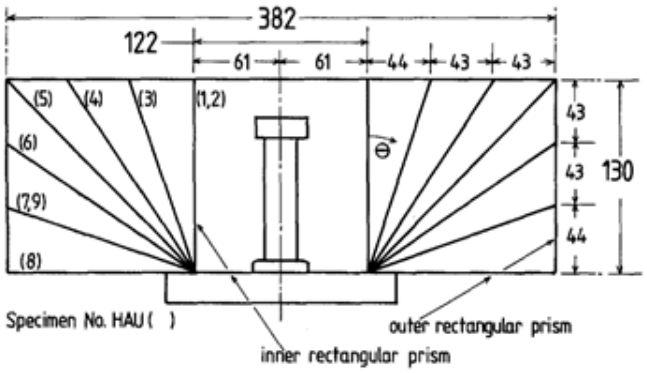

Figure 2.1.3.2 Sloped Haunch (Oehlers and Park 1994)

2.1.3.4. Stud Embedment Length

Ernst (2006) showed that stud embedment length had little effect on improving the ultimate capacity of push-out test specimens. The specimens involving unreinforced haunches and shear studs with lengths of 4 in. and 5 in. were tested and showed little difference on ultimate capacity and failure mode. Based on statistical analyses, Oehlers (1980) concluded that stud length did not significantly affect the ultimate capacity in traditional push-out tests. It remains unclear how stud length may affect the behavior of shear connectors for girders with tall haunches.

2.1.3.5. Stud Diameter

A regression analysis on 125 previous push-out tests performed by Oehlers (1980) showed that the diameter of shear studs critically affected the ultimate capacity of the specimens. The performance of the studs with a diameter larger than 0.75 in. was significantly affected by the concrete strength.

2.1.3.6. Concrete Deck Width

Based on the regression analysis, Oehlers (1980) stated that the width of the concrete decks greatly affected the ultimate capacity of the push-out test specimens. Ernst (2006) suggested that concrete decks in push-out specimens should be at least 600 mm (23.6 in.) to be sufficiently representative, as suggested by CEN (2004a). Although Ernst (2006) developed the conclusion

based on the study including metal decks, it is expected to be valid in this research project as well. An improperly designed deck width might negatively impact the effectiveness of push-out tests for specimens with tall haunches.

2.1.3.7. Shear Stud Arrangement

Ollgard et al. (1971) tested specimens with both one and two rows of shear studs. The results showed that the average strength per stud remained unchanged for both cases. Jayas and Hossain (1988) tested specimens with one to three rows of studs and drew similar conclusions. Despite these observations, test results showed that shear studs in different rows reached their ultimate shear capacity at different times. Using results from prior testing, Ernst (2006) suggested using at least two rows of shear connectors to ensure all studs reach their capacity before a brittle failure occurs.

2.1.3.8. Concrete Recess

As discussed in CEN (2004a), a concrete recess (Figure 2.1.3.3) can be introduced to the test setup to achieve a better distribution of compressive forces across the entire width of the concrete slab. The influence of a concrete recess is shown in the form of a strut and tie model in Figure 2.1.3.4. The resulting increase in the compressive strut angle leads to a better distribution of stress across the concrete slab width and also allows the tensile stress in the bottom tie to reach a larger magnitude. Nonetheless, such geometry does not exactly replicate the actual slab profile from which a push-out test is intended to represent. For a haunched specimen, where longitudinal splitting is a possible failure mode, it may be important to have a concrete recess to get accurate transverse tensile forces (Ernst 2006). The introduction of a concrete recess, however, leads to a reduction of concrete stiffness, which may give larger deformations than the case in which no recess is present.

Figure 2.1.3.3 Push-out Specimen with Recess (Nguyen and Kim 2009)

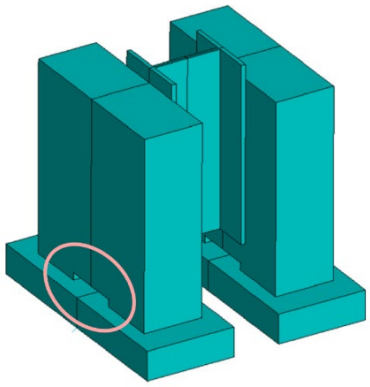

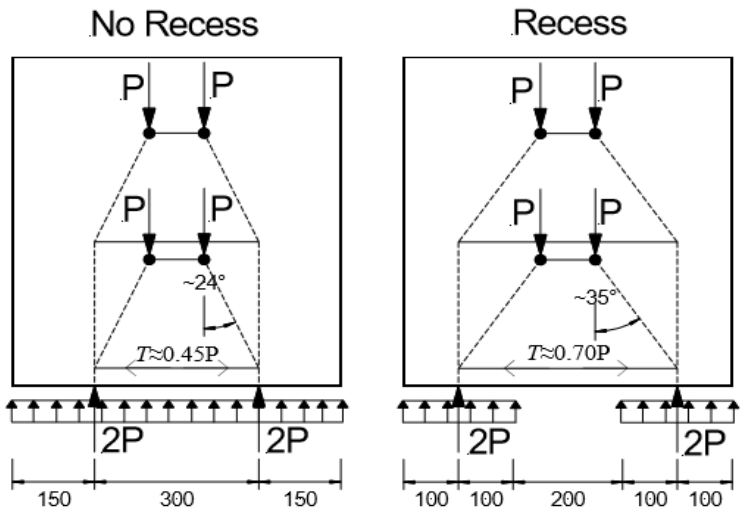

Figure 2.1.3.4 Influence of Concrete Recess (Ernst 2006)

2.1.4. Comparison between the Test Results and the Predicted Values

Test results are often compared with design guidelines and equations given in various guidelines and specifications. Pallares and Hajjar (2010) reviewed 391 monotonic and cyclic push-out tests from the research literature and compared the test results with the predicted strengths from ACI 318 (2008) and AISC (2005). Figure 2.1.4.1 and Figure 2.1.4.2, respectively, show comparisons of the test results with these equations.

In Figure 2.1.4.1, the first plot compares the AISC (2005) predicted strength with strengths measured from all the tests, the second compares with those tests that had steel failures, the third compares with the tests that had concrete failures, and the fourth plot compares with the tests that had a mixed failure. As the average ratio of test/predicted strength is less than 1.0 for all the plots, the strength calculated using AISC (2005) overestimates the average strength from the tests. The ratio is smallest (i.e., the results are least conservative) for the case where the comparison is with those tests that had concrete failures.

Figure 2.1.4.2 shows a comparison of all test results with predicted strength using ACI 318 (2008). As shown in the figure, the average test/predicted strength ratio is 1.35, indicating the predicted strengths are safe, though perhaps unnecessarily conservative. The equations in the current edition of ACI 318 (2019) have been updated and require further evaluation to determine how conservative the current predictions are.

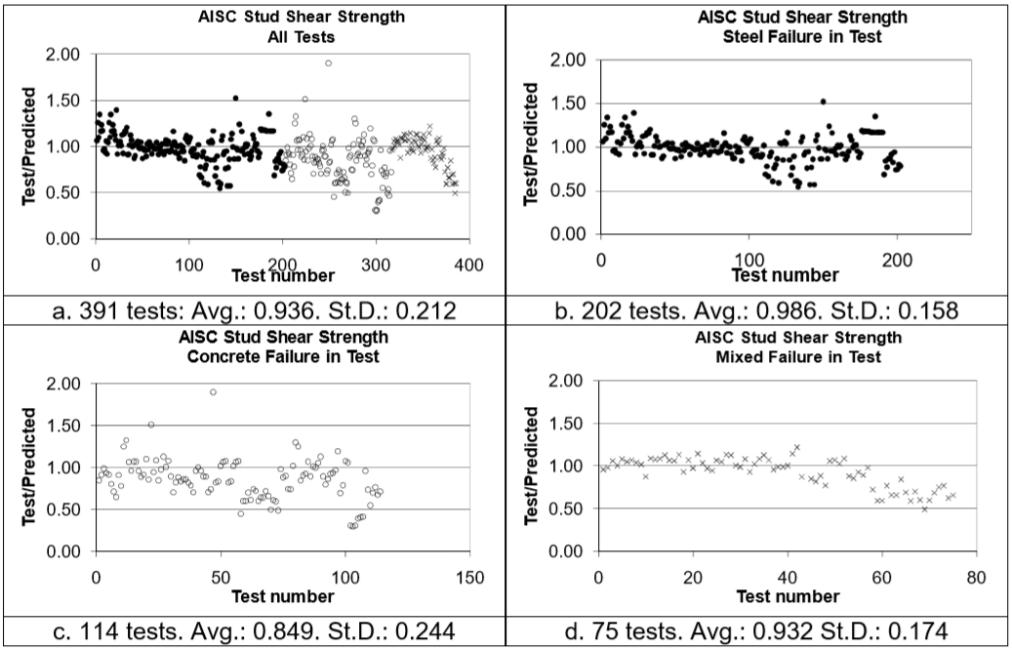

Figure 2.1.4.1 AISC (2005) Predicted Strength Compared with Test Results (Pallares and Hajjar 2010)

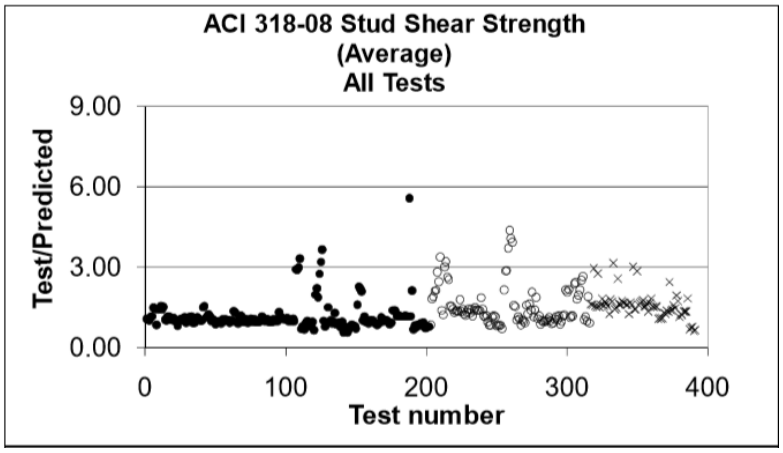

Figure 2.1.4.2 ACI Predicted Strength Compared with Test Results (Pallares and Hajjar 2010)

From the above results, Pallares and Hajjar (2010) recommended providing a reduction factor of 0.65 to the AISC (2005) equation for predicting the steel failure mode in studs. AISC (2016) modified the equation from AISC (2005) to Equation 2.1.4.1, introducing the R_g and R_p factors. The R_g factor accounts for stud grouping effects, while the R_p factor accounts for the weak versus strong position of the stud relative to metal deck forms used in the building industry. Due to the significant difference in the forming systems used in bridges compared to buildings, there will be no R_p factor for bridge applications. The AASHTO LRFD (2020) equation for calculating stud shear strength (Equation 2.1.1.1) has a resistance factor of 0.85 for predicting the steel failure and concrete failure modes in stud connections. For calculation of nominal shear strength of a headed stud embedded in solid concrete or a composite slab, AISC (2016) gives:

$$Q_n = 0.5 A_{sa} \sqrt{f'_c E_c} \leq R_g R_p A_{sa} F_u$$ Equation 2.1.4.1

where: Q_n = nominal strength of shear stud (kips),

A_{sa} = cross-sectional area of a shear stud (in.^{2}),

f_c' = compressive strength of concrete (ksi),

E_c = elastic modulus of concrete (ksi),

F_u = minimum specified tensile strength of stud steel (ksi),

R_g = coefficient to account for group effect,

R_p = position effect factor for shear studs.

While evaluating prior research for this report, the research team compared results from several studies with predicted stud strengths from AASHTO LRFD (2020) and CEN (2005a). The AISC (2016) equation is not compared here because it is applicable to buildings and not bridges. Figure 2.1.4.3 compares results from 43 push-out tests with computed strengths obtained from AASHTO LRFD (2020) and CEN (2005a). The plot shows considerable scatter in the results. The average and standard deviation of test/predicted ratios for both standards are given in Table 2.1.4.1. The average ratios are on the conservative side for both CEN (2005a) and AASHTO LRFD (2020). Nonetheless, no strong conclusions can be drawn from a limited number of data points.

Table 2.1.4.1 Average and Standard Deviation of Test/Predicted Strength Ratios for AASHTO LRFD (2020) and Eurocode 4 (CEN 2005a)

	Eurocode 4 (CEN 2005a)	**AASHTO LRFD (2020)**
Average	1.231	1.082
Standard Deviation	0.260	0.447

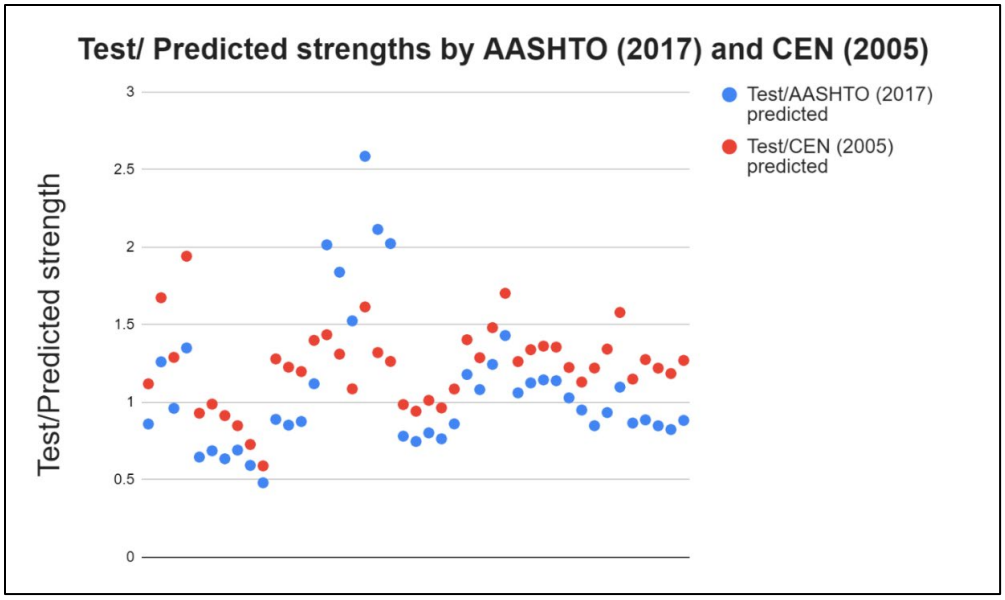

Figure 2.1.4.3 AASHTO LRFD (2020) and Eurocode 4 (CEN 2005a) Predicted Strengths Compared with Test Results

2.1.5. Concluding Remarks

The presence of tall haunches in a composite girder can lead to a significant reduction of shear strength if not properly detailed. Because there are no guidelines available for haunches as tall as 15 in., testing is required to identify the parameters that affect the ultimate shear strength of a haunched specimen. Two-sided push-out tests are often used to analyze the behavior of composite shear connections. Ideally, decks and haunches on both sides should be horizontally cast using concrete of same batch to keep the material properties identical and simulate actual casting conditions. Because different testing approaches and specimen details have been reported in the research literature, the results show significant scatter, even for the same specimen size. The test results are affected by several parameters, such as fabrication method, specimen size, specimen supports, lateral restraint provided, and other factors. These parameters are considered for the design of the test specimens (described subsequently in Chapter 3). The next section summarizes the research literature for composite behavior of PSC girder specimens.

2.2. Push-out Testing in PSC Girders

This section provides a detailed summary of research literature addressing the shear resistance at the interface between PSC girders and the deck/haunch. Section 2.2.1 provides a brief background for interface shear resistance equations used by different specifications. Section 2.2.2 illustrates requirements in some existing guidelines (AASHTO LRFD 2020, CEN 2004b, CEN 2005b ACI 318 2019, TxDOT 2023a, TxDOT 2023b and TxDOT 2022), and Section 2.2.3 summarizes relevant literature reviewed in the study.

2.2.1. Background for Interface Shear Resistance Equations

Shear friction theory, first introduced by Mast (1968), Hanson (1960), and Kaar et al. (1960), postulates that the interface shear resistance for cracked concrete is provided by the reinforcement across the crack. To visualize the shear friction phenomenon, consider the saw-tooth model (Figure 2.2.1.1) presented by Santos and Julio (2012). This visualization suggests displacement occurs normally to the contact surface, simultaneously with tangential displacement. When corresponding peaks on either concrete surface are in contact, it leads to a normal separation of the surfaces, inducing tension in the dowels that cross the shear interface. At maximum strength, the dowels yield, causing a clamping force of $A_s F_y$ to resist the shear.

Mattock and Hawkins (1972) introduced a modification to the original shear friction theory based on a consideration of the cohesion phenomenon. Cohesion describes a chemical bond among the particles of new concrete cast on the old particles of existing concrete. Cohesive bonds resist shearing until they experience stress that exceeds their damage initiation threshold, at which point debonding begins to occur at the contact surface.

Shear friction theory also accounts for contributions from concrete strength (Loov 1978), initially cracked surfaces (Walraven et al 1987), and surface roughness (Santos and Julio 2012). Santos and Julio (2012) suggest that the contributions from each source of shear resistance at the contact interface change with progressive slip of that interface (Figure 2.2.1.2). At low levels of shear stress, the interface experiences no slip, and neither shear friction in concrete nor dowels engage in stress resistance. Only the cohesive bonds resist shear at low levels of stress. As the interface begins to slip, the aggregates interlock, inducing shear friction resistance. At low levels of slip, the dowels experience no deformation and do not yet resist shear. As stresses increase further, the cohesive layer debonds and contributes less shear resistance, while the friction contribution increases. At larger magnitudes of load, the interface slips such that the dowels deform and begin resisting shear stress. At the highest levels of slip, the friction and cohesive forces diminish, leaving dowel action as the primary shear resistance mechanism. In specimens without premature concrete failure, one expects to observe a debonding of the concrete-concrete contact surface followed by yielding of the shear reinforcement.

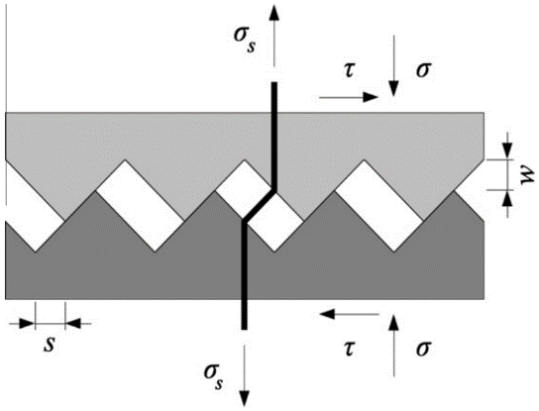

Figure 2.2.1.1 Saw-tooth Model for Shear Friction Phenomenon (Santos and Julio 2012)

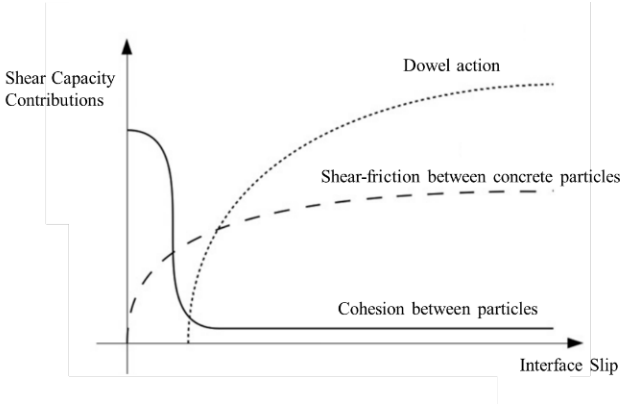

Figure 2.2.1.2 Sources of Interface Shear Resistance with Progressive Slip (Santos and Julio 2012)

2.2.2. Existing Guidelines

This subsection summarizes the haunch and interface shear resistance specifications from AASHTO LRFD (2020), CEN (2004b), CEN (2005b), ACI 318 (2019), TxDOT (2023a), TxDOT (2023b), and TxDOT (2022).

2.2.2.1. AASHTO LRFD (2020) Design Equation

As per AASHTO LRFD (2020) Article 5.7.4.3, the factored interface shear resistance (in kips) is computed as:

$$V_{ri} = \phi V_{ni} \qquad \text{Equation 2.2.2.1}$$

where: ϕ = resistance factor for shear specified in AASHTO LRFD (2020) Article 5.5.4.2

V_{ni} = nominal interface shear resistance (kips)

$$V_{ni} = cA_{cv} + \mu\,(A_{vf}f_y + P_c) \qquad \text{Equation 2.2.2.2}$$

where: $A_{cv} = b_{vi}L_{vi}$

c = cohesion factor

b_{vi} = interface width engaged in shear transfer

L_{vi} = interface length engaged in shear transfer

μ = friction factor

A_{vf} = area of interface shear reinforcement $\geq 0.05A_{cv}/f_y$

f_y = yield strength of reinforcement

P_C = permanent compressive force normal to the shear plane

Also,

$$V_{ni} \leq K_1 f'_c A_{cv} \quad \text{Equation 2.2.2.3}$$

$$V_{ni} \leq K_2 A_{cv} \quad \text{Equation 2.2.2.4}$$

where K_1 = fraction of concrete strength available to resist interface shear

K_2 = limiting interface shear resistance

f'_c = design concrete compressive strength of the weaker concrete on either side of the interface

The values of c, μ, K_1, and K_2 for normal weight concrete (NWC) are shown below in Table 2.2.2.1.

Table 2.2.2.1 Surface Factors Values from AASHTO LRFD (2020)

	CIP on NWC (clean, intentionally roughened to an amplitude of 0.25 in.)	**NWC, Placed monolithically**	**NWC on NWC (clean, intentionally roughened to an amplitude of 0.25 in.)**	**Clean, not intentionally roughened**	**Concrete anchored to steel**
c	0.28	0.4	0.24	0.075	0.025
μ	1.0	1.4	1.0	0.6	0.7
K_1	0.3	0.25	0.25	0.2	0.2
K_2	1.8	1.5	1.5	0.8	0.8

AASHTO LRFD (2020) does not have any specific requirements for tall haunches in PSC girders. The guidelines specify: "All reinforcement present where interface shear transfer is to be considered shall be fully developed on both sides of the interface by embedment, hooks, mechanical methods such as headed studs, or welding to develop the design yield stress."

2.2.2.2. CEN (2004b, 2005b) Design Equation

As per CEN (2004b) Article 6.2.5, the design shear resistance (in MPa) at the interface is computed as:

$$v_{Rdi} = c f_{ctd} + \mu \sigma_n + \rho f_{yd}(\mu \sin\alpha + \cos\alpha) \leq 0.5\, \nu\, f_{cd} \quad \text{Equation 2.2.2.5}$$

where: c = factor depending on interface

f_{ctd} = design tensile strength,

$$f_{ctd} = \frac{\alpha_{ct} f_{ctk}}{\gamma_c} \quad \text{Equation 2.2.2.6}$$

α_{ct} = coefficient taking account of long-term effects on the tensile strength and of unfavorable effects, resulting from the way load is applied,

γ_c = partial factor for concrete,

f_{ctk} = characteristic axial tensile strength of concrete,

$$f_{ctk} = 0.21 f_{ck}^{2/3} \quad \text{Equation 2.2.2.7}$$

f_{ck} = characteristic compressive cylinder strength of concrete in MPa,

μ = friction coefficient depending on interface,

σ_n = stress per unit area caused by normal force,

$\rho = A_s/A_i$,

A_s = area of interface shear reinforcement,

A_i = area of joint,

f_{yd} = design yield strength of reinforcement,

$$f_{yd} = \frac{f_{yk}}{\gamma_s} \quad \text{Equation 2.2.2.8}$$

f_{yk} = characteristic yield strength of reinforcement in MPa,

γ_s = partial factor for steel,

α = angle of shear reinforcement,

ν = strength reduction factor.

$$\nu = 0.6\,[1 - \frac{f_{ck}}{250}] \quad \text{Equation 2.2.2.9}$$

f_{cd} = design compressive strength.

$$f_{cd} = \frac{\alpha_{cc} f_{ck}}{\gamma_c} \quad \text{Equation 2.2.2.10}$$

α_{cc} = coefficient taking account of long-term effects on the compressive strength and of unfavorable effects, resulting from the way load is applied.

The following values are suggested for c, and μ (Table 2.2.2.2)

Table 2.2.2.2 Surface Factors Values from CEN (2004b)

	Very smooth (against steel)	**Smooth (no treatment)**	**Rough (intentionally roughened to 3mm at 40mm spacing)**	**Indented**
c (ksi)	0.25	0.35	0.45	0.5
μ	0.5	0.6	0.7	0.9

2.2.2.3. ACI 318 (2019) Design Equation

As per ACI 318 (2019) Article 16.4.4 and 16.4.5, if the applied longitudinal shear force (in lbs.),

$$V_{uh} \leq \phi 500 A_c \qquad \text{Equation 2.2.2.11}$$

where ϕ = shear strength reduction factor

A_c = area of joint

the nominal horizontal shear strength (in lbs.) for roughened concrete surface is taken as:

$$V_{nh1} = min\left(260 + \frac{0.6 A_v f_y}{b_v s}, 500\right) A_c \qquad \text{Equation 2.2.2.12}$$

where A_v = area of shear reinforcement withing spacing s,

and $A_v \geq \max\left(0.75\sqrt{f'_c}\frac{b_v s}{f_y}, 50\frac{b_v s}{f_y}\right)$

f_y = yield strength for transverse reinforcement in psi

f'_c = specified compressive strength of concrete in psi

b_v = interface width engaged in shear transfer

s = spacing of transverse reinforcement

and $s \leq \min(24, 4 \times least\ dimension\ of\ supported\ element)$

If the applied longitudinal shear force (in lbs.),

$$V_{uh} > \phi 500 A_c \qquad \text{Equation 2.2.2.13}$$

the nominal horizontal shear strength (in lbs.) for roughened concrete surface with shear-friction reinforcement perpendicular to the shear plane is taken as:

$$V_{nh2} = min\left(\mu A_v f_y, 0.2 f'_c A_c, 1600 A_c, (480 + 0.08 f'_c) A_c\right) \qquad \text{Equation 2.2.2.14}$$

μ = coefficient of friction,

f'_c = specified compressive strength of concrete

$fy \leq 60\ ksi$

The values for μ in NWC are shown in Table 2.2.2.3.

Table 2.2.2.3 Surface Factor Values from ACI 318 (2019)

	Concrete placed monolithically	Concrete placed against NWC that is clean and intentionally roughened to 0.25 in.	Concrete placed against NWC that is not intentionally roughened	Concrete placed against steel
μ	1.4	1.0	0.6	0.7

ACI 318 (2019) also specifies that the transverse reinforcement should be anchored on both sides of the interface to develop the yield stress.

2.2.2.4. TxDOT Guidelines

According to TxDOT (2023b), the interface shear resistance should be calculated from AASHTO LRFD (2020) with the surface factor values of CIP on NWC (intentionally roughed to 0.25 in.). TxDOT (2023a) identifies minimum haunch heights of 0.5 in. and 2 in. at mid-span and center of bearing, respectively. This minimum requirement is to allow for bedding strips. The maximum haunch height allowed without reinforcing is 3.5 in.

TxDOT (2022) provides different detailing practices for PSC girders with CIP concrete versus those with PCP decks, as shown in Figures 2.2.2.1 and 2.2.2.2, respectively. The typical bar size to be used for both Bars U and Bars UP is #4. Another detailing practice specified by TxDOT (2019b) when PCPs are used is called a "special grading detail" (SGD) and is shown in Figure 2.2.2.3. The SGD allows engineers to increase the height of the haunch region by including longitudinal reinforcement that engages an inverted bar U extending into the slab. SGDs can be modified to include the top mat of reinforcement as shown in Figure 2.2.2.4. The remaining depth of haunches can be reinforced with Bars U that are used for CIP concrete decks.

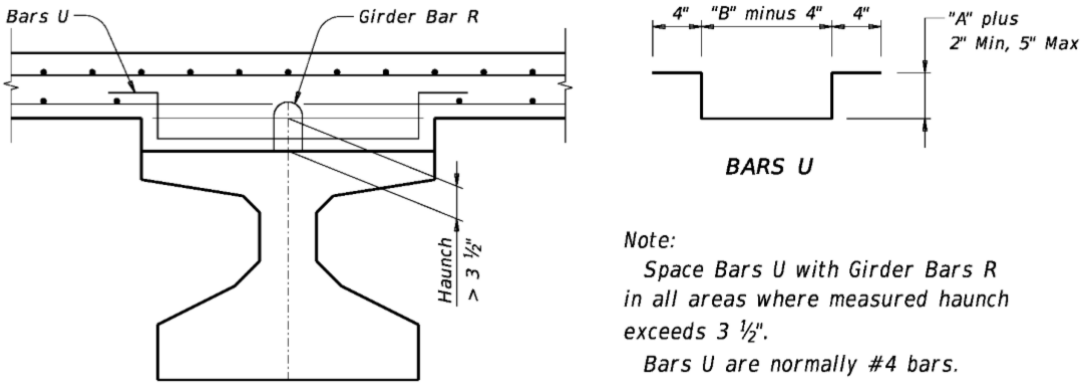

Figure 2.2.2.1 Detailing Practices for PSC Girders with CIP Decks (TxDOT 2022)

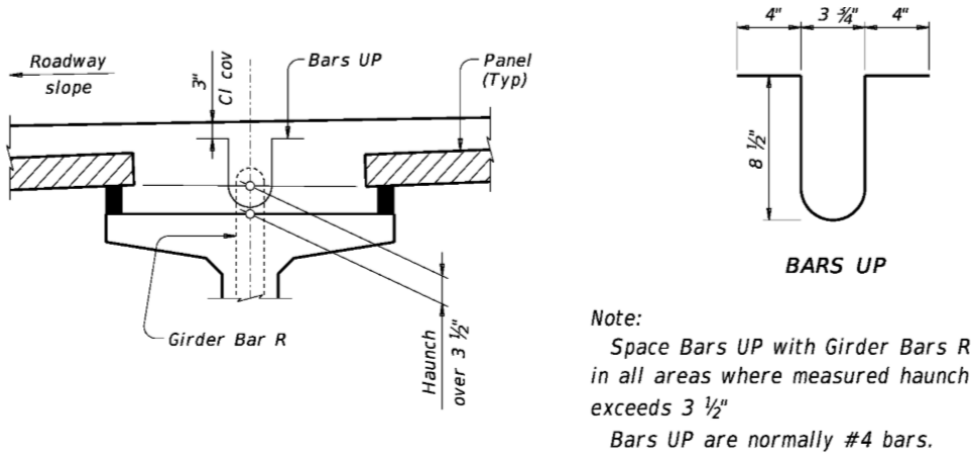

Figure 2.2.2.2 Detailing Practices for PSC Girders with PCPs (TxDOT 2022)

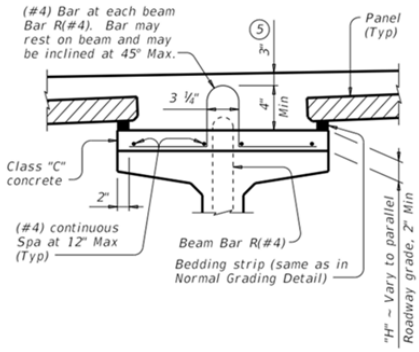

Figure 2.2.2.3 PSC Girders with PCP and SGD (TxDOT 2019b)

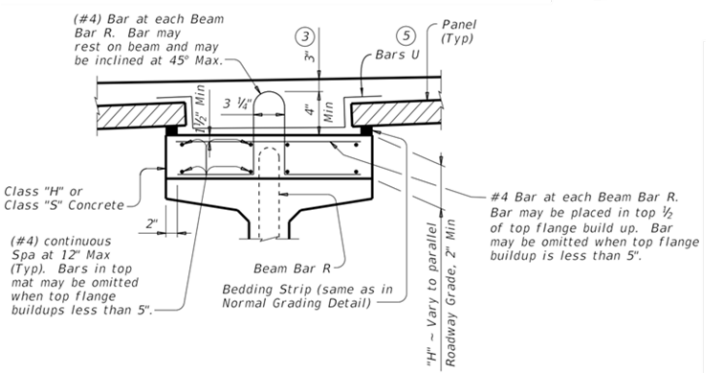

Figure 2.2.2.4 Modified SGD with Bars U (TxDOT 2016)

2.2.3. Past Literature Review for Interface Shear Resistance

The testing methods used to analyze shear behavior, shear-connector type, and other relevant parameters are outlined in this section. This information is based on information available in the published research literature.

2.2.3.1. Specimen Type

Test specimens focused on understanding the behavior of composite PSC girders are often designed using a different approach than steel girder specimens. While it is relatively simple to replicate the welding of headed shear studs to the top flange of a steel girder specimen, past testing to understand composite PSC girder behavior has not typically tried to capture the prestress of the girders. Emphasis is placed on replicating the longitudinal shear transfer mechanism, as shown in Figure 2.2.3.1. These specimens, referred to as push-off or L-shaped specimens, can be loaded either vertically or horizontally. One part of the specimen represents the PSC girder and the other represents a CIP or precast slab. Normally, researchers embed the

shear connector in the bottom part, representing the girder. The connector extends into the top part, representing the slab, which permits the development of composite action between the two parts. This design is convenient for simulating the bond and friction between girders and slabs that may contribute to non-negligible shear capacity in the push-off tests. To reduce the effects of localized stresses in the slab, researchers have included grouted shear pockets that confine the reinforcement in the slab (Noel et al. 2016). Researchers have also included grouted haunches or bedding layers between the two parts; failure appears to occur commonly in these layers (Scholz et al. 2007 and Shim et al. 2004) (Figure 2.2.3.2).

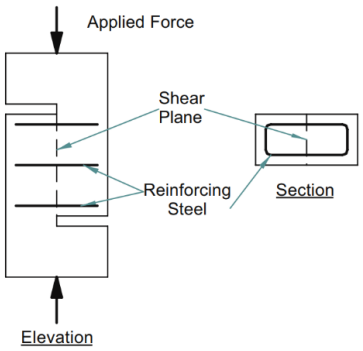

Figure 2.2.3.1 L-Shape Specimens or Push-off Specimens (Menkulasi and Roberts-Wollmann 2005)

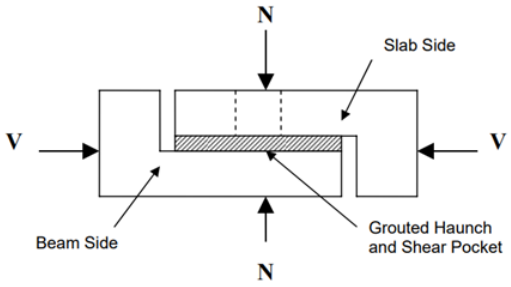

Figure 2.2.3.2 Push-off Specimen with Grouted Haunch (Scholz et al. 2007)

Roskos et al. (2018) tested the shear connection using a different type of specimen, where a 3-in.-thick concrete layer was cast on a steel plate welded with studs and bars R to simulate the PSC girder flange (Figures 2.2.3.3 and 2.2.3.4). The shear studs at the interface between the steel and simulated girders prevent relative slip between the steel flange and the PSC concrete layer, such that the layer of concrete behaves like the top flange of a PSC girder, based on work done by Roskos et al (2018). The studs themselves are not intended to supply the main composite resistance of the system but can fail before the reinforcement at the PSC-haunch interface if the PSC girder fails instead of the composite interface. This type of specimen could capture the bond between the two concrete components while utilizing the same test setup they developed for steel girder specimens (Roskos et al. 2018). A similar approach was used for the test specimens in the current project and is described further in Chapter 4.

Figure 2.2.3.3 Simulation of PSC Girder Flange before Casting (Roskos et al. 2018)

Figure 2.2.3.4 Simulation of PSC Girder Flange after Casting (Roskos et al. 2018)

2.2.3.2. Shear Connectors

To obtain effective composite behavior in PSC girder bridges, a sufficient bond must be provided to connect the girder and the slab so that the transfer of the longitudinal shear from one component to the other will be achieved. TxDOT guidelines (TxDOT 2017) require the use of bars R as shear connectors in PSC girders to provide composite action (Figure 2.2.3.5). With the presence of a tall haunch (≥3.5 in.), the TxDOT guidelines (TxDOT 2022) require haunches to be reinforced with Bars U or Bars UP (mentioned in Section 2.2.2.4). As per Roskos et al. (2018), while the use of bars R and Bars UP commonly occurs in bridge construction, this reinforcement style has not been widely used in experimental research. Most of the past literature focuses on the behavior of headed shear stud connectors embedded in grouted pockets for PSC girder specimens (Chung et al. 2010; Issa et al. 2006; Noel et al. 2016) (Figure 2.2.3.6). The investigation in this project considers bars R and Bars UP to replicate the common bridge design procedure, however, the literature is reviewed for other types of connectors as well.

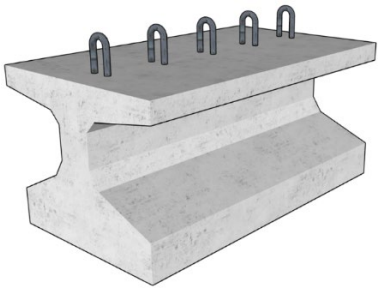

Figure 2.2.3.5 PSC Girder with Bars R

Figure 2.2.3.6 Headed Stud Reinforcement (Noel et al. 2016)

2.2.3.3. Type of Deck

As mentioned in Chapter 1, Task 4 includes testing PSC girders with CIP and PCP decks. The behavior of both types of specimens is different because the number of shear planes present in the former is one whereas the latter has at least two shear planes (three in case of SGD).

Hanson (1960) studied the composite action between PSC girders and CIP slabs. Push-off tests were performed with stirrups as shear reinforcement that extended 4 in. into the slab (Figure 2.2.3.7). The effect of different types of surface bonds (unbonded, smooth, rough) and shear lengths were explored. Bonded specimens developed high shearing stress at a low slip when compared with unbonded specimens that required considerable slip for shear stresses to develop. Shear length varied between 6 in. and 12 in. Based on the average shear stress results obtained for different shear lengths, Hanson concluded that push-off tests will give higher average stress for relatively shorter shear lengths. The failure is progressive from the load application point to the free end. The shear capacity obtained from push-off tests matched well with the girder test also performed by the author. From the load-slip curves, Hanson (1960) provided a critical slip value of 0.005 in., after which composite action ceases.

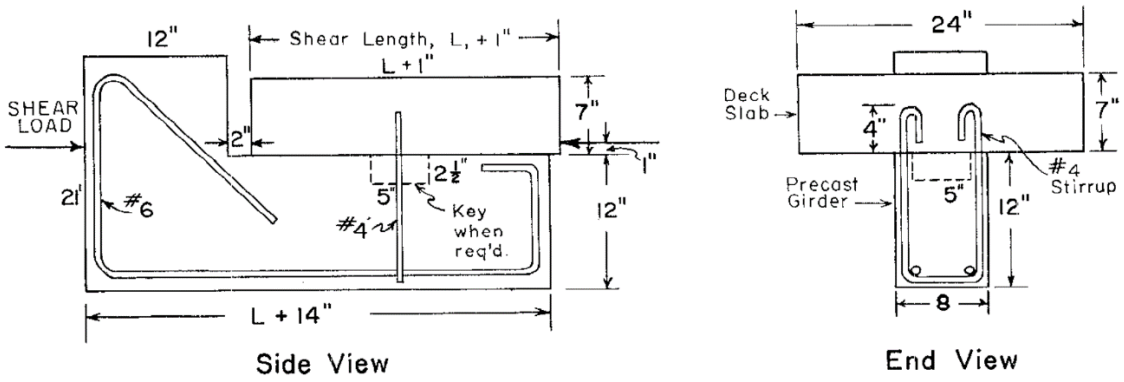

Figure 2.2.3.7 Push-off Test with Stirrups (Hanson 1960)

Waweru (2015) conducted push-off and full-scale beam tests on PSC girders with CIP decks. The shear connector embedment depth varied between 2 in. and 4 in. The push-off specimens with 2-in. embedment depth failed by bar pull-out (Figure 2.2.3.8). The specimens with 4-in. embedment depth saw yielding of bars but not at the peak strength. The author observed that the major contribution for peak strength is from cohesion/aggregate interlock and concrete friction. The relative slip between the girder and deck is negligible at this point. The reinforcement engages in shear transfer only after a small slip/separation occurs. This observation was made from both push-off and full-scale beam tests. Based on the results, the author suggested that the AASHTO LRFD (2020) shear-friction equation could over-estimate the effects of dowel action by assuming yielding of reinforcement at the peak strength.

Figure 2.2.3.8 Bar Pull-out Failure in Push-off Specimen (Waweru 2015)

Trejo and Kim (2011) performed push-off tests on CIP deck specimens with threaded rods as the shear connectors. They observed that for roughened girder surfaces, the cohesion between the girder and haunch provides higher strength than the dowel action of the connector. The sustained load after the drop from the peak load, however, was mainly due to the connector dowel action.

Scholz et al. (2007) performed push-off tests to investigate the shear behavior between full-depth PCPs and a PSC beam with a 1.5-in. grouted haunch. The specimen was loaded at the centerline of the haunch, and a normal force representing dead load on site was also applied. Their results showed that the slab-haunch interface is weaker than the beam-haunch interface due to the trapped air at the interface as shown in Figure 2.2.3.9. Due to the casting orientation shown in the figure, any surface treatment on the PCP did not increase the interface strength. The specimen's casting orientation should therefore align with the procedure on site. Based on their results, the authors recommended using the AASHTO LRFD (2020) interface shear design equation with a smooth interface (c =0.1 ksi, μ =0.6) for a PSC girder with PCPs.

Scholz et al. (2007) also remarked that the failure mode of PSC girder specimens relies heavily upon the amount of reinforcement at the shearing interface. When the shear connections provide less shear resistance than available from contact shear resistance, the specimens experience a sharp drop in capacity after debonding, followed by constant capacity. If the connection resistance approximately equals the contact shear resistance, Scholz et al. (2007) observed only a small drop in specimen resistance following debonding at the contact interface. Finally, if mechanical resistance exceeds the contact resistance, then the shear connectors continue to carry the load, and capacity continues to increase. Figure 2.2.3.10 illustrates the phenomenon outlined by Scholz et al. (2007).

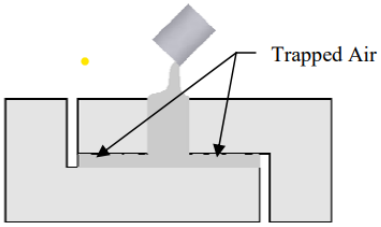

Figure 2.2.3.9 Trapped Air at Slab-Haunch Interface (Scholz et al.2007)

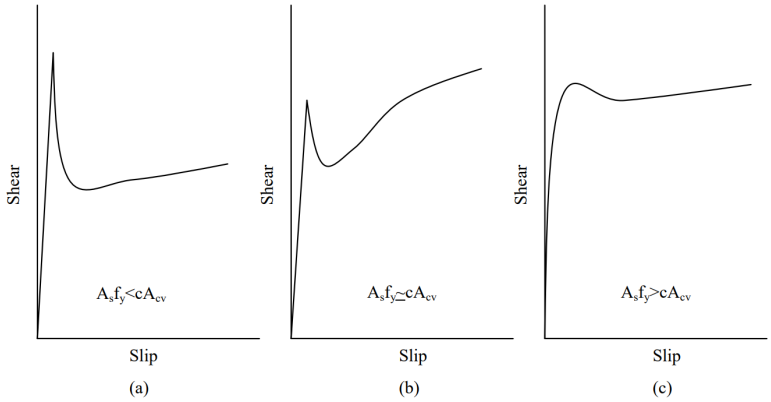

Figure 2.2.3.10 Load-slip Behavior of PSC Girder Push-off Specimens (Scholz et al. 2007)

Menkulaski (2002) performed push-off tests on PSC girders with full-depth PCPs. The author tested specimens with a haunch depth ranging from 1 in. to 3 in. and observed the haunch did not affect the results significantly. An embedment depth of 5 in. into the deck was suggested, however, to avoid concrete cone break-out failure (Figure 2.2.3.11). This failure did not affect the peak strength since it occurs post peak, but it is a brittle failure mode that occurs suddenly. The peak strength increased with an increase in the shear reinforcement area. Reinforcement yielding occurred only after the debonding failure, at which point the cohesion was already lost.

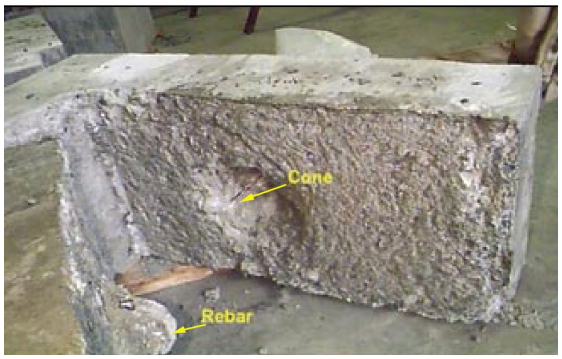

Figure 2.2.3.11 Concrete Cone Break-out Failure (Menkulasi 2002)

2.2.3.4. Other Critical Parameters from Past Experimental Studies

Some other critical parameters, such as the shear plane characteristics (cracked or uncracked), direct stresses (applied force acting parallel or transverse to shear plane), and effect of moment across the shear plane, are also investigated by other researchers and included in this section. Additional findings about the effects of concrete strength and reinforcement are also summarized.

Hofbeck et al. (1969) investigated specimens with initially cracked and uncracked conditions. They observed that the ultimate shear capacity for initially cracked specimens is less than uncracked specimens at low clamping stresses (<1000 ksi). At higher clamping stresses, the capacities calculated for both cracked and uncracked specimens were approximately the same. They also noted that the concrete strength does not affect the initially cracked specimen capacity up to a clamping stress of 600 psi. Another conclusion made was that dowel action does not contribute significantly to the capacity for initially uncracked specimens but has a significant effect on initially cracked specimens. Hofbeck et al. (1969) also noted that with an increase in clamping stress, the ultimate shear capacity for both initially cracked and uncracked specimens increased.

From their push-off test results, Mattock and Hawkins (1972) had similar observations with Hofbeck et al. (1969). Additionally, Mattock and Hawkins (1972) observed that direct tension stresses parallel to the shear plane reduces the interface shear resistance for uncracked specimens but has no effect on cracked specimens. The compressive transverse stresses were found additive to clamping stresses.

Mattock, Johal, and Chow (1975) performed push-off tests to identify the effect of moment acting across the shear plane on the shear transfer strength of cracked specimens. The eccentricity between the loading point and shear plane varied between 0 in. and 7.5 in. Based on their results, the shear transfer strength was not reduced by the additional applied moment at the crack. The authors suggested that shear transfer reinforcement be concentrated in the flexural tension zone when both shear and moment are applied. If both shear and tension are present, the total amount of reinforcement can be calculated by simply adding the reinforcement required to resist both forces.

Kent et al. (2012) performed push-off tests with high strength steel as the shear connector. Based on the results, the authors suggested that the reinforcement ratio affects the shear-friction capacity, but the grade of steel does not. The ultimate shear capacity was controlled by concrete behavior rather than steel yielding. They suggested that due to the complex nature shear friction, the parameters affecting the strength cannot be separated.

Chung et al. (2010) and Noel et al. (2016) performed push-off tests on specimens with shear stud connectors. Chung et al. (2010) suggests that the geometry of the shear connectors, the strength of concrete, and the roughness of concrete greatly affect composite behavior. As per Noel et al. (2016), the rebar detailing around the bearing zone of the shear studs may also affect the performance of the shear connectors. The concrete surrounding the stud is more vulnerable to crushing failure if there is insufficient confinement from reinforcing steel. This confinement may prevent concrete crushing failure, which is a failure mode that has a lower capacity than stud yielding.

2.2.3.5. Failure Mode

Most of these previous research studies reveal that PSC girder push-off test specimens commonly experience failure at the contact interface between the slab and girder, followed by yielding of shear reinforcement. Debonding of the contact interface between the slab and girder describes the first component of specimen failure. With this failure mode, shear stresses exceed the resistance due to friction, cohesion, and aggregate interlock. Figure 2.2.3.12 depicts the failure plane of a push-off test specimen.

After specimens lose shear resistance due to surface contact mechanisms, only the mechanical shear connections remain to resist shear forces. If the shear forces exceed the resistance provided by the mechanical connections, yielding, and shearing of these connections occurs, along with higher slips. In specimens where grouted shear pockets confine the shear connections, local concrete crushing failures are less likely. In specimens without this confinement, Chung et al. (2010) observed local concrete crushing adjacent to the mechanical connections before shear connection failure.

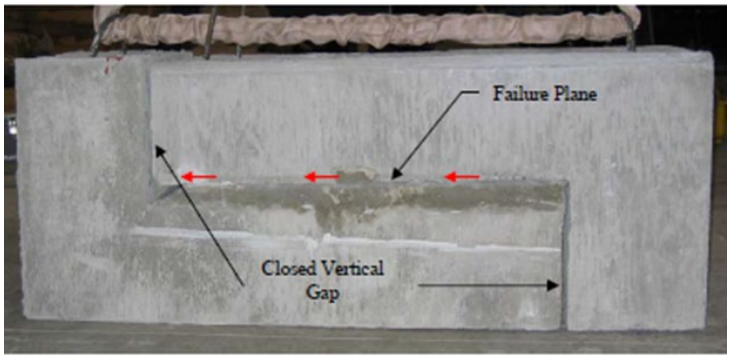

Figure 2.2.3.12 Failure Plane of L-Shape Specimens (Scholz et al. 2007)

Mattock and Hawkins (1972) provided a failure hypothesis for shear transfer strength in uncracked and cracked specimens. External loads on a specimen can cause shear stress along the shear plane and direct stress parallel and transverse to the shear plane. Under increasing load, diagonal tension cracks form as shown in Figure 2.2.3.13.a. Diagonal concrete struts develop in between parallel tension cracks. As shown in Figure 2.2.3.13.b, a truss action occurs where the applied shear is resisted by compression and shear in the struts. Overall specimen failure occurs when the diagonal concrete struts between cracks fail under combined axial and shear force. For cracked specimens, the transfer strength is provided by frictional resistance to sliding surfaces and dowel action.

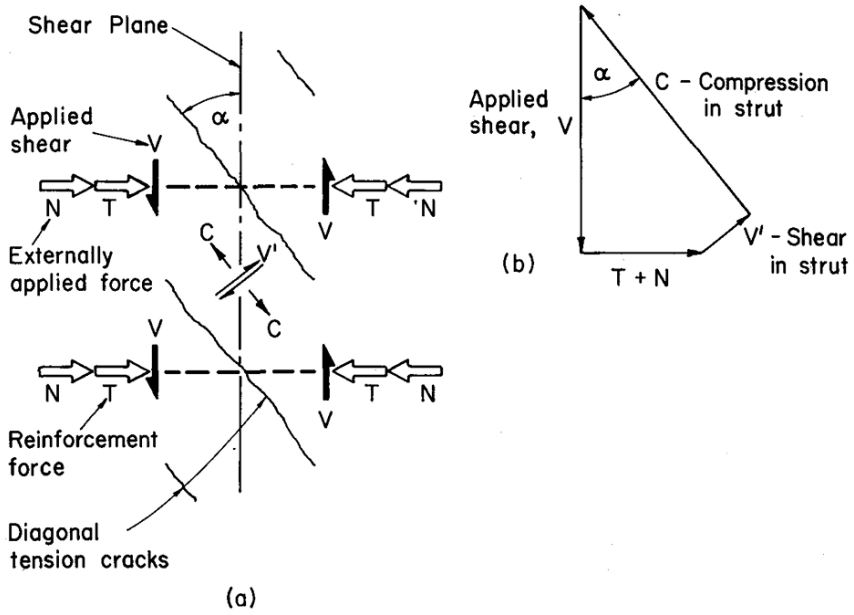

Figure 2.2.3.13 Failure Hypothesis for Shear Transfer Strength in Uncracked Specimens (Mattock and Hawkins 1972)

2.2.4. Concluding Remarks

The observations from past studies indicate that the behavior of the contact surface between the girder flange and slab requires scrutiny. Contact properties such as friction, cohesion, and aggregate interlocking will affect the strength, ductility, and failure modes of PSC girder push-out test specimens with tall haunches. Additionally, shear reinforcement detailing, concrete strength, clamping force, haunch depth, embedment depth, and initial cracked or uncracked conditions can affect the interface shear capacity as well. Most of these parameters have been studied in the past except for haunch depths more than 3 in. As mentioned in Chapter 1, the study described in this final report considers haunch depths up to 12 in. Results from experimental testing and computational simulation are presented in Chapter 4 and 5, respectively. The next section summarizes relevant research literature addressing the computational modeling of push-out tests.

2.3. FE Analysis (FEA)

Several researchers have used detailed finite element (FE) models to simulate push-out tests. Several FE modeling methods based on different assumptions are introduced in this section. Model accuracy is demonstrated through comparisons to measured push-out test data.

Guezouli and Lachal (2012) proposed a 2-dimensional (2D) nonlinear finite element model to investigate shear connection behavior between the concrete slab and steel section in a two-sided push-out test. In addition to nonlinear material models and four-node planar elements, frictional contact elements were considered in the FE model using what the researchers termed the

"Layer/Zone equivalence methodology." The results of the FE model were compared with the results of the push-out experiments performed by the authors.

To implement the layer equivalence methodology, Guezouli and Lachal (2012) first divided push-out specimens into different parts in the FE model: A) steel section web, B) steel section flange, C) prefabricated slabs, D) concrete fill material, and E) studs, as shown in Figure 2.2.3.1. The test setup was then divided into different zones or layers in the X-Z plane each time the part varied. This division is shown in Figure 2.2.3.2. An equivalent material representing each zone had a thickness of 1 mm (0.04 in.). This equivalent material considered the actual depth and modulus of each part in the Y direction. For example, normal and fill concrete in L4 was homogenized to have the same properties as the fill concrete. Similarly, normal concrete, fill concrete and steel studs were homogenized to steel material in L5. Reinforcing steel material was not considered as a different part, but a correction factor was applied to the modulus of the equivalent material.

Guezouli and Lachal (2012) used an elastic-plastic material model for steel and a Drucker-Prager model for concrete. Taking advantage of symmetry, only half of the specimen was modeled in the finite element software. The concrete base was vertically restrained by a roller support, and vertical displacement was prescribed at the top of the steel section. The contact formulation was based on the kinematic method. Load-slip curves were obtained from the FE model, where the load was the reaction at the concrete base and slip was the applied vertical displacement. Results from the FE model were compared with the push-out test results, which allowed for the calibration of the friction coefficients and horizontal boundary conditions in the FE model. The 2D FE modeling method developed by Guezouli and Lachal (2012) was able to achieve both accuracy and time efficiency, but extra calculations were required for the "Layer/Zone equivalence methodology."

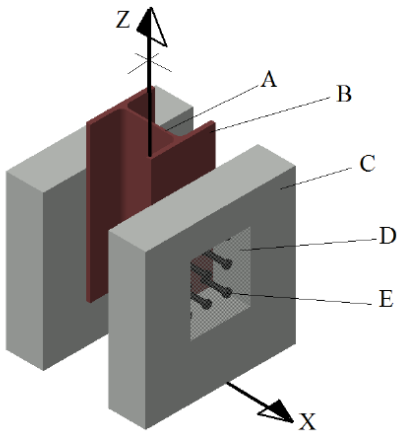

Figure 2.3.1 Push-out Test Specimen with Different Parts (Guezouli and Lachal 2012)

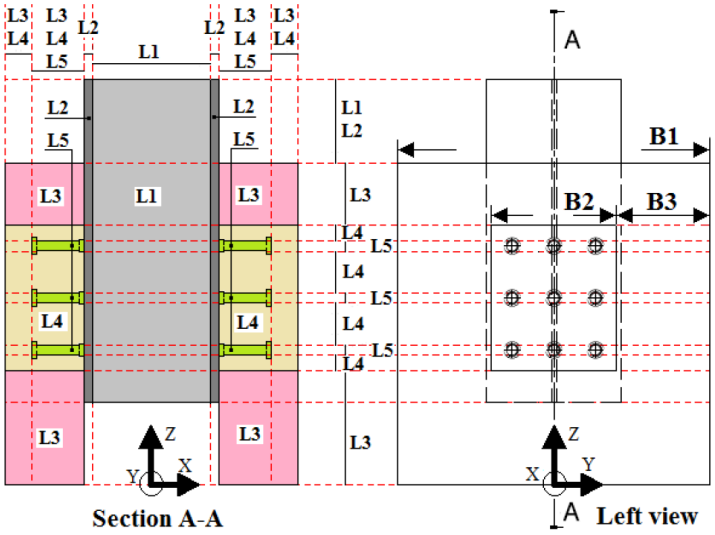

Figure 2.3.2 "Layer/Zone Equivalence Details" (Guezouli and Lachal 2012)

Kim et al. (2001) performed push-out tests to identify the behavior of shear connectors within composite slabs and prepared 2D linear, 2D nonlinear, and 3-dimensional (3D) linear finite element models using the LUSAS FE (2000) software. The 2D model is shown in Figure 2.2.3.3. The profiled sheeting was modeled using bar elements, and all other components were modeled as plane-stress elements. Considering symmetry, only half of the specimen was modeled. The researchers used a reduced stiffness for the bottom elements of the studs to account for possible stud yielding before failure. Meshing was more refined in the vicinity of the studs compared to other parts of the model. Nonlinear material properties were employed in this study and included tension softening for the concrete. A comparison of the computed and measured results is shown in Figure 2.2.3.4. Due to several assumptions made during modeling the specimen, result discrepancies are noticeable in the initial stiffness and strain hardening stages. The initial stiffness in the 3D linear model compared better with the test results than the 2D nonlinear model. An important observation made was that the 2D nonlinear model remained elastic until failure occurred.

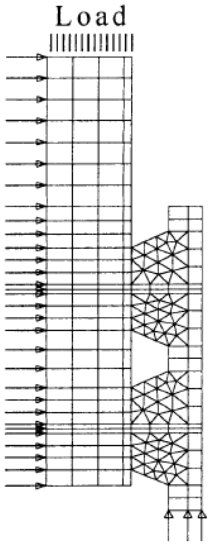

Figure 2.3.3 2D FE Model of Push-Out Test (Kim et al. 2009)

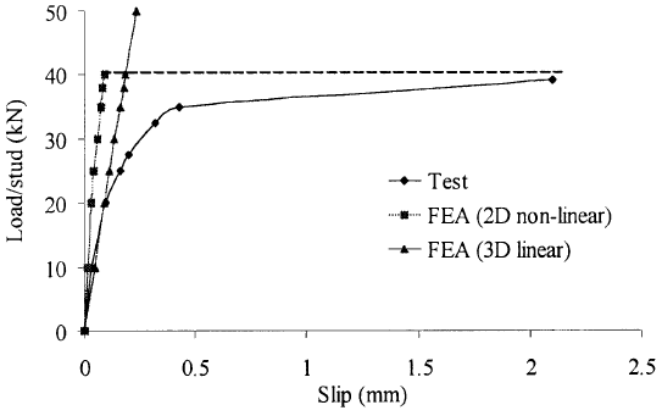

Figure 2.3.4 Test Results Compared with FE Models (Kim et al. 2001)

Lam and El-Lobody (2005) developed a 3D FE model in ABAQUS Version 6.2 for a parametric study that investigated the influence of concrete strength and headed shear stud diameter in two-sided push-out tests. The FE models included one headed shear stud attached to each flange of the steel section, which assumed the load was transferred equally to each individual shear stud. The FE models, as well as the push-out test specimens used to verify the predicted results, were designed based on Eurocode 4 (BSI 1994). A W10×49 was used for the steel section. The slab was 619-mm (24.4-in.) wide, 469-mm (18.5-in.) tall, and 150-mm (6-in.) thick. A recess was used at the bottom of the concrete slabs. One quadrant of the specimen geometry was modeled due to symmetry about two axes. This approach was used to minimize the computational run-time needed to analyze each model.

Brick elements (i.e., 3D solids) were used to mesh the geometry (Figure 2.2.3.5). Apart from the symmetric boundary conditions on Surfaces 1 and 3, vertical restraint (in the z-direction) was applied on Surface 2. Due to the assumption that the concrete could be properly confined by the reinforcement, both steel and concrete in the analyses were modeled as an elastic-perfectly-plastic material. A modified RIKS algorithm, which calculates the load magnitude and displacement simultaneously using an arc-length solution procedure, was used to compute the response. Comparisons between the results of the push-out tests and the FE models demonstrated that this modeling method was able to accurately predict the ultimate shear capacity of the specimens if the concrete strength was less than 7 ksi. The mode of failure was identified by investigating the stress distribution for each incremental step. Figure 2.2.3.6 shows the stress distribution from the FE Model for a push-out specimen with combined stud yielding and concrete failure. Such distributions were studied for each specimen and compared with the failure observed during the test. The comparison showed the validity of the FE model. Relative

to code-predicted strengths, the FE analysis results matched the predicted shear capacity of Eurocode 4 (BSI 1994) but were more conservative than those predicted using BSI (1990) and AISC (1999).

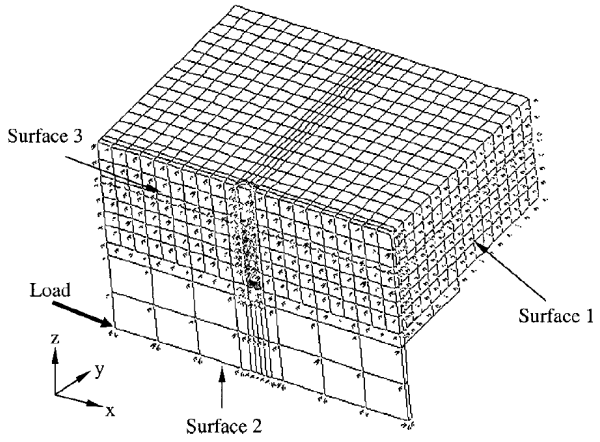

Figure 2.3.5 FE Model of a Quadrant of Push-out Test Specimen (Lam and El-Lobody 2005)

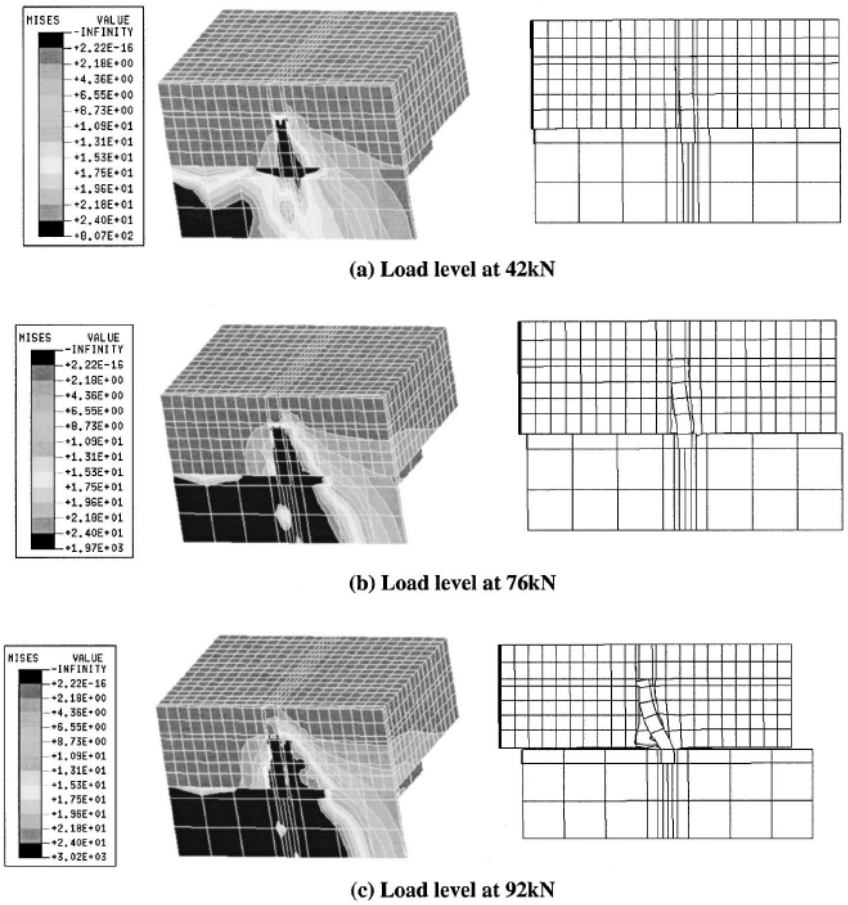

Figure 2.3.6 Stress Distribution from FE Model (Lam and El-Lobody 2005)

Nguyen and Kim (2009) developed a refined 3D FE modeling method in ABAQUS (2006) that accounted for material and geometric nonlinearity to predict the response of push-out tests with large-diameter shear studs. The researchers considered studs with a diameter larger than 22 mm (0.9 in.). Their model included the concrete slab, steel section, slab reinforcement, headed shear studs, cohesive layer, and a rigid base. A trilinear material model, which consisted of an elastic stage, strain hardening stage, and yield plateau, was assigned to all steel parts. The Concrete Damaged Plasticity material model was used for the concrete. This constitutive model was developed primarily to simulate concrete with reinforcement and other quasi-brittle materials using isotropic damage plasticity (ABAQUS 2013). Although this model requires more computational time and resources than other simplified models (e.g., elastic-perfectly-plastic), it can capture concrete crushing and the degradation stage of the load-slip curves (Figure 2.2.3.7). A tie constraint was applied between the stud and concrete to avoid any relative slip. Only the lower half of the headed shear studs were coupled with the surrounding concrete because separation between the concrete and the top surface of the headed shear studs occurred quickly after loading. Embedded constraints were applied to the reinforcing steel in the concrete. Interaction between the loaded steel section and the concrete slabs was due to a cohesive layer with a 0.05-mm (0.002-in.) thickness. The concrete base had a friction coefficient of 0.25 based on past studies. A dynamic-explicit analysis was used to conduct the analyses, and the vertical displacement increased linearly as the analysis progressed. A dynamic-explicit analysis is often used for problems involving impact, progressive damage, material failure, and other similar problems (Nguyen and Kim 2009). The authors suggested that despite being a dynamic analysis method, dynamic-explicit analyses can also be employed for quasi-static push-out tests due to the progressive sequence of damage that occurs prior to failure. The FE model results compared well with the experimental results. The authors also compared the FE model results with AASHTO LRFD (2004) and CEN (2005a). Relative to the test results, AASHTO LRFD (2004) gave higher strength values, while CEN (2005a) gave lower strength values.

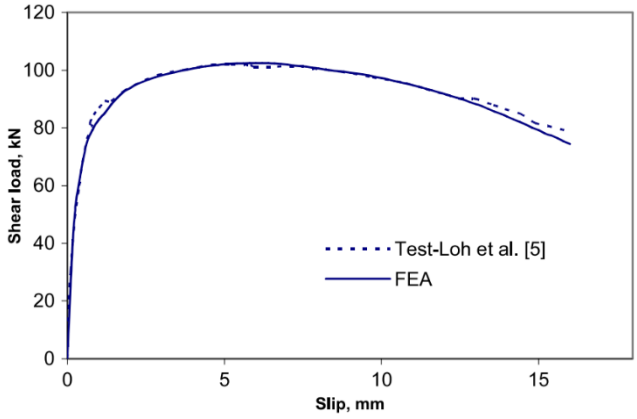

Figure 2.3.7 Comparison of Results between the FE Model and Push-out Test (Nguyen and Kim 2009)

2.3.1. Concluding Remarks

Based on the references to four different FE modeling methods introduced in Section 2.3, several recommendations can be provided for the modeling to predict the behavior of push-out specimens. A 3D FE model is preferable to a 2D model as the latter may introduce discrepancies in initial stiffness and in the strain-hardening stage of the load-slip curve. For the concrete material, several parameters in the Concrete Damaged Plasticity model require calibration after push-out test results are obtained. The elastic-perfectly-plastic model is comparatively easier to define than other models and can reflect the mechanical properties of both steel and reinforced concrete to some extent. More sophisticated material models, such as the Concrete Damaged Plasticity and Drucker-Prager models, are also considered by the researchers for comparison. Due to symmetry about two axes, it is preferred to model only one quadrant of the push-out specimens to reduce the total number of degrees of freedom and computational run-time. Tie constraints can be used at the interface between the shear studs and the surrounding concrete. The concrete and steel parts of the push-out test specimen can be meshed using hexahedral brick elements to achieve acceptable accuracy. Some other aspects of the FE modeling need to be determined by comparing the results of experiments and simulations. For example, several different boundary conditions have been used in previous analyses of push-out tests, but their effect on the computed results has not been clearly documented. Chapter 5 provides the details of the FE models developed for steel and PSC girder specimens

2.4. Conclusion

The literature review presented in this Chapter provides detailed information concerning how push-out and push-off tests are conducted. The behavior of both zero-haunch and haunched specimens was described. In summary, the behavior of a traditional push-out test for steel girder specimens can be affected by the following parameters: stud tensile strength, stud diameter, stud height, stud layout, concrete compressive strength, concrete casting method, transverse reinforcement detailing, longitudinal reinforcement detailing, slab width, slab height, and boundary conditions. The behavior of PSC girder specimens can be affected by the contact surface properties, area, shear reinforcement detailing, concrete strength, clamping force and loading surface. The manner in which some of these parameters affect behavior and overall capacity is well documented in the research literature and does not require further investigation. However, several other parameters, particularly those related to haunch geometry and reinforcement detailing, are critical to TxDOT Project 0-7016. These parameters are given primary consideration in the specimen designs of the steel and concrete girder tests conducted as part of the experimental research for this project. The steel girder specimens are described in Chapter 3, and the PSC girder tests are described in Chapter 4.

Chapter 3. Ultimate Shear Capacity Tests of Haunches on Steel Girder Bridges

In Chapter 3, an overview of the push-out tests for the steel girder specimens is provided, including the specimen design, the push-out test setup, the testing procedure, and the test results. Conclusions based on the test results are provided at the end of the chapter, and preliminary design recommendations are also given.

3.1. Specimen Design

A total of 34 specimens were fabricated and tested to investigate the behavior of the shear connector and various reinforcement details with tall haunches. A typical push-out test specimen is shown in Figure 3.1.1. Several parameters mentioned in Chapter 2 can impact on behavior in the push-out tests, including concrete and shear stud material properties, concrete slab and haunch dimensions, and haunch detailing strategies. The test specimen parameters were therefore selected based on current design specifications, common TxDOT practices, past literature, and preliminary FE analysis results. For instance, stud and steel section geometric and material properties were selected based on AASHTO LRFD (2020), the TxDOT standard drawing SGMD (2019a), and typical TxDOT practices. The concrete slab width and height were based on past literature and preliminary FE analysis results.

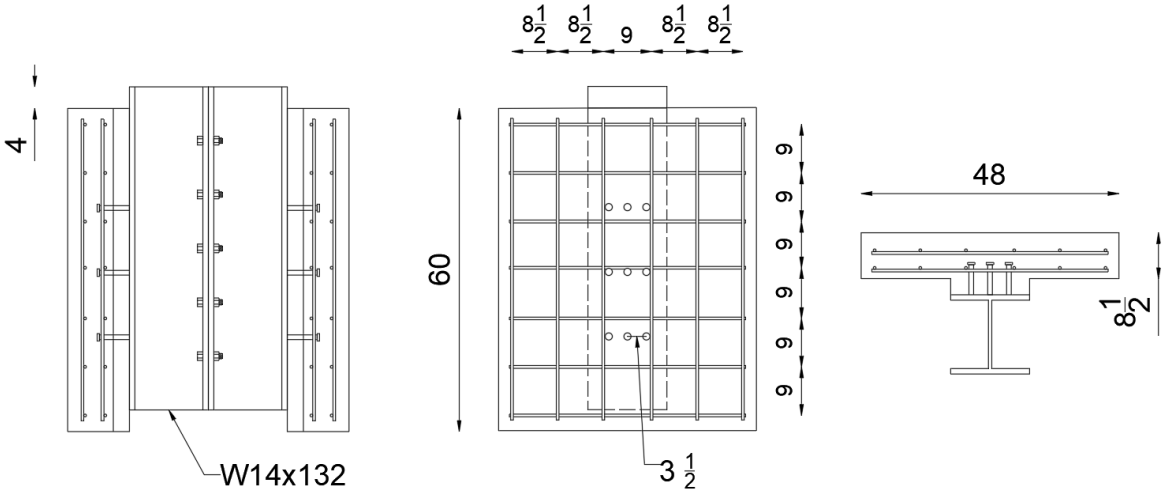

Unit: inch

Figure 3.1.1 Push-out Test Specimen Detailing

As shown in Figure 3.1.1, all steel girder push-out test specimens were designed in symmetric pairs, assembled, and tested simultaneously. This allowed the concrete in the specimens to be cast in the same position that would occur in slab construction. The simulated concrete deck was 60 in. tall, 48 in. wide, and 8.5 in. thick, which were determined by the preliminary FEA to

capture the expected stress state in real girders. The top and bottom rebar mats were consistent for all of the specimens, as illustrated in Figure 3.1.1. The top and bottom clear cover of the rebar mats was 2.5 in. and 1.25 in., respectively. The headed shear studs (7/8 in. dia.) were welded on one flange of a 6-foot long W14×132 section with different arrangements. On the other flange, bolt holes were pre-drilled to accommodate 1 in. diameter A490 bolts used for the connection between the two steel shapes when the specimen was paired with the counterpart. The haunch depth, the haunch reinforcement (not shown in Figure 3.1.1), and the stud arrangement varied among the specimens as outlined in Section 3.4. As per TxDOT guidelines, Class-S concrete (f'_c = 4 ksi) and #4 Grade 60 rebar were used to fabricate the specimens. Detailed sketches of each specimen are available in the Appendix Section A2.

3.2. Specimen Fabrication

A consistent set of guidelines and steps were followed in the fabrication of the steel girder push-out test specimens so as to obtain consistency in specimens. The fabrication consisted of the following steps:

1) A wire brush was used to remove loose mill scale, rust, and debris from the W14x132 steel section. A total of ten 1-1/16 in. bolt holes were then drilled in one of the flanges, as shown in Figure 3.2.1.

Figure 3.2.1 W14×132 Sections with Bolt Holes

2) The section was then flipped and headed shear studs were then welded on the other flange (shown in Figure 3.2.3) using an arc stud welding gun. Prior to stud welding to the specimens, a 90-degree bending test was performed to verify the welding procedures and quality, as shown in Figure 3.2.2.

Figure 3.2.2 Bending Test

Figure 3.2.3 Welded Shear Stud

3) The rebar cages were fabricated with strain gauges at locations where concrete cracking was most likely to occur in the haunch regions, as shown in Figure 3.2.4. The strain gauge wires were labeled and organized for easy identification and protection. The locations of the strain gauges were determined by the preliminary FEA and varied in different specimens. Further discussions about the rebar strain are provided in Section 3.8.

Figure 3.2.4 Rebar Cage with Strain Gauges

4) The steel sections were placed in the formwork. Sealant, as indicated in Figure 3.2.5, was applied to fill the gaps between the steel sections and the formwork. Formwork oil was also applied on the surfaces of the formwork to ease removal of the specimens. Lastly, the rebar cages were placed on top of the steel sections (shown in Figure 3.2.6). Spacer wheels were used to control the clear cover of the rebar cages.

Figure 3.2.5 Casting Preparation 1

Figure 3.2.6 Casting Preparation 2

5) As indicated in TxDOT Bridge Design Manual (2023b), Class S concrete with a compressive strength of 4 ksi was used for decks and haunches. Before each casting, slump testing (shown in Figure 3.2.7) was performed to verify the workability of the concrete. Concrete sampling was simultaneously conducted with casting (shown in Figure 3.2.9), as shown in Figure 3.2.8. For each batch of concrete, a total of 30 cylinders with a dimension of 4 in.× 8 in. were fabricated to measure the compressive strength on the 3rd, 7th, 14th, 21st, 28th, and the testing days. Material testing, including rebar, shear stud, and concrete, is dicussed in Section 3.8. After casting was completed, the concrete surfaces were finished by trowels, as shown in Figure 3.2.10.

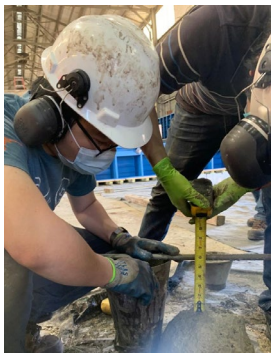

Figure 3.2.7 Slump Test

Figure 3.2.8 Concrete Sampling

Figure 3.2.9 Concrete Casting

Figure 3.2.10 Concrete Finishing

6) After the compressive strength of the concrete reached 3 ksi (design strength of the concrete anchors), the specimens were removed from the formwork and assembled in symmetric pairs for testing, as shown in Figure 3.2.11.

Figure 3.2.11 Assembled Specimen

3.3. Test Matrix

As stated previously, the haunch geometry, the haunch rebar detailing methods, and the stud arrangement were the variables of interest. To fully investigate the effects of these variables on the longitudinal shear capacity of steel girders with tall haunches, a total of 34 specimens were fabricated with various details. The test matrix is provided in Table 3.3.1. Detailed drawings of the specimens are provided in Appendix A2. In the table column with "stud arrangement", a designation N1 ×N2 indicates N1 stud locations with a total of N2 studs at each location. All of the specimens made use of 3 studs per location at 3 locations except Test 17 that had three locations with one stud at each location (3 x 1). All of the tests had a stud pitch of 12 in. except Test 10. Some of the other tests had special cases such as stacked studs or longer studs (8 in. versus 6 in. which was more common in the other tests). The column with the haunch detailing outlines special reinforcing that was included in Appendix A2. Tests with N/A indicate no special details were used for those specimens.

Considering the properties of concrete with a compressive strength of 4 ksi, the shear capacity contribution of each shear stud can be estimated using Equation 2.1.1.1 in Chapter 2 as following:

$$Q_{n,concrete} = 0.5A_{sc}\sqrt{f_c'E_c} = 0.5 \times 0.6in.^2 \times \sqrt{4ksi \times 3986ksi} = 37.9kips \quad \text{Equation 3.3.1}$$

$$Q_{n,stud} = A_{sc}F_u = 0.6in.^2 \times 60ksi = 36kips \quad \text{(controls)} \quad \text{Equation 3.3.2}$$

$$Q_n = \phi_{sc}Q_{n,stud} = 0.85 \times 36kips = 30.6kips \quad \text{Equation 3.3.3}$$

Table 3.3.1 Test Matrix of Steel Girder Specimen

Test #	Specimen #	Haunch Size (in.)	Stud Arrangement	Haunch Rebar Detailing
1	1, 2	9	3×3 double stacked	N/A
2	3, 4	9	3×3	U-bar
3	5, 6	9	3×3	Stirrups
4	7, 8	3	3×3	N/A
5	9, 10	0	3×3	N/A
6	11, 12	15	3×3 triple stacked	N/A
7	13, 14	15	3×3	U-bar
8	15, 16	9	3×3	N/A
9	17, 18	6	3×3 8-in. stud	N/A
10	19, 20	9	3×3 double stacked, 6-in. pitch	N/A
11	21, 22	12	3×3	U-bar
12	23, 24	12	3×3	U-bar (double spacing)
13	25, 26	12	3×3	U-bar (double spacing, alternative location)
14	27, 28	12	3×3	Stirrups
15	29, 30	15	3×3	Stirrups w/ unconfined longitudinal rebars
16	31, 32	15	3×3	Stirrups w/ confined longitudinal rebars
17	33, 34	15	3×1	Stirrups

The specimen pairs had 18 shear studs contributing to the effective shear resisting cross-sections except the pair of Specimens 33 and 34 used in Test 17 which had 6 shear studs. Therefore, the design capacity for Test 17 (the pair of Specimens 33 and 34) was 184 kips, and the other specimens had a design capacity of 552 kips.

3.4. Push-out Test Setup Design

The setup shown in Figure 3.4.1 was designed and fabricated to conduct the push-out tests. The setup accommodated specimens with a maximum haunch depth of 15 in. As shown in the figure,

the setup was capable of accommodating two different test specimens simultaneously. Each side of the testing frame included two actuators with a capacity of 550-kips. The applied load was measured by the load cells connected to the data acquisition system. A spreader beam was used to transfer the applied load to the outside flanges of the W14×132 sections to simulate direct shear between the top flange of the steel girder and the bottom of the concrete haunch (as shown in Figure 3.4.2). A 2 in. gap was provided between the haunch and loading platen of the setup to allow haunch shearing to occur without bearing against the reaction frame. Hydro-Stone gypsum cement, with a compressive strength of 10 ksi, was used to fill the gaps between the foundation plates and the concrete deck and promote a uniform distribution of stress to concrete. Detailed sketches of the members in the push-out test setup are included in Appendix A1.

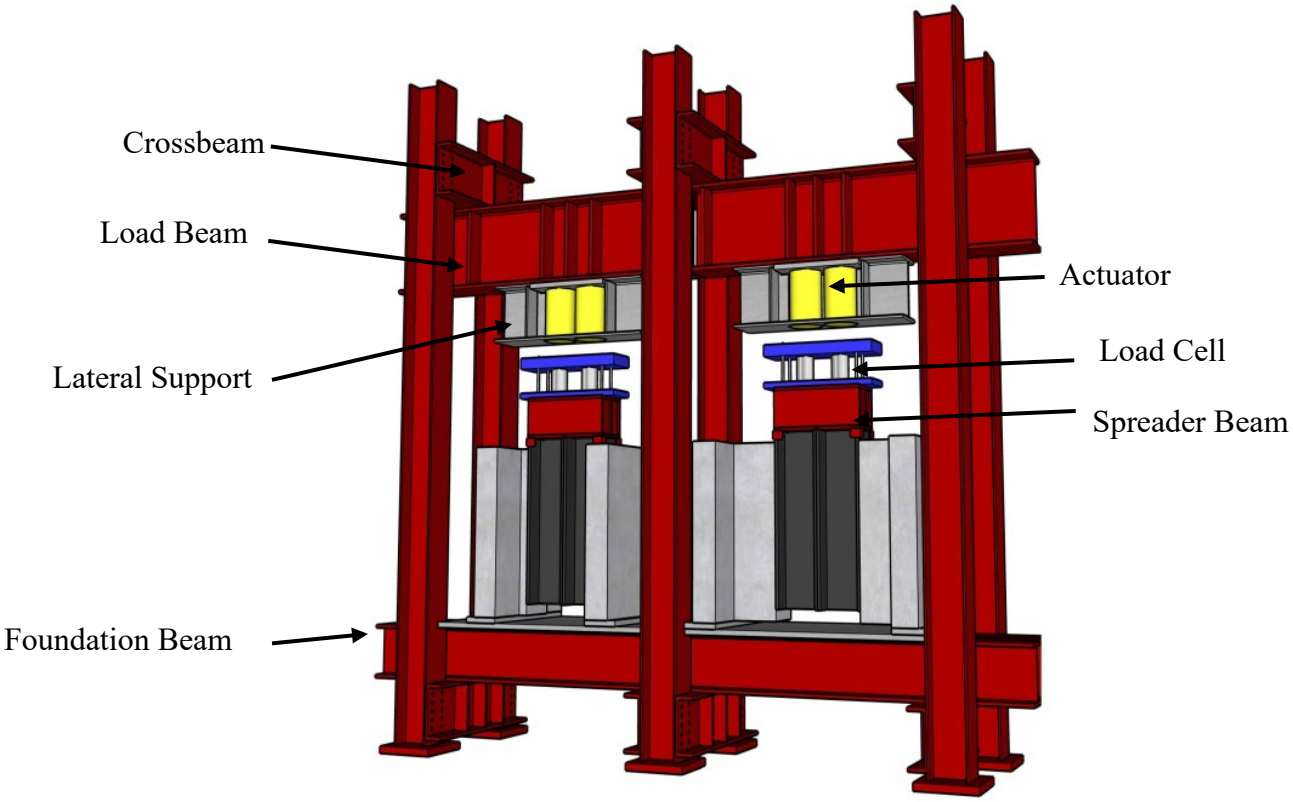

Figure 3.4.1 Push-out Test Setup Illustration

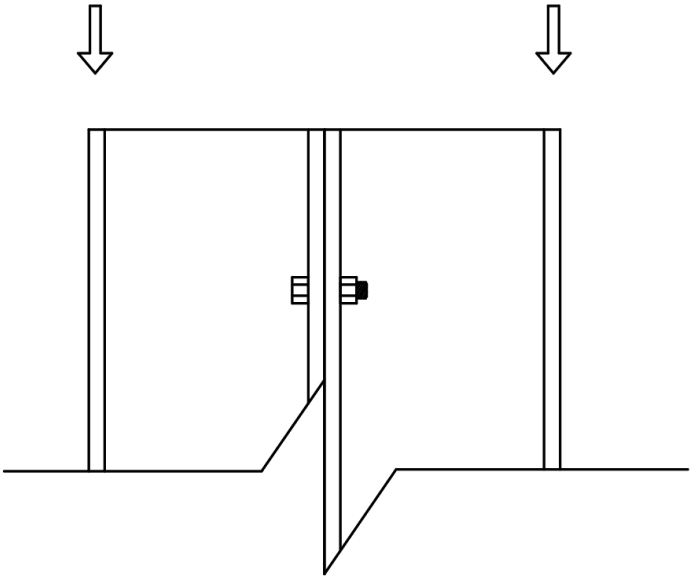

Figure 3.4.2 Load Transferred by the Spreader Beam

3.5. Push-out Test Instrumentation

The load-slip curve was an important indicator of the behavior from the push-out test. The applied load was captured by the load cells, as mentioned in the previous section. The slip between the steel sections and concrete was measured by linear potentiometers (LP) at the concrete-steel interface, as shown in Figure 3.5.1. The LPs were installed at the side surfaces of the steel section flanges and measured the relative displacement of wood blocks bonded to the concrete slab. During the push-out tests, the steel sections were slowly pushed downward causing shear deformation between the concrete haunch and steel flange. The LPs measured the relative slip at 3 locations spaced along each simulated concrete deck. There were a total of 12 LPs used in a push-out test, 6 on each specimen (6 on each side – front and back). The positions of the LPs relative to the shear studs are illustrated in Figure 3.5.2. Multiple LPs along the height of the specimens were able to show the slip distribution in the longitudinal direction.

As shown in Figure 3.2.4, strain gauges were installed on the rebar cages. Figure 3.5.3 illustrates a strain gauge plan for the specimen with a 9 in. haunch and the U-bars specimen. This is just one example with other specimens having similar gauge layouts. The strain gauges were attached to the haunch reinforcement in the vicinity of the shear studs. These locations were expected to have large stress demand as well as significant strains.

Strain gauges were also attached on the webs with a horizontal orientation to measure the strain distribution along the steel section length, as shown in Figure 3.5.4. To study the potential causes of the specimen overstrength, the researchers believe that friction on the steel-concrete interfaces contributed to the ultimate capacity in addition to the shear studs. During the push-out tests, the normal pressure applied on the steel flanges might be remarkable as the concrete tended to bear against the steel sections on the top while prone to be detached near the bottom. This

phenomenon is referred to as the clamping effect. The web strain gauges were only used in Test 15, 16, and 17 as the clamping effect was not discovered until the late stages of the experiments. More web strain data is provided in Chapter 4 of this report as most of the PSC girder specimens incorporated the gauges as a measure of the clamping effect.

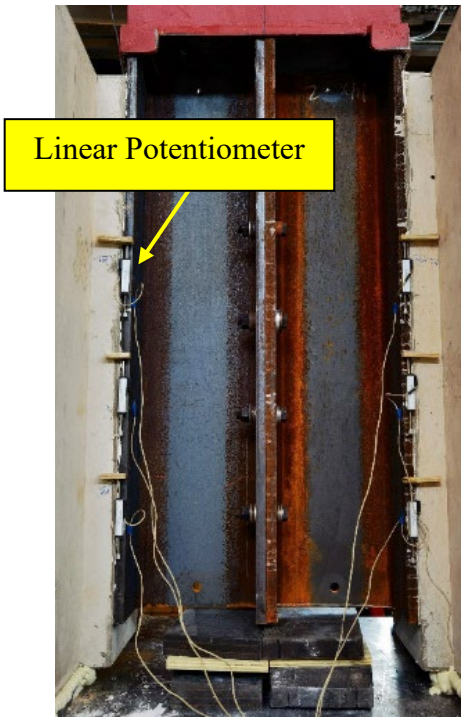

Figure 3.5.1 Linear Potentiometers on Specimen

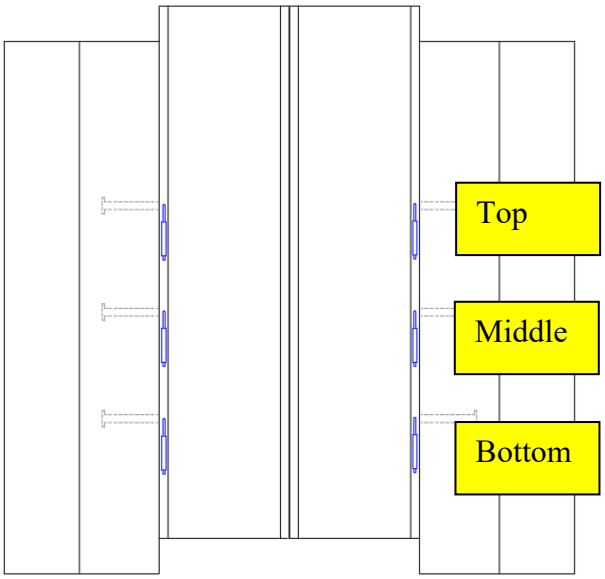

Figure 3.5.2 Linear Potentiometer Plan

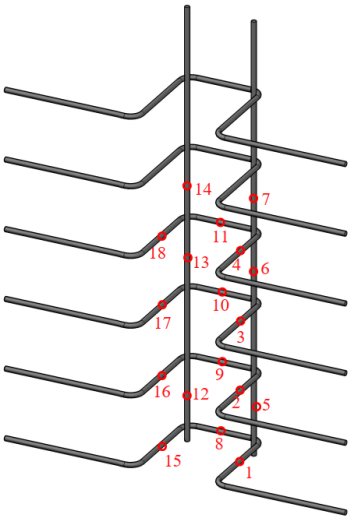

Figure 3.5.3 Strain Gauge Plan on Haunch Reinforcement

Figure 3.5.4 Web Strain Gauge

3.6. Push-out Test Procedure

Before each push-out test, the LPs were tested using 0.5 in and 1 in. displacement shims. The most common cause of malfunctional LPs was wire rupture or disconnection. The strain gauges were checked by their readings after the data acquisition system was initialized. A malfunctioning strain gauge might have remarkable readings (larger than 0.00003) even though there was no applied load. Some gauges on the rebar or the lead wires were inevitably damaged during the concrete castings.

For the sake of safety, passive lateral supports were installed on the columns of the testing frame to avoid large lateral displacement after failure, as indicated in Figure 3.6.1. The 0.5 in. and 0.75 in. thick plywood pieces were stacked and mounted on the columns with a clear spacing between 1 in. to 2 in. to the specimens. The number of the plywood pieces was adjusted based on the haunch size on a given specimen. While some researchers have simulated the frictional forces from loads applied through the concrete slab, in the experiments conducted on this study, there was no active lateral restraint (mentioned in Section 2.1.2.4). Neglecting any added friction in the push-out tests is generally conservative.

Figure 3.6.1 Passive Lateral Restraint

Eurocode 4 (CEN 2004a) provides a standard push-out test procedure to assess the behavior of the composite systems. The procedure requires an initial loading stage of 25 loading cycles between 5% to 40% of the expected ultimate capacity. The method outlines that subsequent loading increments should be such that failure does not occur within 15 minutes. Initial loading cycles are helpful to verify the functionality of the testing system and settle down any initial defects in the specimens, such as flaws and cracks in the concrete. Although the research protocol used in this study did not follow the 25 loading cycles, 2 initial loading cycles were

conducted in the tests between 0 to 150-kip to check the functionality of the hydraulic system, such as pressure leaks, and potential issues with instrumentation (load cells, strain gauges, or linear potentiometers). In the ultimate capacity test stage, the average loading rate was maintained between 0.5 to 1.0 kip/sec. The loading was paused every 50 kips after the load reached 350 kips to examine and mark cracks on the concrete. Observations on the behavior were noted throughout the push-out tests. The experiments were also videoed to capture noteworthy behavior.

Following the completion of each test, pictures were taken so that the failure modes of the specimens were recorded. The researchers conducted a post-test inspection to check concrete cracking, shear stud deformation, and other noteworthy aspects of the specimen behavior. The failed specimens were then secured by chains, as shown in Figure 3.6.2, for easy removal from the setup. The specimens were inspected once more prior to disposal. A jack hammer was occasionally required in these post-test inspections to expose the rebars and shear studs. The same testing procedure was applied to the PSC girder specimens as well as outlined in Chapter 4.

Figure 3.6.2 Tall Haunch Specimen after Push-out Test

3.7. Material Tests

To understand the behavior of the specimens and conduct the numerical analyses, the material properties of the concrete, rebars, and shear studs were examined. The testing methods and results are summarized in this section.

The compression test of the concrete cylinders (mentioned in Section 3.3) followed the guidelines established in ASTM C39/C39M (2021). The cylinders had a diameter of 4 in. and a height of 8 in. During the concrete curing, the cylinders were located next to the test specimens of the same concrete batches and covered by plastic sheets so that the material specimens had a

similar curing condition as the concrete in the specimen. Sulfur capping (shown in Figure 3.7.1) was used to finish the top and bottom surfaces. An average stress rate of 35 psi/sec was applied. Figure 3.7.2 illustrates the compressive failure of concrete cylinders. The test results are included in Section 3.8.

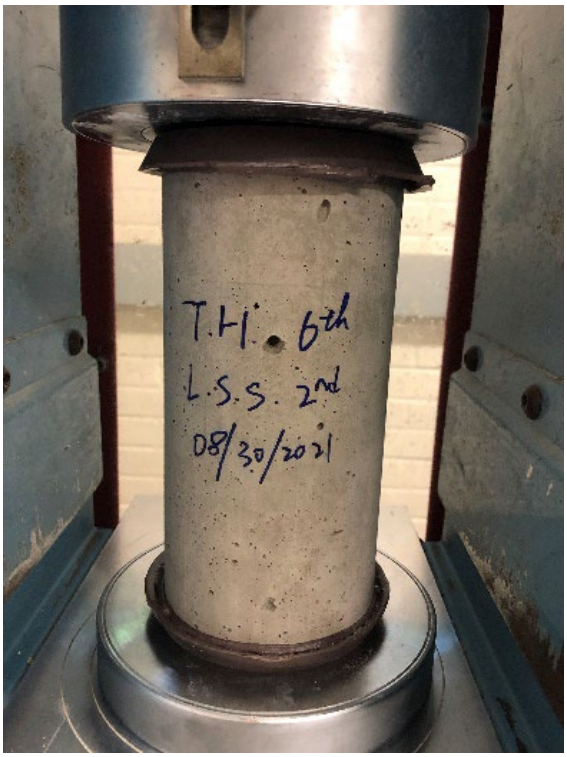

Figure 3.7.2 Cylinder Compression

Figure 3.7.1 Concrete Cylinder with Failure

The provisions of ASTM A370 (2022) was followed to conduct the tension tests of the rebars and the shear studs. Figure 3.7.3 shows the setup of the rebar tension tests. The sample rebars were 36 in. long. The elongation was measured with an extensometer with a gauge length of 2 in. The loading rate was controlled using a displacement control with an applied deformation less than 0.125 in. per min. after 50 per cent of the estimated yield strength was reached. The rebars in the steel girder specimen fabrication were from the same heat. Figure 3.7.4 summarizes the tension tests of the rebars. Based on the test results, the average yield strength of the rebars was 64 ksi, and the average ultimate strength was 98 ksi.

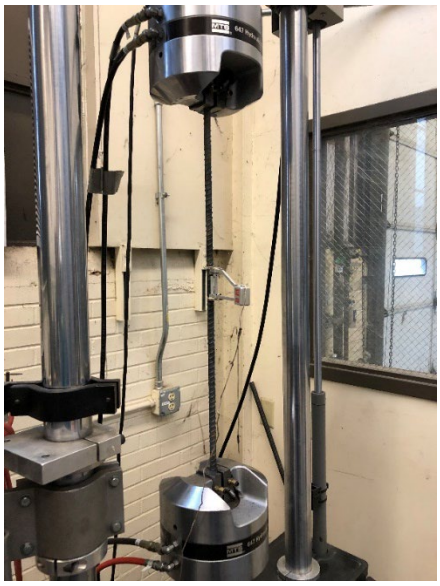

Figure 3.7.3 Rebar Tension Test Setup

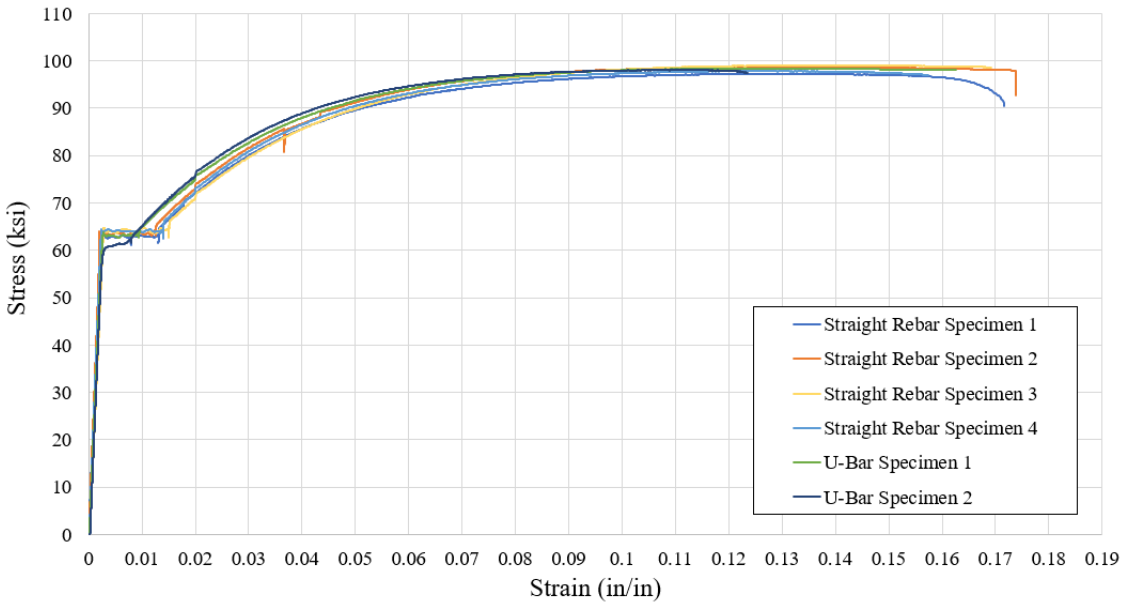

Figure 3.7.4 Rebar Tension Test Results

To investigate the strength behavior of the shear studs, coupon tests were conducted. The sample shear studs were machined into round coupons as shown in Figure 3.7.5. Elongation was measured using an extensometer with a 2 in. gauge length. The test setup is shown in Figure 3.7.6.

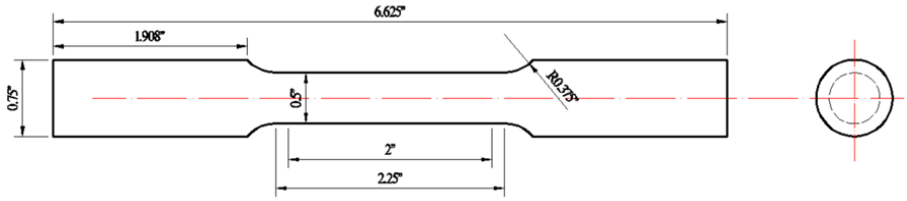

Figure 3.7.5 Shear Stud Coupon Design Sketch (Deng 2023)

To minimize dynamic effects in the stud coupon tests, the loading rate was controlled by specifying a displacement rate of 0.02 in. per min. The loading was paused for 2 minutes every 0.01 strain. Due to the material relaxation, the loading decreased slightly during the interval, as shown in Figure 3.7.7. This loading cycle continued until the dynamic strength was smaller than the 90 per cent of the peak strength. The scattered static strength data points were fitted by polynomial curves, as shown in Figure 3.7.7. The fitting curves were used to estimate the static strength of the shear studs. Six coupon tests were conducted and showed the average static ultimate strength of the shear studs was 77 ksi.

Figure 3.7.6 Stud Coupon Test Setup (Deng 2023)

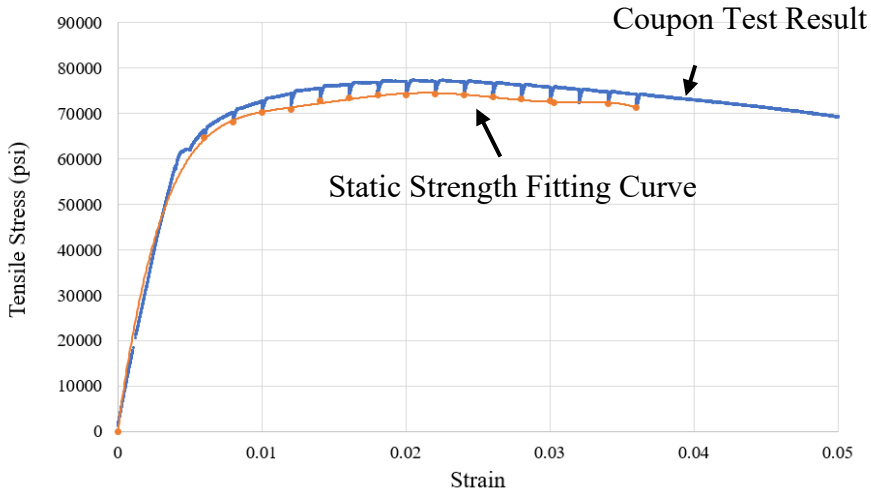

Figure 3.7.7 Shear Stud Coupon Test Result Example

3.8. Push-out Test Result

In this section, the load-slip behavior of the push-out test specimens is discussed with the analyses of the strains measured from the gages on the haunch reinforcement and steel section webs. Due to the complexity of the concrete cracking patterns and asymmetric failures, the slip deformations measured at different locations in a test could significantly vary along the specimen length. To characterize the slip behavior, the researchers developed two methods to process the data. For the specimens with double-sided failure (i.e., failure in both slab specimens), the average of all slip measurements was calculated to account for the behavior. For the specimens with single-sided failure (failure on only one of the concrete decks), the average of the slip measurements on the failure side was used.

There were mainly two different failure modes observed in the push-out tests, shear stud failure and concrete failure. The shear stud failure was characterized by the stud rupture with relatively little concrete damage. In this failure mode, the strength and the ductility of the shear studs was fully developed, which generally resulted in a larger ultimate capacity compared to specimens with concrete failure modes. A typical stud failure specimen is shown in Figure 3.8.1 and 3.8.2. The failure occurred at the shank of the studs near the welding zones. The concrete deck and haunch were easily detached from the steel section after the failure. In general, shear stud failure occurred if the headed shear studs had sufficient spacings and clear edge distances. Failure in the studs is generally preferred compared to the concrete failure modes since the resulting ultimate capacity with shear stud failures is higher and more predictable. The load-slip curve of a pure shear stud failure is relatively smooth (as shown in Figure. 3.8.3).

Figure 3.8.1 Shear Stud Failure (Concrete Deck)

Figure 3.8.2 Shear Stud Failure (Steel Section)

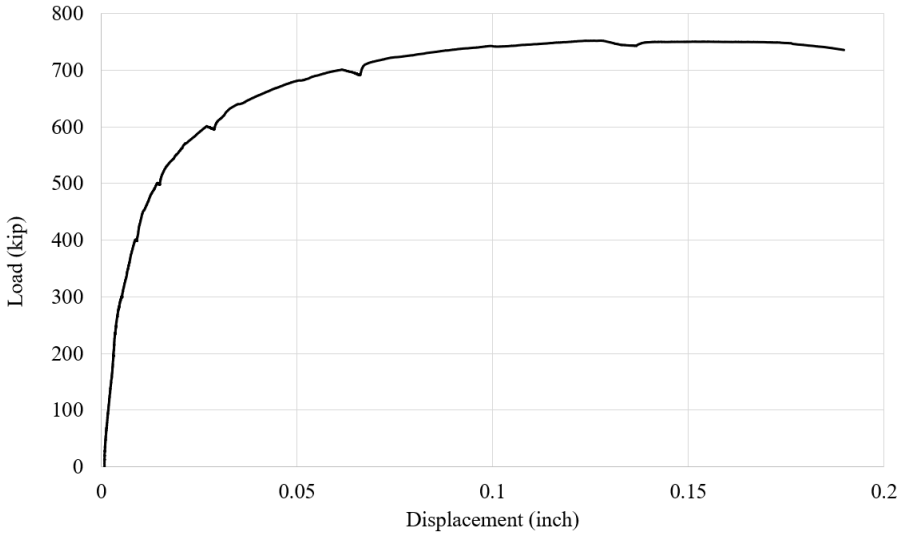

Figure 3.8.3 Typical Load-Slip Curve of Shear Stud Failure

Five different concrete failure modes were observed in the push-out tests, which consisted of 1) concrete breakout, 2) haunch splitting/widening, 3) haunch detachment, 4) localized concrete crushing, and 5) global haunch failure. Figure 3.8.4 shows an example of a concrete failure. Concrete failure modes typically showed an asymmetric pattern, meaning that the deck in one of the two specimens failed, while the deck on the companion specimen did not. In many of the cases with a concrete deck failure, significant concrete cracking often occurred in the haunch region. Because the failure occurred in the concrete, the strength of the shear studs was not fully developed, which resulted in a lower ultimate capacity compared to specimens with shear stud failures. The concrete failure modes might sometimes exhibit large displacement in the wide flanges sections as the cracks resulted in a "rigid body" movement (no bending) in the shear studs. A typical load-slip curve of the concrete failure modes is shown in Figure 3.8.5. The fluctuation of the curve was a result from the crack propagation.

Figure 3.8.4 Concrete Failure in Push-out Test

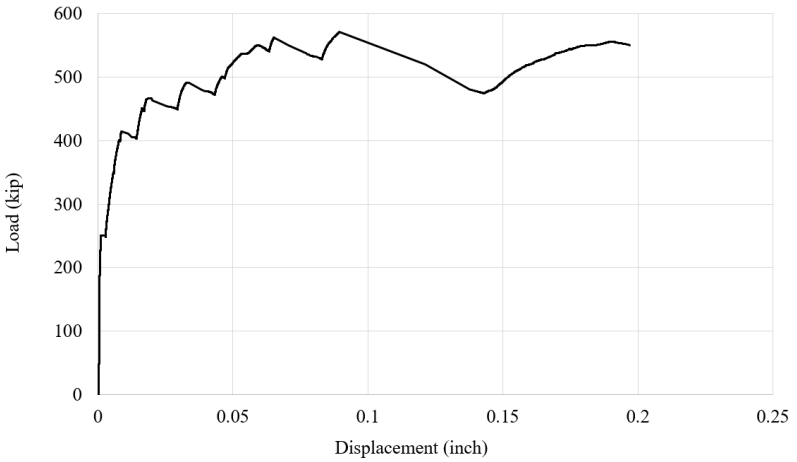

Figure 3.8.5 Load-Slip Curve of Concrete Failure

3.8.1. Shear Stud Failure

Shear stud failure occurred in six push-out tests out of seventeen. The ultimate capacities of these specimens have been listed in Table 3.8.1. The load-slip curves of the stud failure specimens are shown in the Figure 3.8.6. As indicated by Table 3.8.1, specimens with shear stud failure reached at least 136% of the design capacity (552 kips for Test 01 to 05, and 184 kips for Test 17). The concrete strength and haunch size did not significantly affect the ultimate capacity of the shear connectors. The result of Test 01 showed a lower stiffness than the others in the elastic phase as the specimens had been twice loaded to 700 kips for the test setup trial before the ultimate capacity test. As the specimens had higher capacity than the estimation, the first two actuator setups used in the testing system were not able to reach the ultimate capacities in Test 01.

Table 3.8.1 Summary of Specimens with Shear Stud Failure

Test #	Haunch Size & Detailing	Concrete Strength (psi)	Ultimate Capacity (kip)	% of Design Capacity
01	9” Haunch w/ Stacked Shear Studs	5508	868	157%
02	9” Haunch w/ U-bar	5925	780	141%
03	9” Haunch w/ Stirrups	5015	825	149%
04	3” Haunch	4643	832	150%
05	Zero Haunch	5061	751	136%
17	15” Haunch w/ Stirrups, Single stud per row	5233	292	159%

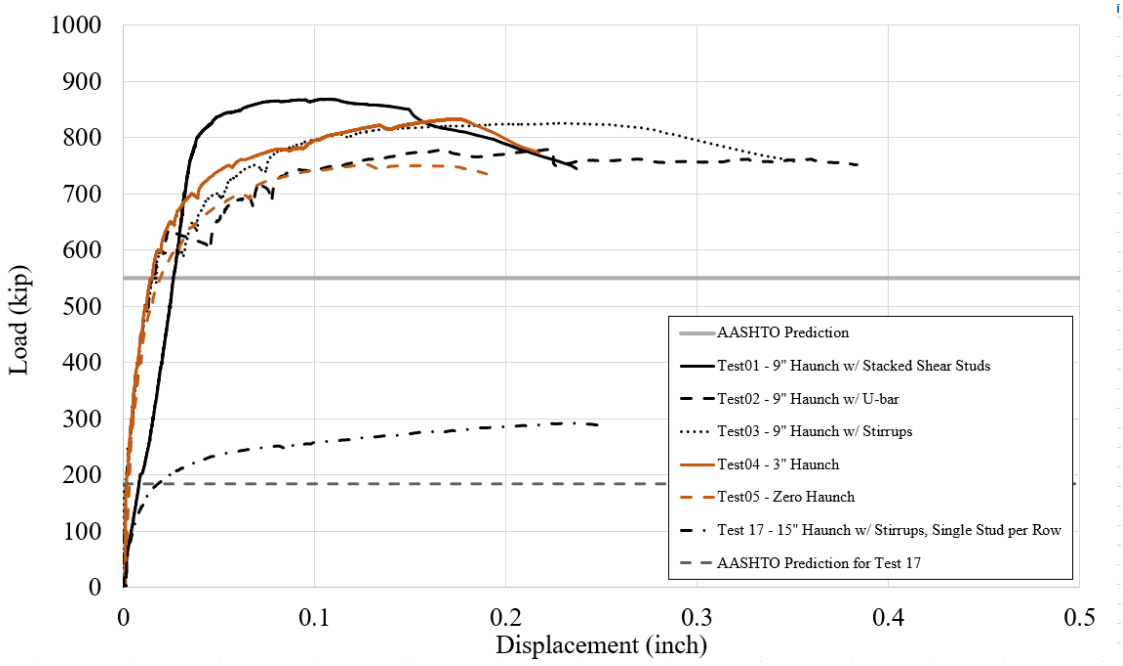

Figure 3.8.6 Load-Slip Curves of Specimens with Shear Stud Failure

A double-sided failure (slabs on the companion specimens) occurred in Test 04 and 05, as shown in Figure 3.8.7 and 3.8.8. Due to the small haunch depths, large concrete cracks did not occur on the specimen. Therefore, the slip did not vary significantly along the longitudinal direction, as shown in Figure 3.8.9 and 3.8.10. The maximum rebar strain observed in Test 04 and 05 was 0.0003, which is essentially negligible. The steel strains were likely small because the concrete haunch remained intact with minor cracking. The slips on the two sides of Test 04 and 05 were asymmetric, as shown in Figure 3.8.11 and 3.8.12.

Figure 3.8.7 Shear Stud Failure (Test 04)

Figure 3.8.8 Shear Stud Failure (Test 05)

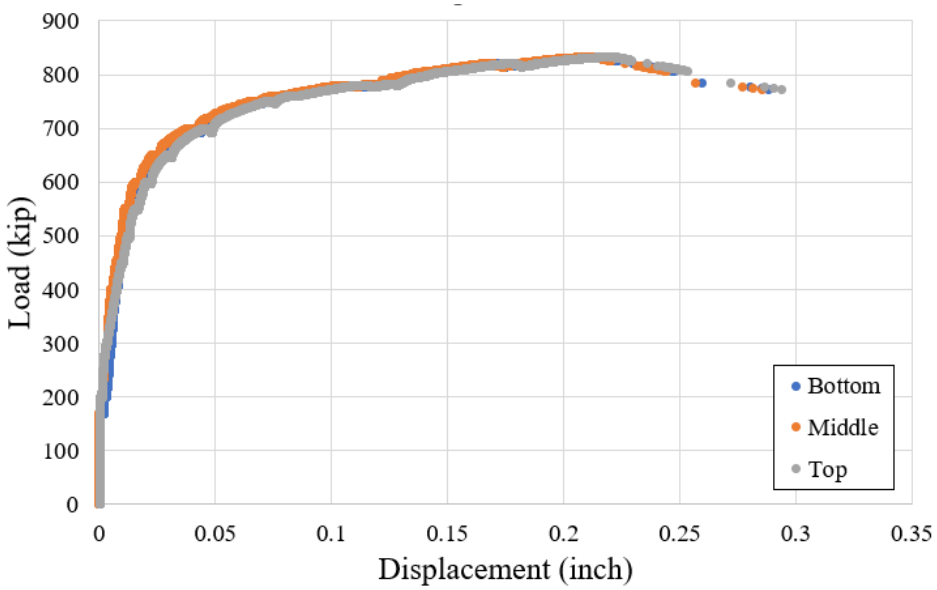

Figure 3.8.9 Load-Slip Curves measured at Different Heights in Test 04

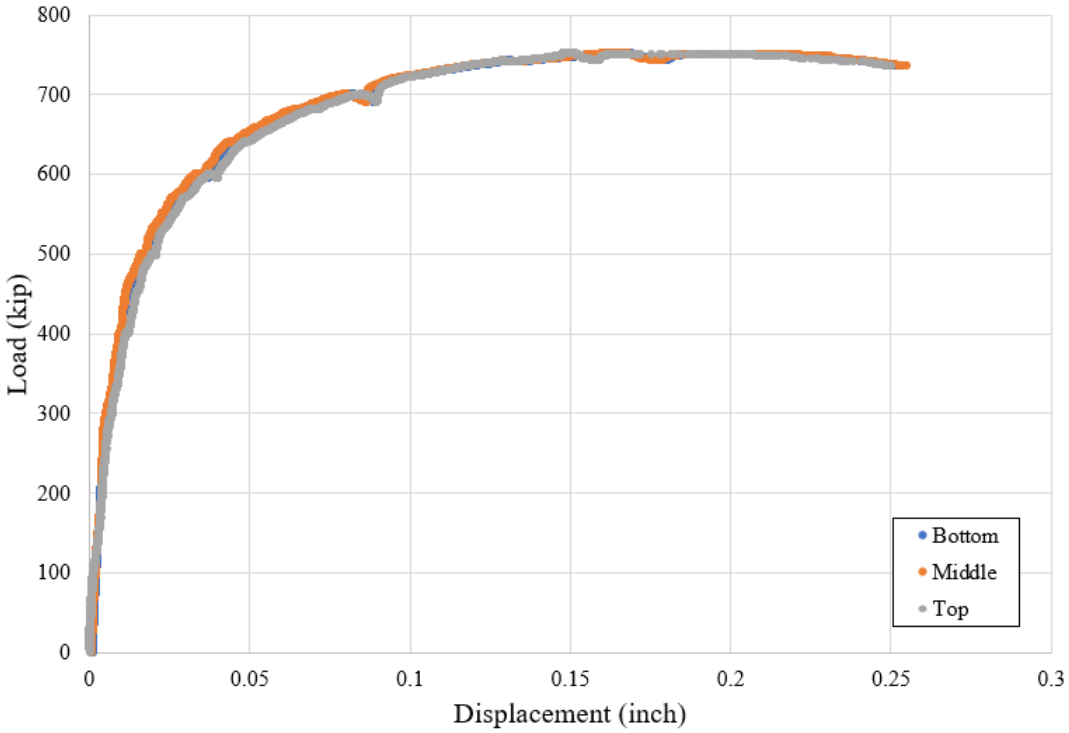

Figure 3.8.10 Load-Slip Curves measured at Different Heights in Test 05

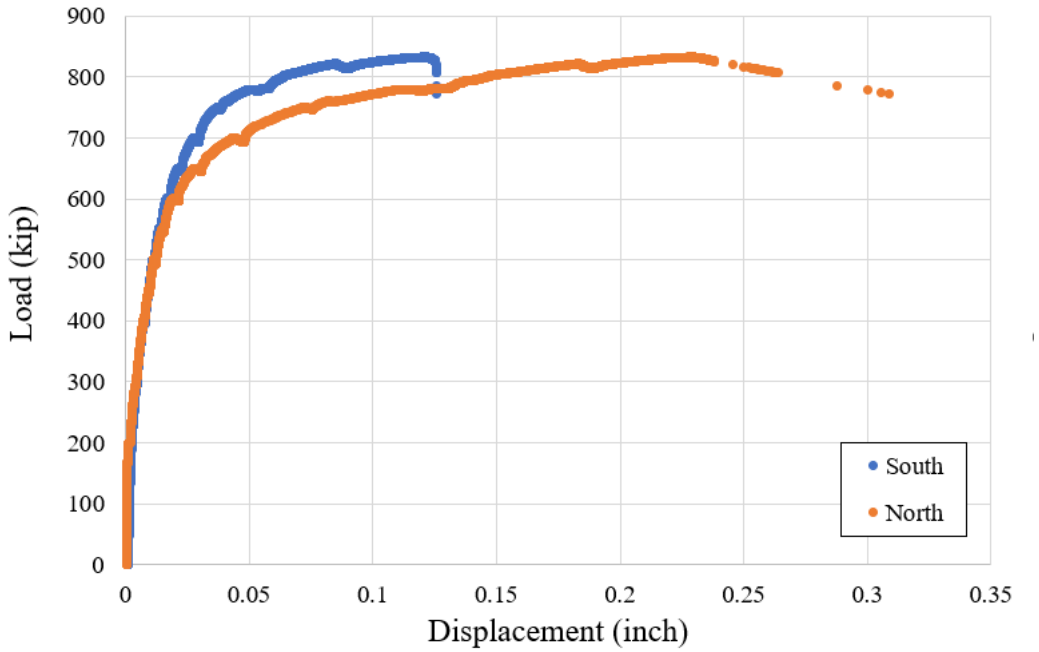

Figure 3.8.11 Load-Slip Curves Comparison between Two Sides in Test 04

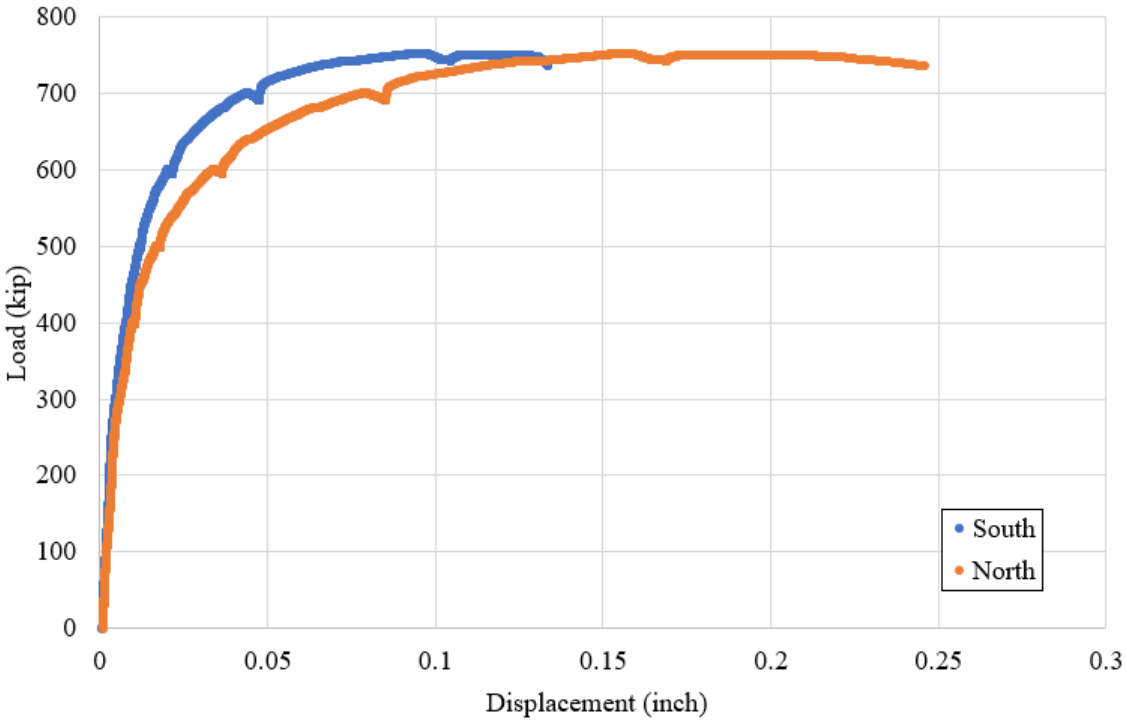

Figure 3.8.12 Load-Slip Curves Comparison between Two Sides in Test 05

Test 01 had a single-sided failure, as shown in Figure 3.8.13. The failure mode included a shear stud failure combined with concrete breakout, which did not control the behavior in this case, near the bottom of the haunch. The concrete breakout likely occurred due to the lack of longitudinal rebars in the haunch. Similar to Test 04 and 05, the slip on the failure interface did not significantly change along the longitudinal direction, as shown in Figure 3.8.14.

Figure 3.8.13 Specimen Failure in Test 01

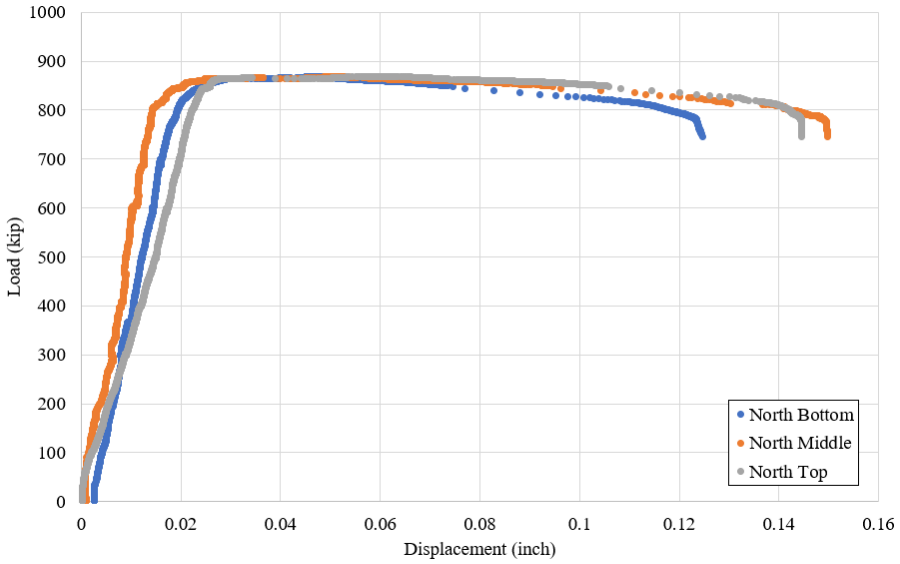

Figure 3.8.14 Load-Slip Curves measured at Different Heights in Test 01

The 9 in. haunch specimen pairs in Test 02 and 03 (shown in Figure 3.8.15 and 3.8.16), which involved U-bars and stirrups respectively, had similar behavior. The fluctuation in the load-slip curves, as shown in Figure 3.8.6, was caused by concrete cracking. The haunch reinforcement prevented the further propagation of the crack, and the haunches were able to bear the shear demands to shear stud failure. Due to the cracks, the haunch concrete could no longer maintain the integrity, which resulted in the relative displacement between different haunch locations. Therefore, the slip between the steel and concrete might not be identical along the length, as shown in Figure 3.8.17. The maximum strains measured in Test 02 and 03 were 0.004 and 0.008 respectively.

Figure 3.8.15 Specimen Failure in Test 02

Figure 3.8.16 Specimen Failure in Test 03

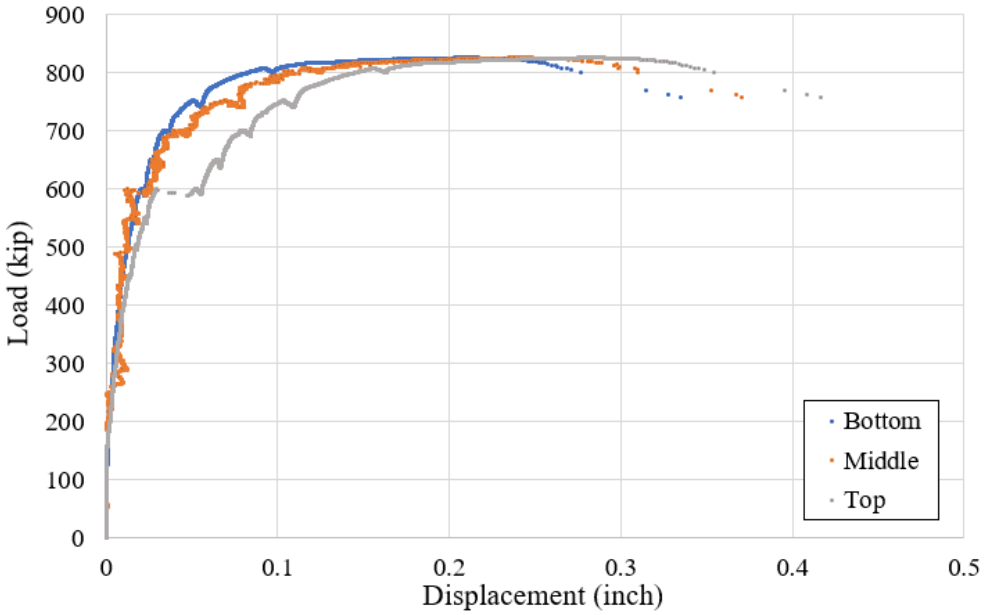

Figure 3.8.17 Load-Slip Curves measured at Different Heights in Test 03

Test 17 was conducted on the specimens with a 15 in. haunch and single shear studs per row. A single-sided failure occurred in the push-out test, as shown in Figure 3.8.18. Due to the sufficient clear edge distance to the studs, shear stud failure occurred in the unreinforced haunch without any visible concrete cracks. Obviously, requiring a single stud or excessively large edge distances is not practical. However, the data from this test indicates that larger edge distances can increase the likelihood of a shear stud failure instead of a concrete failure, which is preferred. As previously mentioned, the steel/concrete slip did not generally vary significantly in the longitudinal direction when the concrete haunch did not experience significant cracking (shown in Figure 3.8.19).

Figure 3.8.18 Specimen Failure in Test 17

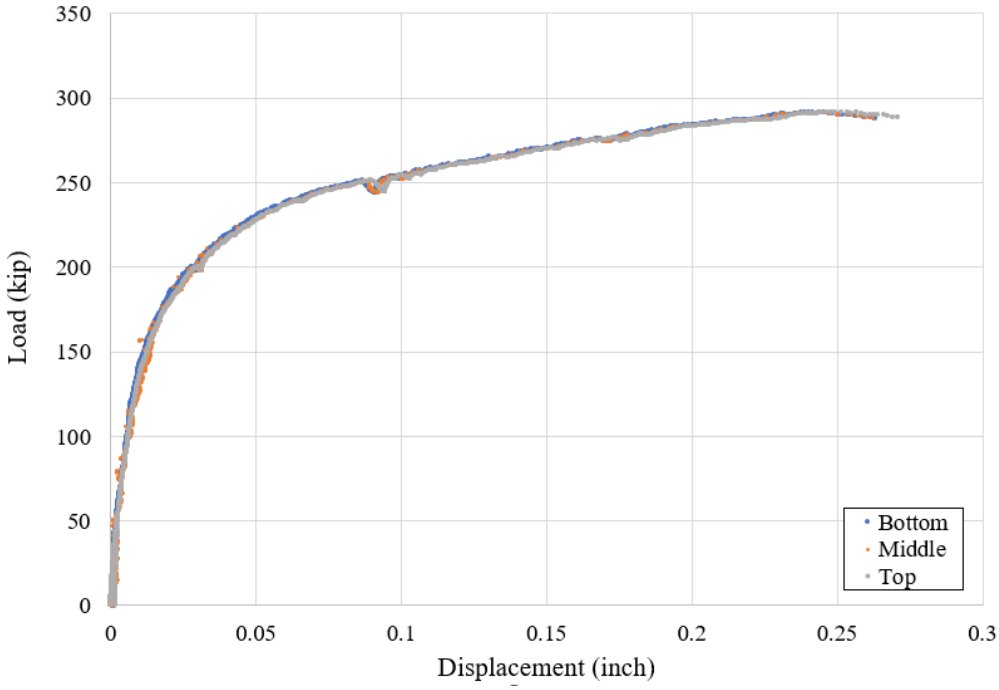

Figure 3.8.19 Load-Slip Curves measured at Different Heights in Test 17

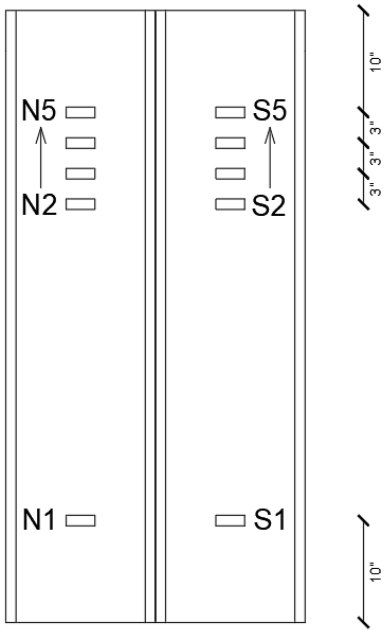

Figure 3.8.20 Web Strain Gauge Plan

Test 17 incorporated web strain measurement in an attempt to measure the clamping effect. Figure 3.8.20 illustrates the strain gauge installation plan. To minimize the impact of web bending on the strain readings, the strain gauges were attached on both sides of the webs, and the

average of the corresponding strains was calculated to characterize the clamping effect at that location. The strain-load curves of the two steel sections are included in Figure 3.8.21 and 3.8.22. The web strains were symmetrically distributed on the steel sections with compression near the top. Tensile strain near the bottom revealed the potential separation between the two specimens. With the limited data points, an assumption can be made that there might be a neutral position on the steel sections. Further study is needed for verification. The development trend of the web strains was deviated when the testing load reached approximately 200 kips, at which the specimens reached the plastic stage. While the data from the web strain readings did not provide direct data that could be used to quantify the shear mechanism between the concrete and steel flange, the readings did corroborate that the slab in push-out specimens tended to "spread" away from the steel beams near the bottom and have a clamping effect (compression) near the top.

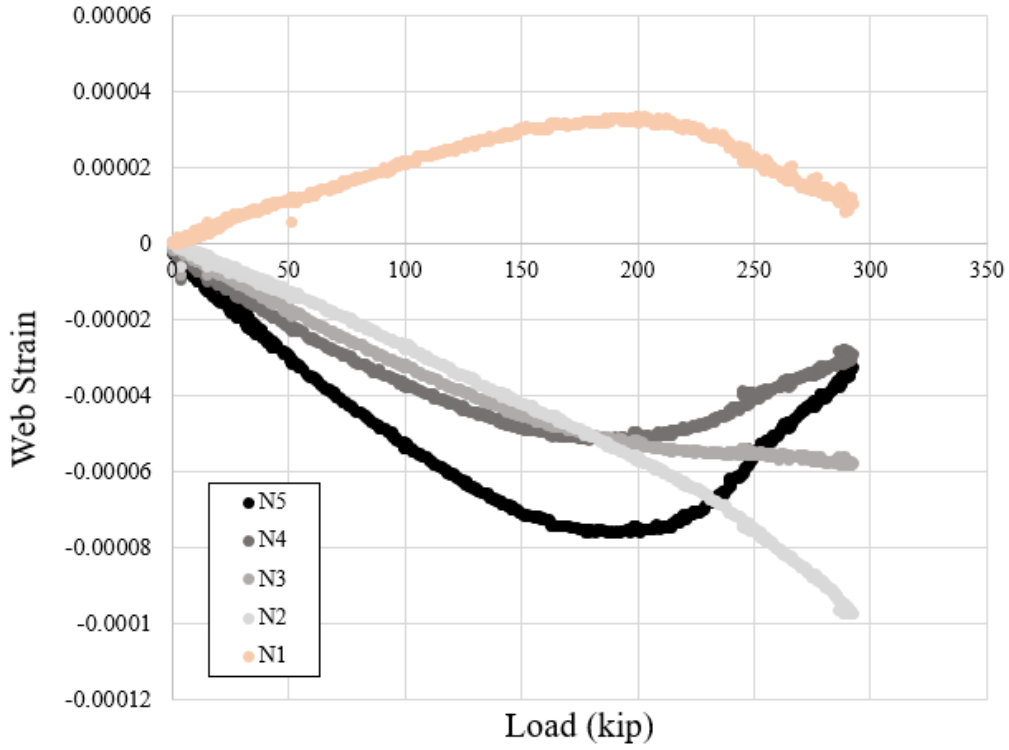

Figure 3.8.21 Web Strain (North) of Test 17

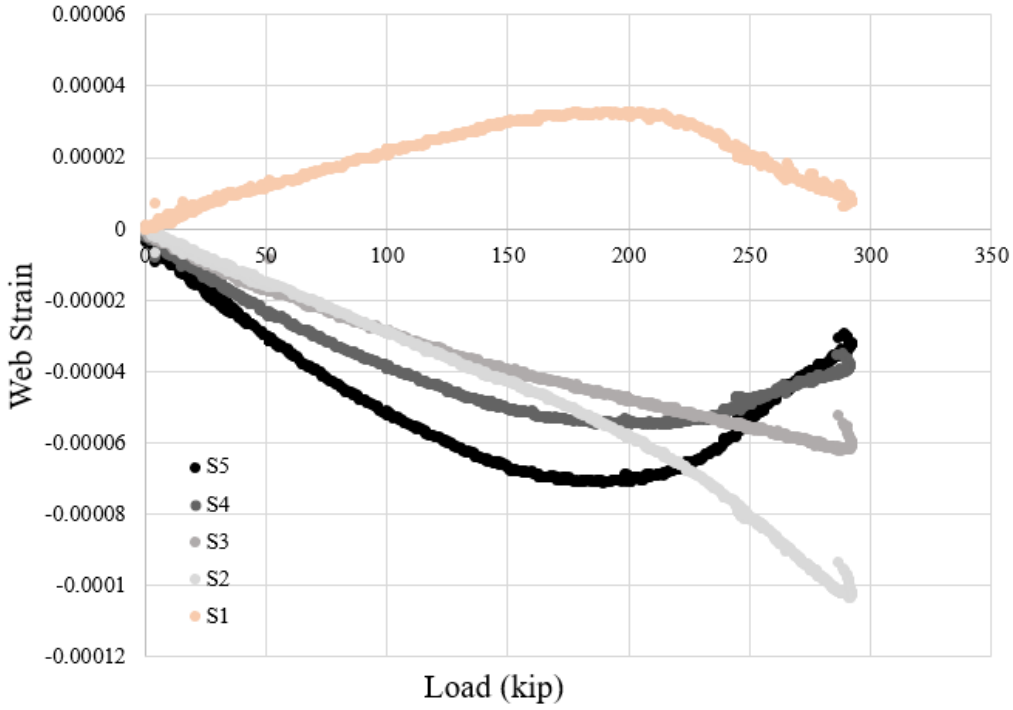

Figure 3.8.22 Web Strain (South) of Test 17

3.8.2. Concrete Breakout Failure

Concrete breakout failure occurred most frequently among the concrete failure modes in the push-out tests. The failure typically involved a triangular concrete block detaching from the haunch on either one or both companion specimens, as shown in Figure 3.8.23. The main causes of the concrete breakout failure were likely insufficient clear edge distance to studs, lack of longitudinal rebars in haunches, and/or extreme haunch sizes. Test 11, 12, and 13 showed the ultimate capacity was not affected by the transverse reinforcement with a spacing not less than 9 in. The push-out tests involving concrete breakout failure are summarized in Table 3.8.2 and Figure 3.8.24.

Table 3.8.2 Summary of Specimens with Concrete Breakout Failure

Test #	Haunch Size & Detailing	Concrete Strength (psi)	Ultimate Capacity (ksi)	% of Design Capacity
06	15” Haunch w/ Triple Stacked Shear Stud	4485	698	126%
07	15” Haunch w/ U-bar	5529	612	110%
11	12” Haunch w/ U-bar	4787	578	105%
12	12” Haunch w/ U-bar (double spacing)	4885	571	103%
13	12” Haunch w/ U-bar (double spacing, alternative location)	4383	610	110%
14	12” Haunch w/ Stirrups	4485	636	115%

Figure 3.8.23 Concrete Breakout Illustration (Test 07)

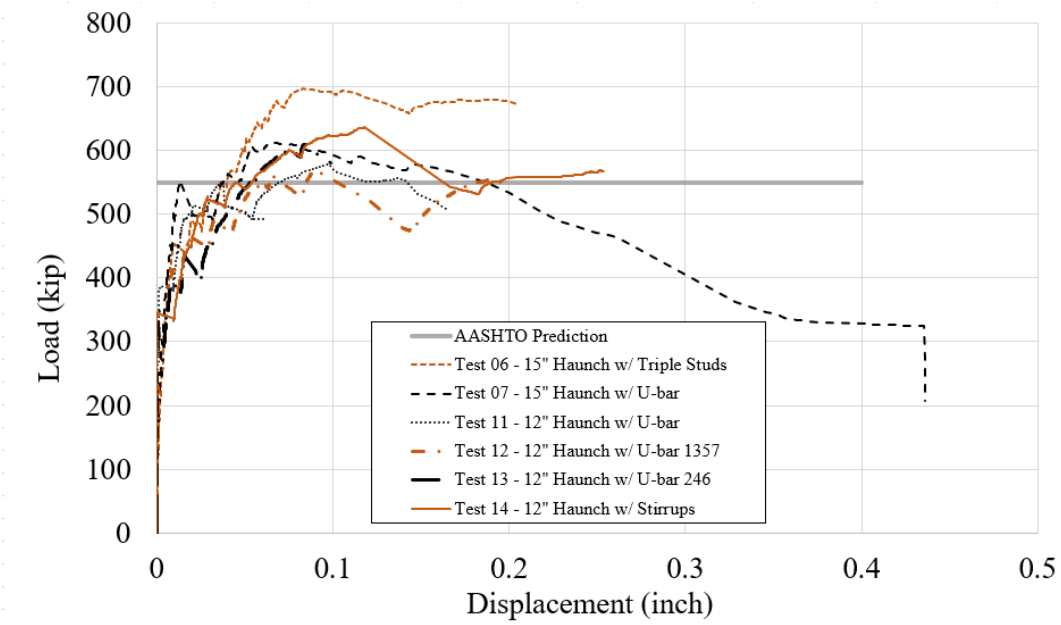

Figure 3.8.24 Load-Slip Curves of Specimens with Concrete Breakout Failure

The specimen pairs in Test 07, 11, 12, 13, and 14 showed similar behavior in terms of the ultimate capacity and the cracking pattern (shown in Figure 3.8.25 to 3.8.29). On the failure side, multiple cracks with significant widths developed across the haunches with concrete breakout in the haunch near the specimen bottom. Due to the cracks, the load-slip behavior was no longer identical in the longitudinal direction, as shown in Figure 3.8.30 to 3.8.34. The discontinuity on the load-slip curves was caused by the sudden cracking of the concrete. The displacement of the steel sections was too fast compared to the scan rate of the data acquisition system to track,

which was the source of “gaps” in data in the graphs. The transverse reinforcement in the vicinity of the large cracks could reach tensile strains between 0.01 to 0.04.

Figure 3.8.25 Specimen Failure in Test 07

Figure 3.8.26 Specimen Failure in Test 11

Figure 3.8.27 Specimen Failure in Test 12

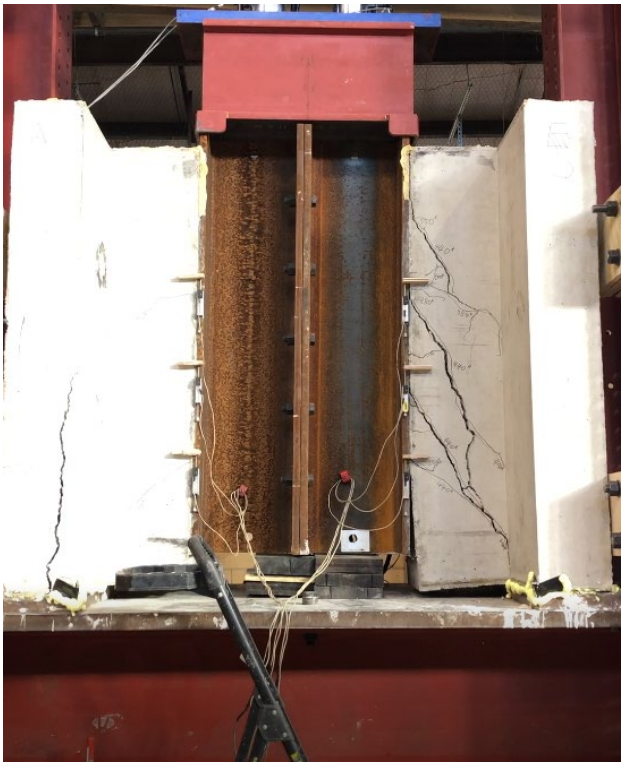

Figure 3.8.28 Specimen Failure in Test 13

Figure 3.8.29 Specimen Failure in Test 14

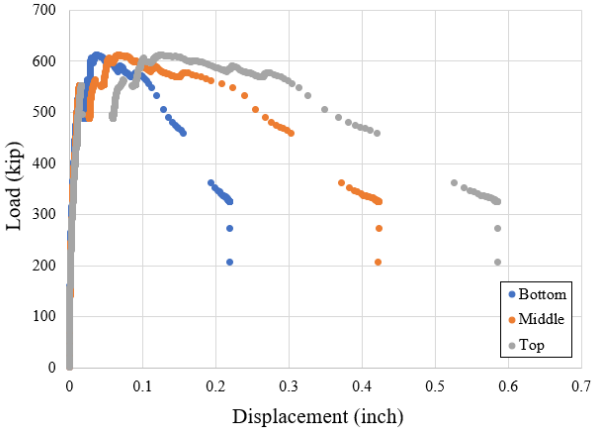

Figure 3.8.30 Load-Slip Curves measured at Different Heights in Test 07

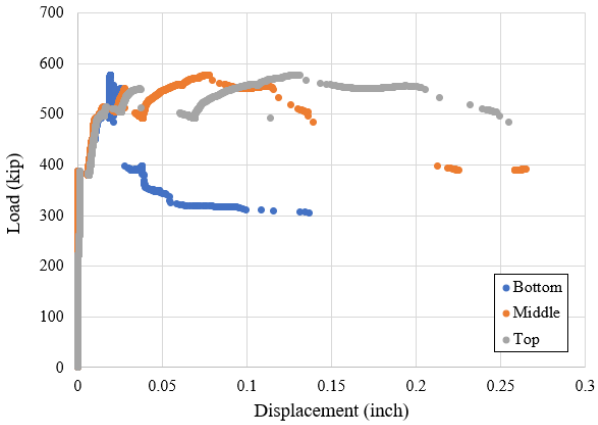

Figure 3.8.31 Load-Slip Curves measured at Different Heights in Test 11

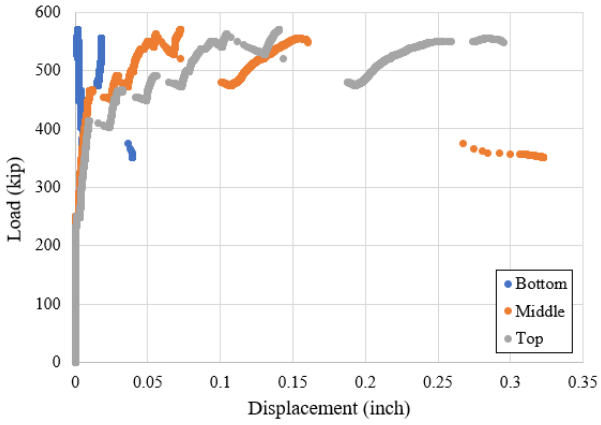

Figure 3.8.32 Load-Slip Curves measured at Different Heights in Test 13

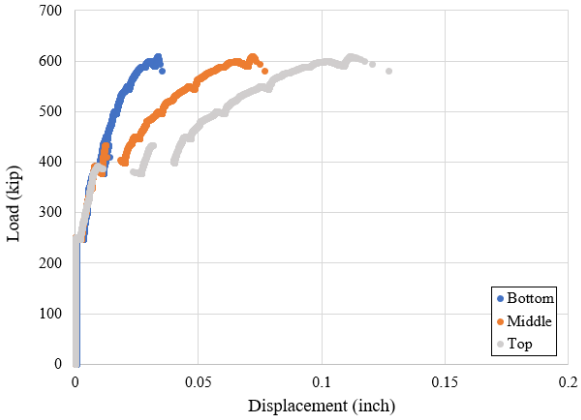

Figure 3.8.33 Load-Slip Curves measured at Different Heights in Test 12

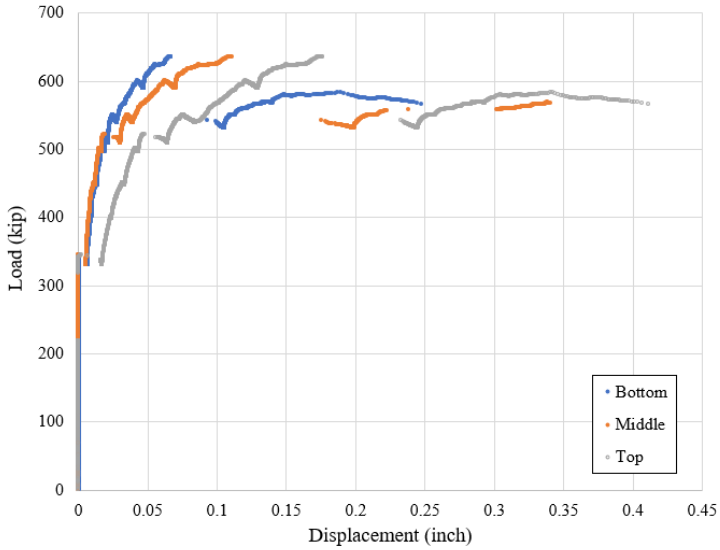

Figure 3.8.34 Load-Slip Curves measured at Different Heights in Test 14

In Test 06, the 15 in. haunch specimens included triple stacked welded shear studs that also failed with concrete breakout, as shown in Figure 3.8.35. Compared with the other concrete breakout specimens, the triple stacked stud specimen had only one major crack starting from the region between the 1st and 2nd row of the shear studs. A similar cracking pattern was observed in Test 01 (9 in. haunch with double stacked shear studs). Shear stud stacking resulted in behavior where the stud strength was developed better than single height studs with more than stirrups or U-bars. The load-slip curves measured at various locations were included in Figure 3.8.36.

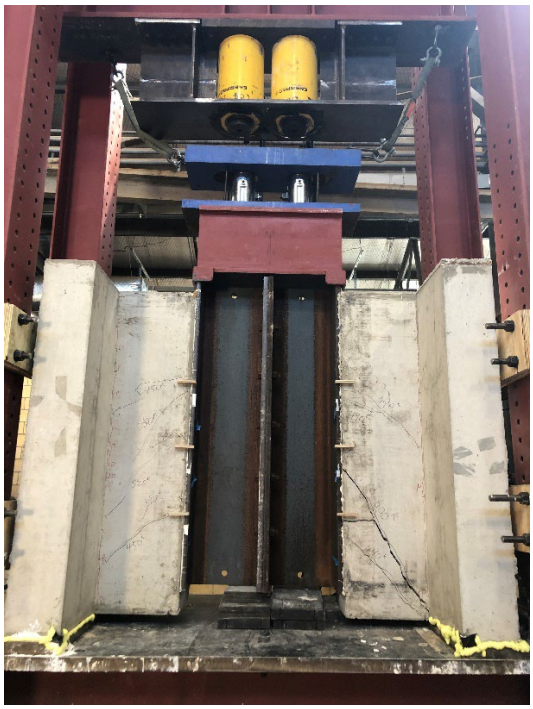

Figure 3.8.35 Specimen Failure in Test 06

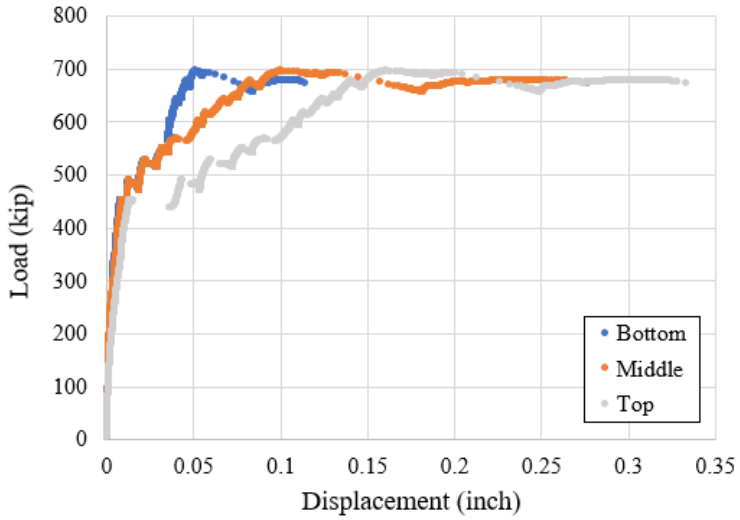

Figure 3.8.36 Load-Slip Curves measured at Different Heights in Test 06

3.8.3. Haunch Splitting/Widening

Test 15 and 16 involved haunch failures, as shown in Figures 3.8.37 and 3.8.38. The failure that was observed consisted of splitting in the concrete haunch along the line of shear studs. This failure mode was characterized by the lateral expansion of the haunches with possible surface concrete spalling, as shown in Figure 3.8.39. The lateral movement of the haunch concrete was caused by the longitudinal rigid body movement of the shear studs widening the concrete cracks. The longitudinal rebars in the haunch acted as restraints to hold back the potential concrete breakout zones (the triangular concrete blocks). The test results related to haunch

splitting/widening are summarized in Table 3.8.3 and Figure 3.8.40. The maximum strain the haunch reinforcement reached was between 0.01 to 0.02.

Based on the test results, it can be concluded that the longitudinal haunch rebars may slightly improve the ultimate capacity of the shear connectors. Providing longitudinal rebars in the haunch region provided improved ductility compared to haunches without the longitudinal rebars.

Table 3.8.3 Summary of Specimens with Haunch Widening

Test #	Haunch Size & Detailing	Concrete Strength (psi)	Ultimate Capacity (kip)	% of Design Capacity
15	15” Haunch w/ Stirrups & Unconfined longitudinal rebars	4731	692	125%
16	15” Haunch w/ Stirrups & Confined longitudinal rebars	4733	635	115%

Figure 3.8.37 Haunch Splitting/Widening 1

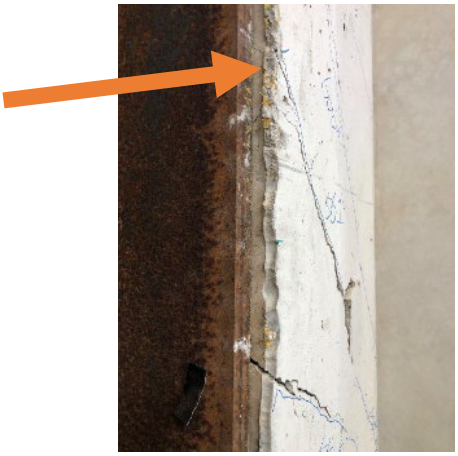

Figure 3.8.38 Haunch Splitting/Widening 2

Figure 3.8.39 Haunch Splitting/Widening 3

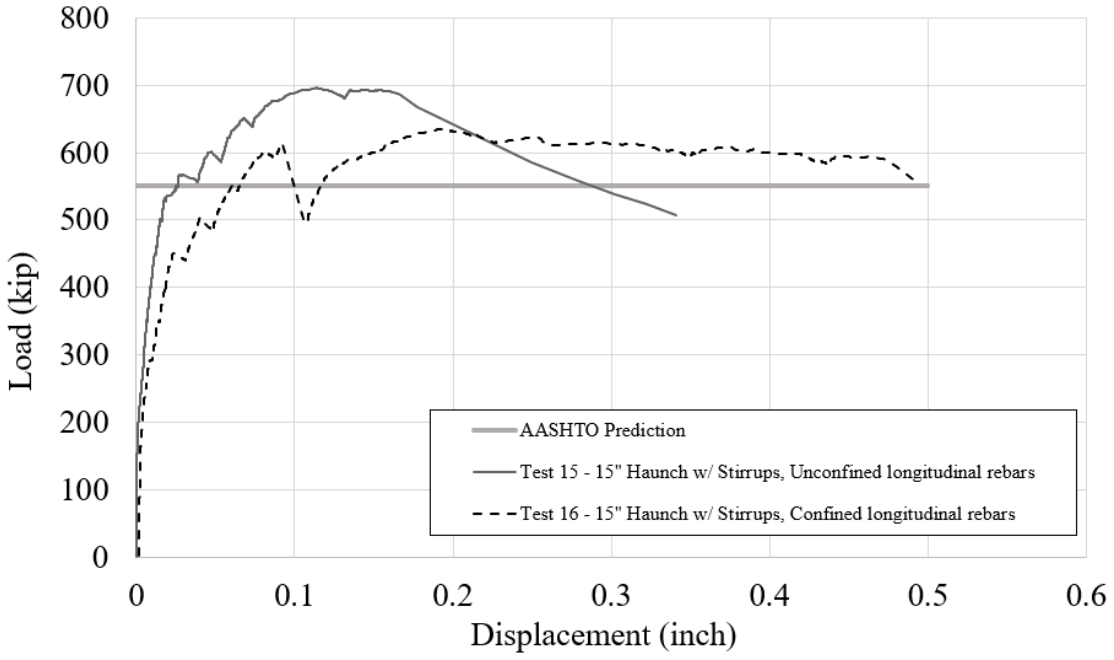

Figure 3.8.40 Load-Slip Curves of Specimens with Haunch Widening

Test 15 and 16 incorporated strain gages on the steel section webs in an effort to characterize the clamping effect from the slab on the upper region of the steel sections. However, because several web strain gauges in Test 16 were accidentally damaged, only results from Test 15 are presented, as shown in Figure 3.8.41 and 3.8.42. Similar to Test 17, the web strains showed compression

near the top and tension near the bottom of the specimens. The strains linearly increased with the increases in the applied load until the specimens reached the plastic stage.

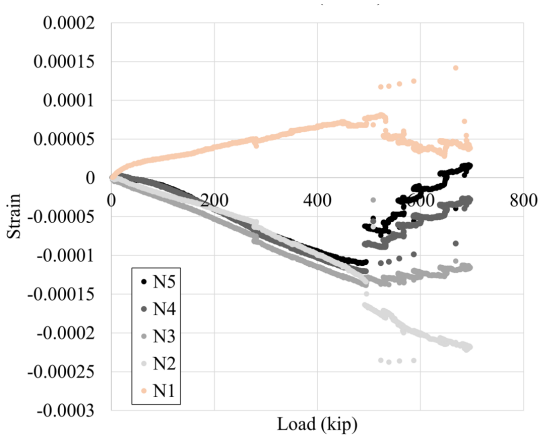

Figure 3.8.41 Web strain (North) in Test 15

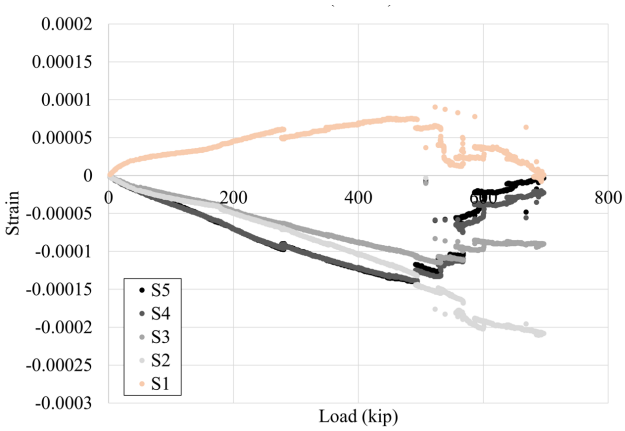

Figure 3.8.42 Web Strain (South) in Test 15

3.8.4. Localized Concrete Crushing

A unique failure mode occurred in Test 10 due to the low stud pitch relative to other specimens. The stud pitch was 6 in. compared with 12 in. for the other specimens. The ultimate capacity was 752 kips (136% of the design capacity). The compressive strength of the concrete was 4642 psi. As shown in Figure 3.8.43, localized concrete crushing was characterized by the concrete damage in the vicinity of the shear stud clusters due to the large stress at localized region. Similar to the other concrete failure modes, the strength of the shear stud was not fully developed prior to the localized concrete crushing. This failure mode can be avoided by increasing the shear stud pitch. The load-slip curve is shown in Figure 3.8.44.

Figure 3.8.43 Localized Concrete Crushing

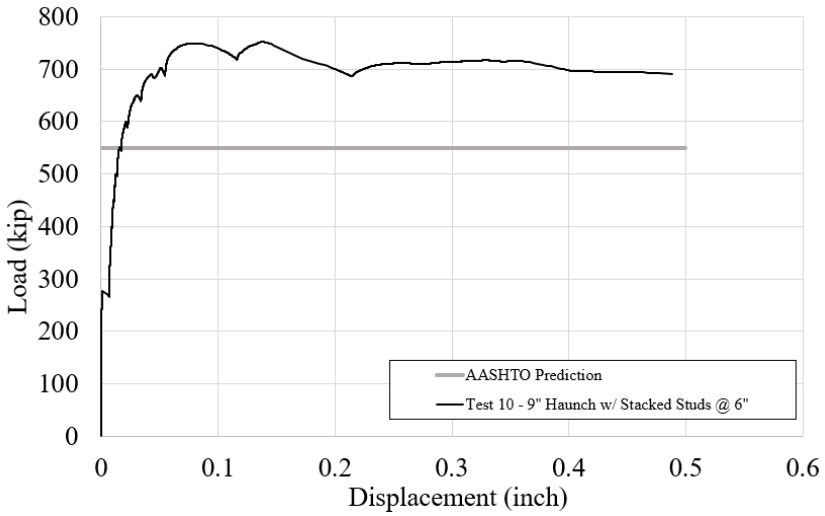

Figure 3.8.44 Load-Slip Curve of Specimen with Localized Concrete Crushing

3.8.5. Haunch Detachment

Test 09 involved a failure mode in which the haunch detached from the steel girder, as shown in Figure 3.8.45. This mode was likely due to the haunch detailing and shear stud length. In Test 09, the specimens had a 6 in. deep haunch and 8 in. long shear studs with a 12 in. pitch. The 8 in. stud length resulted in 2 in. stud penetration into the concrete decks (the minimum deck penetration requirement of AASHTO LRFD 2020). Because there was no other reinforcement penetrating the deck/haunch interface except the shear studs, the interface was not sufficiently strong for the shear studs to reach failure. As shown in Figure 3.8.45, the conical failure planes were formed around the shear studs. Although a concrete failure was identified in this test, the ultimate capacity (851 kips) of the specimens was close to the shear stud failure. The load-slip curve is shown in Figure 3.8.46.

Figure 3.8.45 Haunch Detachment

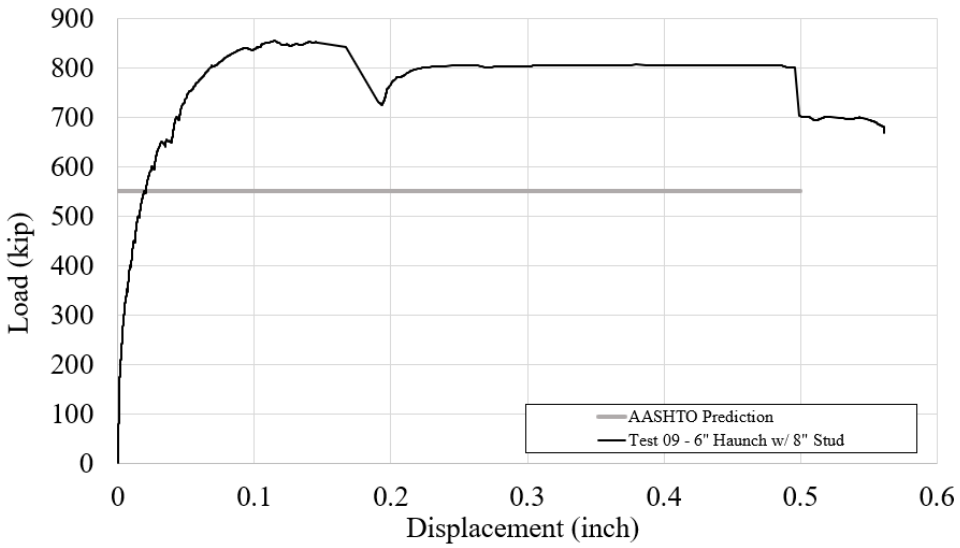

Figure 3.8.46 Load-Slip Curve of Specimen with Haunch Detachment

3.8.6. Global Haunch Failure

Global haunch failure, observed in Test 08, was characterized by a large failure plane through the haunch, as shown in Figure 3.8.47 and 3.8.48. The two specimens in Test 08 were intentionally poor-detailed. They involved a 9 in. haunch and 6 in. shear studs without other reinforcement detailing in the haunch. Although the test result reached 752 kips, 136% of the design capacity, this conclusion should be used with caution. It has not been clear if this failure mode is representative to the composite behavior of a real steel girder bridge. Such a poor detailing method should be avoided in the real construction. The load-slip curve of Test 08 is shown in Figure 3.8.49.

Figure 3.8.47 Global Haunch Failure 1

Figure 3.8.48 Global Haunch Failure 2

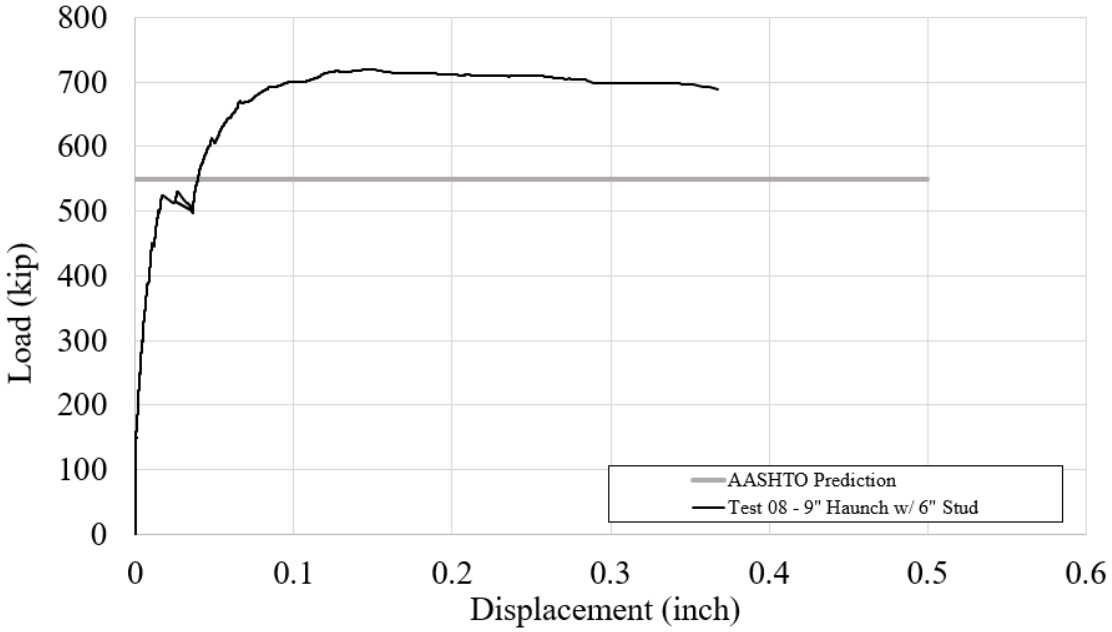

Figure 3.8.49 Load-Slip Curve of Specimen with Global Haunch Failure

3.8.7. Test Result Summary

In this section, all of the push-out test results of the steel girder specimens are included in Table 3.8.4.

Table 3.8.4 Steel Girder Push-out Test Result Summary

Failure Mode	Test #	Haunch Size & Detailing	Concrete Strength (psi)	Ultimate Capacity (kip)	% of Design Capacity
Shear Stud Failure	01	9” Haunch w/ Stacked Shear Studs	5508	868	157%
	02	9” Haunch w/ U-bar	5925	780	141%
	03	9” Haunch w/ Stirrups	5015	825	149%
	04	3” Haunch	4643	832	150%
	05	Zero Haunch	5061	751	136%
	17	15” Haunch w/ Stirrups, Single stud per row	5233	292	159%
Concrete Breakout	06	15” Haunch w/ Triple Stacked Shear Stud	4485	698	126%
	07	15” Haunch w/ U-bar	5529	612	110%
	11	12” Haunch w/ U-bar	4787	578	105%
	12	12” Haunch w/ U-bar (double spacing)	4885	571	103%
	13	12” Haunch w/ U-bar (double spacing, alternative location)	4383	610	110%
	14	12” Haunch w/ Stirrups	4485	636	115%
Haunch Widening	15	15” Haunch w/ Stirrups & Unconfined longitudinal rebars	4731	692	125%
	16	15” Haunch w/ Stirrups & Confined longitudinal rebars	4733	635	115%
Localized Concrete Crushing	10	9” Haunch w/ Stacked Stud @ 6”	4642	752	136%
Haunch Detachment	09	6” Haunch w/ 8” Stud	4773	851	154%
Global Haunch Failure	08	9” Haunch w/ 6” Stud	4643	752	136%

3.9. Conclusion

The results from large scale push out tests on 17 specimens were outlined in this chapter. A discussion of the observed failure modes, load levels, and ductility were discussed for each test. Based on the discussion of the push-out test results, several conclusions can be developed regarding the behavior of the shear connectors and preliminary design recommendations:

1) There were a range of different failure modes related to different detailing in the haunches of the specimens. These modes included failures in the shear studs and failures in the concrete. Despite variations in the various failure modes and ultimate capacities, all of the specimens reached the estimated design capacities. Therefore, the current TxDOT practices beyond the design specifications and guidelines provided specimens that reached required ultimate capacities. However, some of the details demonstrated better behavior than others and therefore, specific details should be encouraged when tall haunches are used. The following observations reinforce these conclusions.
2) Statistically, the average strength of the specimens with shear stud failure reached 149% of the design capacities, while the specimens with concrete failures had an average strength of 121% of the design capacities. The standard deviation of the shear stud failure capacities was 0.09, and 0.16 for the concrete failures. Therefore, modes involving shear stud failure typically had larger capacity and better predictability than the concrete failure modes.
3) The results demonstrated that the depth of the haunch can significantly affect the behavior of the shear connector, particularly if the haunch is unreinforced. Test 05 provides a baseline case with no haunch, while Test 04 had an unreinforced 3 in. haunch. The 3 in. haunch would often be classified as near the upper limit of a "standard" haunch. When the experiments of these two cases are compared with Test 08 that had an unreinforced 9 in. haunch, the behavior was significantly different resulting in a concrete failure. Therefore, haunches above standard values (such as a 3 in. haunch) should be suitably reinforced. Differences in failure modes can also be observed when considering Tests 01 and 06 that had unreinforced haunches but utilized stacked studs that penetrated into the deck. Test 01 had a 9-inch haunch and resulted in a shear stud failure, while Test 06 had a deeper 15 in. haunch and resulted in a concrete breakout failure. Therefore, larger haunch depths need to be accounted for with proper detailing to minimize the likelihood of concrete failures.
4) Penetration of the shear studs into the concrete deck positively impacts affects the shear connector behavior. Test 01 had a total stacked stud length of 12 in. embedded in the haunch of 9 in., which led to the largest ultimate capacity among the specimens with shear stud failure. The same observation was made in Test 06, which had 15 in. haunch and triple stacked shear studs, among the concrete breakout failure specimens. Therefore, at least 2 in. deck penetration is recommended if the haunch is deeper than 3 in.
5) Test 10 to 14 included either U-bars or stirrups with different spacings and identical haunch size (12 in.). These specimens experienced the same concrete failure mode (concrete breakout) and had similar ultimate capacities. Therefore, U-bars and stirrups are alternatives resulting in similar behavior in terms of the shear connector behaviors.
6) The comparison between Test 11 to 16 showed that providing longitudinal rebars confined by either U-bars or stirrups can improve the performance of the shear connector. Test 11 to 14 were associated with U-bars or stirrups and a 12 in. haunch with no

longitudinal reinforcement in the haunch region leading to relatively low capacities and relatively poor ductility. In the contrast, Test 15 and 16 were associated with a 15 in. haunch and confined longitudinal rebars in addition to stirrups, which resulted in larger ultimate shear capacities and better ductility compared to Test 11 to 14.

7) Test 01 and 10 showed that the shear connectors with tall haunches were more vulnerable to increased local stresses in the concrete surrounding the shear studs compared to small haunches. The experiments indicated that the increased concrete stresses can be mitigated by increasing the stud pitch. In the haunches deeper than 3 in., it is recommended to specify the minimum pitch as 12 in. This recommended pitch is also consistent with desired spacings for practical detailing so construction workers can walk on the steel flanges.
8) Just prior to failure, the maximum measured strain in the rebars in the stud failure specimens was 0.008, while strains as large as 0.04 were observed in the concrete failure specimens. As a result, concrete failure may result in higher demand on haunch reinforcement than shear stud failure.
9) More detailed design guidelines are given in Chapter 7 after the parametric study has been conducted. The next chapter introduces the push-out test results of the prestressed concrete (PSC) girder specimens.

Chapter 4. Task 4: Tall Haunches in Prestressed Girder

This chapter describes the testing of tall haunches on PSC girder specimens. Sections 4.1 and 4.2 provide details about specimen design and fabrication method, respectively. Sections 4.3 and 4.4 give testing method and instrumentation locations details. Section 4.5 provides test results. Finally, Section 4.6 includes summary remarks from the tests on PSC girders with tall haunches.

4.1. Specimen Design

The general approach for the PSC girder specimen design was similar to the procedures outlined in Chapter 3 for steel girder systems. Two specimens were arranged in a symmetric configuration. Both specimens were tested together and were horizontally cast at the same time to simulate the actual construction process and to keep the concrete properties identical. Rather than an actual PSC girder, all the specimens consisted of a simulated PSC girder. Similar to the specimens utilized in Roskos et al. (2018), a steel section having a top flange cast with 3 in. of concrete and welded with proper reinforcement detailing was used to simulate a PSC girder. The method captures that same concrete surface with R-bars that engage CIP concrete. As per TxDOT (2017), typical PSC girders often have a top flange width of 36 in. to 42 in. In this project, however, a W14×132, which has a 14.7-in. wide flange, was used as the base section for the simulated PSC girder in place of an actual TxGirder. The studs and bars R were welded to the W14×132 flange, and a 3-in.-thick concrete layer was cast on top of the steel member. This specimen arrangement is referred to as the simulated PSC girder in the remainder of this document and is shown in Figure 4.1.1. As mentioned in Chapter 2, a similar approach was incorporated in past TxDOT research (Roskos et al. 2018). Since the focus of the current research is on the haunch region, a specimen design that can capture the bond interface of the girder with the haunch was used. The simulated PSC girder captures the main features of TxGirder top flange detailing while allowing for details suitable for push-out tests. Because the steel shape was identical to that used for the steel specimens, the same formwork, testing fixtures and reaction frame as for the steel girder system outlined in Chapter 3 were used. A contractor familiar with TxDOT construction practices (Bexar Concrete Works, Ltd.) was hired to fabricate the simulated PSC girders.

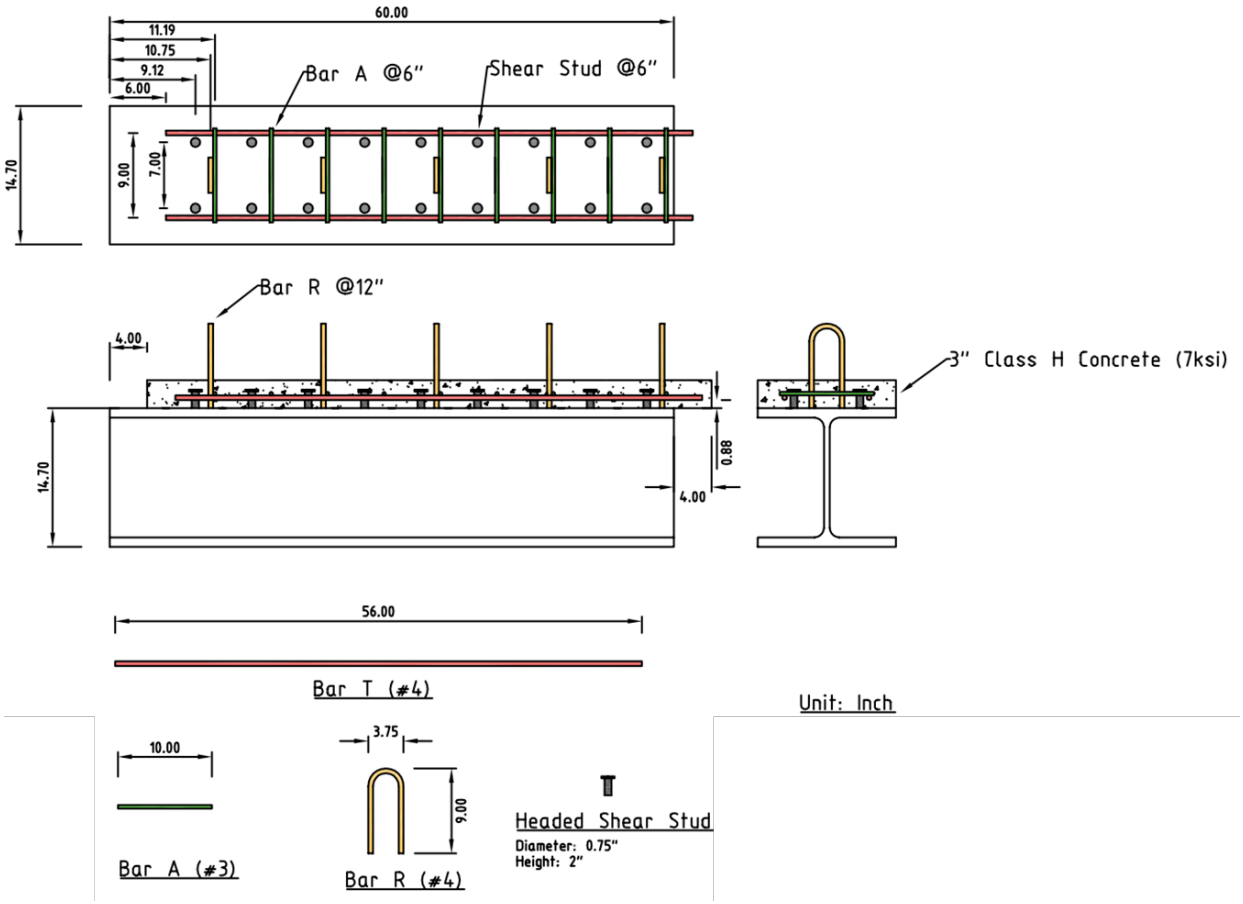

Figure 4.1.1 Simulated PSC Girder Detailing

The test matrix for PSC girders covered haunch depths that range from 2 in. to 12 in. Among the 36 constructed specimens, 18 are referred to as Specimen Group I and were designed to represent PSC girders with fully CIP haunches and slabs. The others, referred to as Specimen Group II, included PCPs. In all the specimens, the bars R configuration was as per TxDOT guideline (2017) and is shown in Figure 4.1.1. The length of bars R outside the 3-in.-thick slab was 6 in. The rebar details of each specimen are collectively shown in Appendix Section A3.1.

Appendix Section A3.1.1 shows plan and elevation sketches for Specimen Group I. Figure 4.1.2 shows a typical specimen for Group I. The 2-in. haunch specimens did not have any haunch reinforcement detailing. In the specimens with haunches taller than 2 in., Bars U, vertical stirrups, SGD rebar cages, and longitudinal rebar were used separately or together to improve the behavior of the tall haunches.

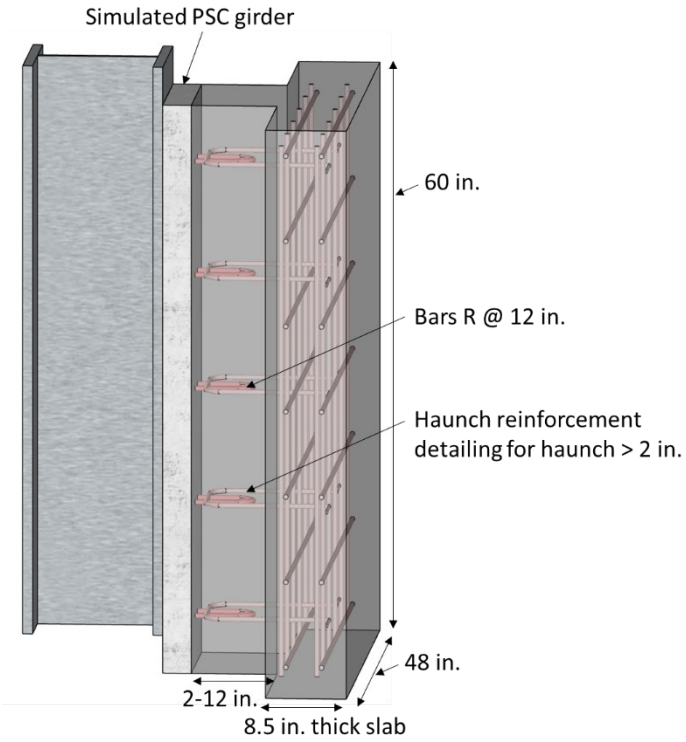

Figure 4.1.2 Typical Specimen for Group I

The Bars U detailing strategy for haunches in Specimen Group I is shown in Figure 4.1.3. Figure A3.1.1.3 shows a specimen with Bars U detailing in the haunch. The width of bar U was taken smaller than the reinforcement spacing in the middle of the slab (9 in.) for easier constructability on site. The extension lengths of Bars U into the top reinforcement of the slab were 4 in., and the clear cover on top and bottom were 3 in. and 1.25 in., respectively. The vertical stirrups strategy shown in Figure 4.1.4 was applied to two 9-in. CIP specimens (Figure A3.1.1.5). Although SGD is used by TxDOT for PSC girders with PCPs (see Chapter 2), researchers used the same reinforcement detailing combined with Bars U (Figure 4.1.5) for two specimens in Group I (Figure A3.1.1.8). Two special 2-in. haunch CIP specimens (Figure A3.2) were designed to develop composite behavior only through concrete cohesion. By eliminating bars R and Bars UP, the researchers intended to characterize the contribution of concrete cohesion to the composite behavior.

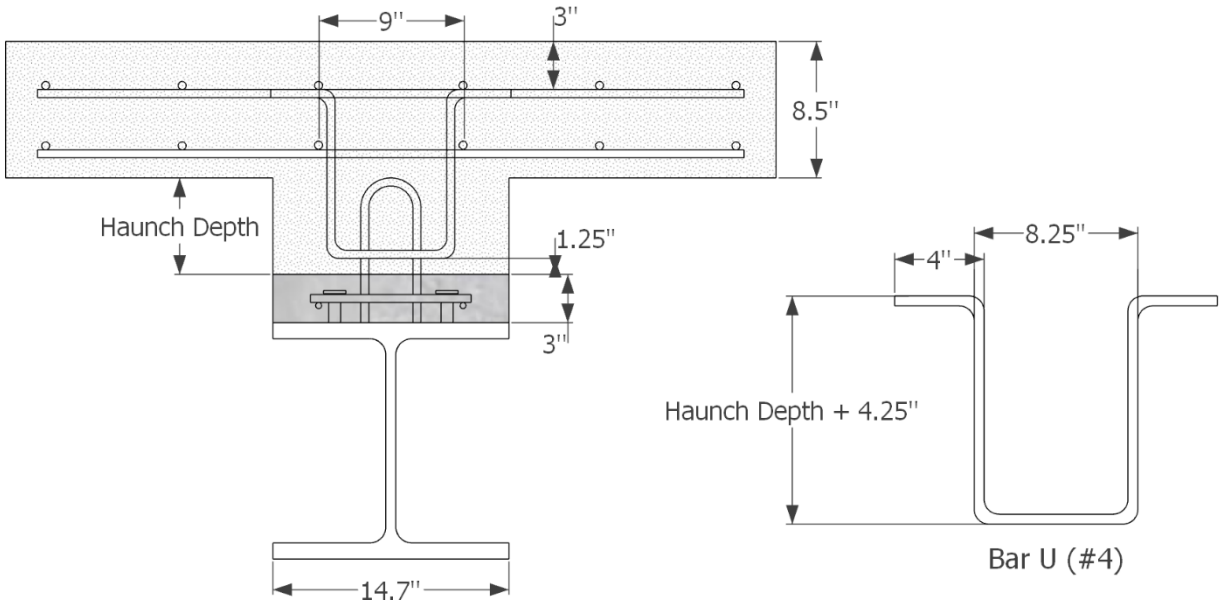

Figure 4.1.3 Configuration of Bar U in Specimen Group I

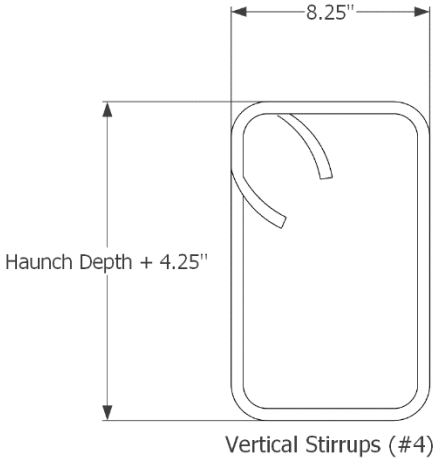

Figure 4.1.4 Configuration of Stirrups in Specimen Group I

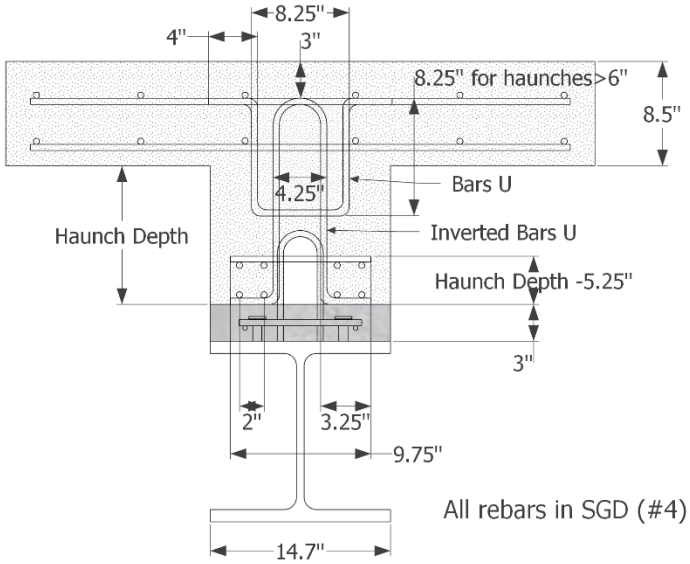

Figure 4.1.5 Configuration of SGD Rebar Cage in Specimen Group I

As mentioned previously, the specimens in Group II were fabricated with PCPs. The detailing for PCPs in the project (shown in Figure 4.1.6) follows guidelines from TxDOT (2019c). Specimen Group II is further subdivided into two groups: those with Bars UP (Figure 4.1.7) and those with SGD (Figure 4.1.8). Appendix Section A3.1.2 shows plan and elevation sketches for Specimen Group II.

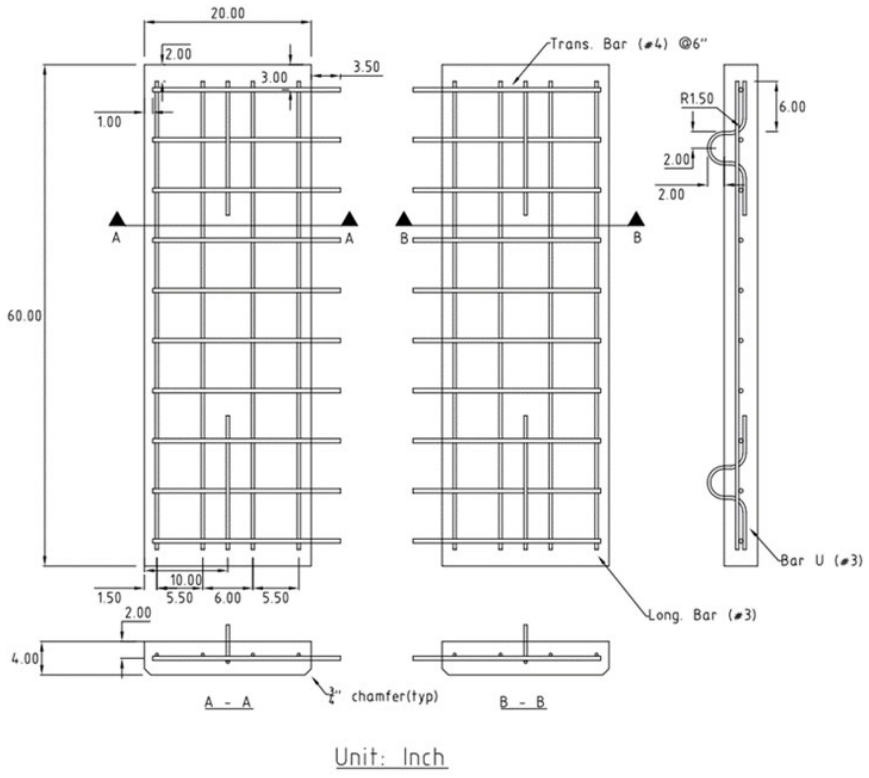

Figure 4.1.6 PCP Detailing

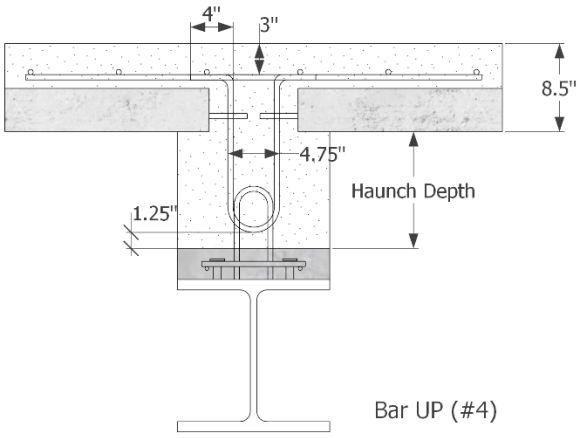

Figure 4.1.7 Configuration of Bar UP in Specimen Group II

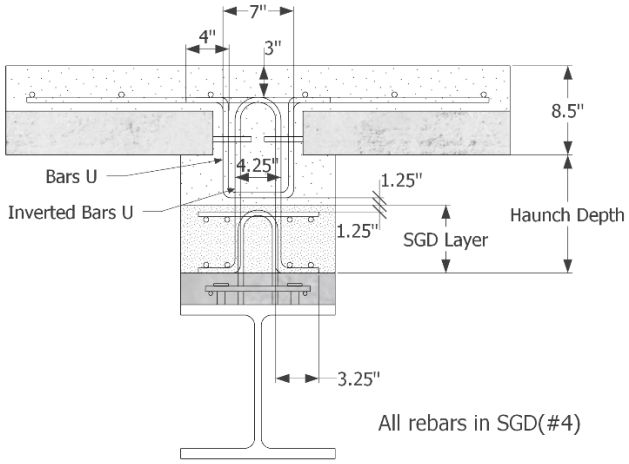

Figure 4.1.8 Configuration of SGD in Specimen Group II

Table 4.1.1 lists the 36 specimens fabricated for PSC girder specimen tests. Test results are discussed in Section 4.5. The specimens in italics were tested with the steel spreader beam (SB_S), and all other specimens were tested with the prestressed spreader beam (SB_P). Both spreader beam types are explained in Section 4.3.

Table 4.1.1 PSC Girders Specimen Test Matrix

Specimen No.	Haunch Depth (in.)	Specimen Group	Haunch Reinforcement Detailing	No. of Bars R
1, 2	2	I	-	-
3, 4	*2*	*I*	-	*5*
5, 6	2	I	-	5
7, 8	6	I	Bars U	5
9, 10	*9*	*I*	*Bars U*	*5*
11, 12	9	I	Stirrups	5
13, 14	12	I	Bars U	5
15, 16	12	I	SGD rebar cage (entire haunch and slab cast together)	5
17, 18	12	I	Bars U with longitudinal rebars	5
19, 20	*2*	*II*	-	*5*
21, 22	2	II	-	5
23, 24	6	II	Bars UP	5
25, 26	6	II	SGD (3-in. layer cast first) with Bars U	5
27, 28	*9*	*II*	*Bars UP*	*5*
29, 30	9	II	SGD (5-in. layer cast first) with Bars U	5
31, 32	12	II	Bars UP	5
33, 34	12	II	Bars UP	3
35, 36	12	II	SGD (8-in. layer cast first) with Bars U	5

4.2. Fabrication Method

TxDOT Class H concrete was specified for the simulated PSC girder concrete and PCPs. The minimum compressive strength required for these two concrete layers was 7 ksi. The simulated PSC girders with bolt holes on one flange and bars R and shear studs on the other were fabricated by Bexar Concrete Works, Ltd. Figures 4.2.1-4.2.2 show simulated PSC girders before and after concrete casting. Researchers had the PCPs utilized for Specimen Group II also fabricated by the same contractor (Figure 4.2.3-4.2.4).

TxDOT Class S concrete was provided for the SGD and CIP layers in all specimens. The minimum specified compressive strength for these was 4 ksi. The SGD and CIP layers were constructed by researchers at FSEL. This work included tying rebar cages, connecting and arranging strain gauges, performing concrete casting, and assembling the cured specimens. Figures 4.2.5-4.2.11 show the fabrication steps needed to prepare the specimens. The contact surfaces between different concrete layers were intentionally roughened as is done on the TxDOT site. The concrete material properties for the CIP layer were tested after 28 days and for all the layers on the day of testing using cylinders prepared during casting.

Figure 4.2.1 Simulated PSC Girder Before Concrete Casting

Figure 4.2.2 Simulated PSC Girder Concrete Casting

Figure 4.2.3 PCPs Before Concrete Casting

Figure 4.2.4 PCPs After Concrete Casting

Figure 4.2.5 SGD Rebar Cages in Formwork

Figure 4.2.6 CIP Rebar Layer with Strain Gauges

Figure 4.2.7 CIP Formwork with Rebar Cages

Figure 4.2.8 Specimen Vibration During Concrete Casting

Figure 4.2.9 Cylinder Preparation During Concrete Casting

Figure 4.2.10 Levelling of Top Concrete Surface

Figure 4.2.11 Specimens Assembled

Tables 4.2.1 and 4.2.2 show the concrete material properties for Specimen Group I and II, respectively.

Table 4.2.1 Specimen Group I Concrete Material Properties

Specimen No.	Haunch Depth (in.)	Haunch Reinforcement Detailing	No. of Bars R	Spreader Beam Used	Concrete Strength (ksi)	
					CIP	PSC
1, 2	2	-	-	SB_P	4.7	9.5
3, 4	2	-	5	SB_S	5.3	9.8
5, 6	2	-	5	SB_P	4.9	7.8
7, 8	6	Bars U	5	SB_P	5.4	10.7
9, 10	9	Bars U	5	SB_S	4.6	9.2
11, 12	9	Stirrups	5	SB_P	3.8	8.6
13, 14	12	Bars U	5	SB_P	5.1	8.8
15, 16	12	SGD with Bars U rebar cage (entire haunch and slab cast together)	5	SB_P	5.2	10.5
17, 18	12	Bars U with longitudinal rebars	5	SB_P	3.8	8.9

Table 4.2.2 Specimen Group II Concrete Material Properties

Specimen No.	Haunch Depth (in.)	Haunch Reinforcement Detailing	No. of Bars R	Spreader Beam Used	Concrete Strength (ksi)			
					CIP	SGD	PCP	PSC
19, 20	2	-	5	SB_S	4.8		7.1	8.9
21, 22	2	-	5	SB_P	4.0		7.0	9.0
23, 24	6	Bars UP	5	SB_P	5.9		7.0	9.2
25, 26	6	SGD (3-in. layer cast first) with Bars U	5	SB_P	3.9	4.6	7.1	9.4
27, 28	9	Bars UP	5	SB_S	5.3		7.1	9.3
29, 30	9	SGD (5-in. layer cast first) with Bars U	5	SB_P	6.2	4.9	7.1	9.3
31, 32	12	Bars UP	5	SB_P	4.5		7.4	9.6
33, 34	12	Bars UP	3	SB_P	5.4		7.3	10.7
35, 36	12	SGD (8-in. layer cast first) with Bars U	5	SB_P	5.1	4.8	6.9	9.5

The material properties for other components in the specimens were also as per TxDOT guidelines (2023a, 2023b). Bars R were A706 Grade 60 #4 steel, and all other reinforcing Bars U were A615 Grade 60 #4. The yield and ultimate strength for bars R specified by the fabricator were 66.5 ksi and 92.6 ksi, respectively. The average yield and ultimate strength measured for other reinforcing bars were 63.5 ksi and 98.2 ksi, respectively. The steel sections used were A992 Grade 50 W14×132 with a specified yield and ultimate strength of 50 ksi and 65 ksi, respectively. The shear studs used in the simulated PSC girder had a specified tensile strength of 60 ksi.

4.3. Testing Method

The push-out tests for both steel and PSC girder specimens were performed on the same test setup (Figure 4.3.1). The spreader beam was modified to load the simulated PSC girder-haunch interface for the PSC girder specimens. The difference between SB_S and SB_P can be seen in Figure 4.3.1 where a PSC girder specimen is shown on the left side of the figure, and a steel girder specimen is shown on the right side of the figure. A few of PSC girder push-out tests performed (discussed in Section 4.5) used the SB_S. Thus, the load was applied to the interface between the steel section and the simulated PSC girder. All remaining tests were performed with the SB_P, where the interface between the simulated PSC girder and haunch was loaded.

Similar to the steel girder specimens, all the layers of concrete in the girder, haunch, and deck for PSC girder specimens were cast horizontally. The testing procedure was the same as the steel girder specimen tests. A minimum of two load cycles of 50 - 150 kips were applied before loading the specimens to failure. The average loading rate was 0.5 kip/sec. At the peak load for each test, there was a sudden drop (minimum 20%) to a smaller residual load. The test was stopped at this point due to the limitations of the setup. LPs were used for all tests to measure relative slip between the following components: steel and simulated PSC girder, simulated PSC girder and haunch, SGD layer in the haunch and CIP layer in the haunch, and the haunch and PCP. The LP locations are described in more detail in Section 4.4. Strain gauges were provided at some critical locations on the reinforcing bars and steel webs and are described further in Section 4.4.

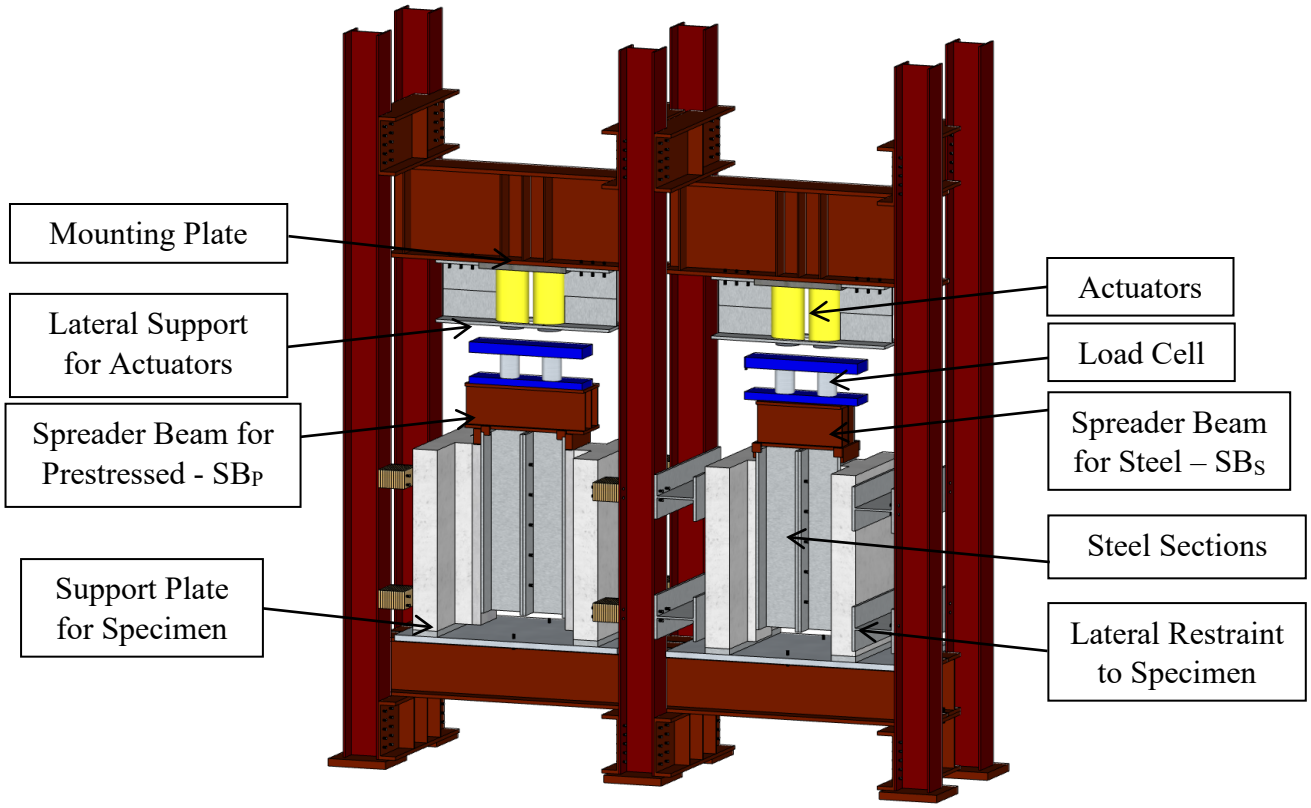

Figure 4.3.1 Test Setup

4.4. Instrumentation Locations

This section describes the instrumentation locations for Specimen Groups I and II. Figure 4.4.1 shows the locations of LPs for Specimen Group I. LPs 1 and 2 are positioned at the simulated PSC girder-haunch interface, and LP A is located at the steel section-simulated PSC girder interface. Figures 4.4.2 and 4.4.3 show the locations of LPs for Specimen Group II with and without SGD, respectively. Table 4.4.1 indicates the locations of LPs for Specimen Group II. Total load versus average slip plots for various interfaces are generated using data from LPs. The total load represents the load applied during each test, with the general assumption that each specimen carries half of the total applied load. The average slip values for LPs 1 and 2 are calculated for the failed specimen to analyze the behavior of the simulated PSC-girder haunch interface. The analysis of LP results is presented in Section 4.5. Individual total load versus average slip for all tests are shown in Appendix Sections A3.3.1 and A3.3.2 for Specimen Groups I and II respectively. Test 8 (2-in. haunch specimens tested with SB_S) did not have LPs at the simulated PSC girder-steel section and haunch-PCP interfaces.

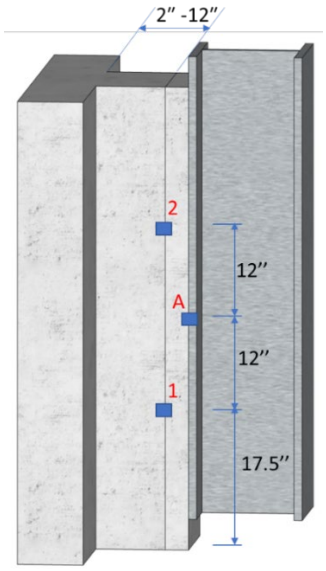

Figure 4.4.1 Specimen Group I LP Locations

Table 4.4.1 Specimen Group II LP Schematics

	Simulated PSC Girder – Steel Interface	Simulated PSC Girder – Haunch Interface	Haunch – PCP Interface	Haunch CIP – Haunch SGD Interface
PCP Specimens without SGD	A	1, 2	B	-
PCP Specimens with SGD	A	1, 2,	B	C

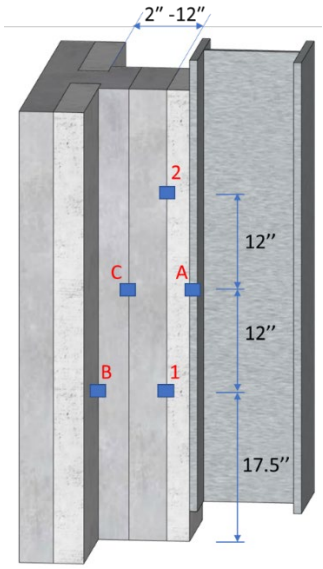

Figure 4.4.2 Specimen Group II with SGD LP Locations

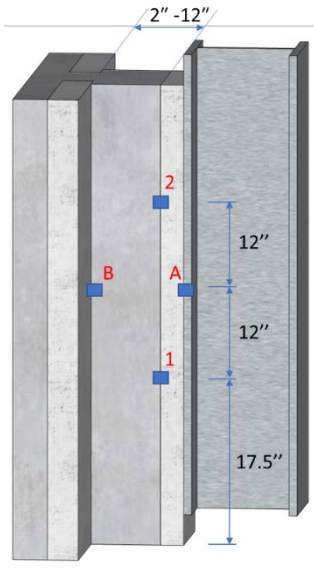

Figure 4.4.3 Specimen Group II without SGD LP Locations

Figure 4.4.4 shows the locations of strain gauges provided on the steel web for Specimen Groups I and II. These strain gauges are provided to understand the effects of load eccentricity in push-out tests for tall haunches. Figure 4.4.5 shows the load application points and the support points for the PSC girder specimens considered in this study. The applied load is resisted by the cohesive stresses between the interfaces and the shear resistance due to friction from the reinforcement bars. Because the forces are not concentric, a counterclockwise moment will act on the specimen shown in Figure 4.4.5. This moment will be resisted by tensile and compressive forces (shown in green) in the shear reinforcement. The resultant forces in the surrounding concrete will be compressive on the top and tensile near the specimen base. The applied strain gauges on the web can provide information about the relative difference between applied moments for different haunch sizes. Strain versus load plots for the steel web, which reveal this relationship, are shown in Section 4.5 for selected tests. The remaining tests can be found in Appendix Sections A3.4.1 and A3.4.2 for Specimen Groups I and II respectively.

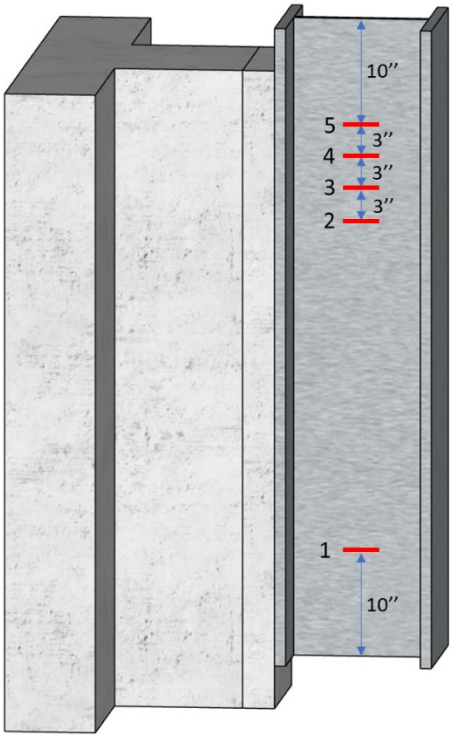

Figure 4.4.4 Steel Web Strain Gauges Locations

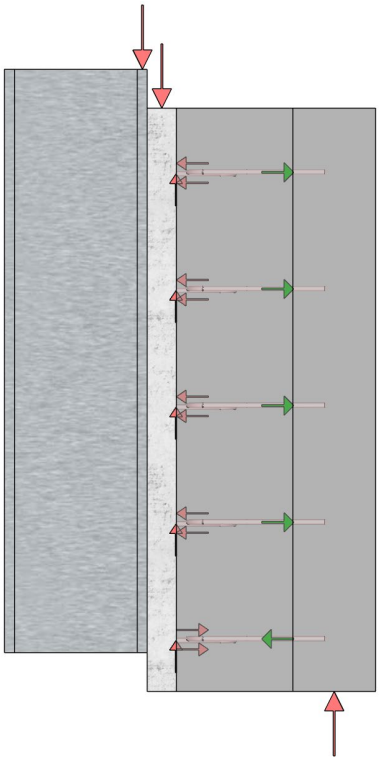

Figure 4.4.5 Force Mechanism in Push-out Tests

Figures 4.4.6 and 4.4.7 depict the locations of strain gauges on Bars U/Bars UP and SGD, respectively. Section 4.5 provides the strain versus load plots for haunch reinforcement, offering insights into the behavior of the reinforcement under load. Some of the strain gauges were damaged during concrete casting; thus, the results obtained from those are not provided.

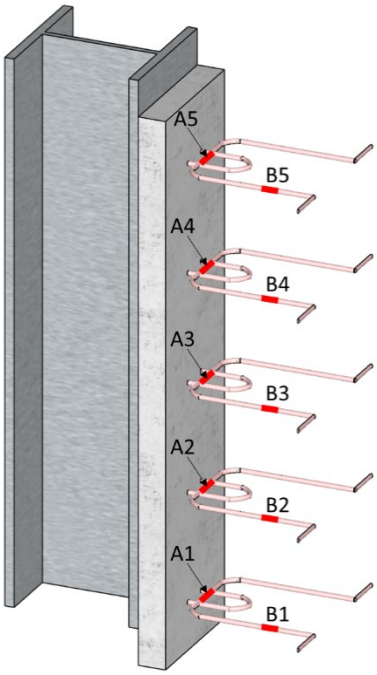

Figure 4.4.6 Strain Gauge Locations for Bars U Haunch Detailing

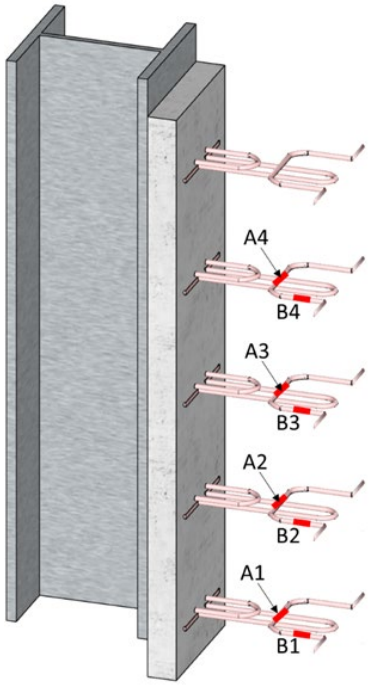

Figure 4.4.7 Strain Gauge Locations for SGD Rebar Haunch Detailing

4.5. Test Results

This section describes the test results and observations for the PSC girder push-out tests. The experimental results are compared with AASHTO LRFD (2020), CEN (2004b), and ACI 318 (2019) predicted shear resistance. Sample calculations of design interface shear resistance from these guidelines are presented in Appendix Section A3.2.

4.5.1. Specimen Group I: CIP Specimens Results

The test results for Specimen Group I are explained in Section 4.5.1.1. Section 4.5.1.2 compares the test results with the predicted capacities.

4.5.1.1. Test Results

In Specimen Group I, the researchers tested 18 specimens as shown in Table 4.5.1. As mentioned in Section 4.3, the load drops suddenly at the test failure load of the specimen. The remaining load carried by the specimens is referred to as residual load (Table 4.5.1). Out of the nine tests performed, two used the SB_S shown in Figure 4.3.1. All other tests were performed with the SB_P. The haunch depth varied between 2 in. and 12 in. The detailing methods used for haunches deeper than 2 in. are discussed in Section 4.1 and shown in Figures 4.1.3, 4.1.4, and 4.1.5. As mentioned previously, the 2-in. haunch specimens with no bars R were tested to quantify the cohesion between the simulated PSC girder and haunch.

Table 4.5.1 Specimen Group I Tests

Test No.	Specimen No.	Haunch Depth (in.)	Haunch Reinforcement Detailing	No. of Bars R	Spreader Beam Used	Test Failure Load (kips)	Residual Load (kips)
1	1, 2	2	-	-	SB_P	742	0
2	3, 4	2	-	5	SB_S	1105	143
3	5, 6	2	-	5	SB_P	997	409
4	7, 8	6	Bars U	5	SB_P	728.5	317
5	9, 10	9	Bars U	5	SB_S	1016	327
6	11, 12	9	Stirrups	5	SB_P	772	393
7	13, 14	12	Bars U	5	SB_P	801	257
8	15, 16	12	Bars U with longitudinal rebars	5	SB_P	627	393
9	17, 18	12	SGD with Bars U rebar cage (entire haunch and slab cast together)	5	SB_P	717	176

The failure modes observed for Specimen Group I can be broadly divided into the following:

a. simulated PSC girder cracking/failure
b. simulated PSC girder-haunch interface debonding and/or failure
c. simulated PSC girder-haunch interface debonding combined with haunch-cracking

a. Simulated PSC girder cracking/failure

The first type of failure mode was observed in Tests 2 and 5 (Figures 4.5.1 and 4.5.2) where the SB_S was used to load the specimens. These tests had a significantly higher specimen capacity compared to the tests performed with SB_P as can be seen in Table 4.5.1. Girder failure was observed in these specimens because of its special design and loading method. Because this failure mode is not expected in real bridges, the researchers fabricated another spreader beam (SB_P) for the PSC girder specimens to better simulate the interface behavior between PSC girders and haunches under actual field conditions. The capacity obtained from this test would therefore be unreliable for the shear interface in consideration. These tests are still useful because they provide insight into the behavior of specimens with different haunch sizes.

Figure 4.5.1 Test 2
(2-in. Haunch SB_S)

Figure 4.5.2 Test 5
(9-in. Haunch with Bars U)

The capacity of 9-in. haunch specimens (Test 5) was lower than the 2-in. haunch specimens (Test 2). The 2-in. haunch specimens did not have major cracks in the haunch, unlike the 9-in. haunch specimens that had major diagonal cracks in the haunch combined with girder failure. The diagonal crack at the specimen failure occurred near the base. This behavior has also been observed for other specimens in Group I loaded with SB_P (shown subsequently in this section). A possible explanation for this crack is the combined flexure and shear stresses on tall haunches in push-out tests (Section 4.4). The combination of shear and tensile stresses near the specimen base will result in major concrete cracking close to or at the failure load.

Figures 4.5.3 and 4.5.4 provide total load versus average slip plots for these tests at the simulated PSC girder-haunch and simulated PSC girder-steel interfaces, respectively. These figures show that at least half the capacity is provided by the cohesive strength at the interface, and the relative slip increased with a lower stiffness value after the loss of cohesion at the shear interface. The maximum slip observed at the simulated PSC girder-steel interface for Tests 2 and 5 is almost twice the slip observed for other tests (Figure 4.5.5). The slip at this interface, therefore, reduced when SB_S was replaced with SB_P.

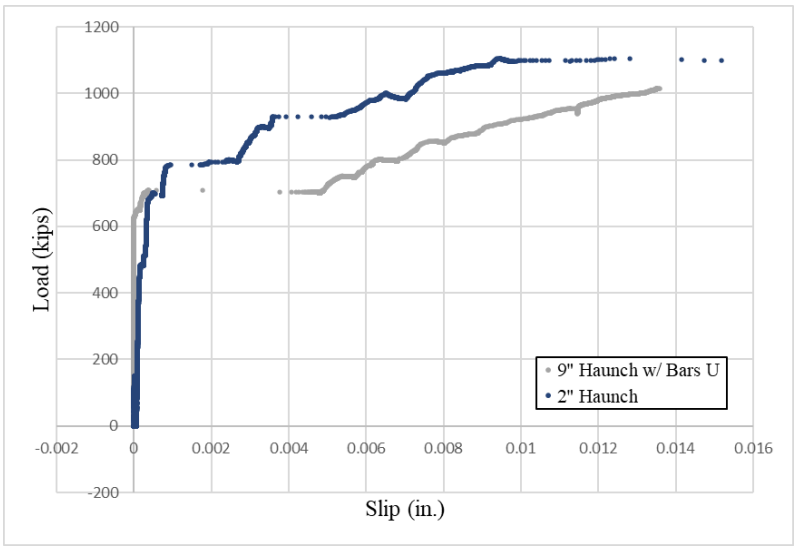

Figure 4.5.3 Load versus Slip at Simulated PSC Girder-Haunch Interface (SB_S)

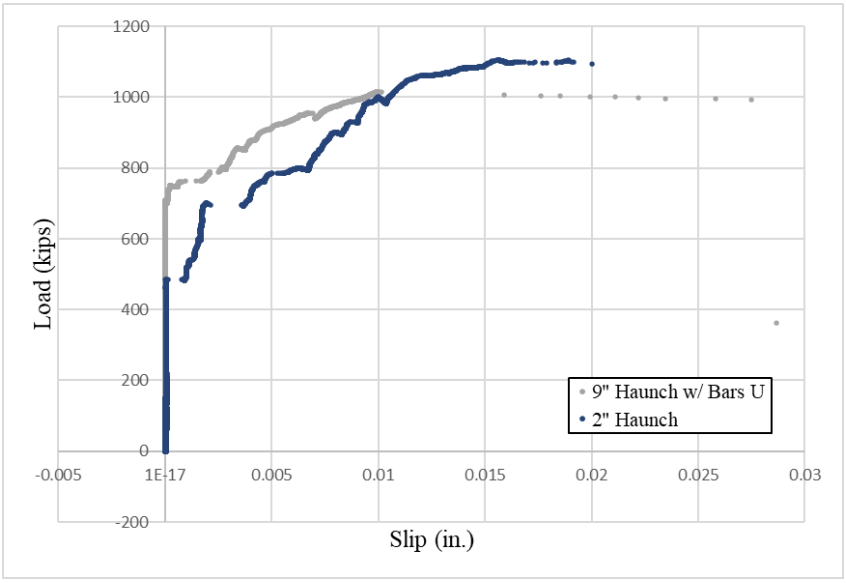

Figure 4.5.4 Load versus Slip at Simulated PSC Girder-Steel Interface (SB_S)

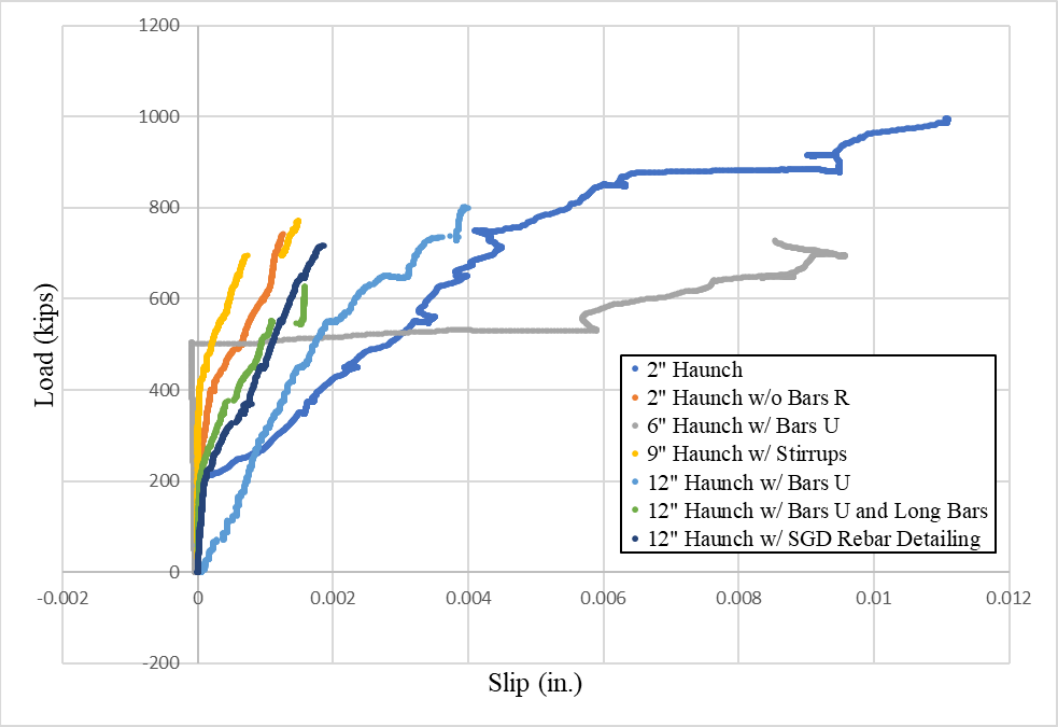

Figure 4.5.5 Load versus Slip at Simulated PSC Girder-Steel Interface (SB_P)

b. Simulated PSC girder-haunch interface debonding and/or failure

The second type of failure mode is observed in Tests 1 (Figure 4.5.6), 3 (Figure 4.5.7), and 9 (Figure 4.5.8). Test 1 (2-in. haunch specimens with no bars R) had complete separation at the simulated PSC girder-haunch interface when the failure load was reached. Test 3 (2-in. haunch specimens with bars R) also had a failure at the simulated PSC girder-haunch interface due to debonding, followed by yielding of the reinforcement bars. Comparing the capacities of the specimens with and without bars R shows that bars R provide approximately 25% of the total capacity in the specimens with bars R. The cohesion or aggregate locking and shear friction between concrete particles (mentioned in Chapter 2) provides the major portion of the capacity in these specimens. Figure 4.5.9 shows the relative slip at the simulated PSC-girder haunch interface is significantly higher for Test 3 compared to Test 1. Also, Test 1 dropped from 742 kips to 0 (Table 4.5.1) at the peak load and therefore had a more brittle failure compared to Test 3.

Figure 4.5.6 Test 1
(2-in. Haunch with No Bars R)

Figure 4.5.7 Test 3
(2-in. Haunch SB_P)

Figure 4.5.8 Test 9
(12-in. Haunch with SGD Rebar Cage)

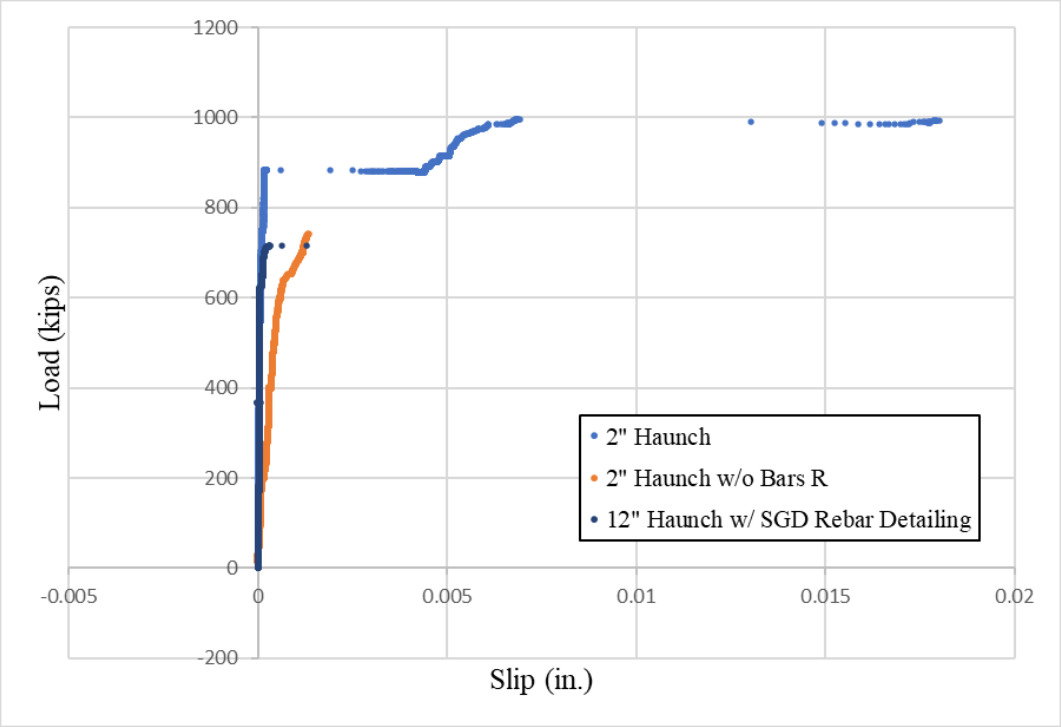

Figure 4.5.9 Load versus Slip at Simulated PSC Girder-Haunch Interface (SB_P) (Debonding Failure)

Test 9 had an SGD rebar cage with 12-in. haunch specimens. Although these specimens did not have any cracks in the haunch, their peak load was lower than that of 2-in. haunch specimens with bars R. Furthermore, the peak load of Test 9 specimens decreased significantly from 717 kips to 176 kips (Table 4.5.1), indicating a notable reduction in load-carrying capacity. This drop occurred during the initiation of interface debonding, with a slip that was insufficient to fully activate the reinforcement bars (Figure 4.5.9). Therefore, the shear reinforcement's contribution to the peak load is negligible. The strain versus load plots for haunch reinforcement in Test 9 (Figures 4.5.10 and 4.5.11) reveal negligible strain values in Bars U (<0.000015), also indicating a minimal contribution from the shear reinforcement. With minimal participation from the shear reinforcement, 12-in. haunch specimens can have a lower peak load than the 2-in. haunch specimens. Another explanation for the earlier debonding failure is the larger load eccentricity in 12-in. haunch specimens compared with 2-in. haunch specimens. This can be seen from the steel web strain versus load plots for Tests 3 (Figure 4.5.12) and 9 (Figure 4.5.13). These figures show that the web strain gauge nearest to the specimen base has about 2-3 times higher strains for 12-in. haunch specimens than 2-in. haunch specimens. The tensile forces combined with the shear forces lead to an earlier debonding failure and smaller ultimate capacity for Test 9.

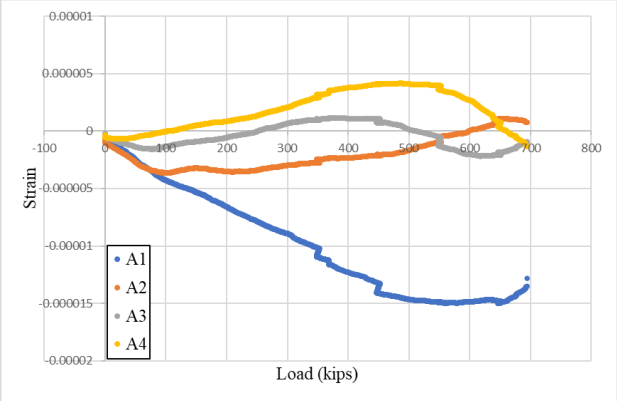

Figure 4.5.10 Strain versus Load Plot 1 for Haunch Reinforcement in Test 9

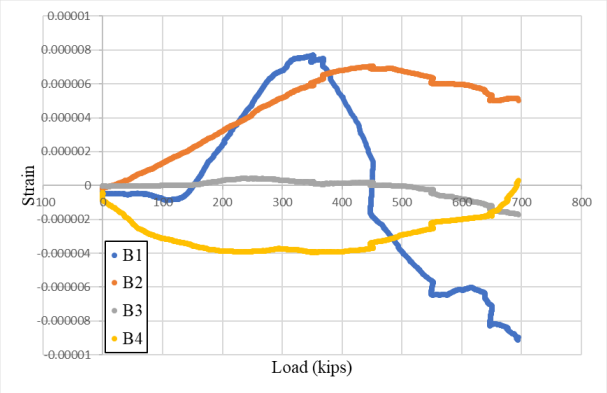

Figure 4.5.11 Strain versus Load Plot 2 for Haunch Reinforcement in Test 9

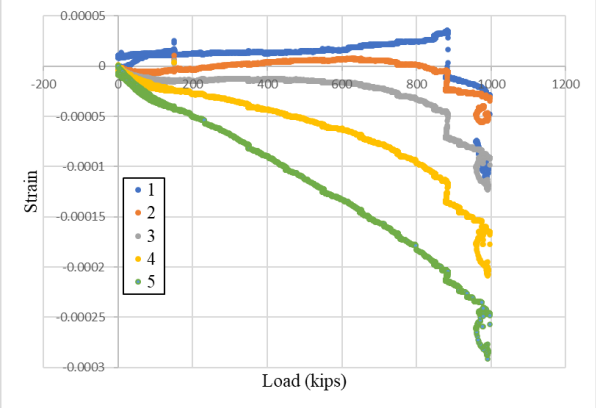

Figure 4.5.12 Strain versus Load Plots for Steel Web of Simulated PSC Girder in Test 3

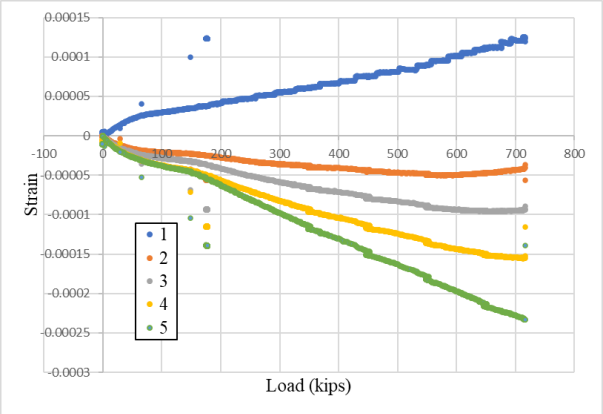

Figure 4.5.13 Strain versus Load Plot for Steel Web of Simulated PSC Girder in Test 9

c. Simulated PSC girder-haunch interface debonding combined with haunch-cracking

The third type of failure mode is observed in Tests 4 (Figure 4.5.14), 6 (Figure 4.5.15), 7 (Figure 4.5.16), and 8 (Figure 4.5.17). All four tests saw debonding failure combined with the cracking of the haunch near the specimen base. This response also can be explained by the combination of shear and tensile stresses for tall haunches in push-out tests. First, the cohesive bonds are exceeded by the applied load. These cracks are already present before the complete loss of cohesive bond. As a result of these cracks, strains are induced in the Bars U or vertical stirrups, which can be observed in the strain versus load plots for haunch reinforcement in the mentioned tests (Figures 4.5.18-4.5.25). Additionally, Figure 4.5.26 presents the total load versus slip plot at the simulated PSC girder-haunch interface for these tests, showing that the load-carrying capacity continues to increase (as shown in Figure 4.5.26) until the combined stresses are sufficient to cause the failure of the concrete strut near the base of the specimen (as discussed in Chapter 2).

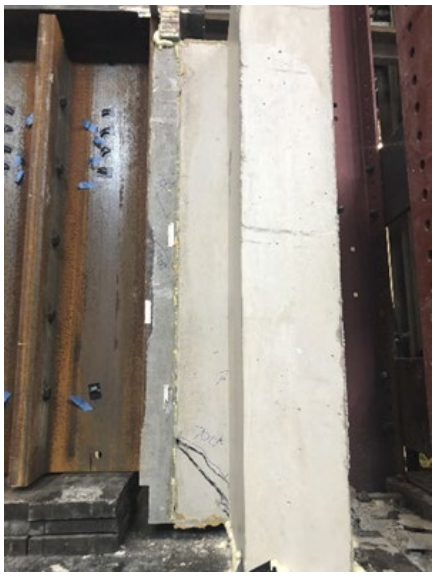

Figure 4.5.14 Test 4
(6-in. Haunch with Bars U)

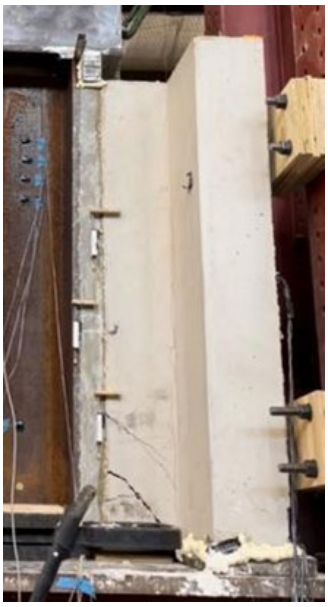

Figure 4.5.15 Test 6
(9-in. Haunch with Vertical Stirrups)

Figure 4.5.16 Test 7
(12-in. Haunch with Bars U)

Figure 4.5.17 Test 8
(12-in. Haunch with Bars U and Longitudinal Bars)

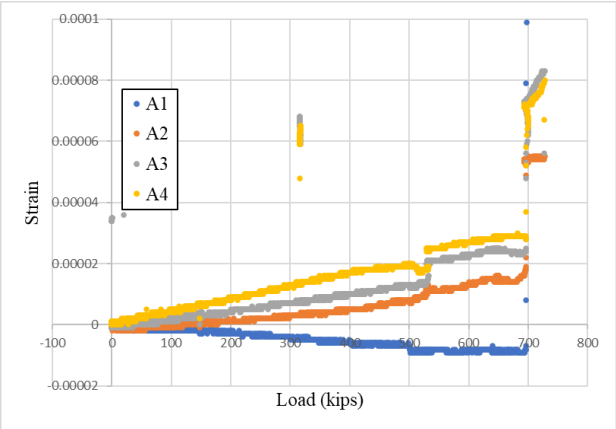

Figure 4.5.18 Strain versus Load Plot 1 for Haunch Reinforcement in Test 4

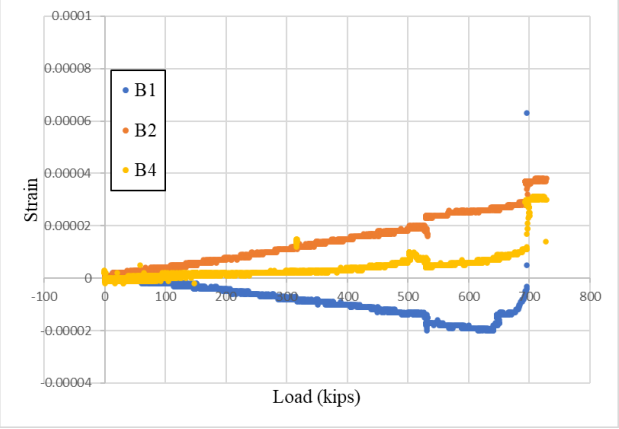

Figure 4.5.19 Strain versus Load Plot 2 for Haunch Reinforcement in Test 4

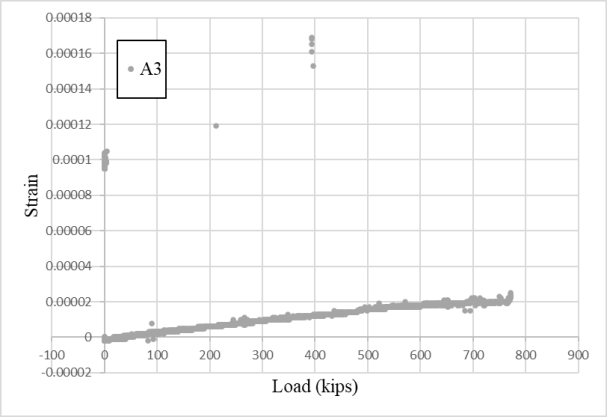

Figure 4.5.20 Strain versus Load Plot 1 for Haunch Reinforcement in Test 6

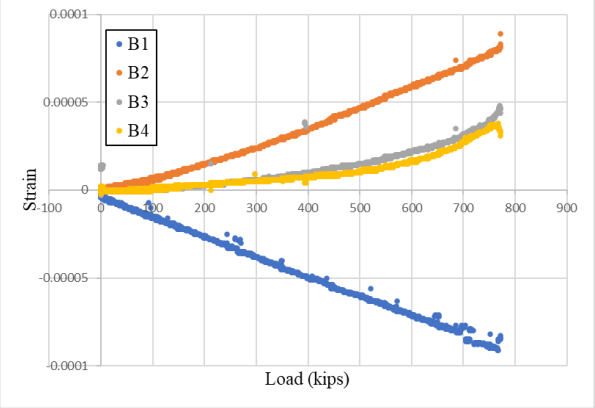

Figure 4.5.21 Strain versus Load Plot 2 for Haunch Reinforcement in Test 6

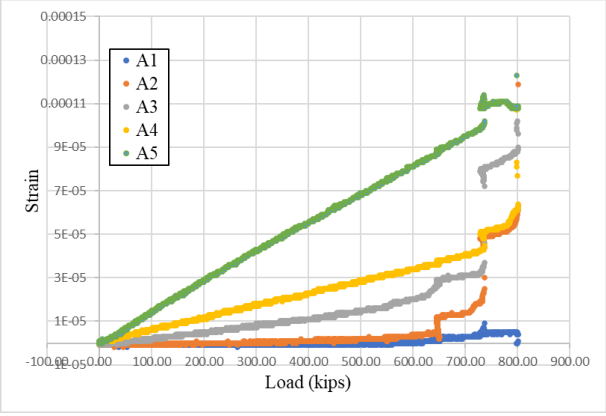

Figure 4.5.22 Strain versus Load Plot 1 for Haunch Reinforcement in Test 7

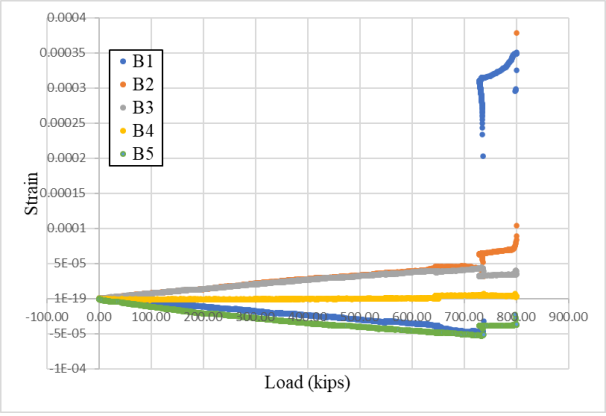

Figure 4.5.23 Strain versus Load Plot 2 for Haunch Reinforcement in Test 7

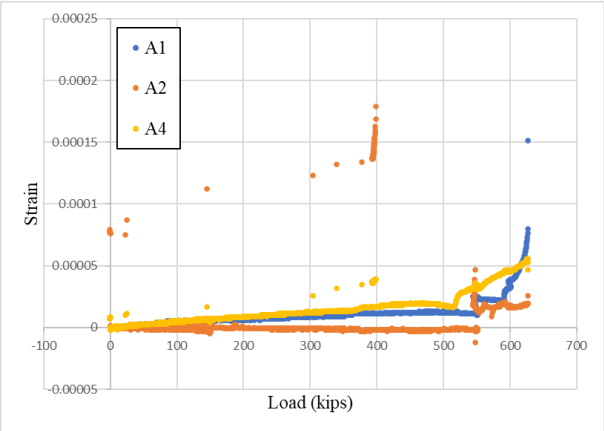

Figure 4.5.24 Strain versus Load Plot 1 for Haunch Reinforcement in Test 8

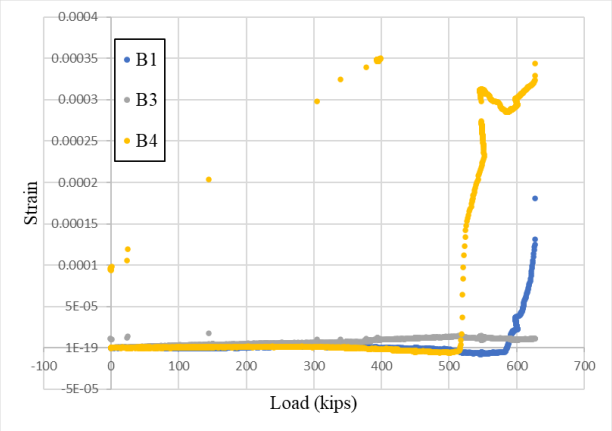

Figure 4.5.25 Strain versus Load Plot 2 for Haunch Reinforcement in Test 8

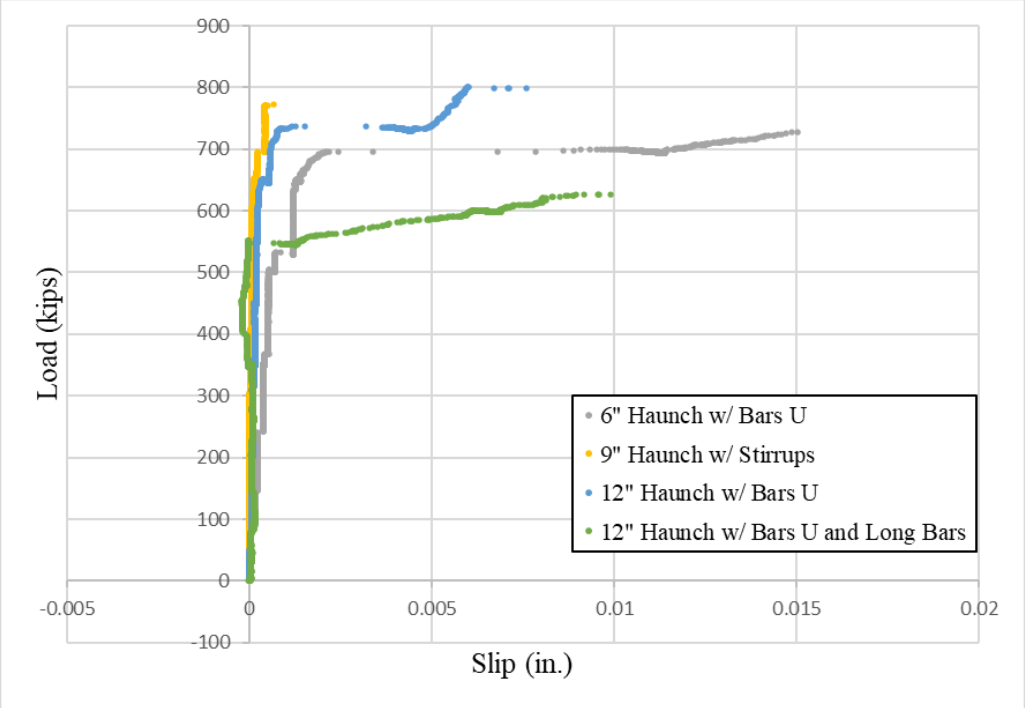

Figure 4.5.26 Load versus Slip at Simulated PSC Girder-Haunch Interface (SB_P) (Debonding Failure combined with Haunch Cracking)

Figures 4.5.19, 4.5.21, and 4.5.23 show the increase in tensile stresses in reinforcement bars with an increase in haunch depth. Higher tensile stresses in reinforcement bars imply higher compressive forces on the shear interface (Section 4.4). The application of compressive stresses will provide a larger clamping effect by the bars R, leading to an increase in capacity measured from the tests. This phenomenon can explain the increase in peak load with an increase in haunch depth for Tests 4, 6, and 7.

The detailing provided for Test 6 (vertical stirrups) behaved similarly in terms of peak load and failure mode to the detailing provided for Tests 4 and 7 (Bars UP). Figure 4.5.26 shows the relative slip at peak load for Test 6 is smaller than for Tests 4 and 7. The residual load, however, is larger for Test 6 compared to Tests 4 and 7 (Table 4.5.1). The confinement provided by vertical stirrups may provide more residual capacity and less cracking, leading to a smaller slip.

Test 8 (12-in. haunch with longitudinal bars) also experienced the third type of failure mode, but the capacity was lower relative to other specimens. Figure 4.5.26 shows the stiffness reduced due to cohesion loss at a relatively smaller load for this specimen. The concrete used for these specimens had a higher slump test value (6.5 in.) compared to other specimens and the TxDOT requirement for class S concrete (3-5 in.). Higher water content can cause more drying shrinkage and lead to cracking in the specimens before testing. After the cohesive bond loss, the bars R provide an increase in capacity until the diagonal crack occurs near the specimen. Figures 4.5.24 and 4.5.25 show an increase in Bars U strains after the load was sufficient to cause cohesive bond loss.

4.5.1.2. Comparison with Predicted Capacities

The capacity of specimens with no bars R, when equated with the AASHTO LRFD (2020) equation, gives a cohesion factor of about 0.4. The suggested value is 0.28; therefore, the experimental result for this test is on the conservative side. Figure 4.5.27 shows that aside from Test 8 (12-in. haunch specimen with Bars U and longitudinal bars), all specimens had a higher capacity than that estimated using Equation 6.6 from the AASHTO LRFD (2020). The lower capacity obtained in Test 8 can be attributed to poor concrete properties for these specimens.

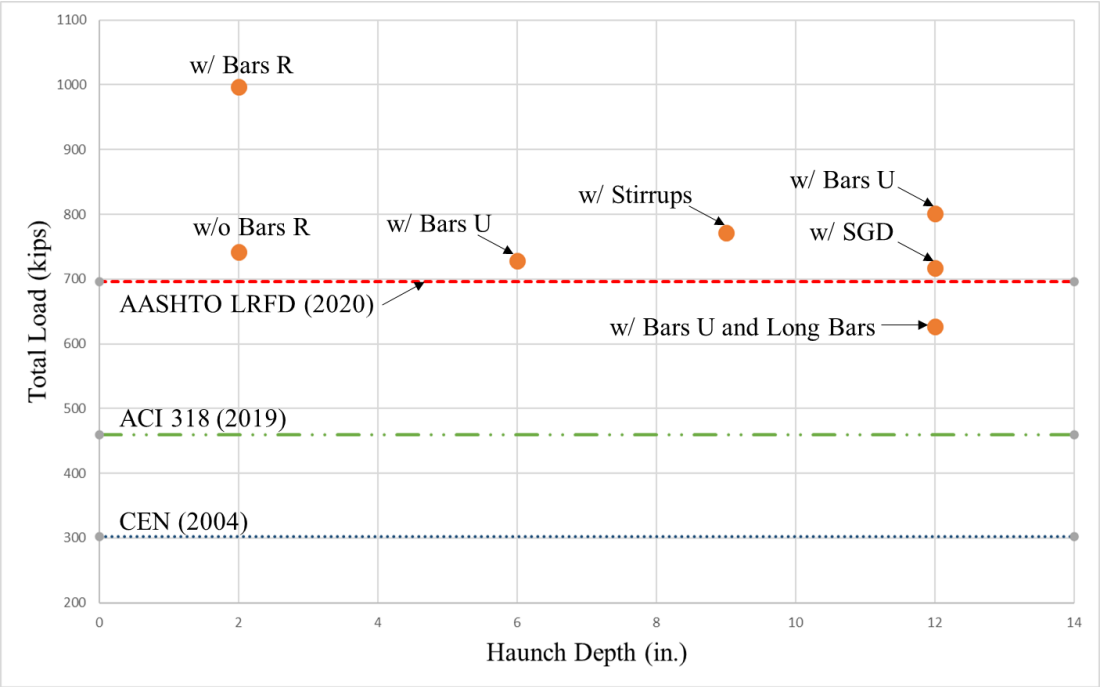

Figure 4.5.27 Specimen Group I Test Results Peak Load Comparison with Predicted Capacities

4.5.2. Specimen Group II: PCP Specimens Results

The test results for Specimen Group II are presented in Section 4.5.2.1. Section 4.5.2.2. provides a comparison of test results with the predicted capacities from the guidelines that are considered.

4.5.2.1. Test Results

In Specimen Group II, the researchers tested 18 specimens as shown in Table 4.5.2. Out of the tests performed, two used SB_S shown in Figure 4.3.1. The haunch depth tested varied from 2 in. to 12 in. The detailing method used for haunches deeper than 2 in. was either Bars UP (Figure 4.1.7) or SGD detailing with Bars U (Figure 4.1.8). Two of the 12-in. haunch specimens had fewer bars R and Bars UP than the other specimens. The bars R at the top and bottom of the specimens were removed to observe the effects of reducing bars R on the capacity and governing limit state.

Table 4.5.2 Specimen Group II Tests

Test No.	Specimen No.	Haunch Depth (in.)	Haunch Reinforcement Detailing	No. of Bars R	Spreader Beam Used	Test Failure Load (kips)	Residual Load (kips)
10	19, 20	2	-	5	SB_S	862	227
11	21, 22	2	-	5	SB_P	582	423
12	23, 24	6	Bars UP	5	SB_P	1013	300
13	25, 26	6	SGD (3-in. layer cast first) with Bars U	5	SB_P	1038	380
14	27, 28	9	Bars UP	5	SB_S	864	235
15	29, 30	9	SGD (5-in. layer cast first) with Bars U	5	SB_P	1060	480
16	31, 32	12	Bars UP	5	SB_P	783	340
17	33, 34	12	Bars UP	3	SB_P	976	0
18	35, 36	12	SGD (8-in. layer cast first) with Bars U	5	SB_P	751	300

The failure modes observed for Specimen Group II can be broadly divided into the following:

a. PCP-haunch interface debonding combined with pull-out failure
b. PCP-haunch interface debonding combined with haunch cracking
c. Simulated PSC girder-haunch interface debonding
d. Simulated PSC girder-haunch interface debonding with haunch cracking

a. PCP-haunch interface debonding combined with pull-out failure

Tests 10 (Figure 4.5.28) and 11 (Figure 4.5.29) had a debonding failure at the PCP-haunch interface. Test 10 was performed using SB_S and had a higher capacity compared to Test 11. As explained previously in Section 4.5.1, the capacities measured from the specimens tested with SB_S have damage or cracks in the simulated girder, therefore, the peak load values may be unreliable. The failure mode, however, can still provide insight into the specimen behavior. In both specimens, bars R pulled out of the CIP deck as shown in Figures 4.5.30 and 4.5.31. This type of failure has been observed in past studies (see Chapter 2). This failure occurs if the embedment depth of the shear connectors into the deck is insufficient.

Figure 4.5.28 Test 10 (2-in. Haunch SB_S)

Figure 4.5.29 Test 11 (2-in. Haunch SB_P)

Figure 4.5.30 Pull-out Failure in 2-in. Haunch (Girder Image)

Figure 4.5.31 Pull-out Failure in 2-in. Haunch (Slab Image)

Figure 4.5.32 shows the load versus slip plot for Test 11. The cohesive bond loss of Test 11 specimens occurred earlier than the other specimens in Group II tested with SB_P (Figure 4.5.33). Because Test 11 specimens were cast with Test 8 specimens in Group I, the concrete slump for these was also higher (6.5 in.) than the required value for TxDOT Class S concrete (3-5 in.). Beyond the loss of cohesion, the load increases with the increase in shear reinforcement stresses until the pull-out failure strength was reached. Figure 4.5.34 shows the load versus slip plot at the haunch-PCP interface for Test 11. The slip for Test 11 is higher at this interface compared to the simulated PSC girder-haunch interface. The relative slip obtained beyond 0.04 in. (Figure 4.5.34) is unreliable because contact was established with the specimens' lateral supports near the end of the test after the peak load.

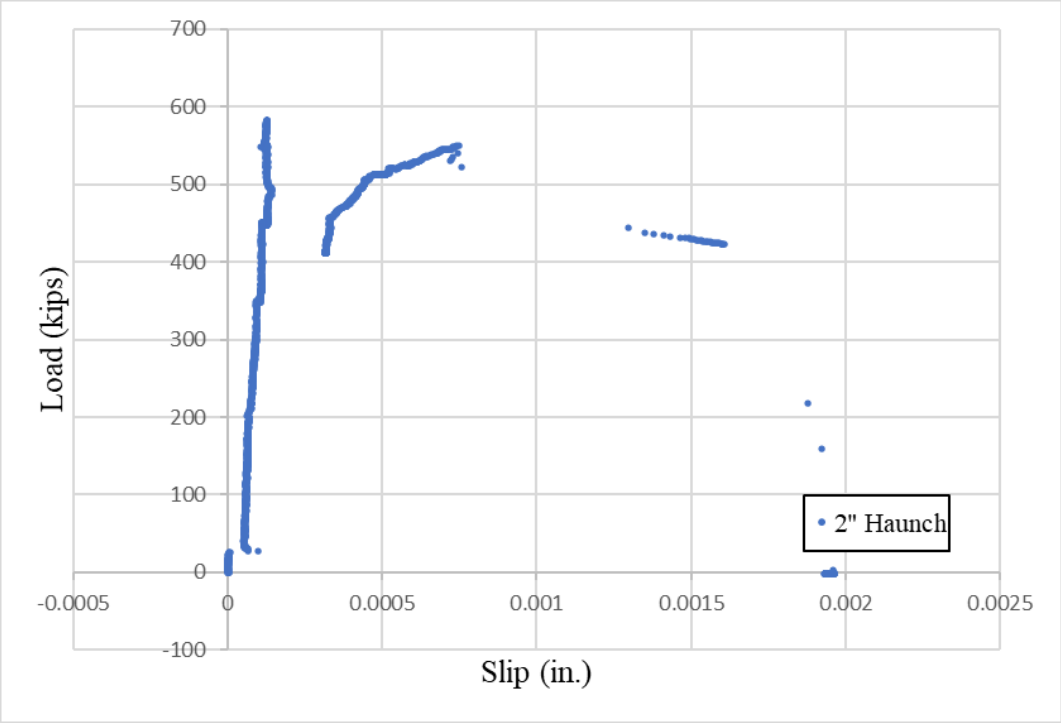

Figure 4.5.32 Load versus Slip at Simulated PSC Girder-Haunch Interface for Test 11 (SB_P)

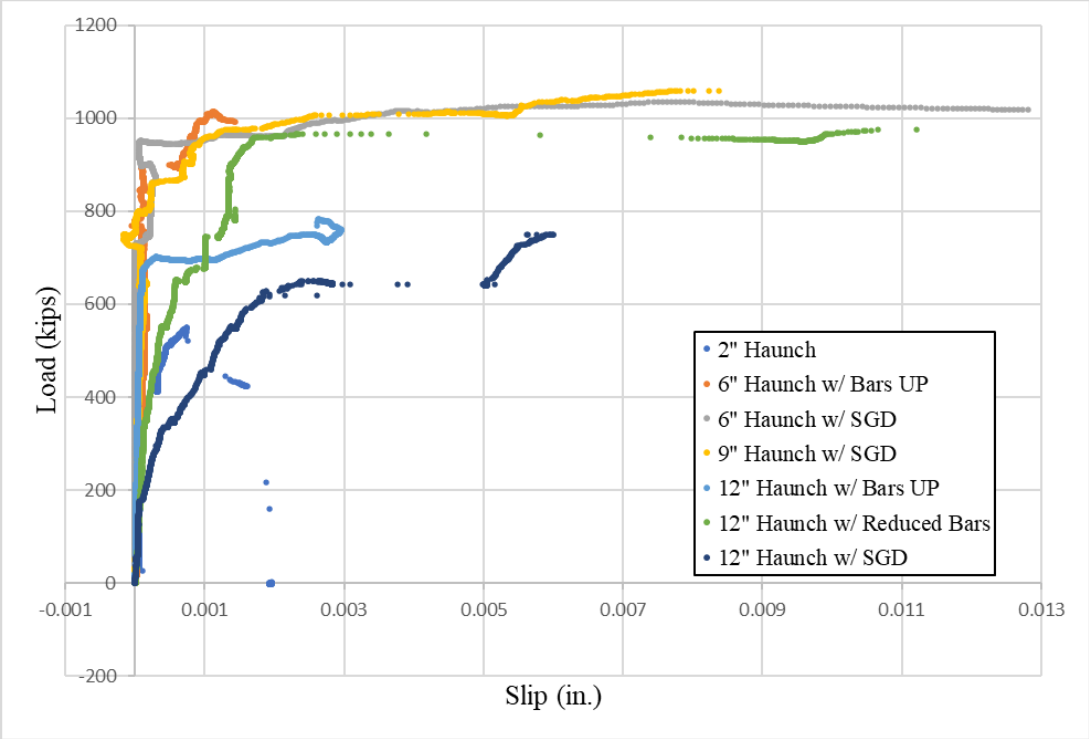

Figure 4.5.33 Load versus Slip at Simulated PSC Girder-Haunch Interface for Specimen Group II (SB_P)

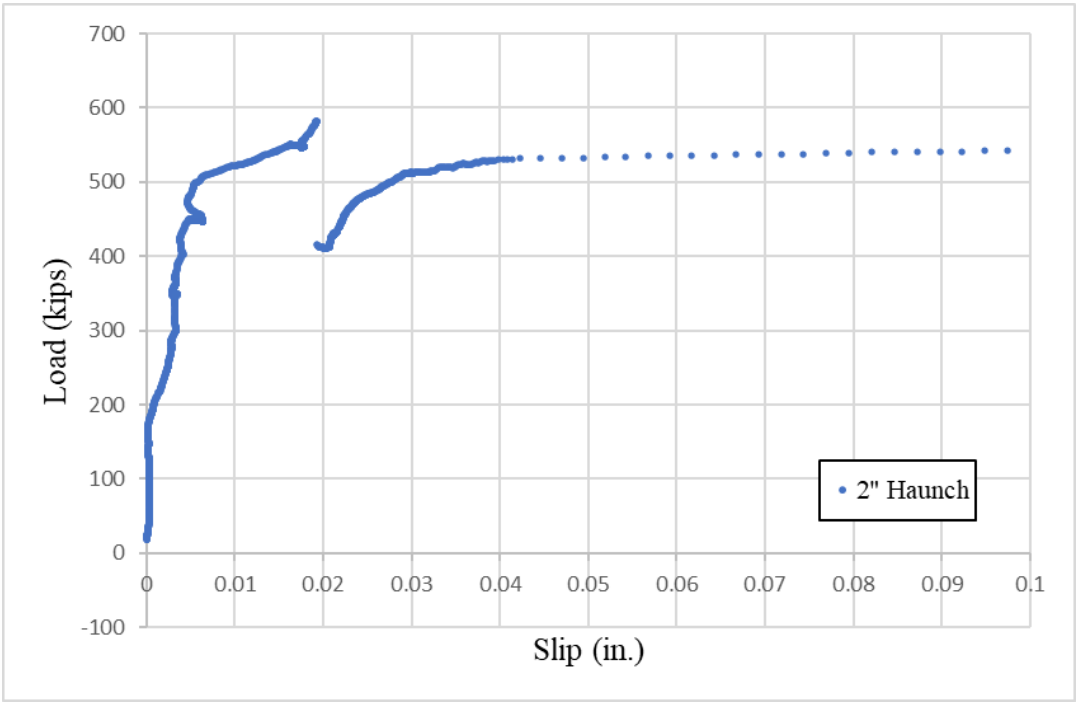

Figure 4.5.34 Load versus Slip at PCP-Haunch Interface for Test 11 (SB_P)

The behavior of 2-in. haunch specimens tested with SB_S was similar to the one tested with SB_P. Figure 4.5.35 shows the load versus slip plot at the simulated PSC girder-haunch interface for

Test 10. The relative slip is almost negligible at the simulated PSC girder-haunch interface until the loss of cohesive bond. The slip increases slightly until a brittle debonding failure combined with pull-out failure at the PCP-haunch interface occurs.

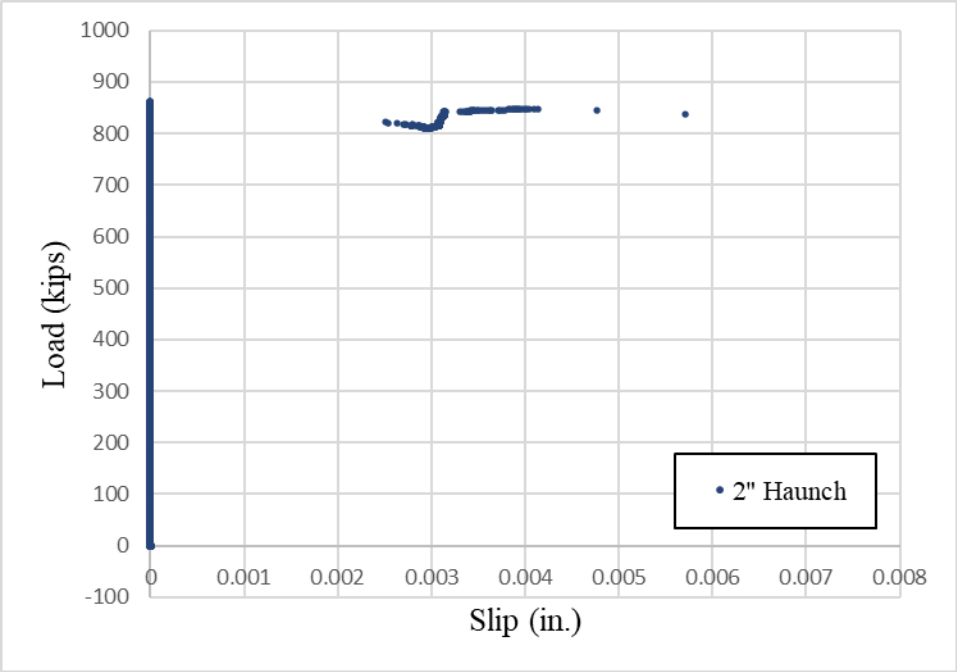

Figure 4.5.35 Load versus Slip at Simulated PSC Girder-Haunch Interface for Test 10 (SB_S)

b. PCP-haunch interface debonding combined with haunch cracking

Tests 12 (Figure 4.5.36), 14 (Figure 4.5.37), and 16 (Figure 4.5.38) had debonding/cracking at the PCP-haunch interface combined with major diagonal cracks in the haunch. Test 14 (9-in. haunch specimens) was performed using SB_S and had major cracks in the simulated girder as well. The relative slip obtained at the simulated PSC girder-steel interface was highest for this test compared to other specimens in Group II (Figures 4.5.39 and 4.5.40).

Figure 4.5.36 Test 12
(6-in. Haunch with Bar UP)

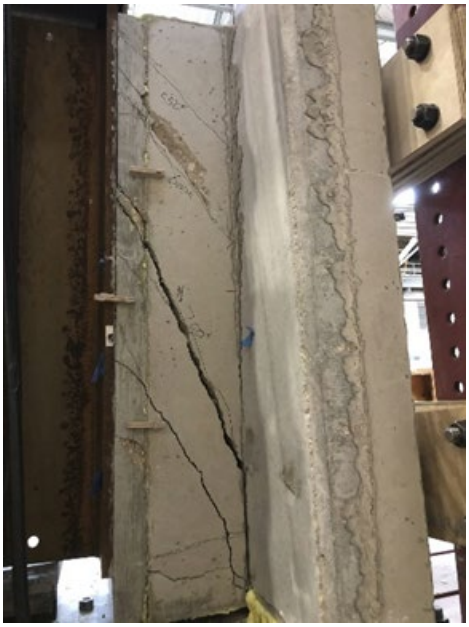

Figure 4.5.37 Test 14
(9-in. Haunch with Bar UP)

Figure 4.5.38 Test 16
(12-in. Haunch with Bar UP)

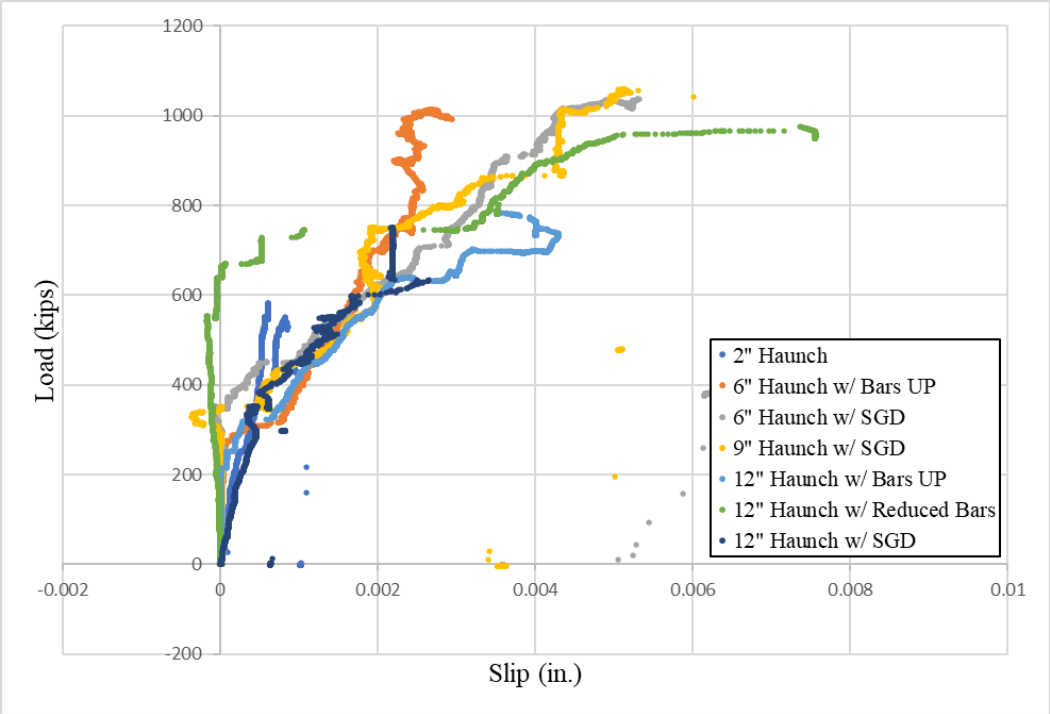

Figure 4.5.39 Load versus Slip at Simulated PSC Girder-Steel Interface (SB_P)

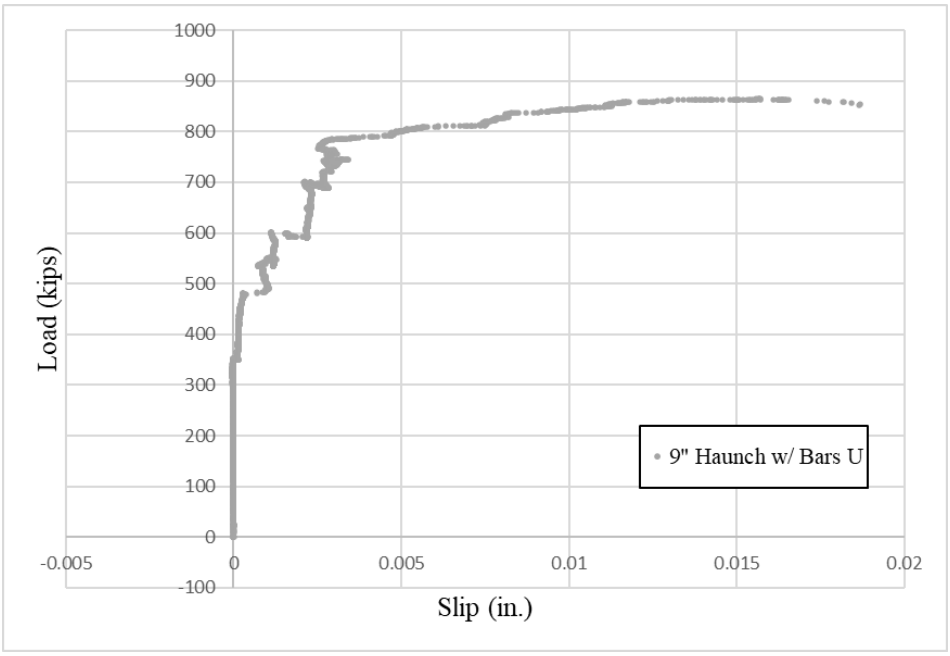

Figure 4.5.40 Load versus Slip at Simulated PSC Girder-Steel Interface for Test 14 (SB_S)

As mentioned in Chapter 2, the shear plane at the PCP-haunch interface is weaker compared to the simulated PSC girder-haunch interface. The combination of parallel and transverse stresses acting on this plane cause the formation of diagonal tensile cracks. A truss action is developed in the haunch where the concrete struts in between the diagonal tension cracks resist the applied

shear (Section 2.2.3.5). The failure occurs when the reinforcement bars yield or concrete struts in between these diagonal cracks fail. The truss action can explain the failure mode observed in these tests.

Figures 4.5.41 and 4.5.42 show that all three tests had small slips until cohesive bond loss took place, beyond which the load increased until failure occurred. The slip for the PCP-haunch interface (Figures 4.5.43 and 4.5.44) is higher compared to the simulated PSC girder-haunch interface (Figures 4.5.41 and 4.5.42). Another behavior evident from both the shear interface plots is that the cohesive bond stresses were lower for the PCP-haunch interface compared to the simulated PSC girder-haunch interface.

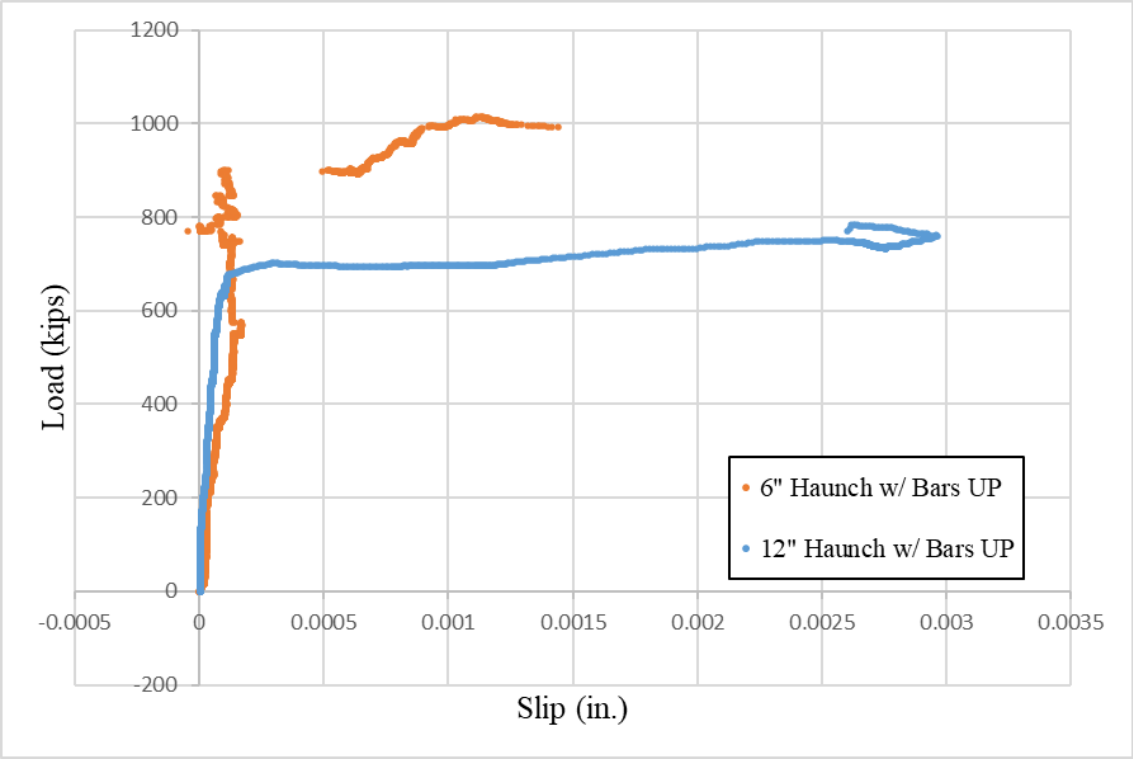

Figure 4.5.41 Load versus Slip at Simulated PSC Girder-Haunch Interface for Tests 12 and 16 (SB_P)

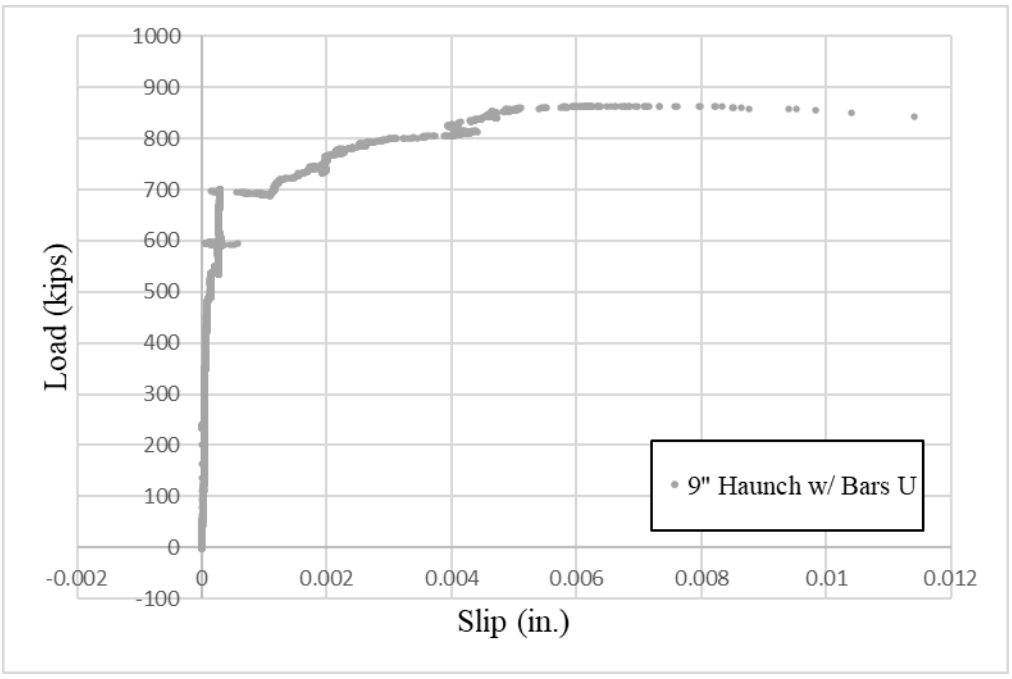

Figure 4.5.42 Load versus Slip at Simulated PSC Girder-Haunch Interface for Test 14 (SB_S)

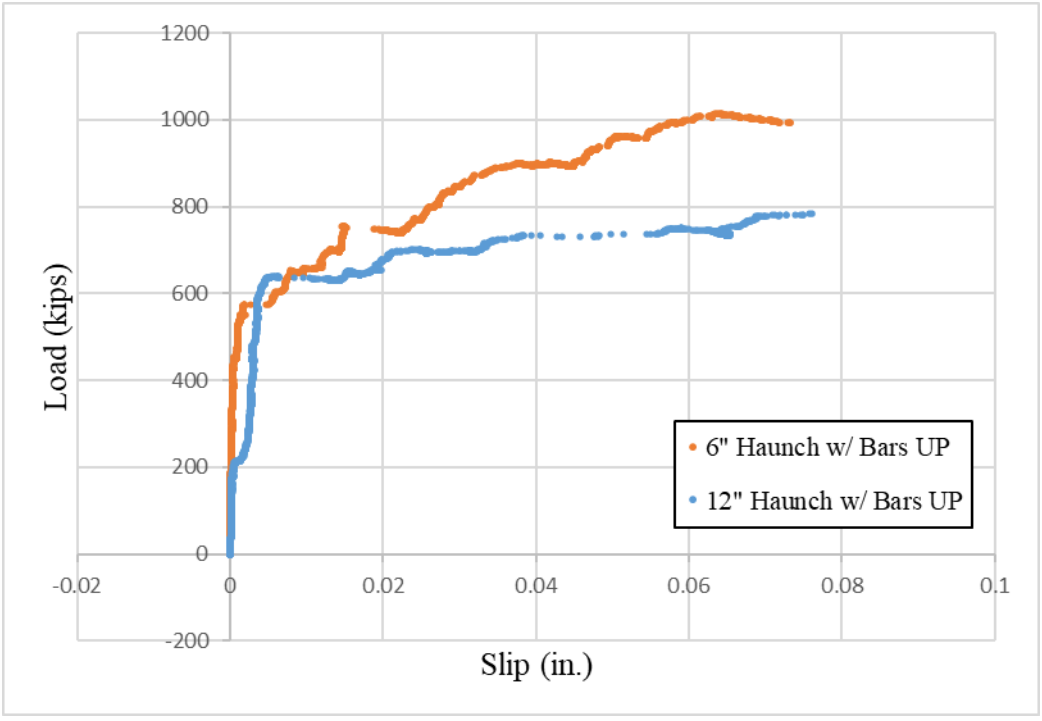

Figure 4.5.43 Load versus Slip at CIP Haunch-PCP Interface for Tests 12 and 16 (SB_P)

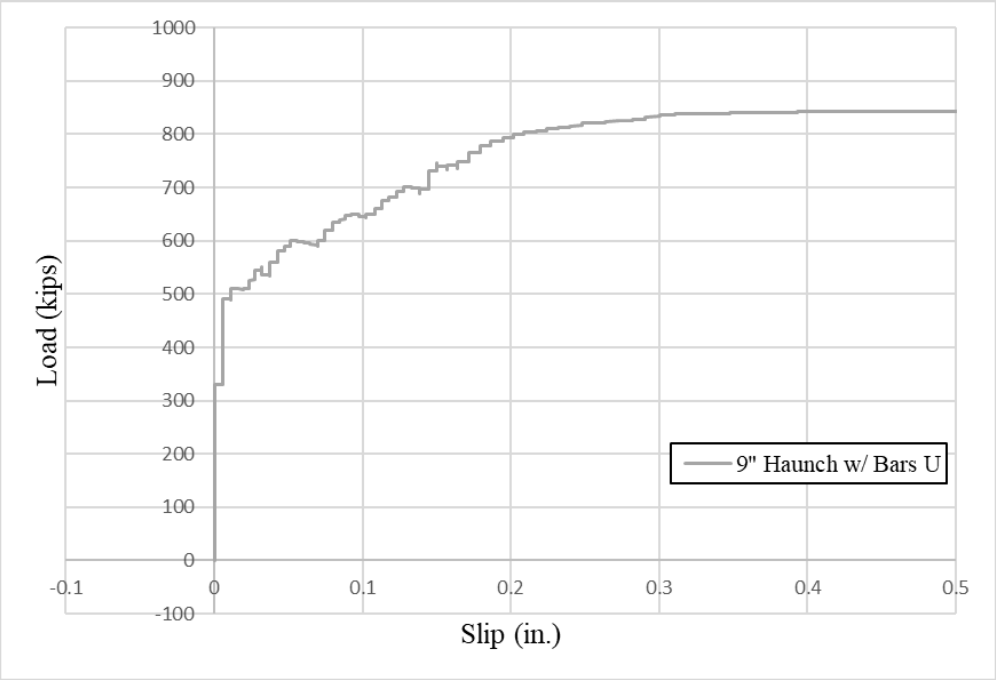

Figure 4.5.44 Load versus Slip at CIP Haunch-PCP Interface for Test 14 (SB_S)

The strain versus load plots for the strain gauges on the steel web are different for Test 12 (Figures 4.5.45 and 4.5.46) compared to other tests. The plot is unsymmetrical after approximately 850 kips for the two specimens tested together. Test 12 established contact with the specimens' lateral support at this test load. Before contact was established, the load transfer mechanism is similar to other specimens with compression observed in the top four strain gauges of the steel web and tension observed in the bottom-most strain gauge (Figure 4.5.47). The peak load for Test 12 may have increased beyond 850 kips due to the lateral supports.

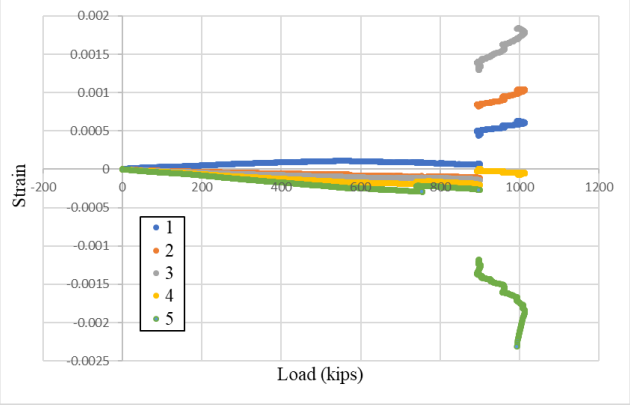

Figure 4.5.45 Strain versus Load Plot for Steel Web of Simulated PSC Girder in Test 12 (North Specimen)

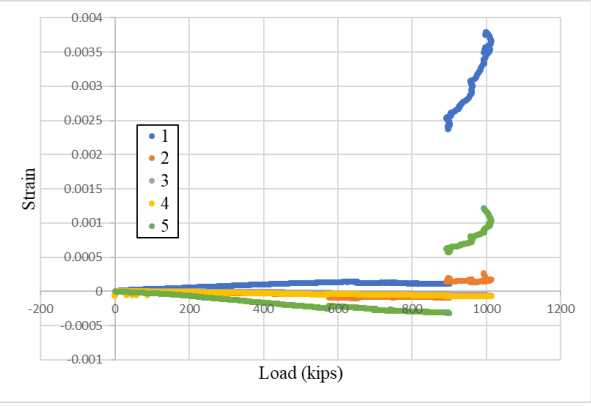

Figure 4.5.46 Strain versus Load Plot for Steel Web of Simulated PSC Girder in Test 12 (South Specimen)

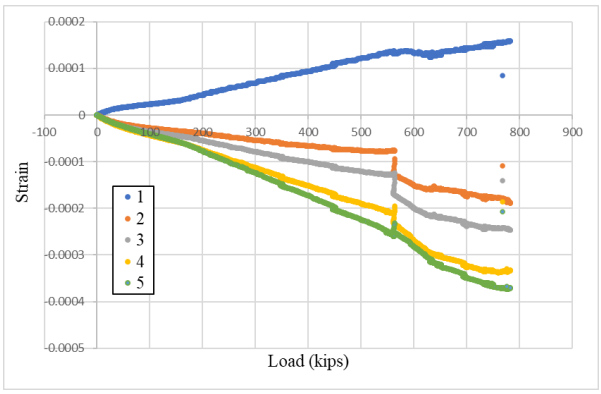

Figure 4.5.47 Strain versus Load Plot for Steel Web of Simulated PSC Girder in Test 16

The strain in reinforcement bars in Tests 12 and 16 increased after cohesive bond loss at the PCP-haunch interface (Figures 4.5.48, 4.5.49, 4.5.50, and 4.5.51). Some of the reinforcement bars in the cracked regions yielded at the peak load.

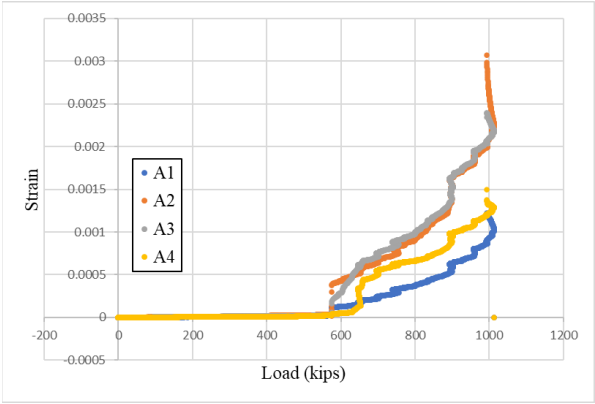

Figure 4.5.48 Strain versus Load Plot 1 for Haunch Reinforcement in Test 12

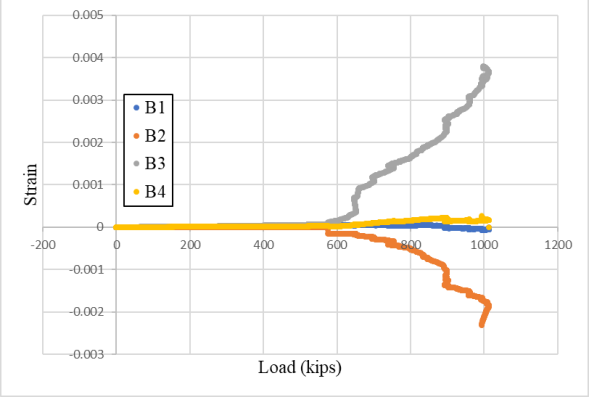

Figure 4.5.49 Strain versus Load Plot 2 for Haunch Reinforcement in Test 12

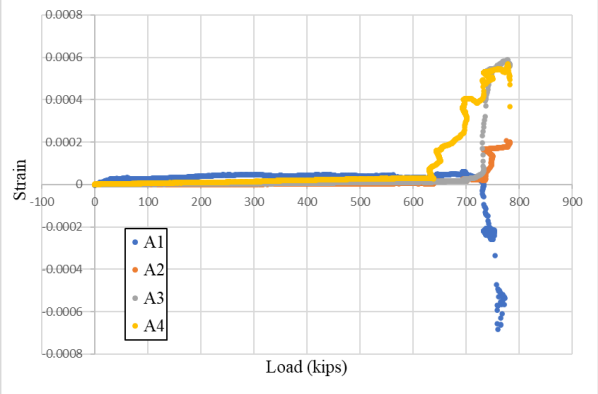

Figure 4.5.50 Strain versus Load Plot 1 for Haunch Reinforcement in Test 16

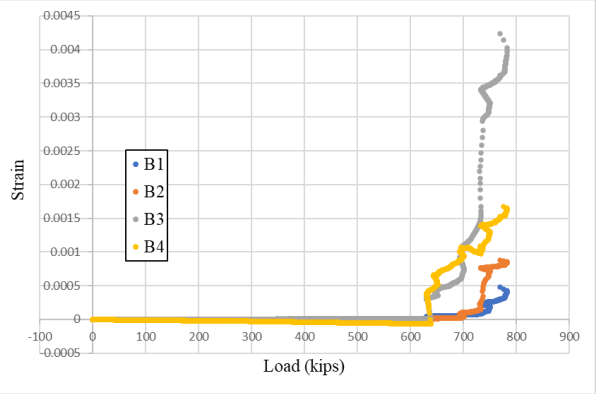

Figure 4.5.51 Strain versus Load Plot 2 for Haunch Reinforcement in Test 16

c. Simulated PSC girder-haunch interface debonding

Tests 13 (Figure 4.5.52) and 15 (Figure 4.5.53) had a debonding failure at the simulated PSC girder-haunch interface. Diagonal tensile cracks were observed in Tests 13 and 15, but the crack width was small. These tests had a higher peak load than all other specimens (Table 4.5.2). Test 18 also failed at the simulated PSC girder-haunch interface but did not have any diagonal cracks in the haunch (Figure 4.5.54).

Figure 4.5.52 Test 13
(6-in. Haunch with SGD)

Figure 4.5.53 Test 15
(9-in. Haunch with SGD)

Figure 4.5.54 Test 18
(12-in. Haunch with SGD)

Figures 4.5.55 and 4.5.56 show the load versus slip plots for Tests 13, 15, and 18 at the simulated-PSC girder haunch interface and PCP-haunch interface, respectively. Tests 13 and 15 had a cohesive bond loss at the PCP-haunch interface, leading to stress in reinforcement bars and stiffness reduction in Figure 4.5.56. The load increases until failure at the simulated PSC girder-haunch interface. These specimens have better ductility than the other specimens (Figure 4.5.39).

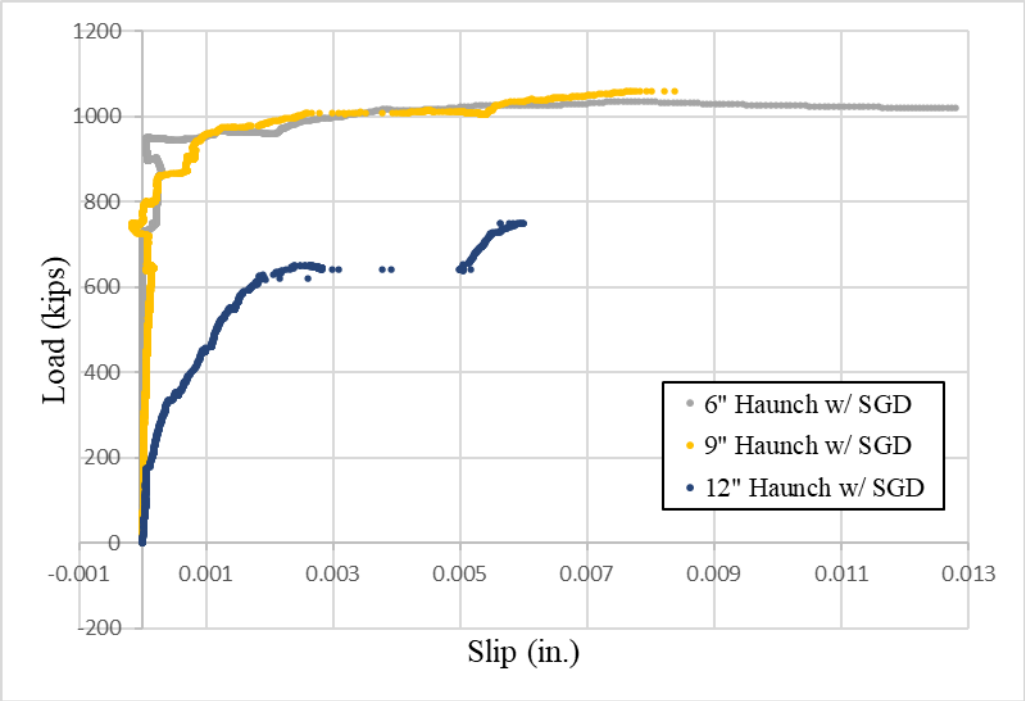

Figure 4.5.55 Load versus Slip at Simulated PSC Girder-Haunch Interface for Tests 13, 15, and 18 (SB_P)

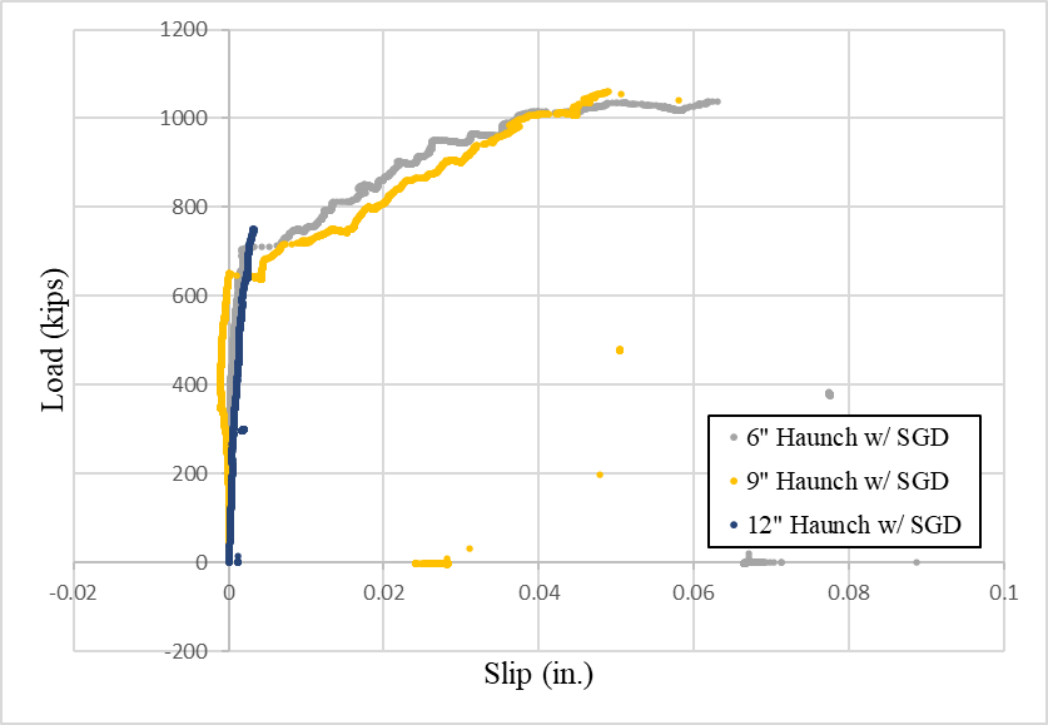

Figure 4.5.56 Load versus Slip at CIP Haunch-PCP Interface for Tests 13, 15, and 18 (SB_P)

The peak load for Test 18 is significantly smaller than Tests 13 and 15. Also, Test 18 had a significantly smaller slip at the PCP-haunch interface (Figure 4.5.56). The strains in Bars U for Test 18 (Figures 4.5.57 and 4.5.58) were also small compared to Test 13 (Figures 4.5.59 and 4.5.60). Test 18 specimens behaved like Test 9 specimens in Group I. Figures 4.5.61-4.5.64 show that the web strain gauge nearest to the specimen base has the highest strain value for 12-in. haunch specimens compared to other specimens. The tensile forces combined with the shear forces lead to an earlier debonding failure and smaller ultimate capacity for Test 18. The SGD-haunch interface slip for all three specimens is small compared to other interfaces (Figure 4.5.65).

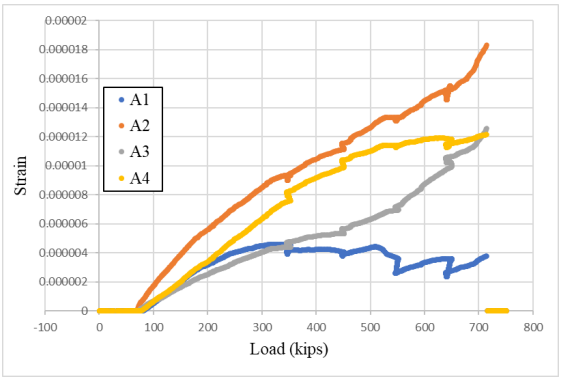

Figure 4.5.57 Strain versus Load Plot 1 for Haunch Reinforcement in Test 18

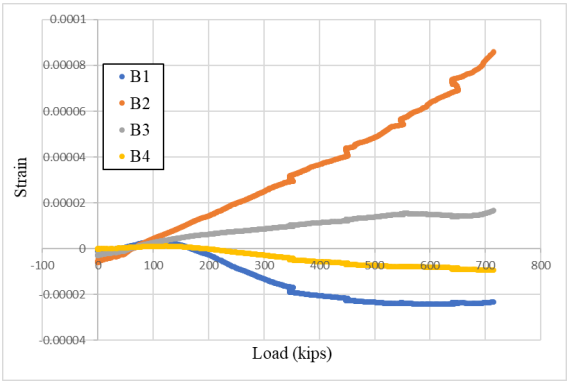

Figure 4.5.58 Strain versus Load Plot 2 for Haunch Reinforcement in Test 18

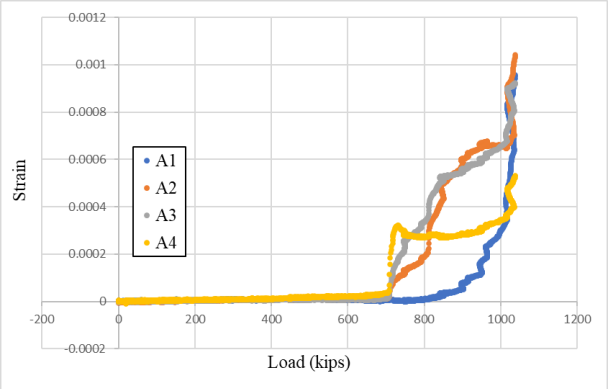

Figure 4.5.59 Strain versus Load Plot 1 for Haunch Reinforcement in Test 13

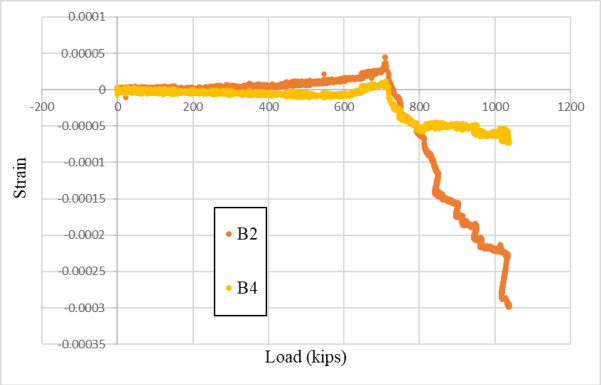

Figure 4.5.60 Strain versus Load Plot 2 for Haunch Reinforcement in Test 13

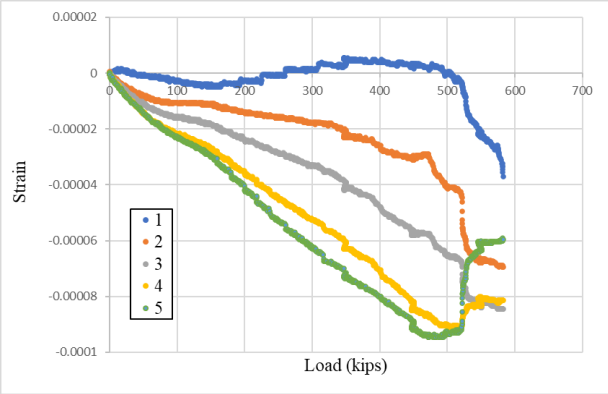

Figure 4.5.61 Strain versus Load for Steel Web of Simulated PSC Girder in Test 11

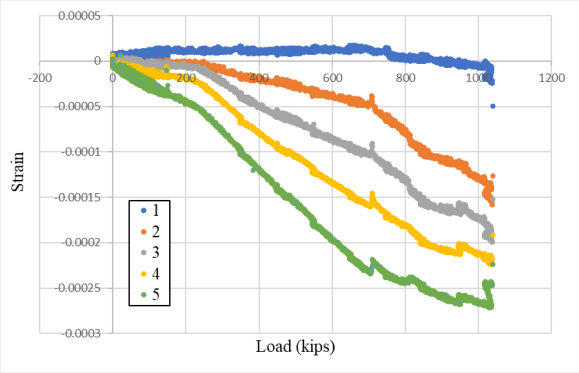

Figure 4.5.62 Strain versus Load for Steel Web of Simulated PSC Girder in Test 13

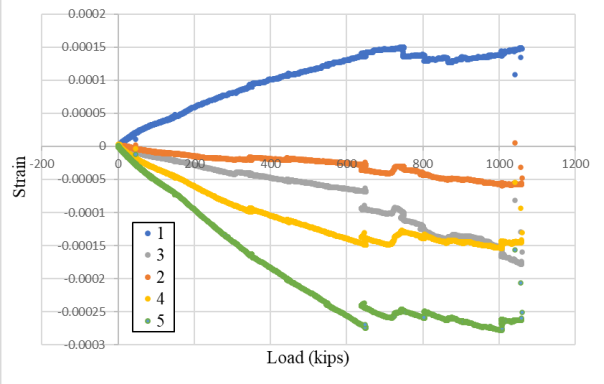

Figure 4.5.63 Strain versus Load for Steel Web of Simulated PSC Girder in Test 15

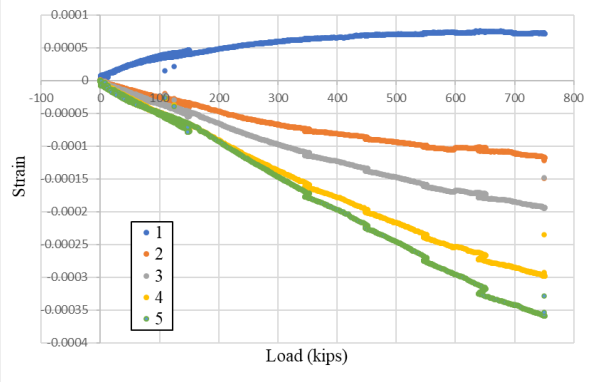

Figure 4.5.64 Strain versus Load for Steel Web of Simulated PSC Girder in Test 18

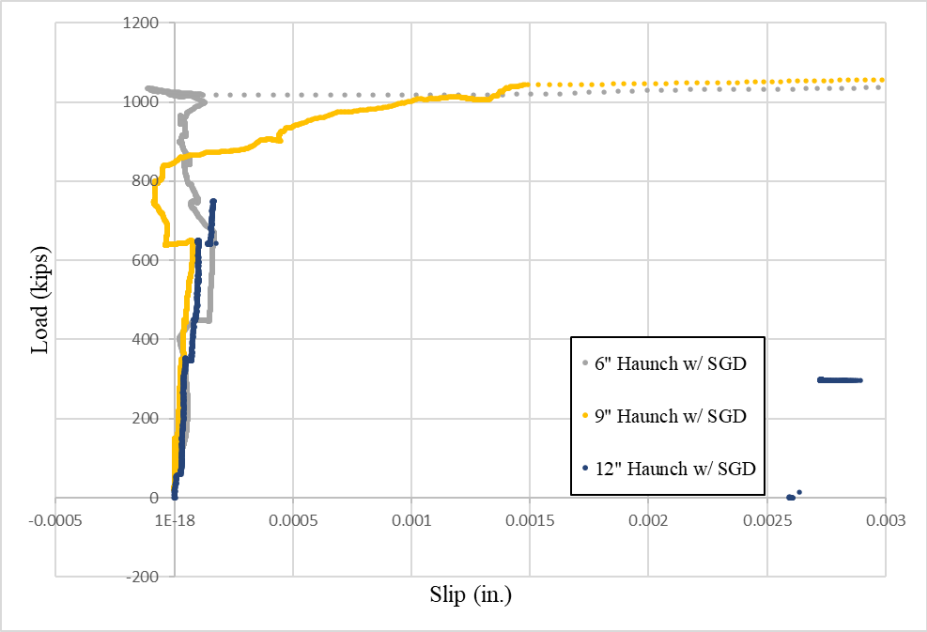

Figure 4.5.65 Load versus Slip at Haunch CIP-Haunch SGD Interface (SB_P)

d. Simulated PSC girder-haunch interface debonding with haunch cracking

Test 17 (Figure 4.5.66) had separation at the simulated PSC girder-haunch interface combined with major diagonal cracking in the haunch. This test had higher capacity than other 12-in. haunch specimens tests and no residual load after failure (Table 4.5.2). Figures 4.5.67 and 4.5.68 show that the cohesive bond was lost at the PCP-haunch interface first, and then the load increased until reinforcement yielded. Another observation from Figure 4.5.69 is that the relative slip at the simulated PSC girder-steel interface is negligible until the load reached approximately 700 kips.

Figure 4.5.66 Test 17
(12-in. Haunch with Reduced Bar UP)

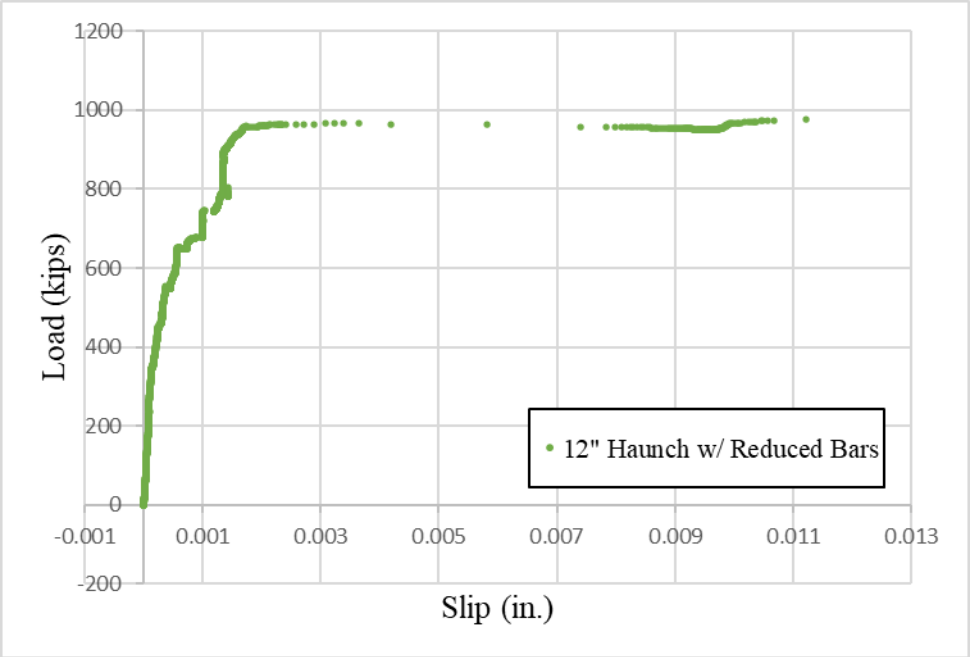

Figure 4.5.67 Load versus Slip at Simulated PSC Girder-Haunch Interface for Test 17 (SB_P)

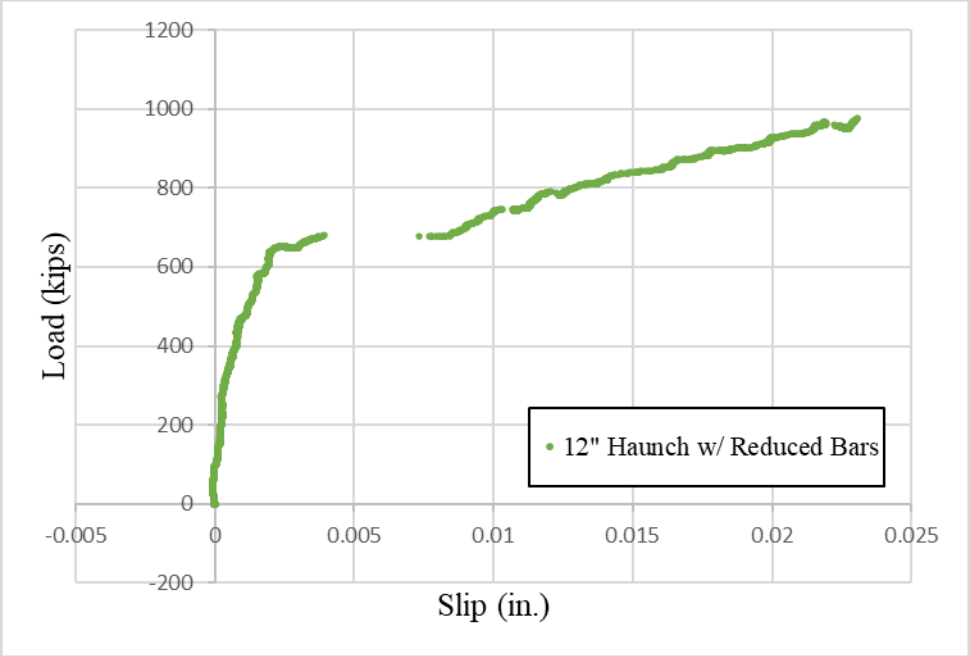

Figure 4.5.68 Load versus Slip at CIP Haunch-PCP Interface for Test 17 (SB_P)

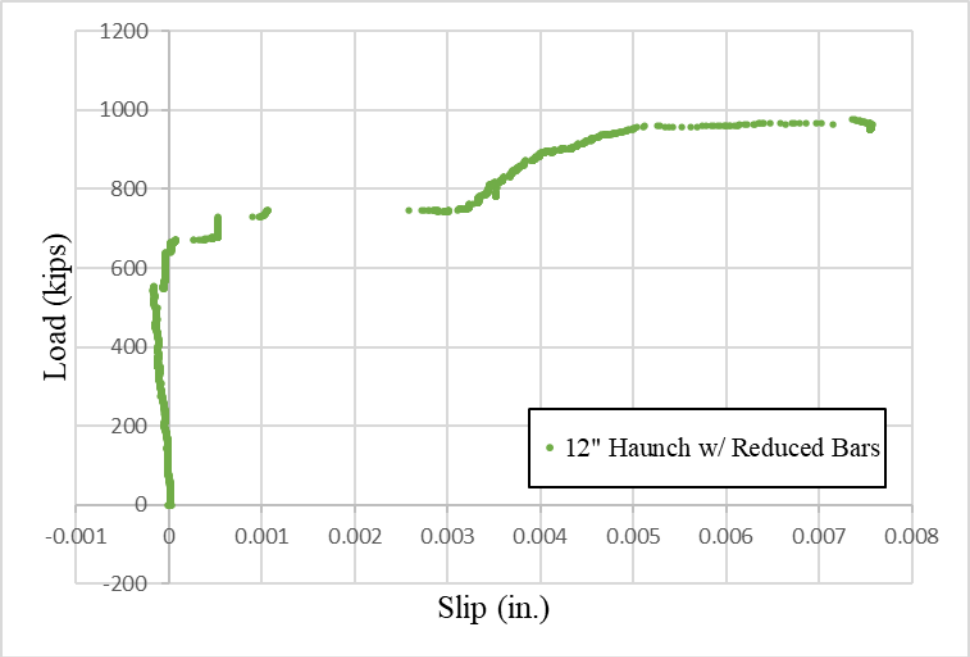

Figure 4.5.69 Load versus Slip at Simulated PSC Girder-Steel Interface for Test 17 (SB_P)

The load transfer mechanism remains the same as in Test 16. The shear plane at the PCP-haunch interface is relatively weak, and diagonal tension cracks are developed due to transverse, parallel, and shear stresses acting on the shear plane. This crack can be seen at both ends of the specimen in Figure 4.5.66. The failure occurs when the reinforcement bars yield or concrete struts in between these diagonal cracks fail. The concrete strut near the specimen base fails first for Test 17.

An explanation for the higher peak load compared to Test 16 is the different testing conditions. Test 17 had no relative slip between the simulated PSC girder-steel interface until about 700 kips (Figure 4.5.69). This behavior was observed in other specimens loaded with SB_S (Figure 4.5.44). All the specimens loaded with SB_S had higher peak load values compared to specimens loaded with SB_P. The loading may have been applied to steel only initially and then to both steel and PSC after a certain amount of displacement occurred in the specimens.

Another explanation for the debonding failure at the simulated PSC girder-haunch interface is the presence of flexural stresses in push-out tests. As explained previously in Section 4.4, the surrounding concrete near the bottom-most bars R for tall haunch specimens is in tension. Thus, a combination of tensile and shear stresses are present near the specimen base. For Test 17, the bottom-most and top-most bars R are removed, thereby increasing the edge distances on both ends. The strain in Bars UP for these specimens is in tension from the beginning of the test (Figures 4.5.70 and 4.5.71). The surrounding concrete for all three bars R will then be in compression, thereby increasing the resisting stresses to the applied load until steel yielding or concrete strut failure. Failure occurred in these specimens when all three bars R yielded and the weakest concrete strut near the base failed.

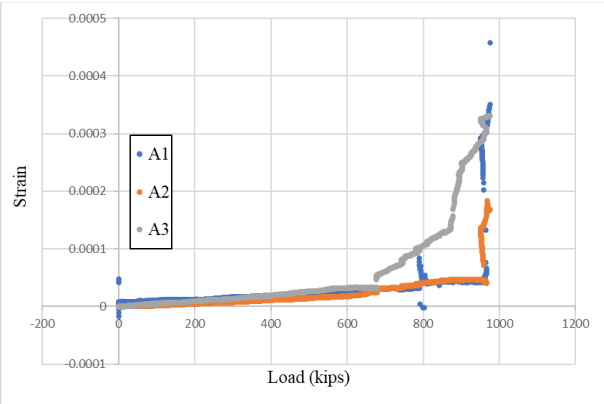

Figure 4.5.70 Strain versus Load Plot 1 for Haunch Reinforcement in Test 17

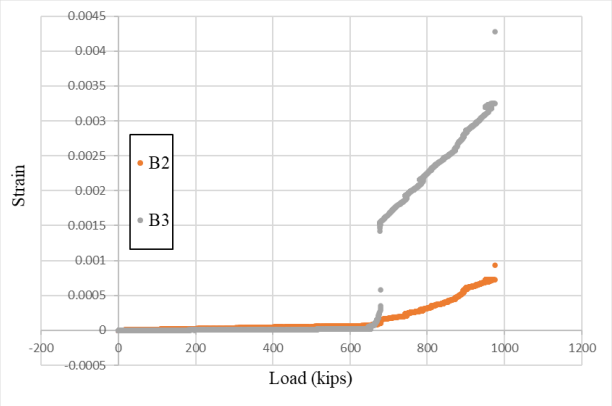

Figure 4.5.71 Strain versus Load Plot 2 for Haunch Reinforcement in Test 17

4.5.2.2. Comparison with Predicted Capacities

All specimens have a higher capacity than that predicted by the AASHTO LRFD (2020) except for Test 11 specimens (2-in. haunch) (Figure 4.5.72). The lower capacity obtained in Test 11 can be attributed to poor concrete properties for these specimens and the pull-out failure of bars R.

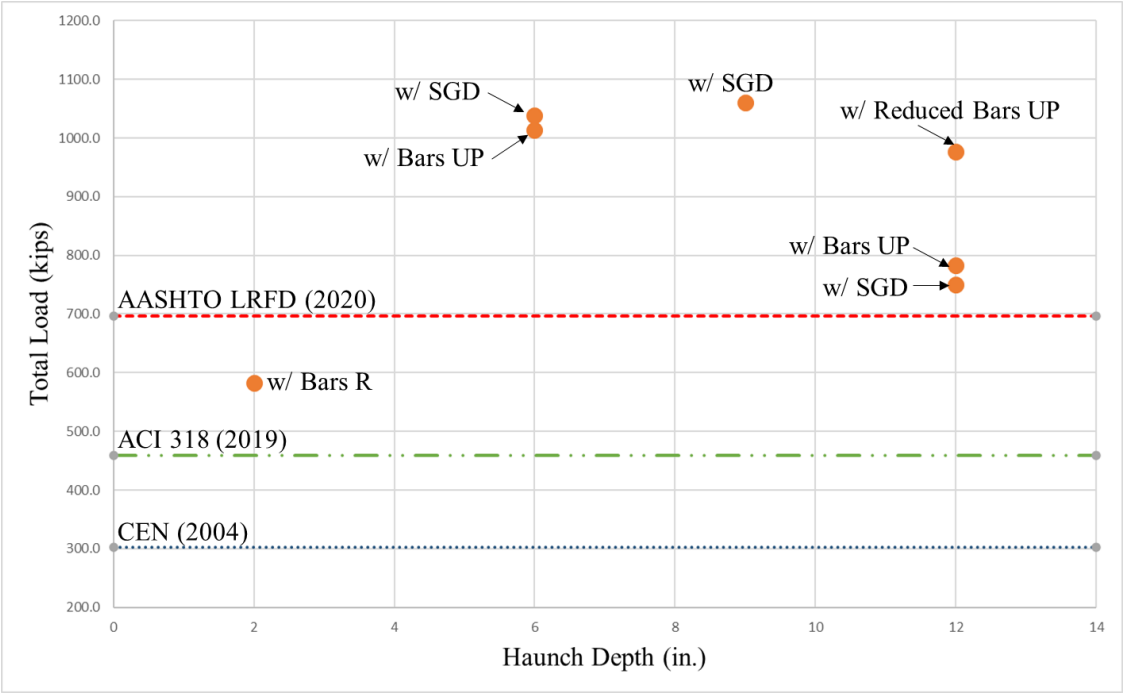

Figure 4.5.72 Specimen Group II Test Results Peak Load Comparison with Predicted Capacities

4.6. Concluding Remarks

For Specimen Group I (CIP specimens), the majority of the peak load (about 75%) is provided by the cohesive strength at the simulated PSC girder-haunch interface. The reinforcement bars

contribute mostly after the cohesive bond is lost. The specimens with no reinforcement bars had no residual load. Some amount of residual load is preferred since the relative slip in these specimens is quite small. The 2-in. haunch specimens with reinforcement bars had the maximum capacity. All other specimens had lower strength due to a combination of debonding and concrete cracking near the specimen base for tall haunches. The inclusion of longitudinal reinforcement bars or vertical stirrups or SGD rebar detailing in the haunch reduced the cracking but did not increase the capacity. Nevertheless, all the detailing strategies were able to provide cohesive strength greater than the AASHTO LRFD (2020) predicted capacity. The concrete material properties to be used should conform with TxDOT Class S concrete (TxDOT 2022).

For Specimen Group II (PCP specimens), the cohesive bond stresses were lost first at the PCP-haunch interface. If the embedment depth of bars R is insufficient, pull-out failure can occur. A minimum embedment depth of 5.5 in. is recommended for girders with PCP decks to allow for the shear reinforcement to penetrate the bottom mat of the CIP deck. If bars R have sufficient embedment depth, the reinforcement stresses increase beyond the cohesive bond loss at the PCP-haunch interface. The load drop occurs at the reinforcement bars yielding or concrete struts failing, whichever occurs first. If the reinforcement bars yield, the cracks rotate parallel to the simulated PSC girder-haunch interface causing interface shear failure. Both the yielding and strut failure modes have higher capacity than the AASHTO LRFD (2020) predicted capacity, but the specimens with steel yielding failure have more ductility. The SGD can provide steel-yielding failure in push-out specimens for haunches up to 9-in. Since the bond is relatively weak at the PCP-haunch interface, modification to the AASHTO LRFD (2020) equation is suggested to consider the area and cohesion factor of the PCP-haunch interface when PCPs are used.

To provide more detailed guidelines, project researchers expanded the range of parameters investigated for PSC girder specimens by performing analytical study. Chapter 5 describes the FE model developed for steel and PSC girder specimens. The model was validated with the test results presented in the current and previous chapters. The validated model is then used to perform parametric study in Chapter 6.

Chapter 5. Finite Element Validation Studies

This chapter describes the development of a computational modeling approach based on experimental observations from the push-out test results of steel and PSC girder specimens with tall haunches. The computational research presented in the chapter focuses on model validation, wherein researchers attempt to recreate the load-slip behavior and failure modes observed in the experimental specimens. From these baseline validation specimens, researchers interpolate findings from specimens having a broad range of design parameters. This chapter addresses both specimens with steel and with PSC girders. Both types of specimens include CIP slabs and haunches, while PSC specimens also utilize PCPs.

5.1. Steel Girder

FE analyses are used to computationally extend full-scale push-out tests conducted to investigate the behavior of shear connectors. Kim et al. (2001) developed a numerical model for push-out specimens and explored the behavior of shear connections in composite beams. These researchers simulated a push-out test using both 2D and 3D FE models and obtained a concrete crack pattern that agreed with their experimental tests. Lam and El-Lobody (2005) developed an effective numerical model using the FE method to simulate push-out tests considering both linear and nonlinear material properties for the concrete and shear studs.

Nguyen and Kim (2009) developed an accurate nonlinear FE model of their experimental push-out specimen to investigate the capacity of large shear stud connectors embedded in a solid slab. The model used a cohesion layer between the steel beam and concrete slab interface, and it predicted the experimental load-slip behavior and failure mode of the studs. Titoum et al. (2016) present the results of their experimental study and FE models on a specimen with a novel I-shaped shear connector. For simplicity, Titoum et al. (2016) used the results from a two-dimensional FE model to propose an equation for the prediction of the ultimate load capacity of I-shape shear connectors. Mefleh and Kovács (2022) developed a finite element model of an experimental specimen with a Y-type perfobond shear connector and demonstrated a positive correlation between concrete compressive strength and specimen strength and ductility. These past studies suggest FE analyses can provide valuable information about the response of push-out specimens under a wide range of model parameters.

5.1.1. Geometry

The geometry developed for the steel girder models reflects the dimensions of the experimental specimens. Taking advantage of symmetry, the quarter-model shown in Figure 5.1.1.1 is used to improve computational efficiency compared to a model of the whole specimen. FE models in this study take advantage of symmetry along the YZ and XZ planes. Partitioning the wide flange, shear studs, and slab components controls the mesh size of different parts.

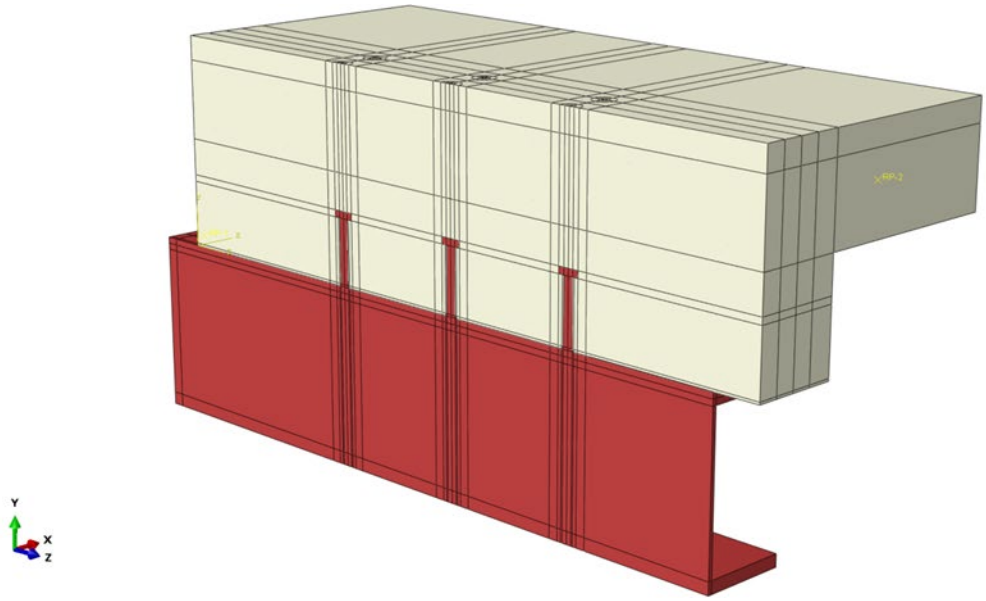

Figure 5.1.1.1 Quarter-model

The geometry of the welds surrounding the base of a shear stud influences the computed behavior because these regions are subjected to high stress concentrations. Figure 5.1.1.2 and Figure 5.1.1.3 compare the stresses at the base of shear studs with and without welds explicitly modeled. Project researchers find that by including the welds in the FE model, a numerical result that more accurately captures the response observed in the lab can be obtained. Therefore, project researchers have included the weld geometry in their models.

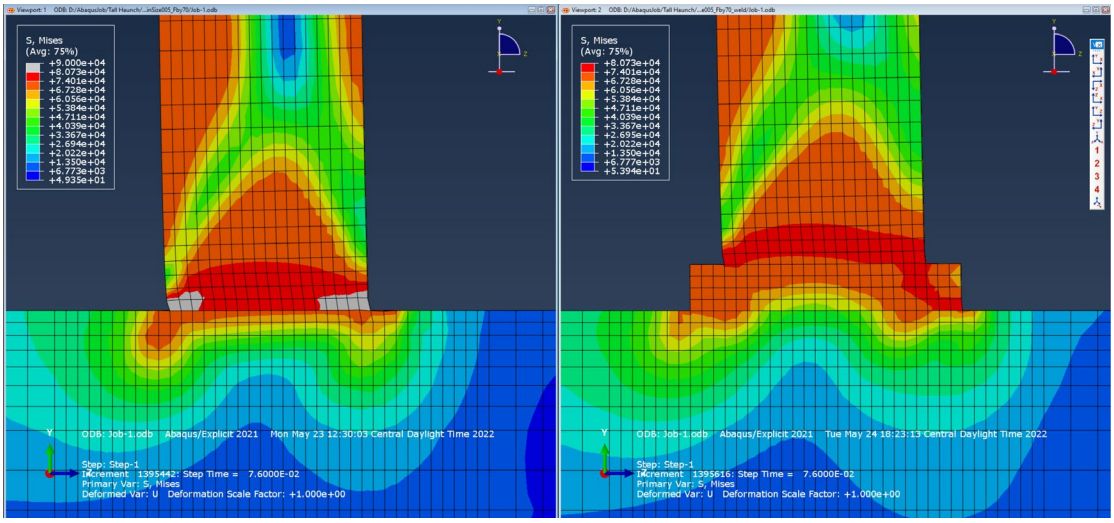

Figure 5.1.1.2 Stress State Comparison with and without Weld Geometry

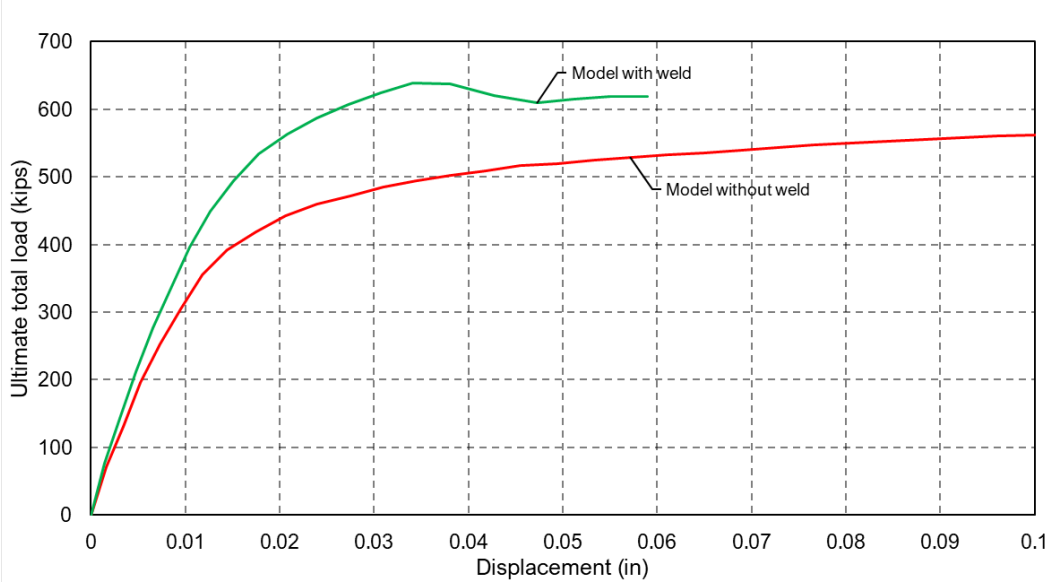

Figure 5.1.1.3 Load-displacement Curve Comparison with and without Weld Geometry

5.1.2. Material Models

Because the specimens consist of several parts with different materials, various constitutive models are specified in the FE analyses. To account for the large deformations and strong nonlinearities the specimen will experience during simulation, the Concrete Damage Plasticity (CDP) material model is adopted to simulate the concrete in the haunches and slabs, and Abaqus/Explicit is used as the solver. The CDP model is defined by seven parameters: 1) density, 2) Poisson's ratio, 3) dilation angle, 4) eccentricity, 5) f_{b0}/f_{c0}, 6) K, and 7) viscosity parameters (defined in Table 2.1). By varying these seven parameters, it is possible to determine the magnitudes of each term that provide the best match between the FE model numerical results and the laboratory test data. Results of this parametric evaluation lead to the values shown in Table 5.1.2.1.

Table 5.1.2.1 Concrete Damage Plasticity Input

Parameter	Meaning	Value
Density	Density of concrete (lbf s^2 / in^4)	2.25×10^{-4}
Poisson's Ratio	Poisson's ratio of concrete	0.2
Dilation Angle	A parameter that controls plastic volumetric strain developed during plastic shearing	40°
Eccentricity	Flow potential eccentricity in concrete's plastic flow equation.	0.1
f_{b0}/f_{c0}	The ratio of biaxial compressive strength to uniaxial compressive strength.	1.16
K	The ratio of the second stress invariant on the tensile meridian to that on the compressive meridian.	0.72
Viscosity Parameter	A parameter representing the relaxation time of the viscoplastic system, usually used to improve FE model's convergence rate.	0.04

Additionally, this model needs to specify the compressive and tensile behavior of the concrete. For compressive behavior, the Chang and Mander (1994) model is adopted, with the corresponding stress-strain relationship shown in Figure 5.1.2.1. For tensile behavior, to avoid unreasonable mesh sensitivity, the fracture energy cracking model is used in this study. In this model, the tensile stress-strain relationship of concrete is linear before the maximum tensile strength is reached. Afterwards, the concrete starts to crack, and the tensile stress-cracking width relationship is shown in Figure 5.1.2.2. The G_f variable in the figure is the area under the curve, which is obtained, according to the Abaqus user manual (Dassault Systemes 2022), from interpolation between 0.22 lb./in. for concrete with a strength of 2850 lb./in.^{2} and 0.67 lb./in. for concrete with a strength of 5700 lb./in.^{2}. The tensile strength of concrete is calculated from its compressive strength using an equation specified in Eurocode-2 (CEN 2004b).

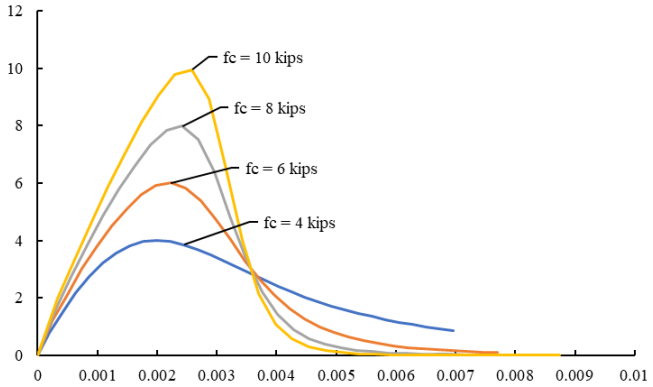

Figure 5.1.2.1 Stress-strain Relationship of Concrete (Chang and Mander 1994)

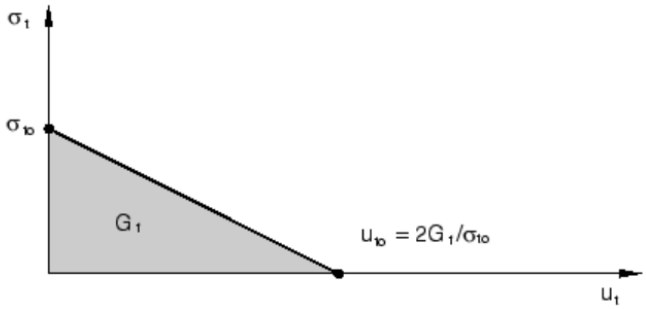

Figure 5.1.2.2 Tensile Stress Cracking Width Relationship of Concrete (Dassault Systemes 2022)

The FE model has three kinds of steel materials. The elastic modulus and Poisson's ratio of all steel used in the model is 29000 ksi and 0.3, respectively. The stress-strain relationships for the wide flange sections and the reinforcing steel are elastic-perfectly-plastic as shown in Figure 5.1.2.3, with a yield stress of 50 ksi for the wide flange sections and 60 ksi for the rebar. For studs, a trilinear stress-strain relationship is used, shown in Figure 5.1.2.4, with a yield stress of 60 ksi and an ultimate stress of 80 ksi, which is based on the material test results the researchers conducted for this project.

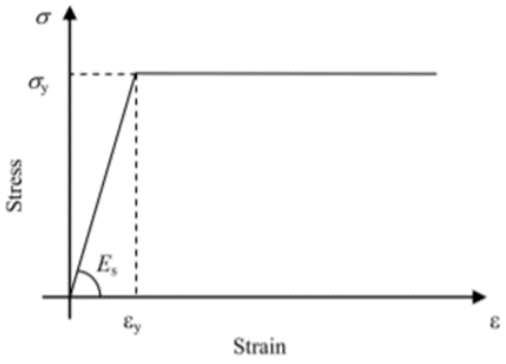

Figure 5.1.2.3 Stress-strain Relationship for Beam and Rebar

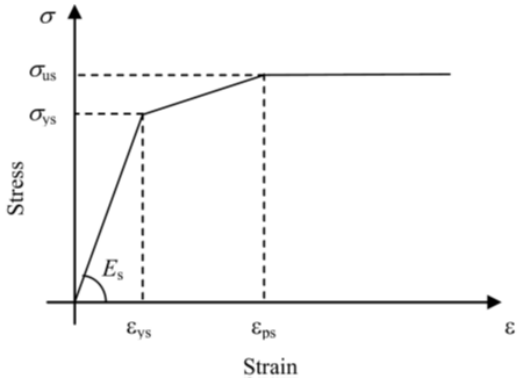

Figure 5.1.2.4 Stress-strain Relationship for Shear Studs

5.1.3. Interactions

In the FE model, contact occurs at the interface between the concrete parts (haunch and slab) and the steel parts (studs and beam), shown in Figure 5.1.3.1. This contact interaction is simulated using general contact, and the contact property is "hard" contact with a friction coefficient of 0.25. In this case, the cohesive effect between the concrete haunch and the studs and beam is ignored. This is acceptable because of the small cohesive strength between steel and concrete. Additionally, the FE model results obtained without cohesion will provide a conservative estimate of the capacity which is appropriate for parametric evaluation. The rebar in the slab and haunch, shown in Figure 5.1.3.2, are bonded to the concrete using an "embedded region" constraint, and slip between these components is prevented.

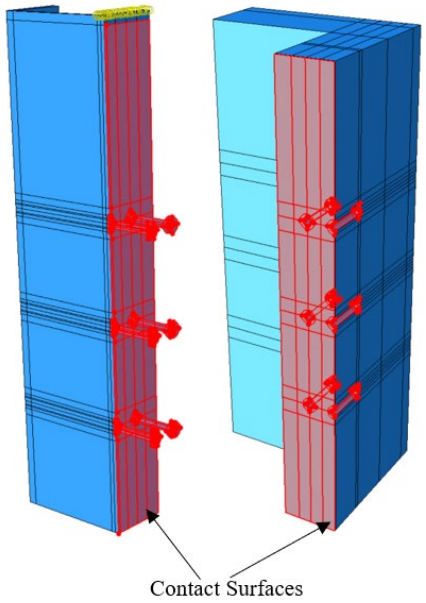

Figure 5.1.3.1 Interface in Contact Interaction

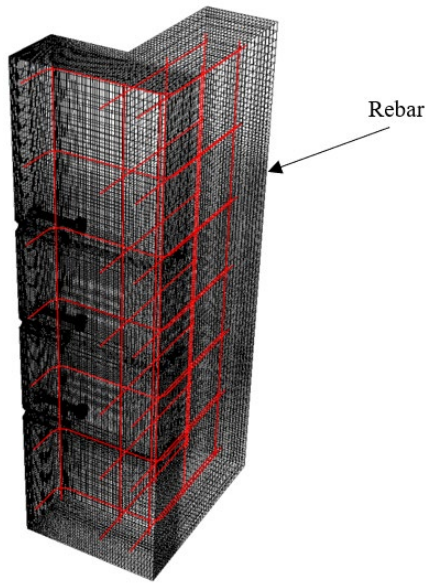

Figure 5.1.3.2 Rebar Inside Haunch and Slab

5.1.4. Loading and Boundary Conditions

Because the FE model represents one-quarter of the specimens tested in the lab, symmetry boundary conditions are applied to the faces shown in Figure 5.1.4.1. Rigid body constraints are applied to the loading and supporting surface shown in Figure 5.1.4.2. With this approach, the displacements of these two surfaces are tied to the reference points associated with them, becoming a rigid surface. Then, a controlled displacement is applied to the reference point of the loading face, and an "ENCASTRE" (i.e., fixed) boundary condition is applied to the reference point of the supporting surface.

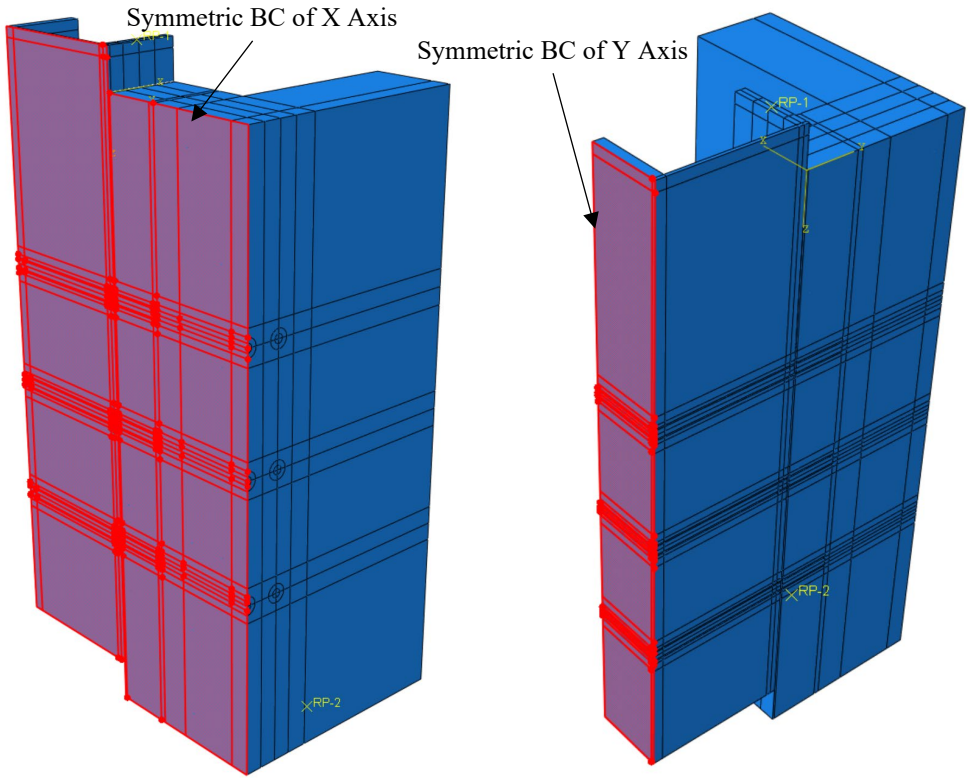

Figure 5.1.4.1 Symmetric Boundary Conditions

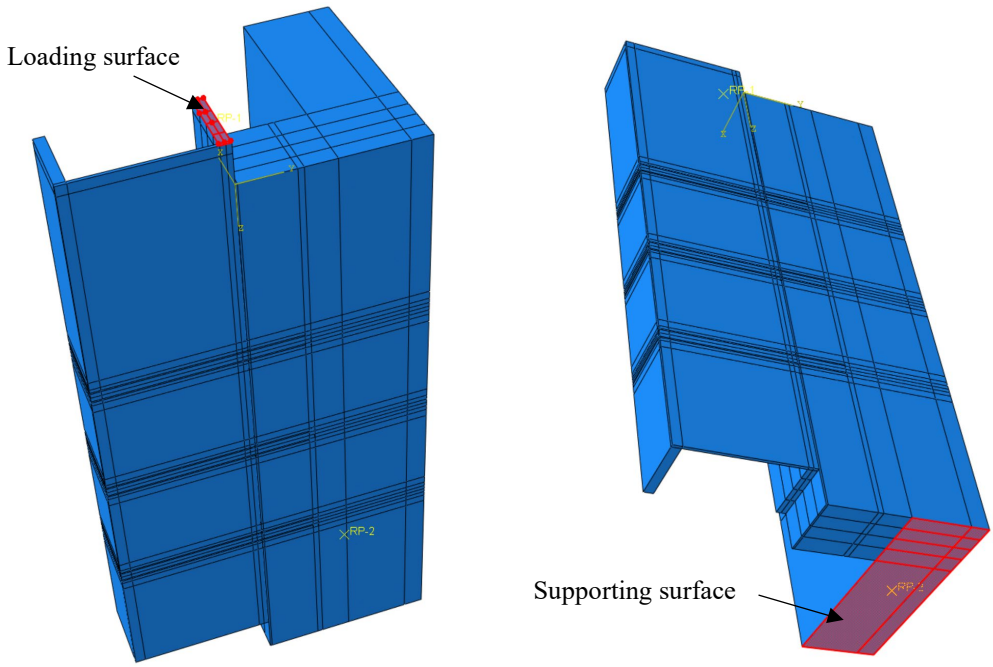

Figure 5.1.4.2 Loading and Supporting Surfaces

5.1.5. Meshing and Elements

For 3D parts in the FE model, including the studs, beam, haunch and slab, the solid element C3D8R (an 8-node linear solid) is used. The truss element T3D2 (a 2-node linear 3D truss) defines the 1D parts used to represent the rebar. In this FE model, significant stress concentrations exist around the area at the bottom of studs, as shown in Figure 5.1.5.1. The FE mesh in this area should be the finest in the model. In contrast, for areas far from the studs, such as around the edge of the slab, the stress gradient is small. Relatively larger mesh sizes can be used in these regions to reduce computational demand. According to these guidelines, after carefully partitioning, the model FE mesh is shown in Figure 5.1.5.2.

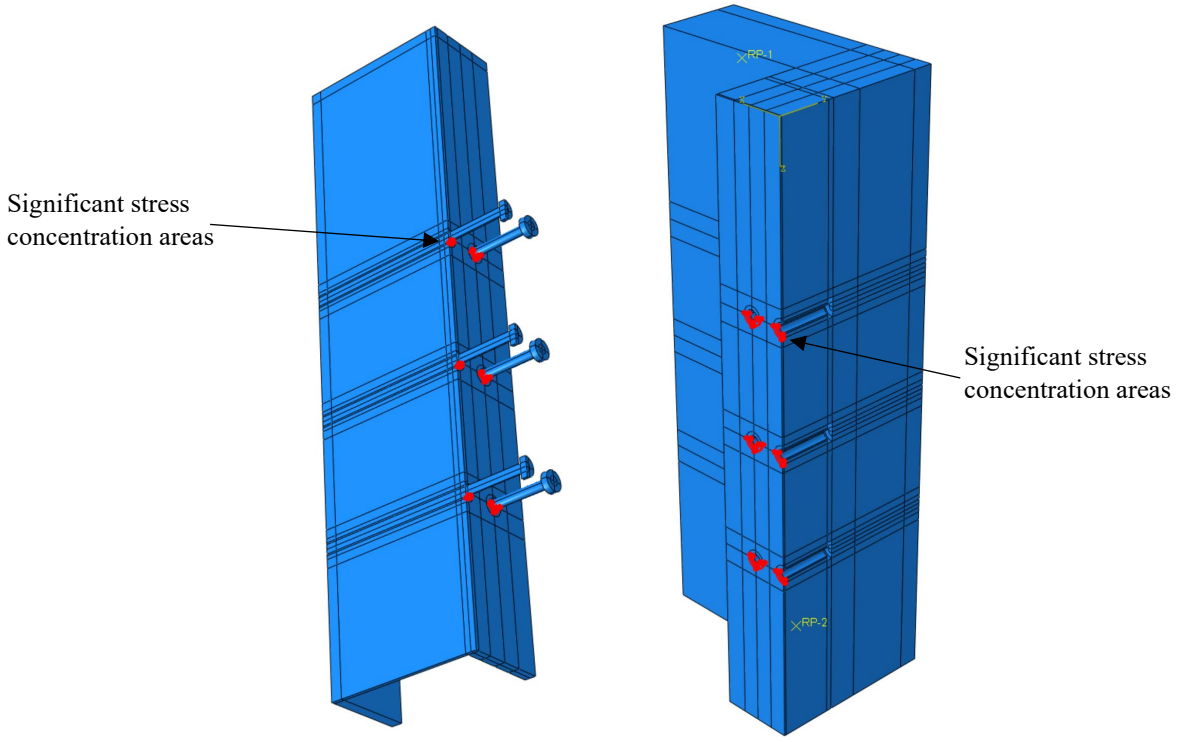

Figure 5.1.5.1 Areas in the Model with Significant Stress Concentrations

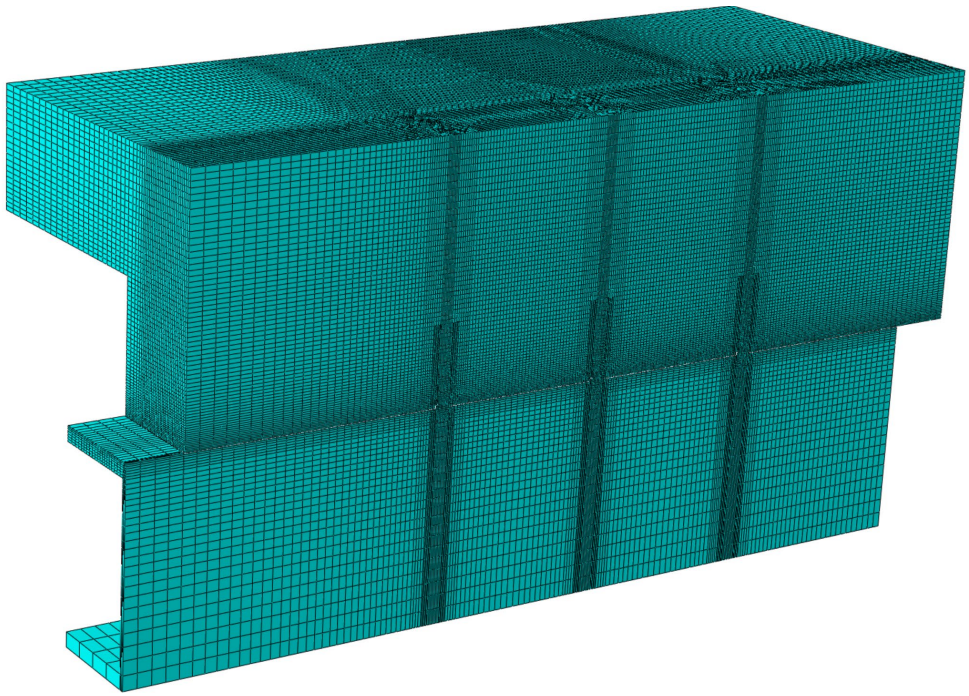

Figure 5.1.5.2 Mesh of the Model

Mesh sensitivity studies are conducted to determine the mesh size required by the model. By continuously refining the mesh, project researchers find that when the average element length in the finest mesh areas reach 0.05 in., the simulation result is similar to when the length is 0.1 in.,

as shown in Figure 5.1.5.3. Therefore, an average element length of 0.1 in. is adopted in the areas that have a significant stress concentration, and an average element length of 1.0 in. is used in the areas that have small stress gradients, as shown in Figure 5.1.5.4.

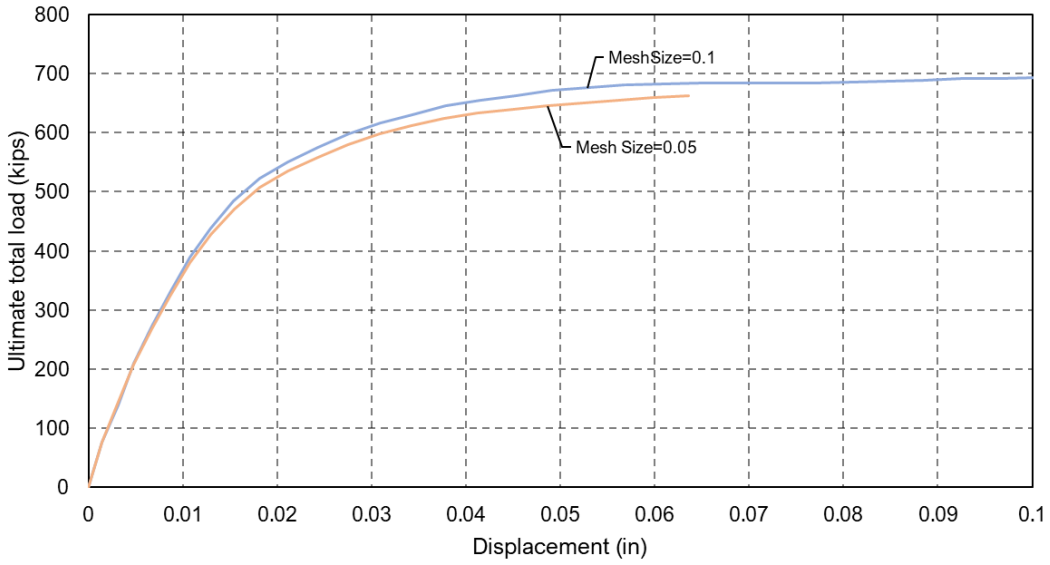

Figure 5.1.5.3 Load-displacement Curve Comparison between Different Mesh Sizes

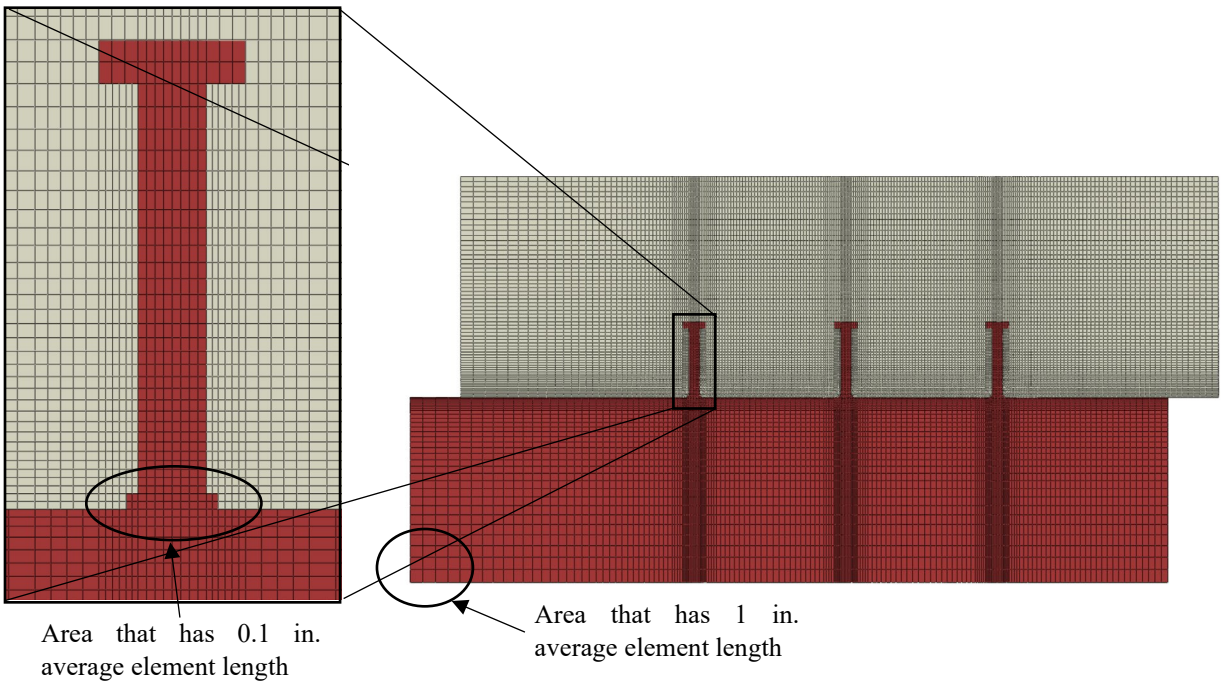

Figure 5.1.5.4 Mesh Size in Different Areas

5.1.6. Analysis Method

Results from the laboratory tests indicate push-out specimens experience large deformations, concrete cracking, steel yielding, and abrupt motions as parts come into and out of contact or slip. These behaviors are challenging to represent in an FE model and can result in large run times or the inability to converge to a solution unless special care is taken. For this reason, Abaqus/Explicit is used as the primary solver. Typically, Abaqus/Standard is used to model structural response under pseudo-static loading like that used during the testing program. When abrupt motions occur, however, Abaqus/Standard may not converge to a solution. If dynamic response is considered in shifting abruptly from one equilibrium position to the next, Abaqus/Standard relies upon an implicit numerical integration scheme (Cook et al., 2002), which may require a large number of iterations to converge to a solution. Such models have a large computational demand and are not efficient. Abaqus/Explicit, conversely, uses and explicit numerical integration scheme (Cook et al., 2002), which is the approach favored by other commercial FE software (e.g., LS-DYNA) when simulating scenarios involving abrupt changes in problem parameters associated with contact and nonlinear material response. Other researchers have reached similar conclusions when modeling push-out tests (Nguyen and Kim 2009). Accordingly, Abaqus/Explicit was used for the FE analyses.

5.1.7. FEA and Test Results Comparison

Seventeen steel girder experiments were performed in the laboratory, eight of which were used in model validation studies (see Table 5.1.7.1). Figures 5.1.7.1-5.1.7.8 compare the FE analyses and experimental results. The average discrepancy in failure load between the test specimens and the FE models is 15%. The FE modeling results indicate that Test 5 failed due to shear stud fracture, while all other cases failed due to haunch cracking. These failure modes are consistent with what project researchers observed in the laboratory tests. Table 5.1.7.2 shows the results comparison summary.

Table 5.1.7.1 Specimens used for FE Model Validation

Test No.	Haunch Depth (in.)	Haunch Reinforcement Detailing	Layers of Stud	Stud Height (in.)
1	9	-	2	6
2	9	U-Bar	1	6
3	9	Stirrup	1	6
4	3	-	1	6
5	0	-	1	6
9	6	-	1	8
11	12	U-Bar	1	6
16	15	Stirrup	1	6

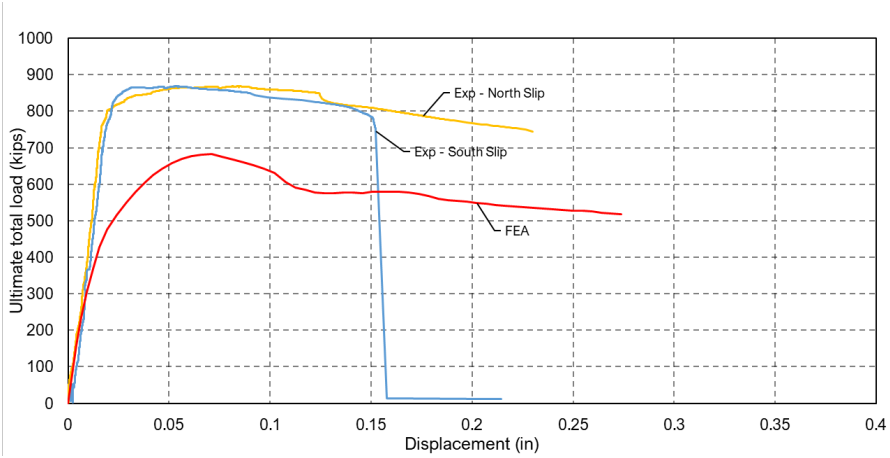

a) Result comparison

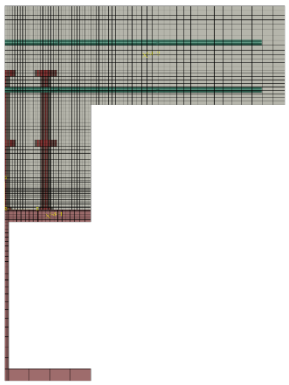

b) Specimen section

Figure 5.1.7.1 Load-displacement Curve Comparison between Test and FEA for Test 1

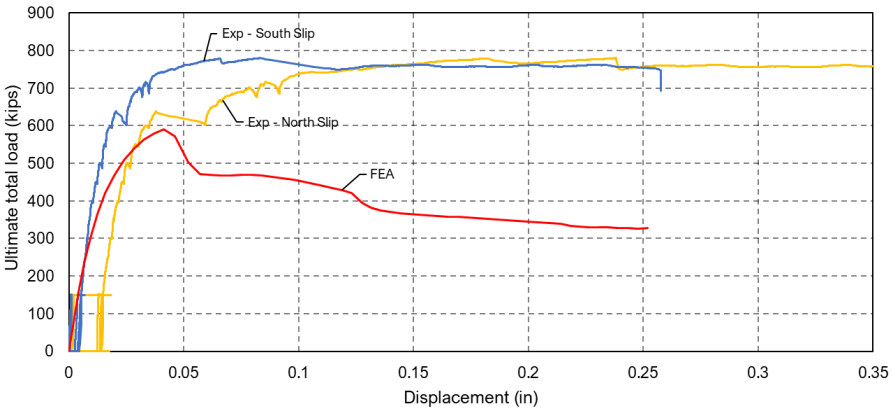

a) Result comparison

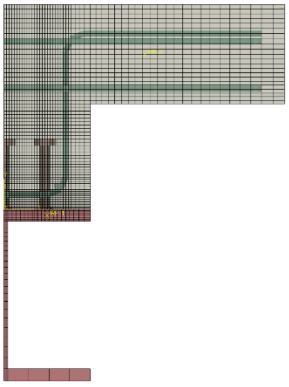

b) Specimen section

Figure 5.1.7.2 Load-displacement Curve Comparison between Test and FEA for Test 2

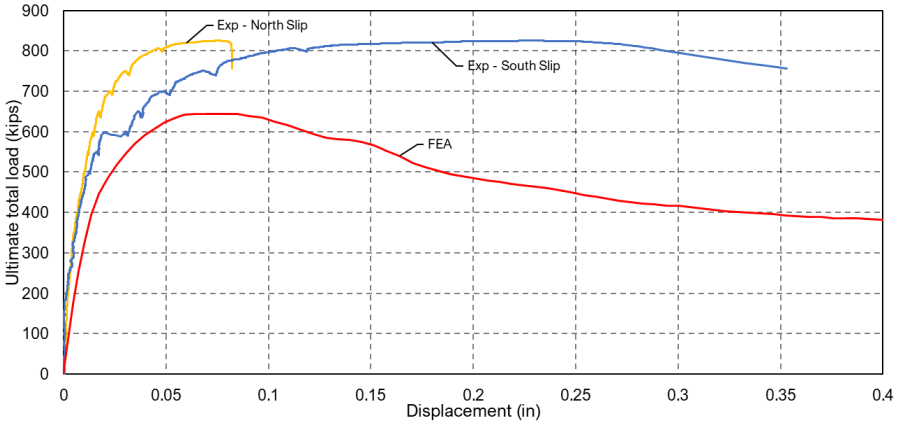

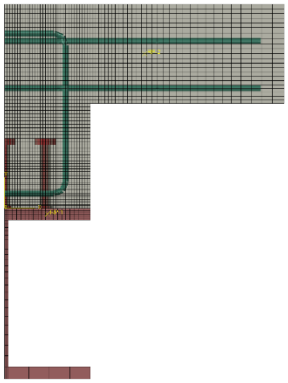

a) Result comparison b) Specimen section

Figure 5.1.7.3 Load-displacement Curve Comparison between Test and FEA for Test 3

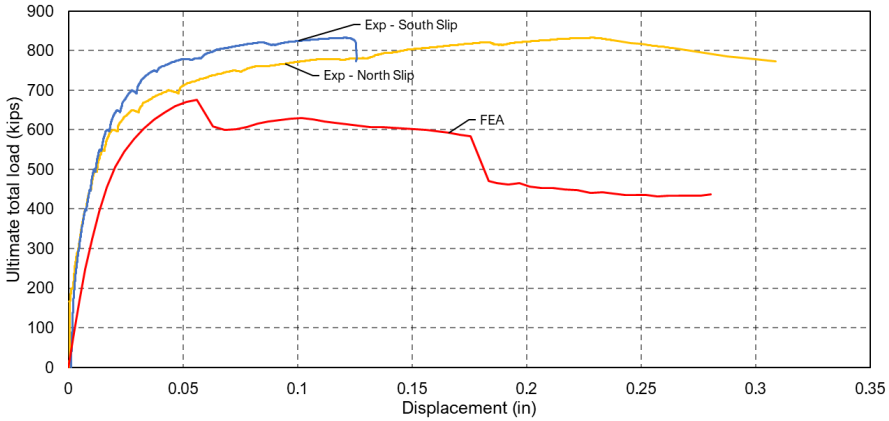

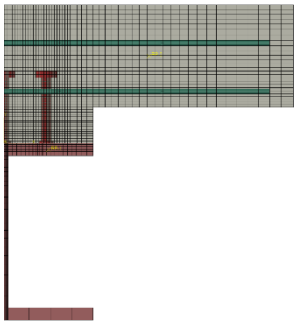

a) Result comparison b) Specimen section

Figure 5.1.7.4 Load-displacement Curve Comparison between Test and FEA for Test 4

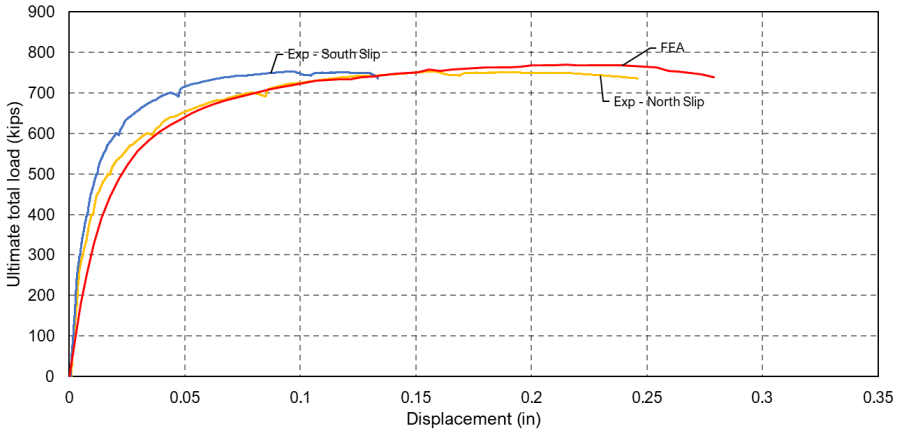

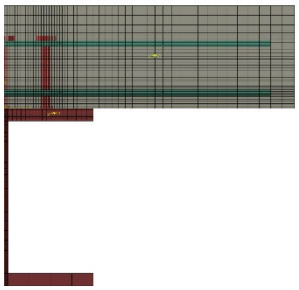

a) Result comparison b) Specimen section

Figure 5.1.7.5 Load-displacement Curve Comparison between Test and FEA for Test 5

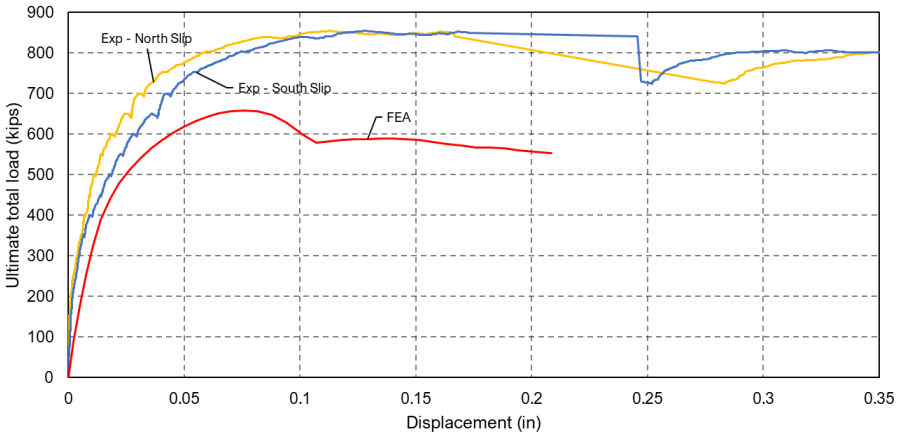

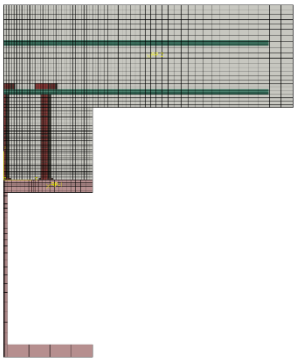

a) Result comparison b) Specimen section

Figure 5.1.7.6 Load-displacement Curve Comparison between Test and FEA for Test 9

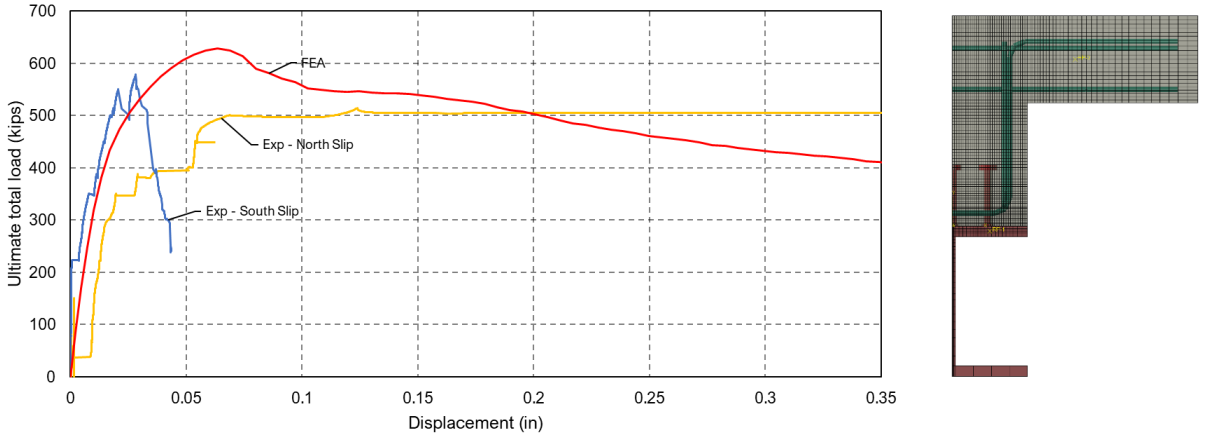

a) Result comparison b) Specimen section

Figure 5.1.7.7 Load-displacement Curve Comparison between Test and FEA for Test 11

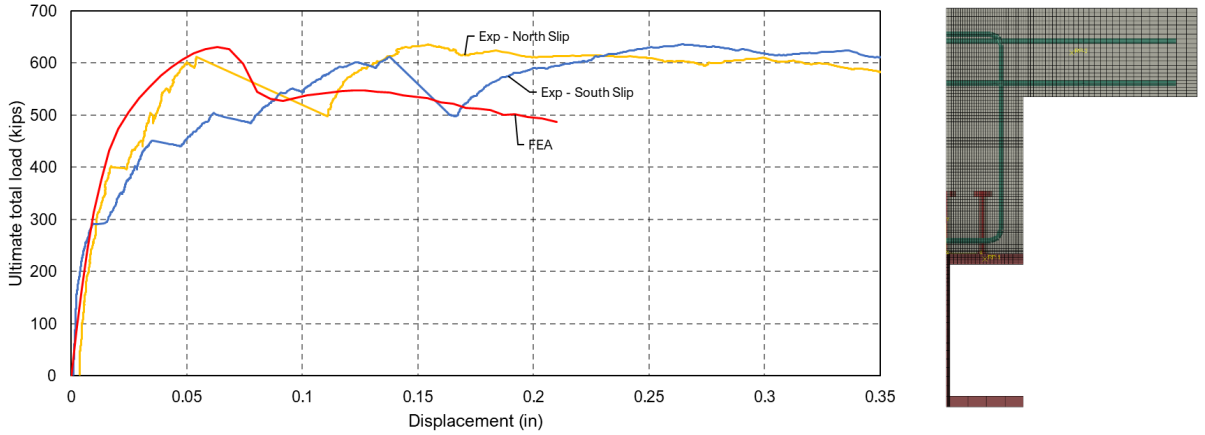

a) Result comparison b) Specimen section

Figure 5.1.7.8 Load-displacement Curve Comparison between Test and FEA for Test 16

Table 5.1.7.2 Result Comparison Summary

Test No.	Concrete Strength (ksi)	Test Failure Load (kips)	FEA Failure Load(kips)	Discrepancy (%)
1	5.5	868	683	-21.3
2	5.5	780	590	-24.4
3	5.0	825	644	-21.9
4	5.0	832	676	-18.8
5	5.1	751	769	2.3
9	5.5	855	658	-23.0
11	4.8	578	628	8.0
16	4.7	635	630	-0.8

5.1.8. Concluding Remarks

From 17 push-out experiments, eight were used for validation of the developed FE model. After carefully selecting the input parameters and conducting a mesh sensitivity study, the FE model can predict the capacity of the experiments with an average accuracy of 85%. This percentage of error is expected considering the non-linear behavior of the push-out tests and variation in material properties. Other factors such as inelastic material properties, imperfections of the test setup can also introduce some level of error. Because the FE model predicts the correct failure mode, an error of 15% or less is acceptable for capturing overall behavior and associated limit states of specimens. Therefore, the FE model is considered to be acceptably accurate for the purposes of evaluating design details in a parametric study of tall haunch steel girder specimens. The next section describes the validation model development for PSC girder specimens.

5.2. PSC Girder

This section describes the FE models used to simulate the laboratory tests for the PSC girder specimens. Information obtained the from Abaqus (Dassault Systemes 2022) manual and literature review (Chapter 2) are used to guide the selection of interaction and material properties for the PSC girder numerical model.

5.2.1. CIP Specimens

This section provides information about the FE model developed and validated for Specimen Group I (CIP specimens). A validation model approximates the behavior of an experimental specimen by estimating its capacity, the slip between the PSC flange (the simulated PSC girder flange) and the steel flange, and the slip between the haunch and the PSC flange. When developing the validation specimen for each experimental case, the FE model should account for the experimental specimen's geometry, material properties, boundary conditions, and loading conditions. A thorough literature review and independent verification guides the assumptions about unknown FEA meshing, interaction, and material properties.

5.2.1.1. Geometric Properties

Figure 5.2.1.1 depicts a computational specimen used for Specimen Group I (with CIP decks) with symmetric boundary conditions on one face of the steel girder flange. Symmetry is employed to increase numerical efficiency when performing structural analysis. A symmetric model cannot account for the redistribution of loads from one specimen to the other. Therefore, the experimental tests that did not experience a symmetric and simultaneous failure in both specimens may not be accurately captured by the FE model. Nonetheless, this approach is suitable for parametric evaluation of tall haunch specimens where the primary concern is assessing how changes in various modeling parameters influence the computed capacity.

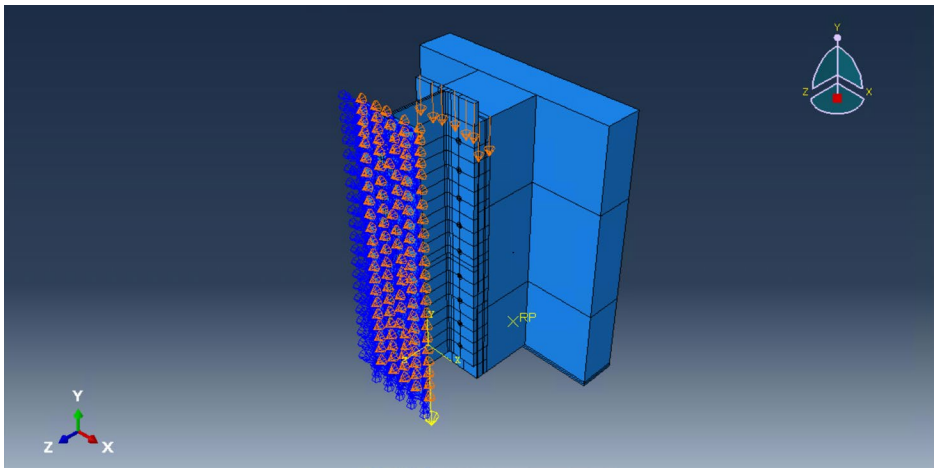

Figure 5.2.1.1 Computational Model with Symmetric Boundary Conditions (CIP Specimens)

The FE models use the geometric properties described in Chapter 4. The parts of the computational model consist of the slab, haunch, wide flange, shear studs, and deformed bars. The slab, haunch, and wide flange shapes are extruded from 2D drawings. The shear studs are 3D parts created from revolutions of 2D drawings. The deformed bars are 3D wire parts with uniform cross-sections. The bars R and U contain 3-in. fillets.

Unlike the steel girder specimen, the shear studs in the simulated PSC girder should not fail if the specimens behave as expected. The weld geometry is still provided in the FE model surrounding the stud to allow for smooth stress transfer from one metal to the other. Shear studs with weld geometry, bars R, and steel section are merged together to act as a single component in the FE model.

5.2.1.2. Material Properties

The concrete properties are simulated using the CDP material model in Abaqus (Dassault Systemes 2022). The CDP model parameters such as dilatancy angle, viscosity, and concrete compressive strength influence the computed behavior of the specimens. These parameters require verification through numerical evaluation. Post-failure load-slip data from computational validation efforts indicate some dynamic effects immediately after debonding of the simulated girder from the haunch. A reasonably large viscosity parameter of 1% reduces the dynamic response after failure.

An evaluation of dilation angles between 30 and 40 degrees indicates a limited correlation between this parameter and the specimen capacity (Figure 5.2.1.2). The validation models for this project use a dilation angle of 40 degrees based on recommendations from a past push-out test study (Silva et al. 2021) and the parametric study (Figure 5.2.1.2) that indicates essentially no influence of concrete dilation angle on specimen capacity. Other CDP parameters considered are based on default values from the Abaqus (Dassault Systemes 2022) manual.

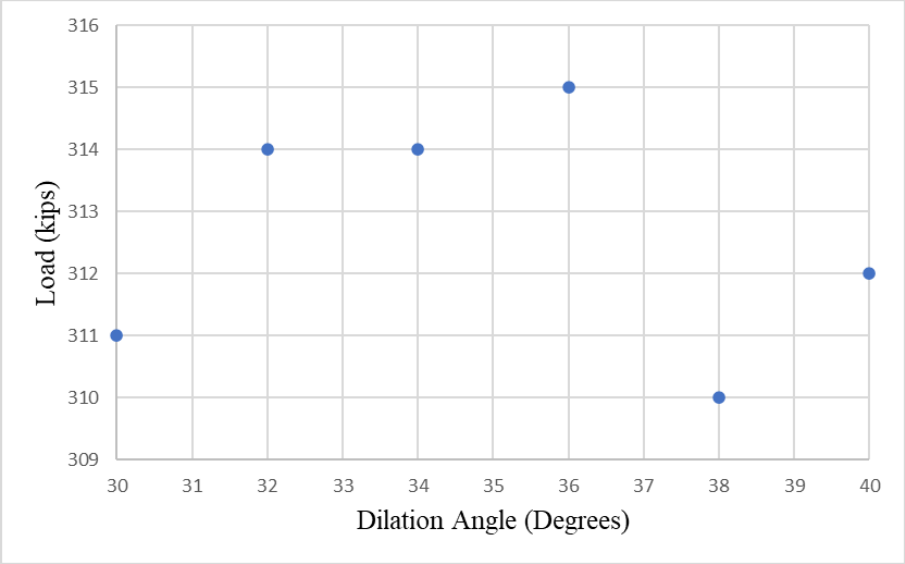

Figure 5.2.1.2 Capacity as a Function of Concrete Dilation Angle (6-in. Haunch Specimen)

As mentioned previously, the CDP model requires definitions of the elastic and plastic behavior of concrete in both uniaxial tension and compression. A compression plot is adopted from CEN (2004b) for all concrete layers present in the FE model. The tension plot is linear up to the tensile strength estimated as $7.5\sqrt{f'_c}$ (ACI 318 2019). The post-cracking curve formulation is obtained from Collins-Mitchell (1980). Figures 5.2.1.3 and 5.2.1.4 show the compression and tensile model for one of the 12-in. haunch specimens with $f'_c = 4.5\ ksi$.

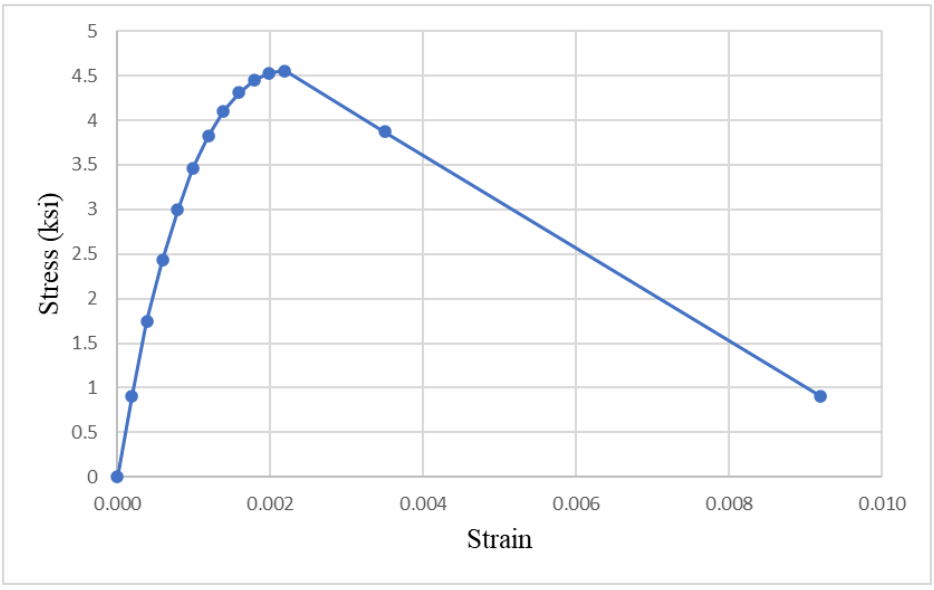

Figure 5.2.1.3 Concrete Compression Properties (12-in. Haunch Specimen)

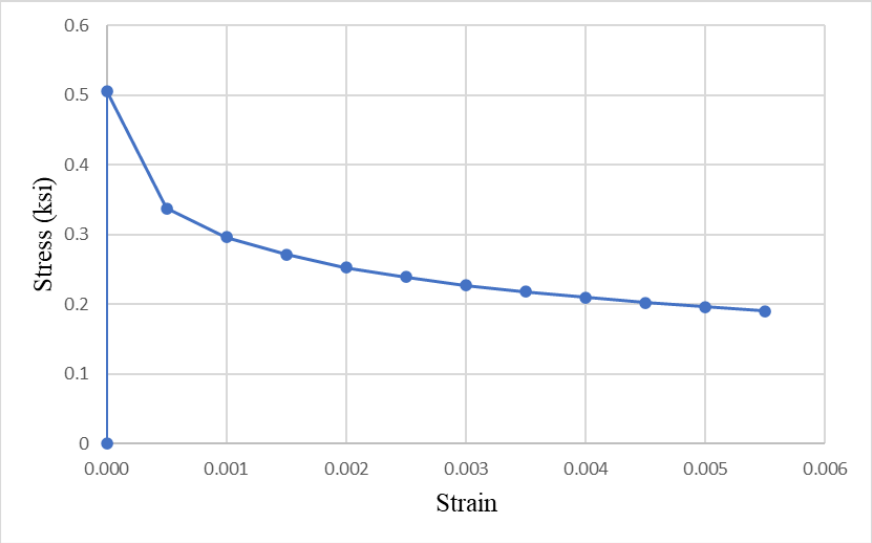

Figure 5.2.1.4 Concrete Tension Properties (12-in. Haunch Specimen)

A trilinear stress-strain curve is used to define the properties for steel sections, bars R, and reinforcement bars and is shown in Figure 5.2.1.5. The stress-strain relationship for shear studs is elastic-perfectly-plastic with $f_y = 60\ ksi$. These properties are based on the material tests performed by the research team and by the fabricators (mentioned in Chapter 4).

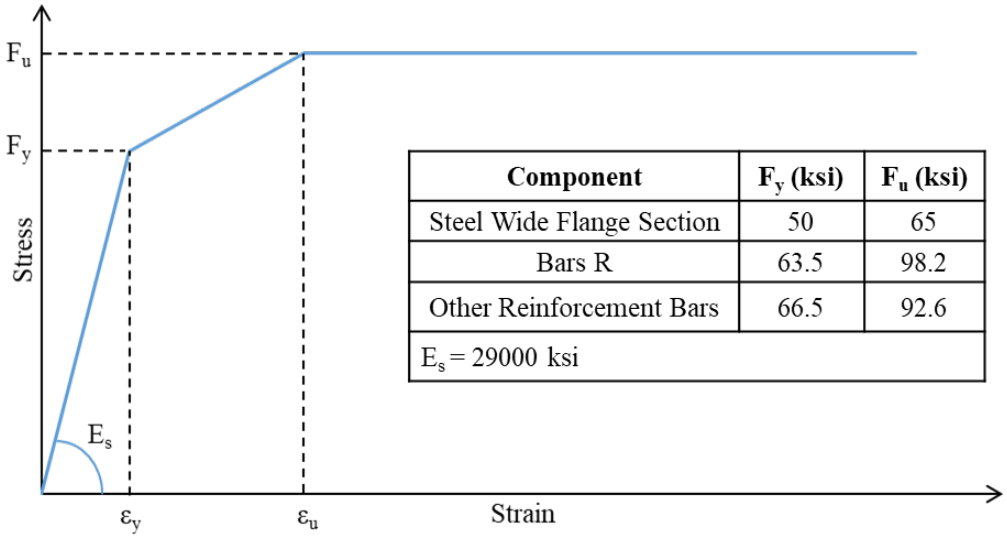

Component	F_y (ksi)	F_u (ksi)
Steel Wide Flange Section	50	65
Bars R	63.5	98.2
Other Reinforcement Bars	66.5	92.6
E_s = 29000 ksi		

Figure 5.2.1.5 Steel Section and Reinforcement Properties

5.2.1.3. Interaction Properties

As mentioned in previous sections, Abaqus (Dassault Systemes 2022) provides a "hard" contact definition to model normal contact between solid materials. Hard contact prevents penetration of one part's surface through adjacent parts. To model tangential contact between two parts, Abaqus (Dassault Systemes 2022) defines friction contact as rough, frictionless, or friction

penalty. Cohesive contact can be defined in Abaqus (Dassault Systemes 2022) in the form of a contact interaction property with elastic stiffness, damage initiation, and damage evolution. One of the cohesive damage models included in Abaqus (Dassault Systemes, 2022) is a quadratic separation model. The cohesive layer behaves elastically until a user-defined threshold is reached (Figure 5.2.1.6). This threshold is referred to as the damage initiation value. Damage evolves after initiation such that the capacity degrades gradually to zero at a user-defined deformation value (Figure 5.2.1.6).

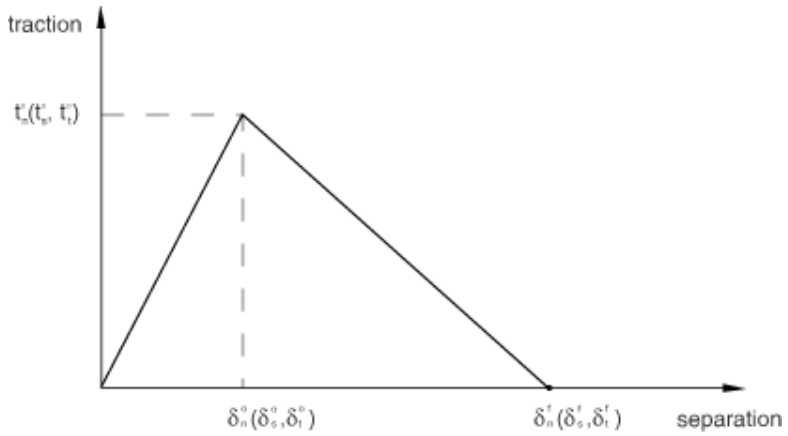

Figure 5.2.1.6 Traction-separation Model used for Cohesive Damage Definition in Abaqus (Dassault Systemes, 2006)

The FE models assume the interface between the steel section (welded with shear studs and bars R) and the simulated PSC girder has a rough friction definition in Abaqus (Dassault Systemes, 2022). In the experimental tests, actuators apply load to both the steel girder and the simulated PSC girder at the same rate, minimizing the slip between these parts. Experimental data confirm the simulated PSC girder and steel experience minimal relative displacement compared to the simulated PSC girder-haunch interface. The interface between the slab base and the rigid base uses a friction coefficient of 1.5 to permit minimal slip between these surfaces, which is also consistent with test observations.

The reinforcement bars in the slab, haunch, simulated PSC girder are bonded to the concrete using the “embedded region” constraint in the FE model. Iterative calibration and information from the research literature inform the selection of contact properties between simulated PSC girders and the haunch. The following subsections provide information about the effects of different contact properties at this interface.

5.2.1.3.1. Friction Coefficient

AASHTO LRFD (2020) provides a range of friction coefficients between 0.7 and 1.4 for interface shear transfer between concrete cast at different times. The following friction coefficients between the simulated girder and haunch aid in the parametric evaluation of the FE models: 0.7, 1.0, 1.1, and 1.4. At high coefficients of friction, the strength at the haunch-girder interface exceeds that of the steel-girder interface for the 12-in. haunch specimen (Figure 5.2.1.7), leading to a premature failure between the simulated PSC girder and the steel flange.

The 6-in. haunch specimen data (Figure 5.2.1.8) suggest a positive correlation between the friction coefficient and specimen capacity. The researchers selected a friction coefficient of 1.2 to accurately represent the frictional resistance to shear in the experimental specimens.

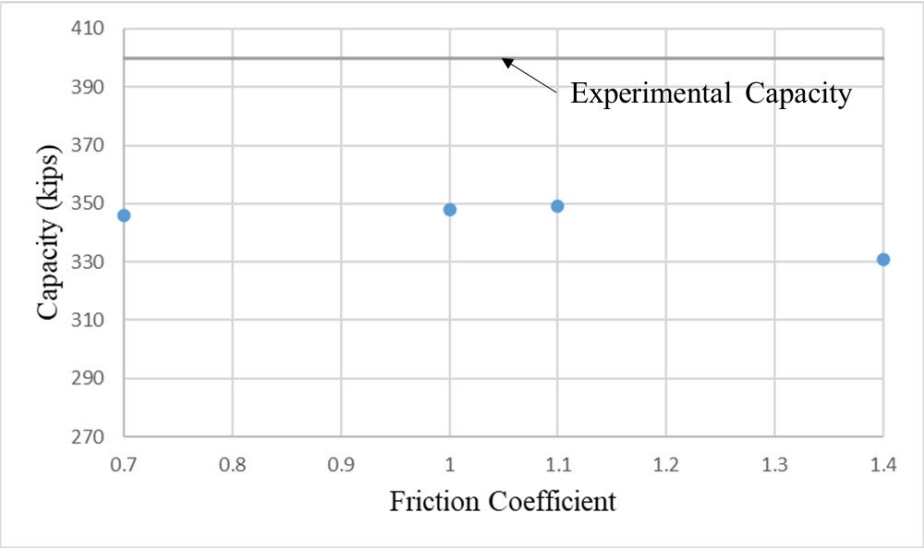

Figure 5.2.1.7 Specimen Capacity versus Friction Coefficient (12-in. Haunch Specimen)

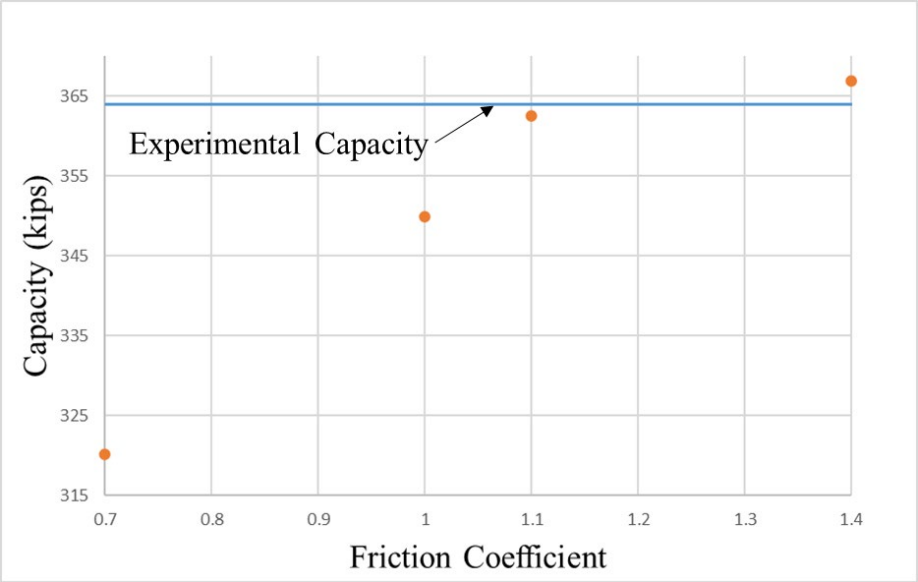

Figure 5.2.1.8 Specimen Capacity versus Friction Coefficient (6-in. Haunch Specimen)

5.2.1.3.2. Cohesive Damage Initiation

The capacity of PSC girder push-out specimens directly correlates to the cohesive strength of the interface between the simulated girder and the haunch. Therefore, this study examines the effects of a range of cohesive damage initiation thresholds specified in AASHTO LRFD (2020)

including 0.28 ksi, 0.32 ksi, 0.36 ksi, and 0.40 ksi (Figures 5.2.1.9 and 5.2.1.10). These cohesive damage initiation variables refer to the cohesion at the interface of the simulated girder and haunch. A positive correlation exists between the capacity and the cohesive damage initiation magnitude.

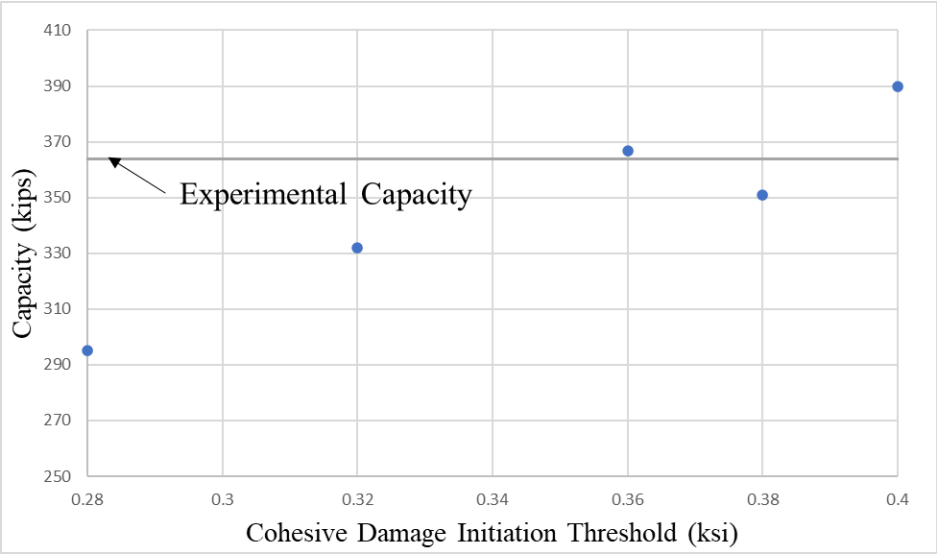

Figure 5.2.1.9 Specimen Capacity versus Cohesive Damage Initiation Threshold (6-in. Haunch Specimen)

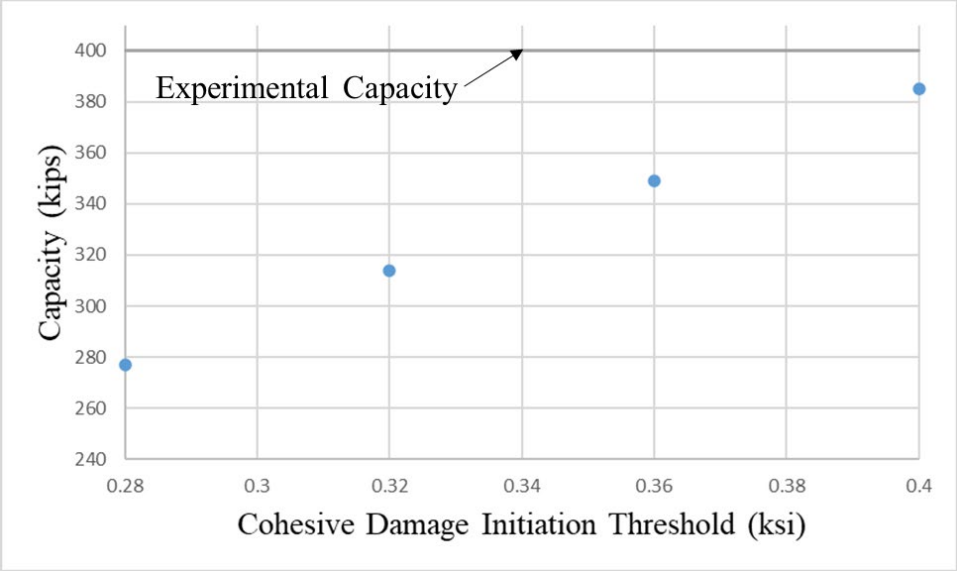

Figure 5.2.1.10 Specimen Capacity versus Cohesive Damage Initiation Threshold (12-in. Haunch Specimen)

The cohesive damage initiation thresholds outlined in AASHTO LRFD (2020) underpredict the strength of prestressed concrete composite sections in the model. The validation models use a cohesive damage initiation threshold equal to 0.50 ksi, which gives computed capacities between 80% and 100% of the experimental capacities.

5.2.1.3.3. Cohesive Damage Evolution

Iterative evaluation of different FE models suggests a correlation between cohesive damage evolution parameters (i.e., total and plastic displacement after damage initiation) and the amount of slip experienced by the computational specimen at failure. An increase in the total and plastic displacement causes the cohesive layer's stiffness to degrade less rapidly as its deformation increases, based on the traction-separation cohesive damage model used by Abaqus (Dassault Systemes, 2022) (Figure 5.2.1.11). The difference between separations at points A and B in Figure 5.2.1.11 equal the plastic displacement after damage initiation. For cohesive layers with a larger plastic displacement definition, the associated specimen endures more load after cohesive damage initiation compared to a specimen with a smaller plastic displacement definition.

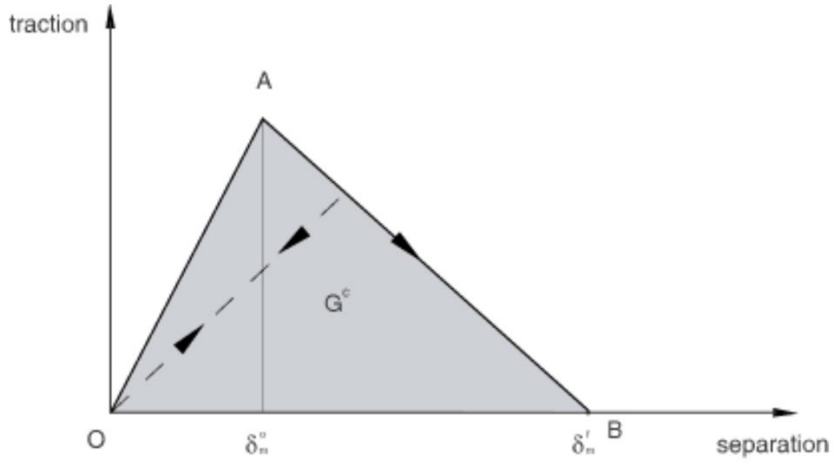

Figure 5.2.1.11 Damage evolution on Abaqus (Dassault Systemes, 2006)

Plastic displacement theoretically only influences the behavior of the specimen after cohesive damage initiation. Therefore, the cohesive damage evolution parameters should not influence a specimen's failure mode or load-slip behavior before failure. Because the specimens experience a brittle failure (Chapter 4), the plastic displacement should have a small value, representing an abrupt loss of cohesive stiffness after cohesive damage initiation.

The following plastic displacements between the simulated PSC girder and the haunch are examined: 0-in., 0.01-in., 0.025-in., 0.035-in., and 0.05-in. Abaqus (Dassault Systemes, 2022) requires a non-zero definition of the cohesive damage evolution parameter to model damage to the cohesive layer after its initial failure.

The 12-in. haunch specimen results (Figure 5.2.1.12) indicate the plastic displacement has little correlation with the specimen capacity, but it does have a positive correlation to the load at which damage to the cohesive layer initiates (indicated as break in Figure 5.2.1.12). The 6-in. haunch specimen data (Figure 5.2.1.13) indicate the plastic displacement correlates to an increase in specimen capacity. The FE models use a damage evolution parameter of 0.05 in. for the parametric study because models with this plastic displacement predict the experimental capacities within 80%-100%, which is the established accuracy goal for this study.

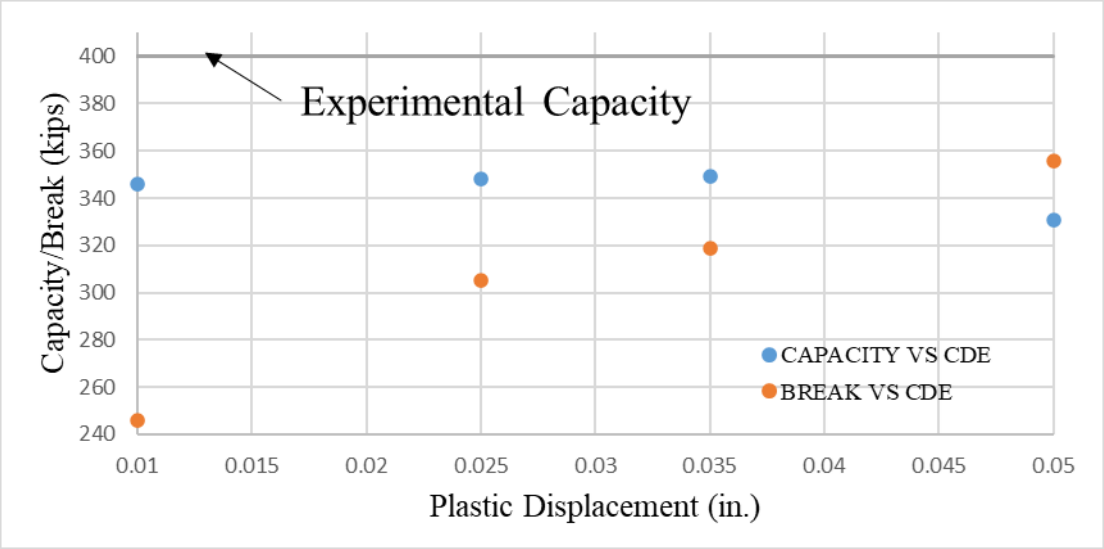

Figure 5.2.1.12 Specimen Capacity versus Cohesive Damage Evolution (12-in. Haunch)

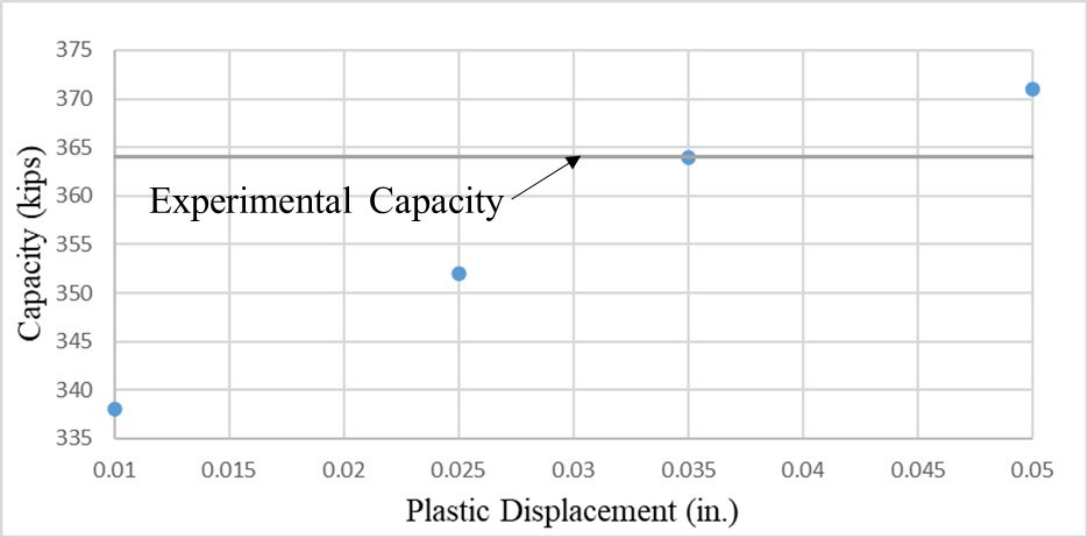

Figure 5.2.1.13 Specimen Capacity versus Cohesive Damage Evolution (6-in. Haunch)

5.2.1.4. Loading and Boundary Conditions

Hydraulic actuators apply loads to experimental specimens at the top surface of the wide flange and simulated PSC girder. Displacement boundary conditions in the model induce deformations at the same locations of the FE model (Figure 5.2.1.14).

The experimental specimens rest on a steel plate within a rigid testing frame. The computational model simulates the test apparatus as a discrete rigid part, defined with extremely large mass and rotational inertia. Hard normal and tangential contact definitions (friction coefficient = 1.5) between the base of the specimen and the rigid part restrict specimen penetration and simulate friction from the hydrostone between the specimen base and the test apparatus.

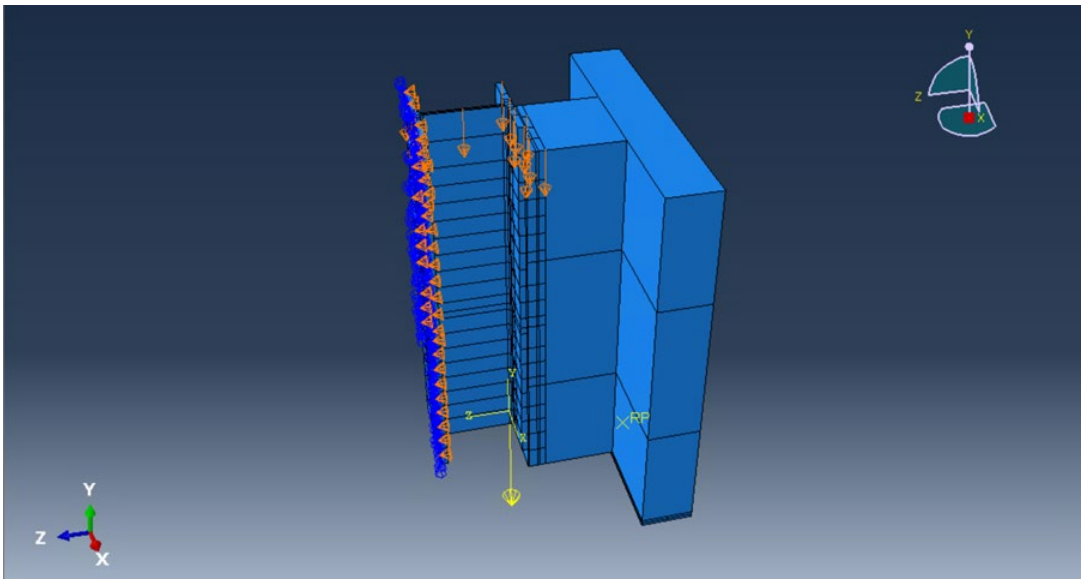

Figure 5.2.1.14 Applied Loading and Boundary Conditions

The presence of gravity load in the FE model influences the post-failure behavior (Figure 5.2.1.15). Including gravity does not significantly impact the capacity of a specimen but limits vibration or motion in the direction opposite of the applied load before instability occurs. The validation models use a standard gravitational acceleration of -386.4 in./s^2.

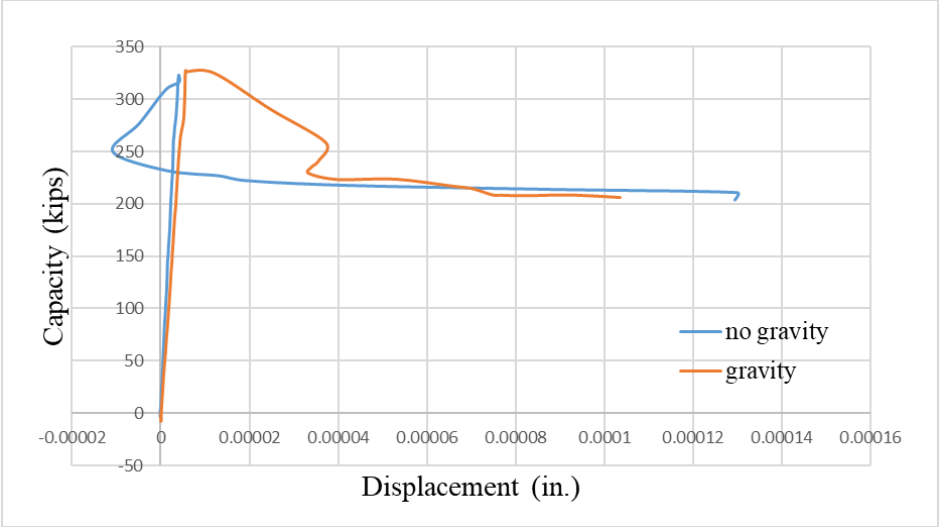

Figure 5.2.1.15 Influence of Gravity Load (12-in. Haunch Specimen)

5.2.1.5. Meshing

All elements are modeled with explicit linear elements. All parts, except for reinforcing bars, consist of C3D8 (8-node linear 3D continuum) solid elements. The reinforcement consists of T3D2 (2-node linear 3D truss) elements. The base consists of rigid elements. Elements in the

model have an aspect ratio of less than 10:1, based on the recommendations of Stith (2010). Thus, the longest dimension of any 3D element does not exceed ten times the length of the shortest dimension of that element.

The validation models use meshing seeds of the following sizes:

- studs, weld collars, PSC stud holes = 0.18 in.
- hot-rolled steel = 0.56 in.
- simulated PSC girder = 0.57 in.
- shear reinforcement (Bars U, bars R, vertical stirrups) = 0.20–0.25 in.
- haunch, slab, and discrete rigid base = 2 in.

5.2.1.6. Validated Models

Computational models can be validated by comparing their load-slip behavior at discrete locations where linear potentiometers recorded the load-slip behavior of experimental specimens (Section 4.4). Using the previously investigated parameters, numerical models can be used to predict the capacity of the experimental specimens. First, consider the results of the 12-in. haunch specimen, which aided in the calibration of unknown parameters. Figure 5.2.1.16 shows the test results compared with the FE model results. The FE model load results are doubled to account for two specimens tested together during the experiments (refer to Chapter 4). The data demonstrate that the FE models predict the capacity of the experimental specimen within 1% accuracy.

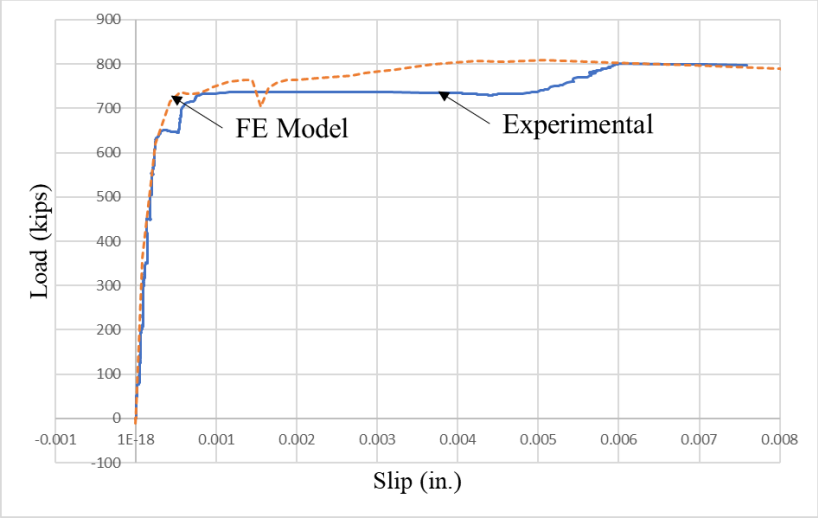

Figure 5.2.1.16 Numerical and Experimental Load-slip Data (12-in. Haunch with Bars U)

The 2-in., 6-in., and 9-in. haunch specimens did not aid in the calibration of unknown modeling parameters and served as validation models only. Figures 5.2.1.17–5.2.1.20 compare the computational and experimental results. These data demonstrate that the FE model closely represents the capacity of the experiment within 20%. Some differences arise in experiments due to variability in concrete material properties, and contact properties (such as friction, and cohesion). Note that the numerical model experiences a gradual loss of capacity after reaching its peak rather than an immediate and total loss of stiffness. The differences in slip can also be attributed to the precision of the linear potentiometers used to measure the slip of the experimental specimens.

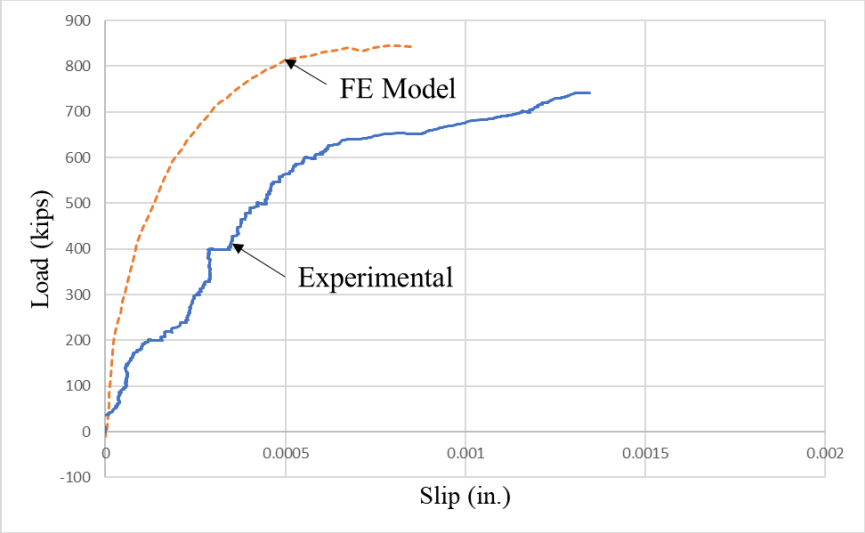

Figure 5.2.1.17 Numerical and Experimental Load-slip Data (2-in. Haunch without Bars R)

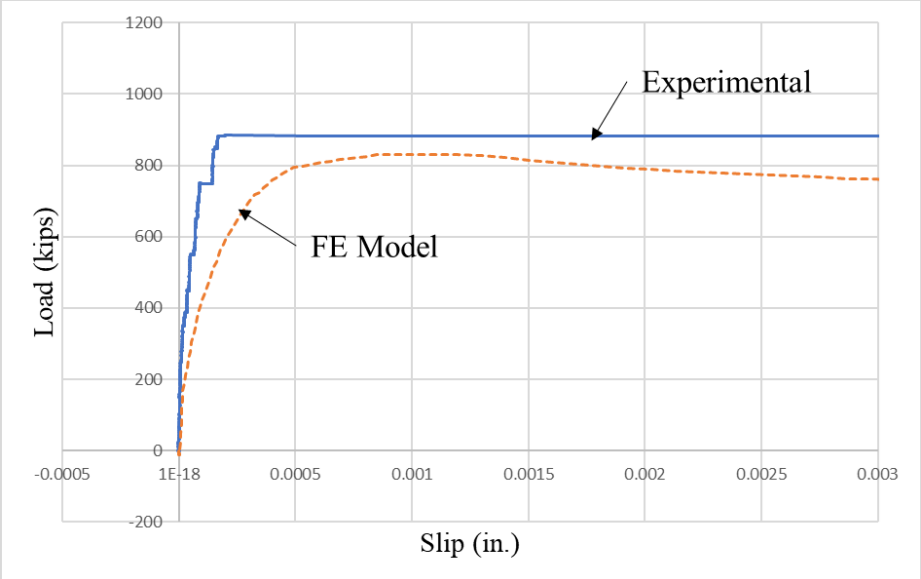

Figure 5.2.1.18 Numerical and Experimental Load-slip Data (2-in. Haunch)

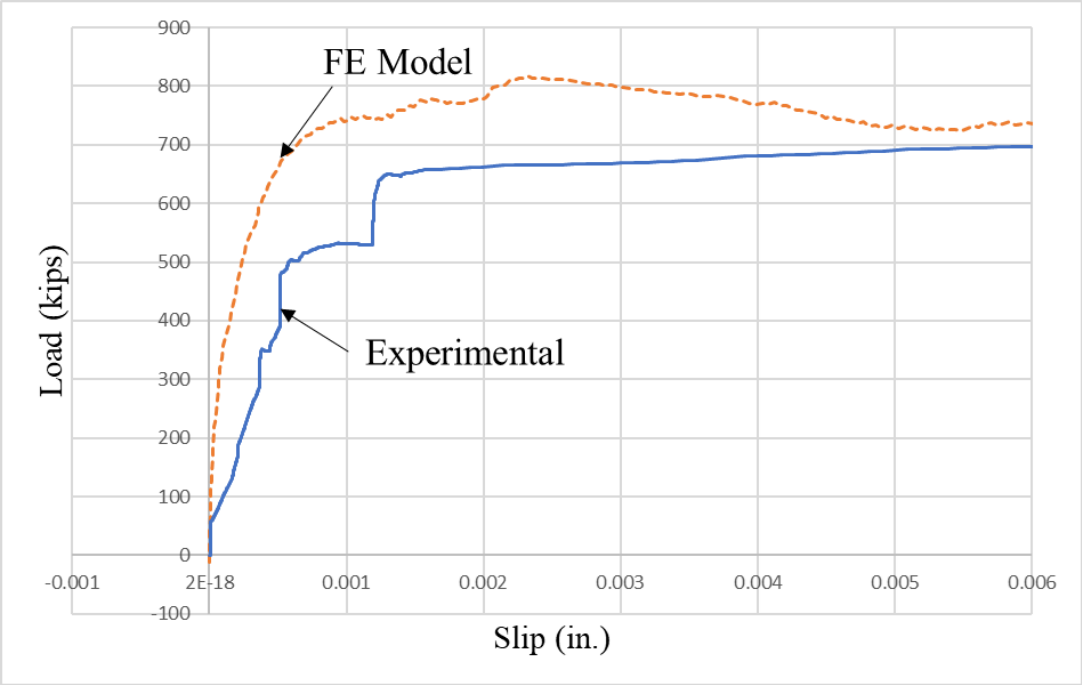

Figure 5.2.1.19 Numerical and Experimental Load-slip Data (6-in. Haunch with Bars U)

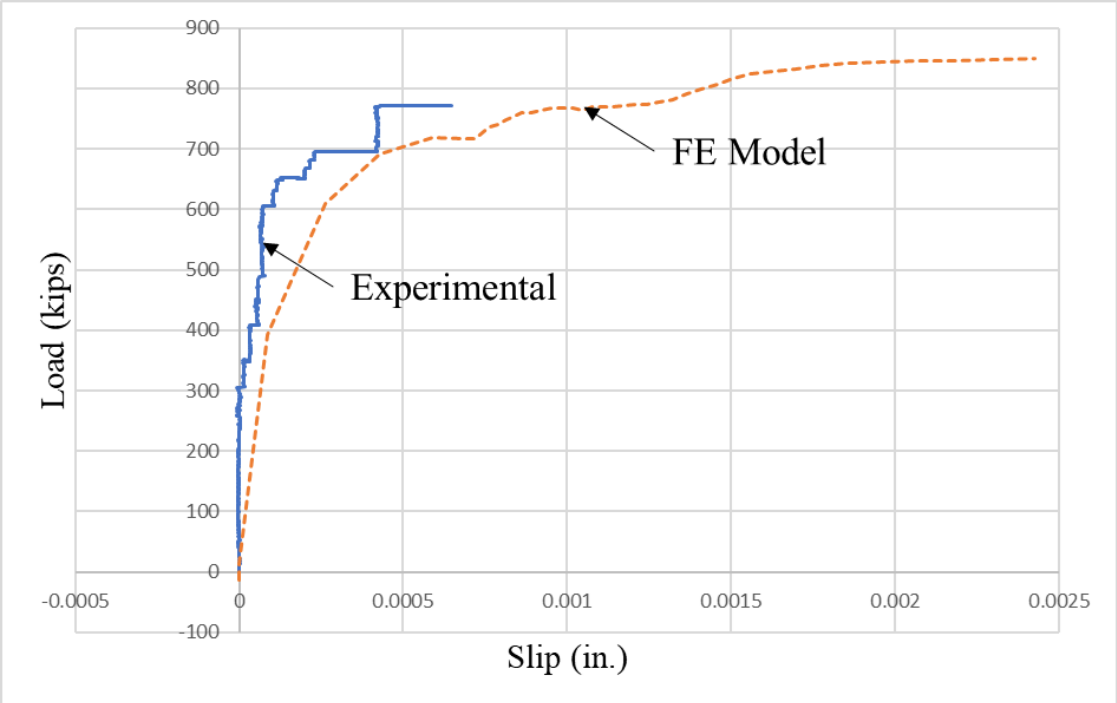

Figure 5.2.1.20 Numerical and Experimental Load-slip Data (9-in. Haunch with Vertical Stirrups)

Despite the differences between the computational and experimental load-slip behaviors, the ability of the FE models to predict experimental capacity makes them valuable for studying the relative effectiveness of changes to a specimens' design and detailing. This level of accuracy is judged as reasonable given the governing brittle failure mode and typical variations in concrete material properties. The next section provides validated model details for PSC girder specimens with a PCP deck.

5.2.2. PCP Specimens

This section provides information about the validation model developed for Specimen Group II (PCP deck specimens). The main difference between Specimen Groups I and II is the number of shear planes. The PCP specimens have at least two interfaces (simulated PSC girder-haunch, PCP-haunch) that needs to be considered. Three shear planes need to be considered for the SGD specimens (Section 4.1). Some of the FE model properties in this section are derived from the CIP specimens' model and are described in the following subsections.

5.2.2.1. Geometric Properties, Loading, and Boundary Conditions

Figure 5.2.2.1 shows the FE model developed for Specimen Group II (with PCP decks) with symmetric boundary conditions on one face of the steel girder flange. As mentioned previously, the experimental tests that did not experience a symmetric and simultaneous failure in both specimens may not be accurately represented by the FE model. The loading surfaces, displacement and support boundary conditions, and gravity load are consistent with those for CIP specimens presented in Section 5.2.1.

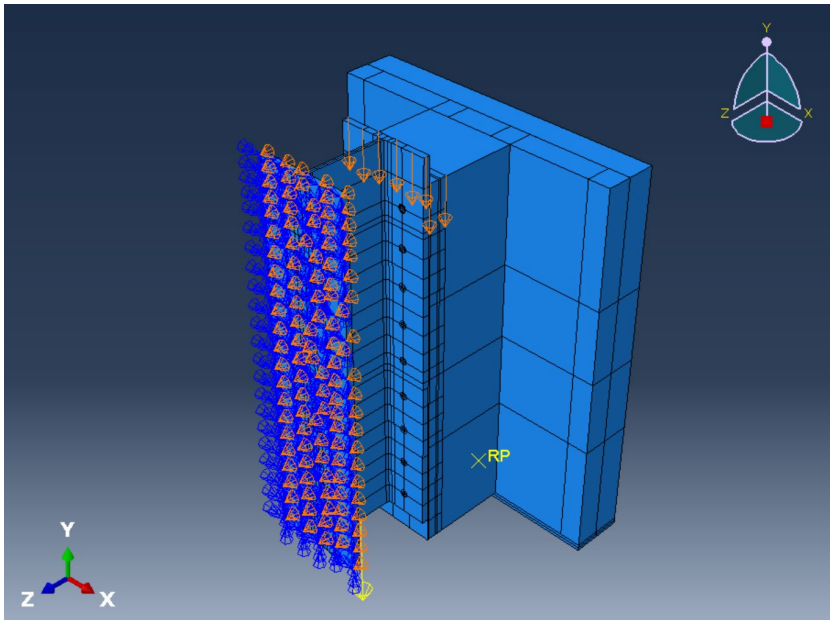

Figure 5.2.2.1 Computational Model with Symmetric Boundary Conditions (PCP Specimens)

The geometric properties for PCP specimens are as described in Chapter 4. The additional parts for these specimens compared to CIP specimens are a PCP concrete layer and reinforcement mat. Bars UP are used instead of Bars U (refer to Section 4.1 for configuration). An SGD concrete layer with inverted Bars U (refer to Section 4.1 for configuration) is used for some specimens.

5.2.2.2. Material Properties

The parameters for the CDP model in Abaqus (Dassault Systemes 2022) remain the same as for the CIP specimens. Compression and tension plots for the CDP model are developed for CIP, PCP, simulated PSC girder, and SGD concrete layers. The concrete compressive strength for all the layers is derived from the tests and plots developed in the same manner as for CIP specimens. The properties for steel components are identical to those in CIP specimens.

5.2.2.3. Interaction Properties

The interaction properties between the steel section and the simulated PSC girder, slab base and the rigid base, and reinforcement bars and concrete are as mentioned for the CIP specimens in Section 5.2.1. The interaction at the simulated PSC girder-haunch and PCP-haunch interfaces are selected based on iterative calibration using similar procedure to that performed on CIP specimens in Section 5.2.1.3. Hard contact is defined for both interfaces. Other interaction properties for both the interfaces are shown below in Table 5.2.2.1:

Table 5.2.2.1 PSC Girders Test Matrix

Interface	Cohesive Damage Initiation (ksi)	Cohesive Damage Evolution (in.)	Friction Coefficient
PCP-Haunch	0.1	0.01	1
Simulated PSC Girder-Haunch	0.28	0.05	1

5.2.2.4. Meshing

The mesh element types are as mentioned for CIP specimens. The additional concrete layer/s in PCP specimens also consist of C3D8 (8-node linear 3D continuum) explicit linear elements. The PCP reinforcement bars consists of T3D2 (2-node linear 3D truss) explicit linear elements. The validation models use meshing seeds of the following sizes:

- studs, weld collars, PSC stud holes = 0.2 in.
- hot-rolled steel = 0.5 in.
- simulated PSC girder = 0.5 in.
- shear reinforcement (Bars UP, bars R, SGD Rebars) = 0.5 in.
- haunch, PCP, slab = 0.5 in.

- discrete rigid base = 10 in.

5.2.2.5. Validated Models

The load versus slip plots are compared for the linear potentiometer locations at all the shear interfaces (refer to Section 4.4). The PCP-haunch interface is the most critical interface with maximum slip for all the specimens. Figures 5.2.2.2–5.2.2.6 show five out of seven test results performed using SB_P compared with the FE model results for the PCP-haunch interface. The FE model load results are doubled to account for two specimens tested together during the experiments (refer to Chapter 4). The data demonstrate that the FE models predict the capacity of the experimental specimen within 20% accuracy. As mentioned previously, differences arise in experiments due to variability in concrete material properties and contact properties. The failure observed in the FE model specimens was consistent with the experimental results with maximum slip at the PCP-haunch interface and diagonal cracking in the haunch. Therefore, the accuracy of the FE model developed for PCP specimens is considered acceptable.

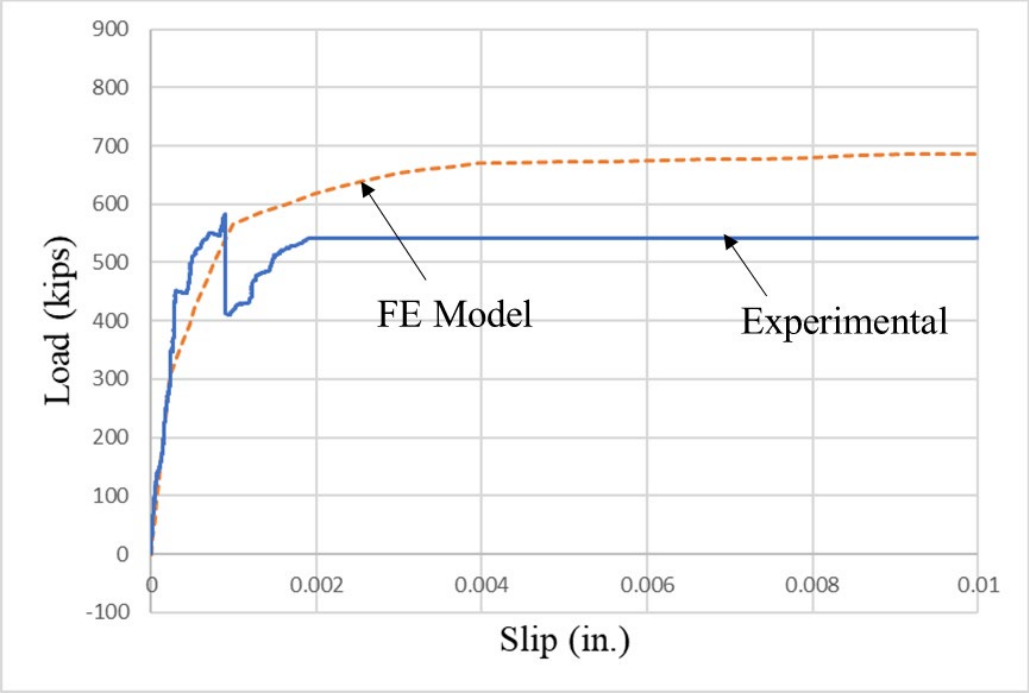

Figure 5.2.2.2 Numerical and Experimental Load-slip Data (2-in. Haunch)

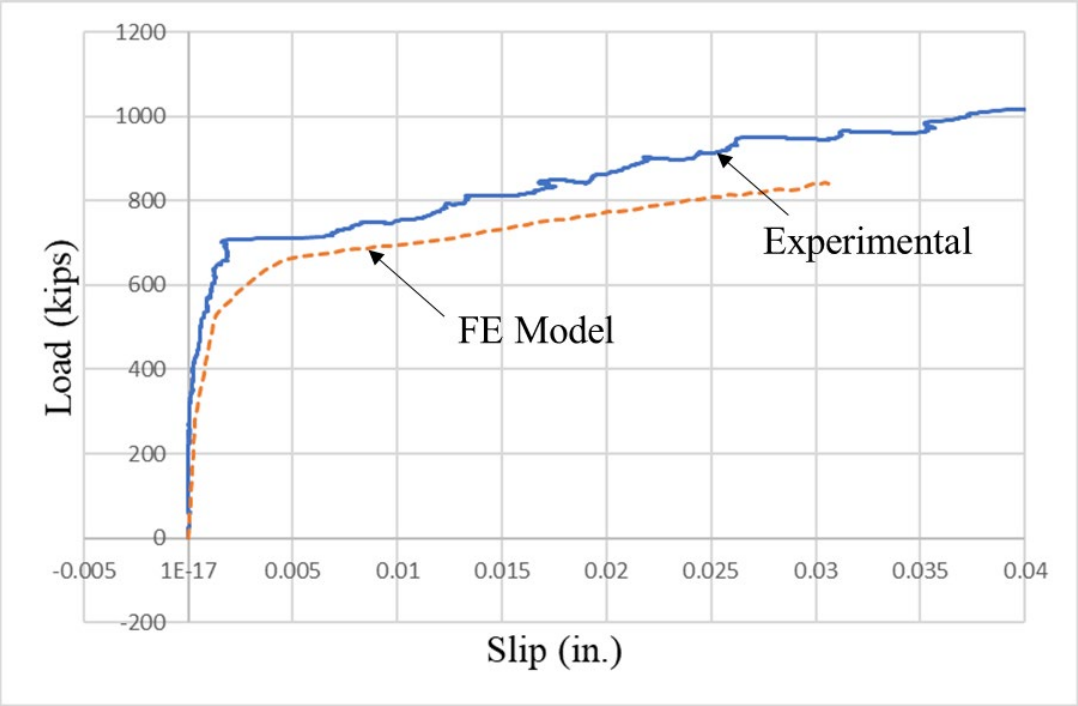

Figure 5.2.2.3 Numerical and Experimental Load-slip Data (6-in. Haunch with SGD)

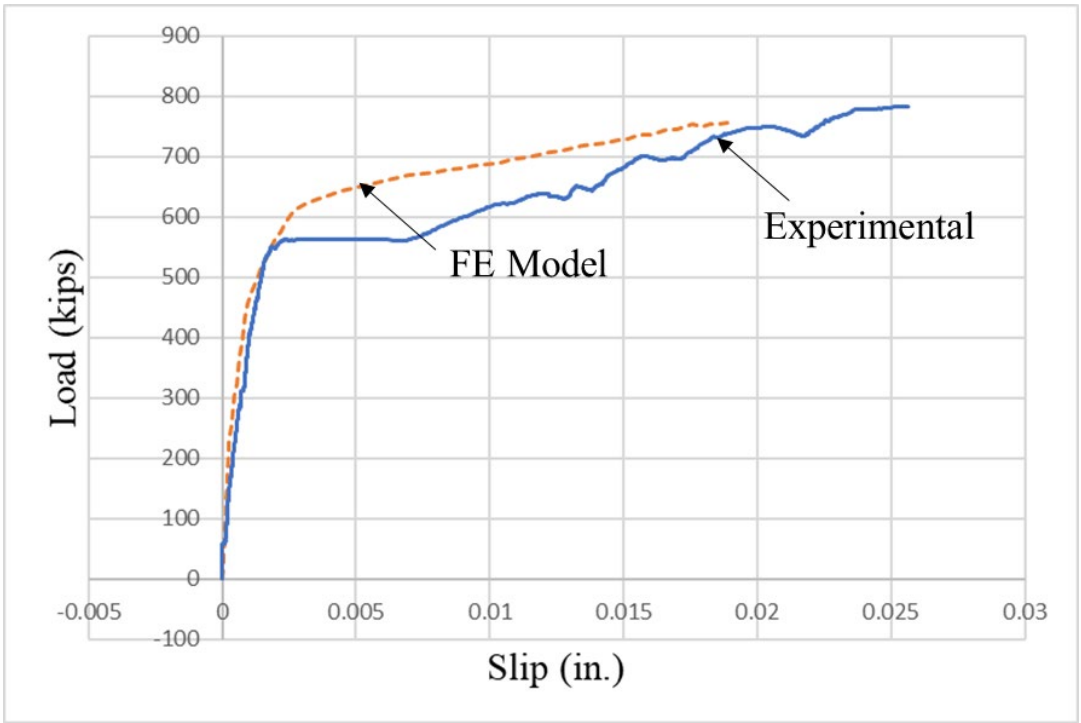

Figure 5.2.2.4 Numerical and Experimental Load-slip Data (12-in. Haunch with Bars U)

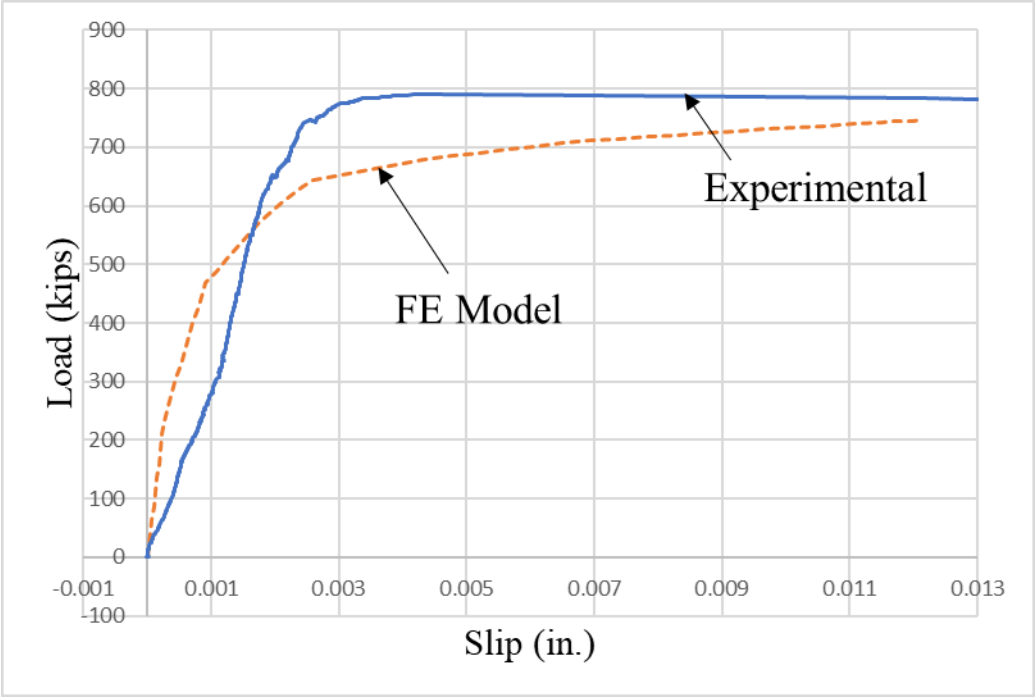

Figure 5.2.2.5 Numerical and Experimental Load-slip Data (12-in. Haunch with Reduced Bars)

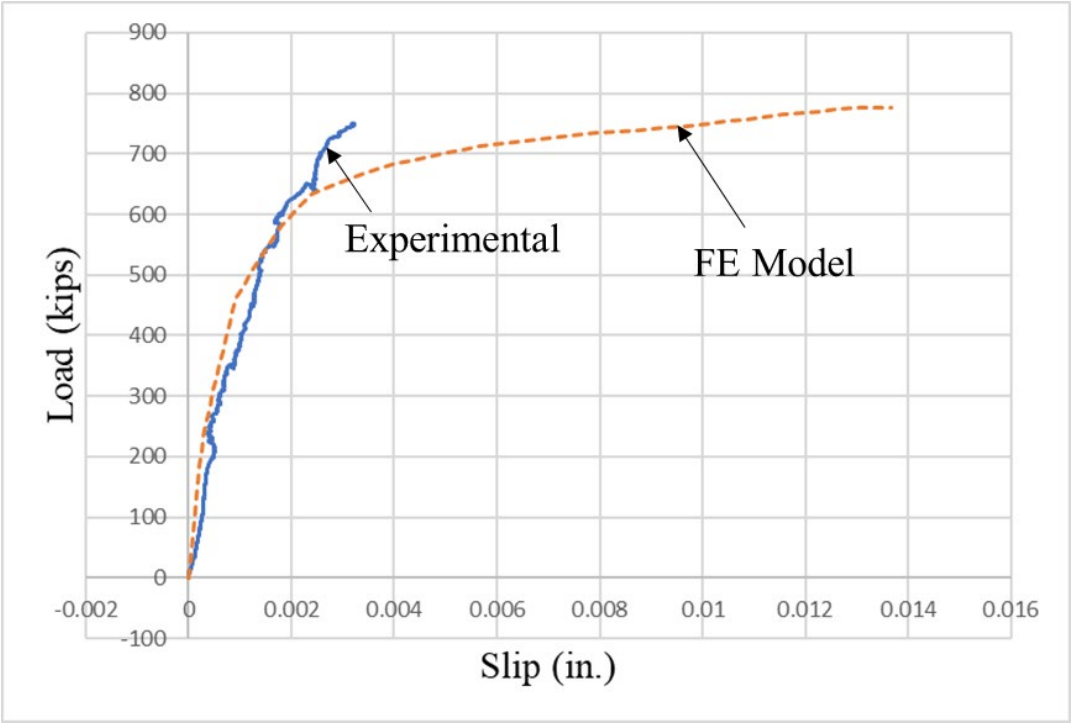

Figure 5.2.2.6 Numerical and Experimental Load-slip Data (12-in. Haunch with SGD)

5.3. Conclusion

The FE model developed for parametric study of tall haunch steel girder specimens has been validated using the results of laboratory push-out tests performed by the project researchers. The validated model shows good agreement with the collected test data and is used in a parametric study in the next chapter to predict the behavior of tall haunch steel girder specimens.

Additionally, a literature review and iterative calibration process have informed the creation of validated FE models of PSC girder specimens. The validation process shows that the strength of PSC girder push-out specimens strongly depends upon the contact properties at the composite interface. The influence of reinforcement detailing, concrete strength, and haunch geometry on the strength and ductility of PSC concrete push-out specimens is studied in Chapter 6.

Chapter 6. Finite Element Parametric Study

The parametric study serves as a numerical extension to the experimental testing program conducted at FSEL. Experimental tests examined the effects of varying haunch depths, reinforcement detailing, and concrete strength on the capacity of push-out test specimens and their associated failure modes. Based on the validation efforts in the previous chapter, a predictive model considers the effects of various design parameters on specimen capacity and ductility, allowing the development of steel and PSC girder design and detailing recommendations.

6.1. Steel Girder

This chapter summarizes the parametric study conducted for the steel girder push-out test specimens. The effect of stud length, stud pitch, and haunch width were qualitatively investigated to extend the research scope limited by the experimental work discussed in Chapter 3. Conclusions made from the parametric study are used to develop the design guidelines of the shear connectors associated with tall haunches.

6.1.1. Finite Element Model of Parametric Study

All of the numerical models in the steel girder specimen parametric study adopted the design of 9 in. haunch with U-bars and longitudinal rebars near haunch bottom, and stud length, stud pitch, and haunch width varied for each model. The validated FE model mentioned in Chapter 5 was incorporated with an updated meshing size in the parametric study. As shown in Figure 5.1.4.5, the meshing size near the high stress concentration areas was 0.1 in., and an average length of 1.0 in. was used in the other areas with mild stress gradient. In the parametric study, as shown in Figure 6.1.1.1, the minimum length of the elements on the shear studs was adjusted to 0.3 in., and the surrounding concrete part was meshed with a minimum length of 0.5 in. The concrete deck had an average meshing size of 1 in. as it was less critical than the haunch and studs. This change was made to reduce the degree of freedom and shorten the computational time. The updated meshing size produced more conservative numerical analysis results than the original one, as shown in Figure 6.1.1.2. The qualitative effect of the parameters on the shear connector behavior was investigated and summarized in the following sections.

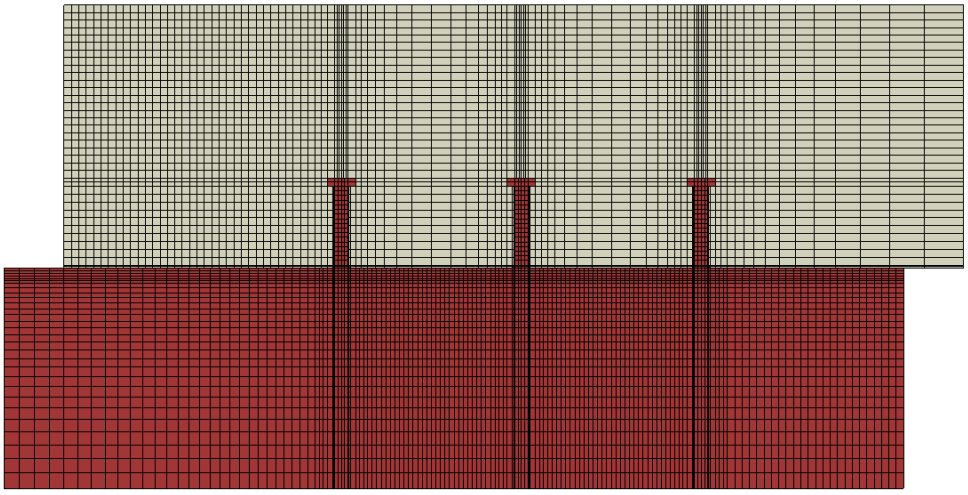

Figure 6.1.1.1 Updated Meshing Size

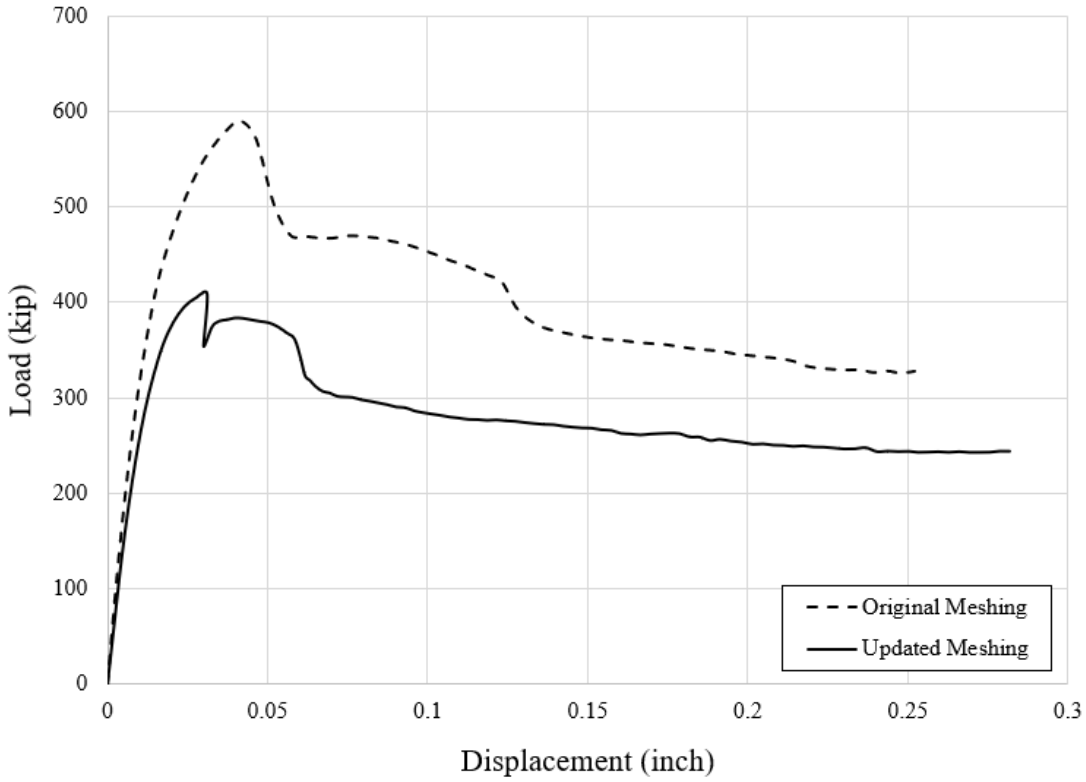

Figure 6.1.1.2 Meshing Size Comparison

6.1.2. Shear Stud Length

As mentioned in Section 2.1.3.4, stud length may not play a significant role in traditional push-out tests. In the ultimate capacity tests of the steel girder specimens, however, the researchers found that stud length could affect the shear connectors involving tall haunches. In Test 09, the specimens with 6 in. haunch and 8 in. shear studs failed in haunch detachment, while in Test 01,

the 9 in. haunch specimens embedded with stacked shear studs, which was 12 in. long totally, had shear stud failure. The effect of stud length was also verified by the parametric study. The models (shown in Figure 6.1.2.2 to 6.1.2.5) with 6 in., 8 in., 10 in., and 12 in. shear stud were analyzed, and the results are summarized in Figure 6.1.2.1.

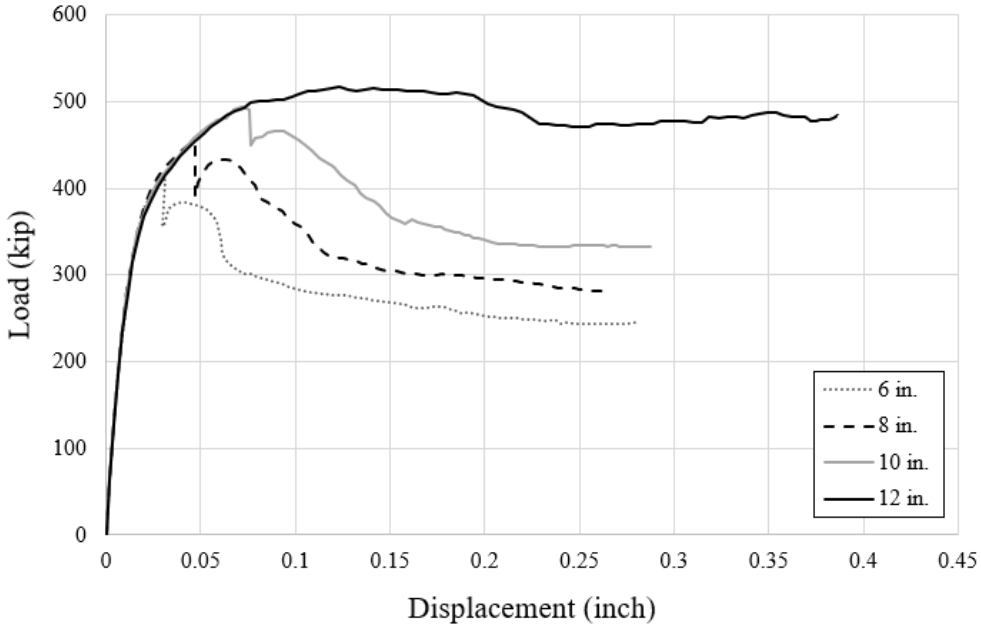

Figure 6.1.2.1 Parametric Study of Stud Length

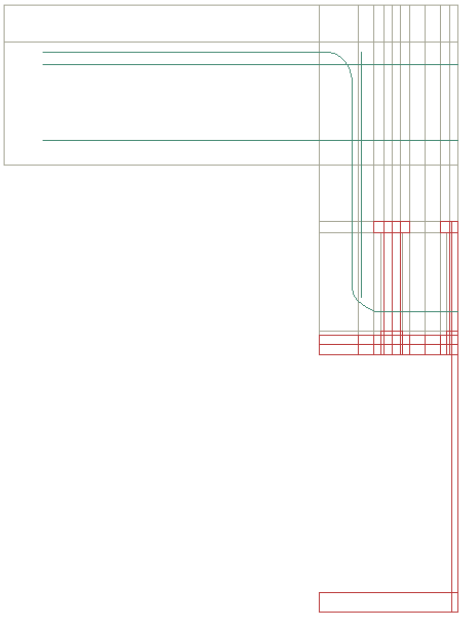

Figure 6.1.2.2 6 in. Shear Stud

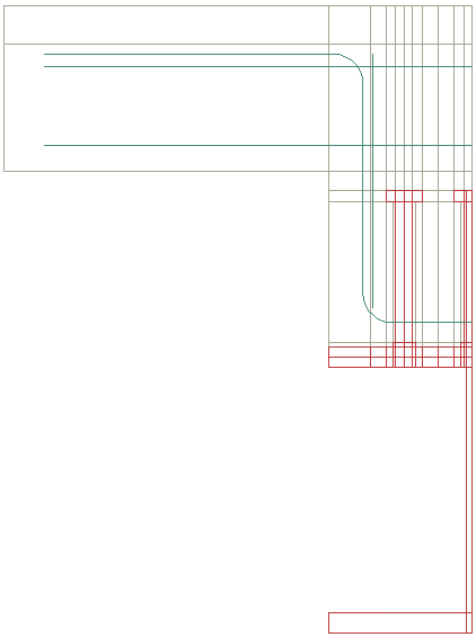

Figure 6.1.2.3 8 in. Shear Stud

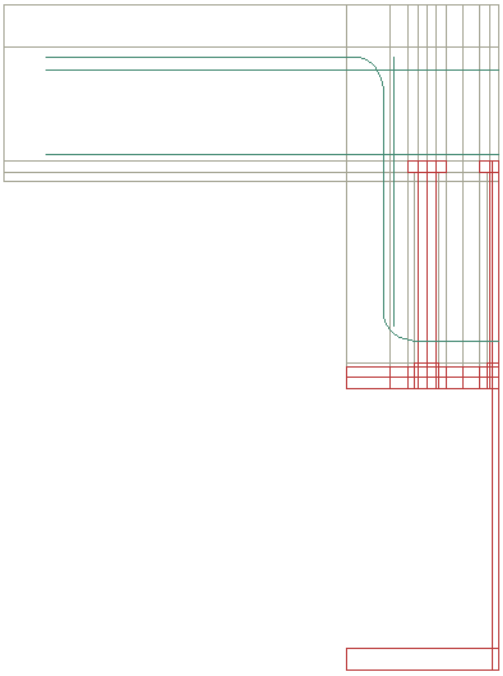

Figure 6.1.2.5 12 in. Shear Stud

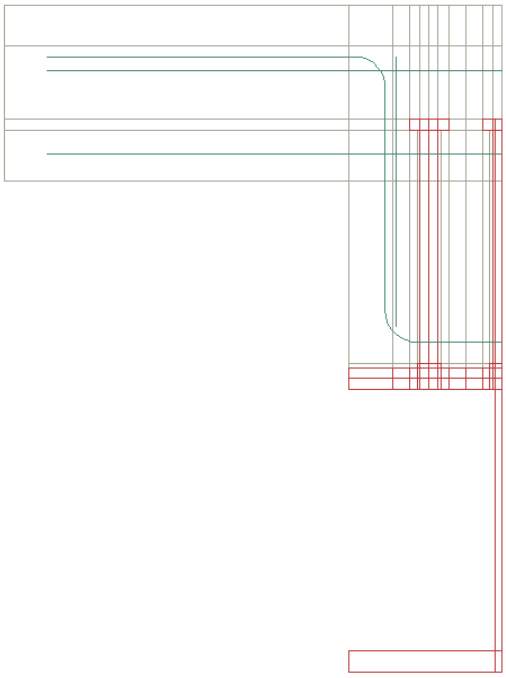

Figure 6.1.2.4 10 in. Shear Stud

The numerical analysis results demonstrated that the ultimate shear capacity was positively related to the stud length. The model with 12 in. studs had better ductility than the other ones due to the deck penetration. The advantage of sufficient stud length was also shown in the push-out tests. Among the shear stud failure specimens with 9 in. haunches, the Test 01 showed the largest ultimate capacity. Therefore, the length of the shear studs, including stacked length, should be sufficient to reach the decks and have ample penetration. Based on the push-out test results and the numerical analysis, a minimum deck penetration of 3 in. is recommended for haunches no less than 6 in.

6.1.3. Shear Stud Pitch

It is mentioned in Section 2.1.3.2 that small stud pitches may result in concrete failure (Jayas and Hosain 1988). This was also observed in the push-out tests. The comparison between Test 01 and 10 showed that stud pitch could change the failure modes of the shear connector with tall haunches. The 12 in. pitch specimen in Test 01 had shear stud failure while the 6 in. pitch in Test 10 let to localized concrete crushing with less shear capacity.

The stud pitches of 6 in. 12 in. and 18 in. (shown in Figure 6.1.3.1 to 6.1.3.3) were systematically analyzed and proved the importance of adequate stud spacing in the longitudinal direction. In the models with 6 in. and 12 in. stud pitches, the studs on the middle row were fixed, and the pitches were adjusted by moving the other shear studs. In the model associated with 18 in. pitch, the studs near the bottom lined up with the ones in 12 in. pitch model in the longitudinal direction. The other two rows were moved towards the opposite direction of the loading. This modeling method can avoid insufficient edge distance between the bottom surface of the concrete and the shear studs. The test results are shown in Figure 6.1.3.4.

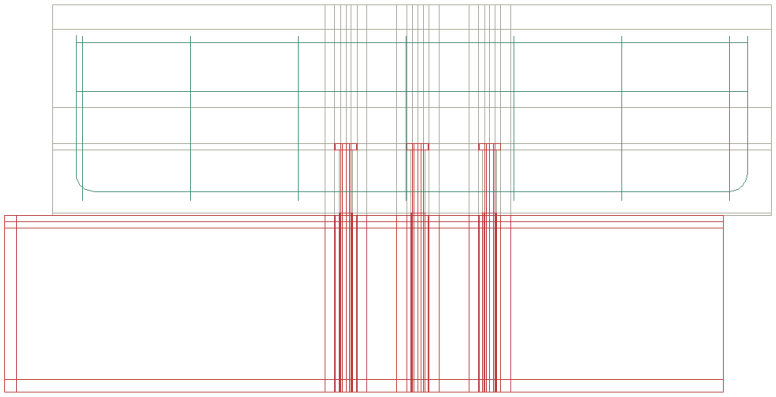

Figure 6.1.3.1 Parametric Study - 6 in. Stud Pitch

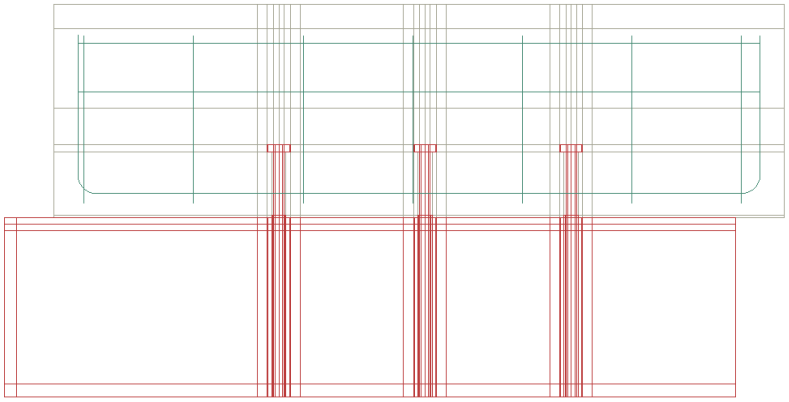

Figure 6.1.3.2 Parametric Study - 12 in. Stud Pitch

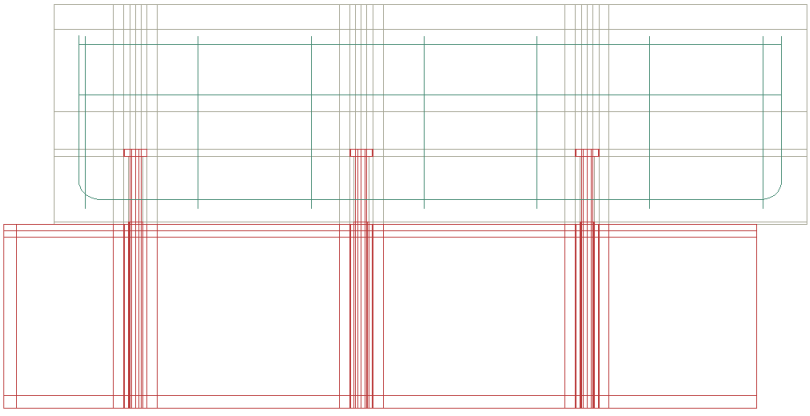

Figure 6.1.3.3 Parametric Study - 18 in. Stud Pitch

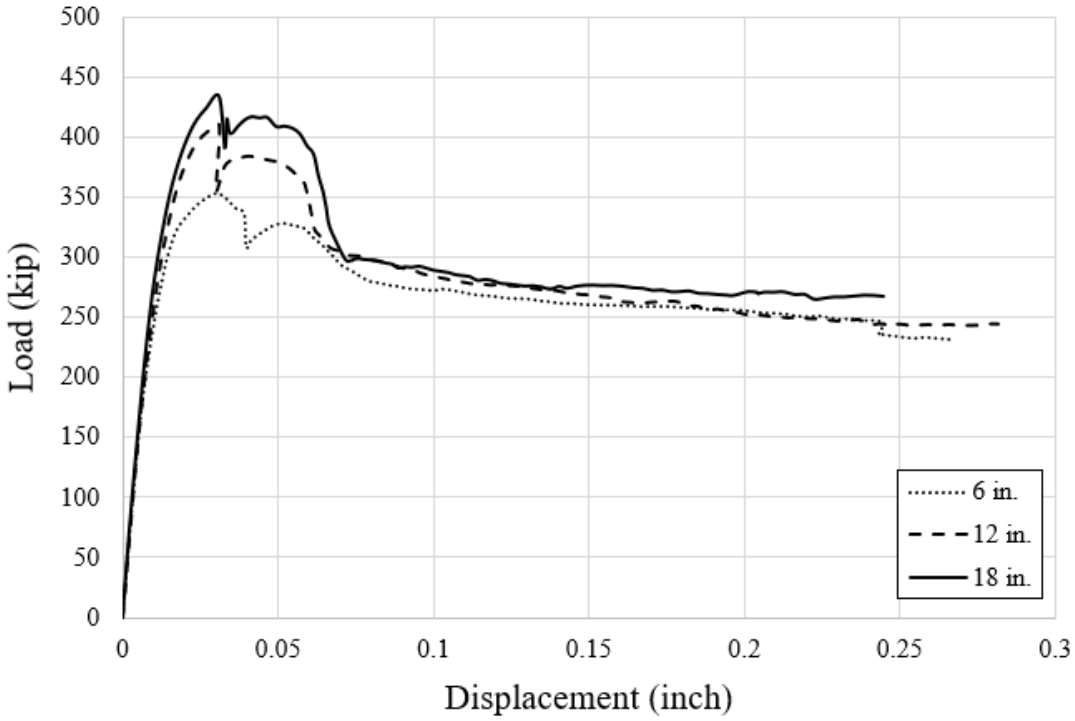

Figure 6.1.3.4 Parametric Study of Stud Pitch

The analysis results showed that larger stud pitch resulted in higher ultimate capacity. The difference between the 12 in. and 18 in. cases was less than the one between the 12 in. and 6 in. cases because the benefit would diminish with the increasing of the pitch, and the ultimate capacity would eventually converge to a certain value.

Based on the analysis and test results, it can be concluded that at least 12 in. pitch is recommended in tall haunch regions of steel composite girders given adequate longitudinal shear strength.

6.1.4. Haunch Width

Due to the limitation of the experiment conditions, the effect of haunch width on the shear connector behavior could not be experimentally investigated. Therefore, the researchers conducted the parametric study for the variable, incorporating the haunch width of 14.7 in., 17 in., 19 in., and 21 in. The U-bars in the models were modified to maintain the consistent clear cover. The flange widths remained consistent with the haunch widths to simulate real bridge construction. The sectional views of the models are shown in Figure 6.1.4.1 to 6.1.4.4. The analysis results are included in Figure 6.1.4.5.

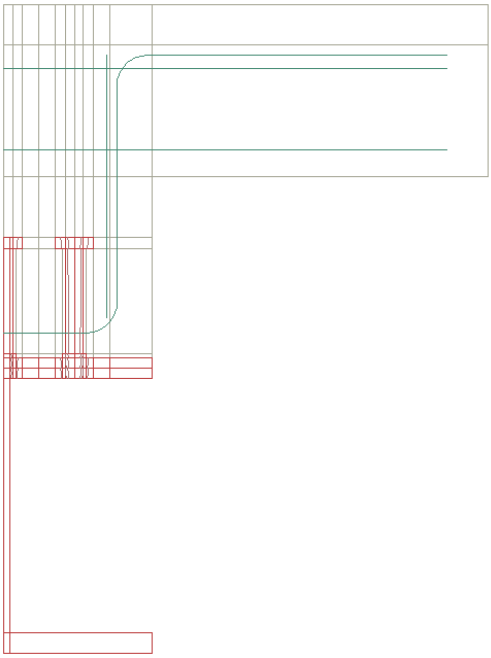

Figure 6.1.4.1 Parametric Study - Steel Girder Width 14.7 in.

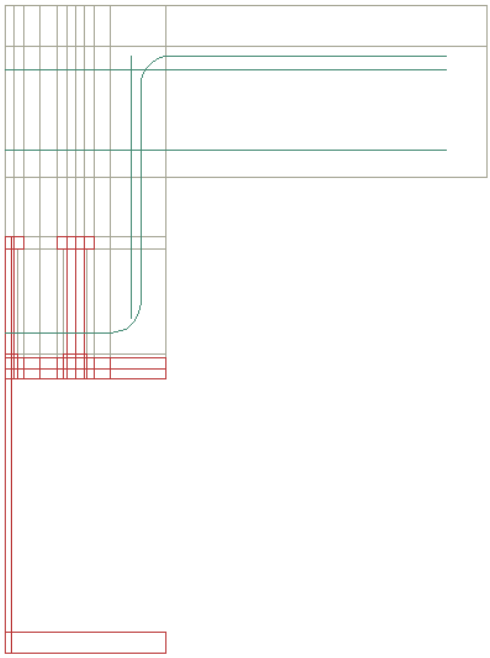

Figure 6.1.4.2 Parametric Study - Steel Girder Width 17 in.

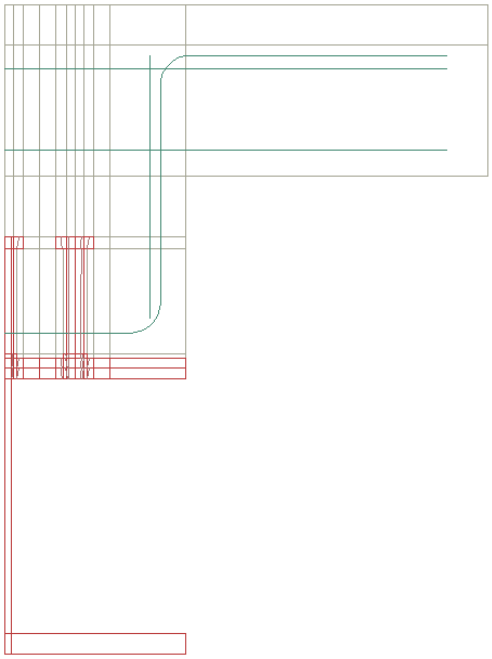

Figure 6.1.4.4 Parametric Study - Steel Girder Width 19 in.

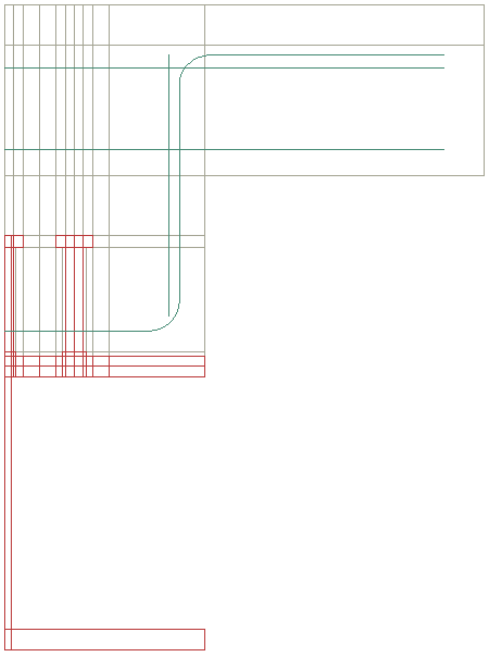

Figure 6.1.4.3 Parametric Study - Steel Girder Width 21 in.

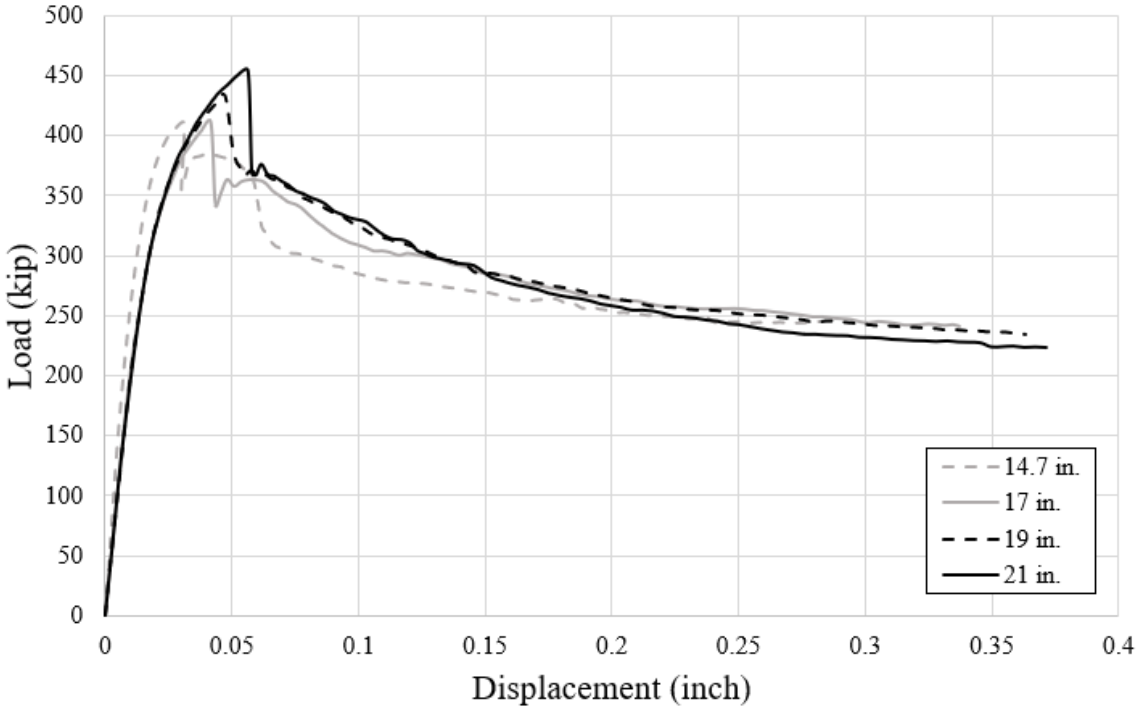

Figure 6.1.4.5 Parametric Study of Haunch Width

As shown in Figure 6.1.4.5, the models with 14.7 in. and 17 in. had little difference in the ultimate capacity, and the other two showed obvious capacity increment due to the increasing of haunch width. Given a shear stud arrangement, a larger haunch width resulted in more clear edge distance from the haunch sides to the studs and higher ultimate capacity of concrete failure. When the haunch is sufficiently wide, shear stud failure controls the behavior rather than concrete, as occurred in Test 17. The mechanism of stud arrangement and clear edge distance affecting shear connector behavior, however, has not been clear yet. Further study is needed for it.

6.1.5. Concluding Remarks

The parametric study of the steel girder specimens was conducted to qualitatively evaluate the effect of stud length, stud pitch, and haunch width on the behavior of shear connectors involving tall haunches. Based on the results, the following conclusions can be developed:

1) Stud length may affect the behavior of shear stud composite system including tall haunches. It is ideal to have shear studs penetrate into decks by at least 3 in.
2) Increasing stud pitch is beneficial for each stud to develop strength in tall haunch cases, while its effect gradually diminishes. The ultimate shear capacity will converage to a certain value with the increasing of stud pitch.
3) Haunch width contributes to the clear edge distance given a certain stud plan. There might be a threshold of haunch width between shear stud failure and concrete failure. Further research is required to reveal the mechanism.

The parametric study serves as a numerical extension to the experimental testing program conducted at FSEL. Experimental tests examined the effects of varying haunch depths, reinforcement detailing, and concrete strength on the capacity of push-out test specimens and their associated failure modes. Based on the validation efforts in the previous chapter, a predictive model considers the effects of various design parameters on specimen capacity and ductility, allowing the development of steel and PSC girder design and detailing recommendations.

6.2. PSC Girder

This section provides details of the parametric study performed on PSC girder specimens with CIP and PCP decks. Chapter 4 provides experimental work details for these specimens.

6.2.1. CIP Specimens

This section presents the parameters studied for CIP specimens. To keep the load versus slip plots in this section consistent with Section 4.4, the load represents the total load applied on two specimens, and the relative slip is calculated in the same manner as the PSC girder specimen push-out tests. All the load versus slip plots shown in this section are for the simulated PSC girder-haunch interface since this interface was most critical for CIP specimens with maximum relative slip.

6.2.1.1. Reinforcement Detailing

The researchers investigated the effects of varying reinforcement types, sizes, and spacing in the FE model for CIP specimens. The effect of including longitudinal reinforcement in the specimens is also studied. Additionally, the minimum penetration requirements and interaction length of Bars U and bars R (explained subsequently in this section) have been examined.

6.2.1.1.1. Type of Shear Reinforcement

Figures 6.2.1.1–6.2.1.4 show the types of reinforcement studied for the CIP specimen parametric study. All four types of reinforcement were included in the experimental program (Section 4.1) for haunches ≥ 6 in. For specimens with haunch depth ≤ 3.5 in., no additional shear reinforcement is provided other than bars R. The configuration for bars R (shown in Section 4.1) in all the specimens is in accordance with TxDOT guidelines (TxDOT 2017).

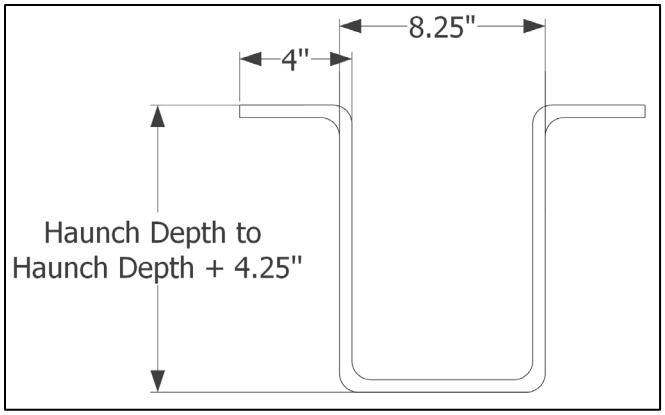

Figure 6.2.1.1 Bars U Configuration

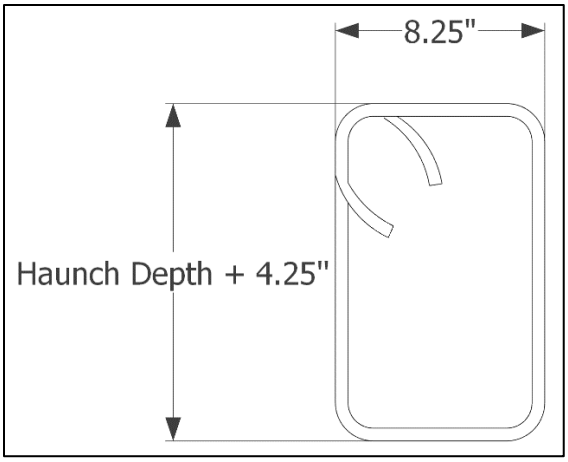

Figure 6.2.1.2 Vertical Stirrups Configuration

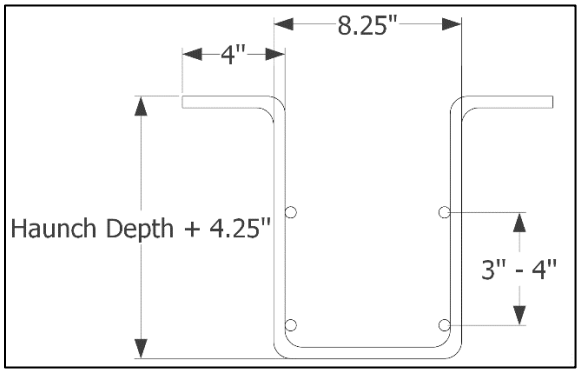

Figure 6.2.1.3 Bars U with Longitudinal Bars (Haunches > 6 in.)

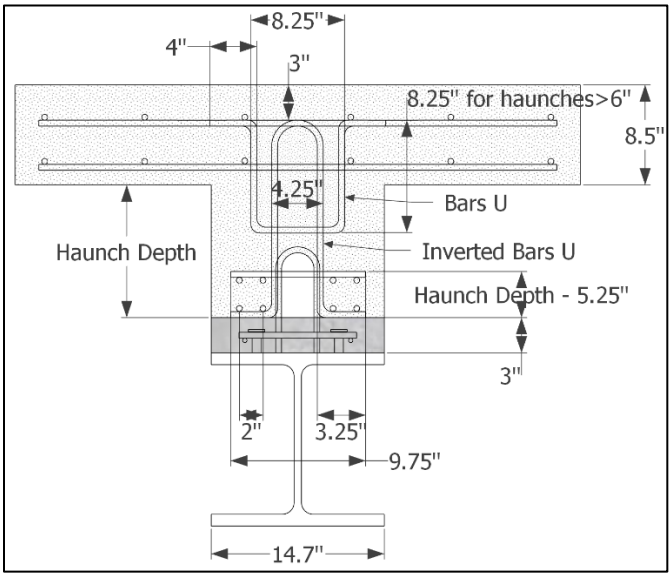

Figure 6.2.1.4 SGD Rebar Detailing (Haunches > 6 in.)

Figure 6.2.1.5 shows the load versus slip plots for 2-in. haunch push-out test specimens with 5 bars R and without bars R. The small slip before the specimens' peak load indicates the occurrence of a debonding failure mode at the composite interface—the cohesive layer between the simulated PSC girder and haunch fails, leading to failure before the shear reinforcement engages and provides shear resistance. Because the shear reinforcement does not provide shear resistance before debonding failure, it does not improve the direct shear capacity. Although the peak loads for both cases are similar, the specimens with no shear reinforcement have a smaller slip and a more brittle failure. The residual capacity in the specimens with no bars R will be zero after the debonding failure, unlike the specimens with shear reinforcement (as mentioned in Chapter 4). The peak capacities are higher compared to the value predicted by AASHTO LRFD (2020) for specimens with 5 bars R (Appendix Section A3.2.1).

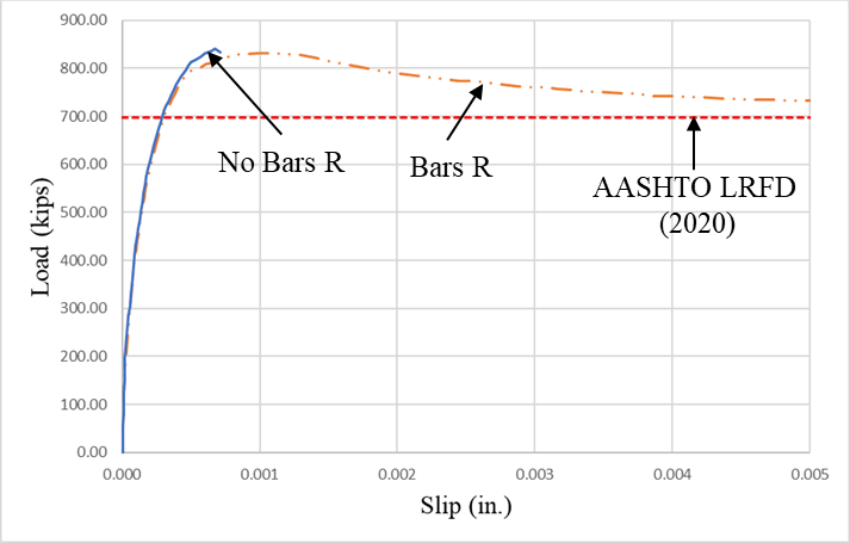

Figure 6.2.1.5 Load versus Slip with and without Bars R (2-in. Haunch)

Figure 6.2.1.6 shows the load versus slip plots for 6-in. haunch push-out test specimens with different detailing strategies. The specimens with no haunch detailing (only bars R as shear reinforcement) have similar peak load values compared to the specimens with Bars U haunch detailing with or without longitudinal bars. As indicated previously, shear reinforcement does not provide shear resistance before debonding failure for smaller haunch specimens. The slip, however, is smaller for specimens with no haunch detailing, and the failure is more brittle as mentioned for the 2-in. haunch specimens. The post-peak behavior of the specimens with Bars U is similar to the specimens with Bars U and longitudinal bars, but the specimens with longitudinal bars are expected to have lesser cracking. The capacities for all the specimens are higher than the predicted value from AASHTO LRFD (2020).

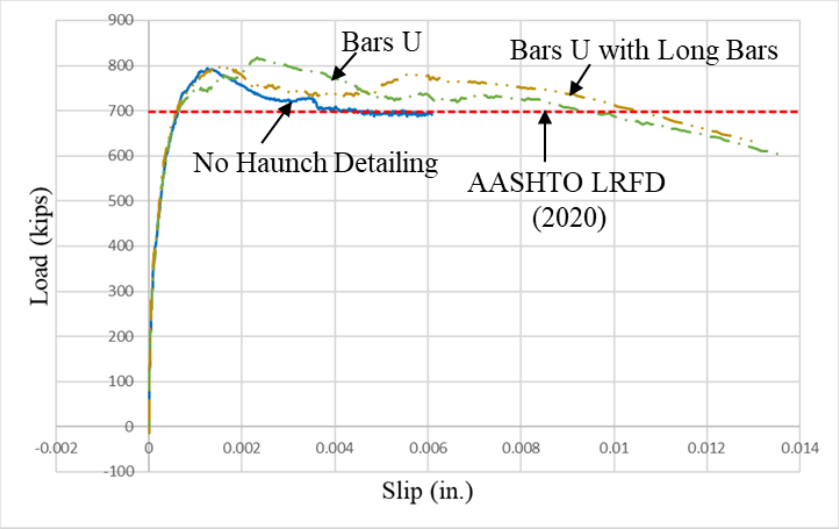

Figure 6.2.1.6 Load versus Slip with Different Haunch Detailing Strategies (6-in. Haunch)

Figure 6.2.1.7 compares the load versus slip plots for 9-in. haunch push-out test specimens with Bars U and with vertical stirrups. The specimens with vertical stirrups performed slightly better than the specimens with Bars U because the former has a higher peak load and slip than the latter. The specimens examined have peak load values higher than that predicted by AASHTO LRFD (2020).

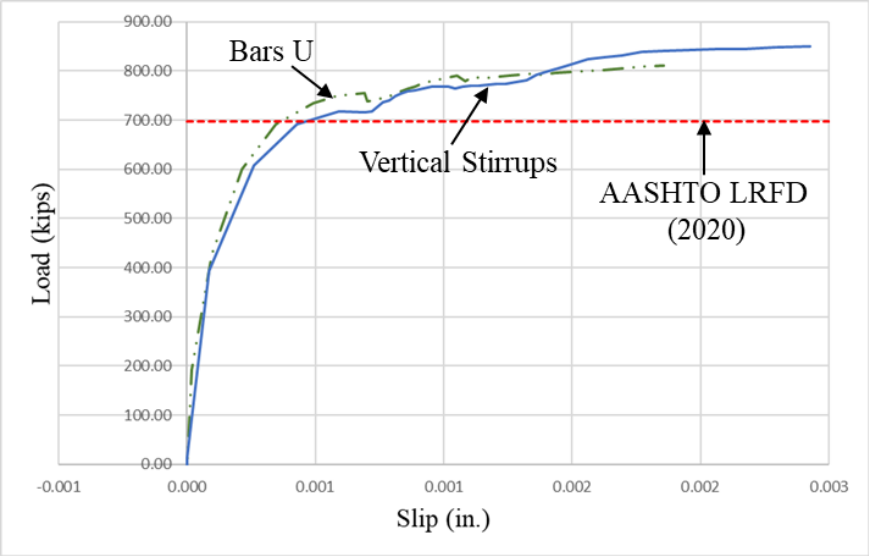

Figure 6.2.1.7 Load versus Slip with Different Haunch Detailing Strategies (9-in. Haunch)

Figure 6.2.1.8 show load versus slip plots for 12-in. haunch specimens with Bars U, Bars U with longitudinal bars, and SGD rebar detailing. All three detailing practices have higher peak load values compared to the AASHTO LRFD (2020) predicted value. The specimen with the SGD rebar detailing has a slightly higher peak load compared to the Bars U specimen.

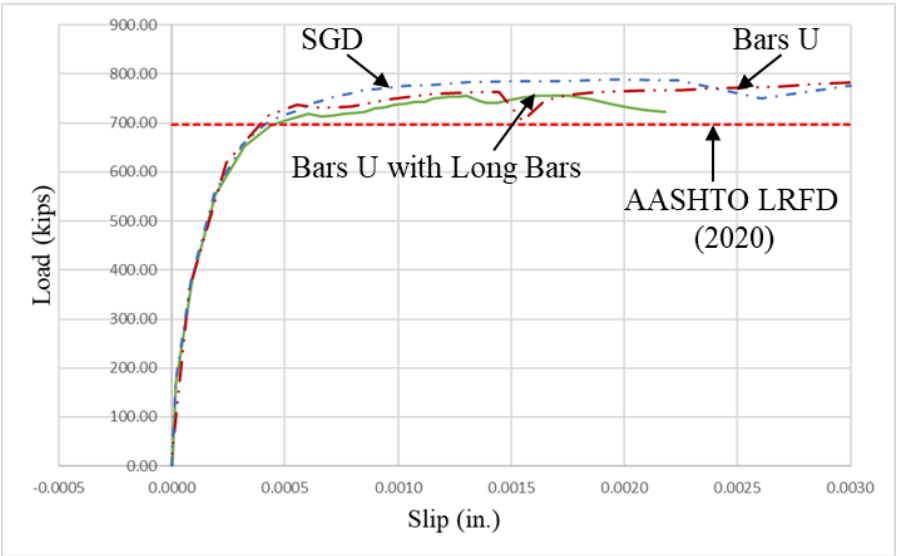

Figure 6.2.1.8 Load versus Slip with Different Haunch Detailing Strategies (12-in. Haunch)

6.2.1.1.2. Shear Reinforcement Layout

The effects of varying the spacing and amount of shear reinforcement are considered in this section. A 12-in. haunch push-out specimen with three bars R and Bars U is investigated (Figure 6.2.1.9). The spacing between bars R and U are varied between 6 in. and 24 in. TxDOT (2017) specifies a maximum spacing of 18 in. for the shear reinforcement. Because the length of the specimen is considered constant from the experiment (60 in.), the edge distances of bars R vary with the change in spacing. The location of the central bar R is kept constant for all the specimens. Figure 6.2.1.10 shows the load versus slip plots for specimens with different spacings. The failure of the specimens with 6 in. and 12 in. spacing is governed by debonding followed by participation of the shear reinforcement. The specimens with 18 in. or 24 in. spacing have a higher participation from bars R before debonding occurs possibly, due to the moment existing in 12-in. haunch specimens (due to load eccentricity as explained in Section 4.4). The final failure in these specimens is debonding combined with diagonal cracking near the haunch base. All the specimens have higher peak load values than the predicted value by AASHTO LRFD (2020), with a slight decrease in capacity with an increase in spacing.

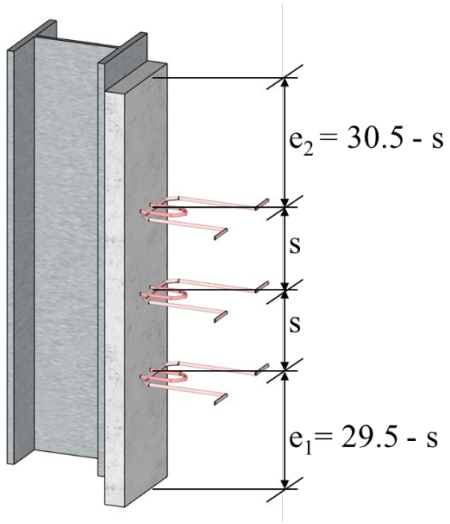

Figure 6.2.1.9 Shear Reinforcement Spacing Variation

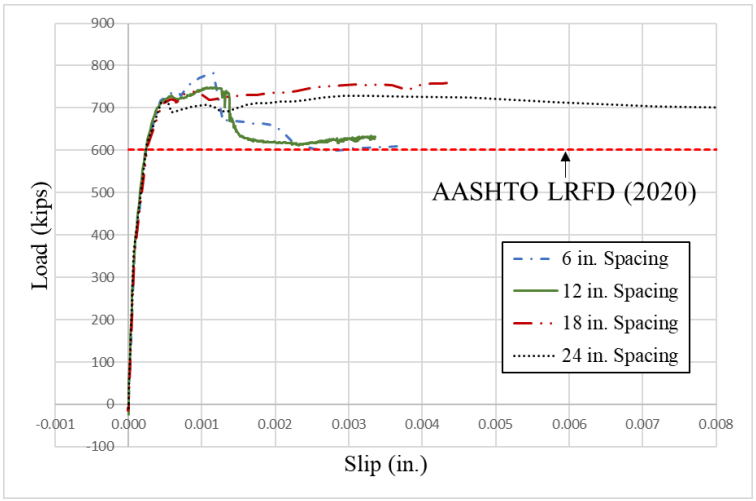

Figure 6.2.1.10 Load versus Slip Variation with Spacing (12-in. Haunch with Bars U)

The number of Bars U are varied for 6-in. and 12-in. haunch specimens (Figures 6.2.1.11). The spacing for specimens with 3 and 5 bars is kept constant (12 in.), while the spacing for specimens with 9 bars is kept at 6-in.

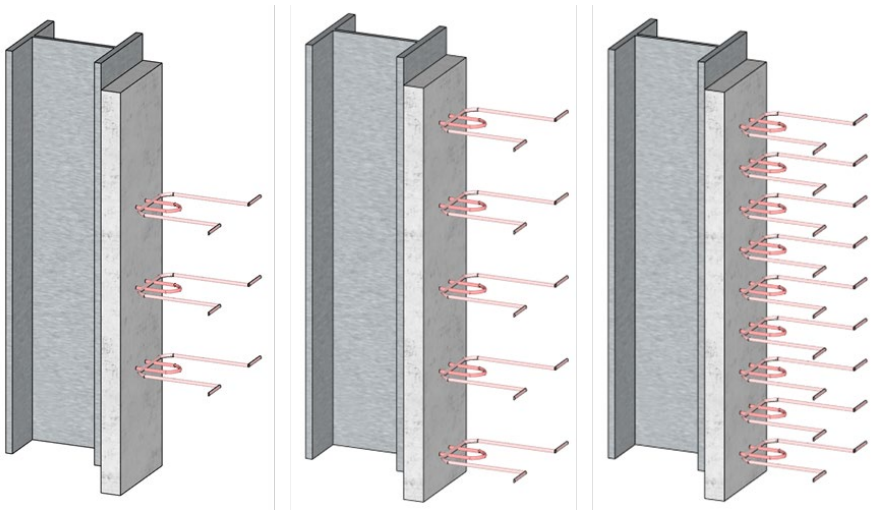

Figure 6.2.1.11 Variation of No. of Shear Reinforcement

Figure 6.2.1.12 shows load versus slip plots for 12-in. haunch specimens with different amounts of shear reinforcement. The load drops in the specimens with 3 and 5 bars for shear reinforcement at approximately 0.0015 in. when the cohesive layer between the simulated PSC girder and the haunch breaks. Beyond this point, the load is only carried by the mechanical connection and is higher for the specimens with more shear reinforcement. The peak load for the specimens with 9 bars is slightly higher than the other specimens, possibly due to increased frictional effects from the moment on a 12-in. haunch specimen (refer to Section 4.4).

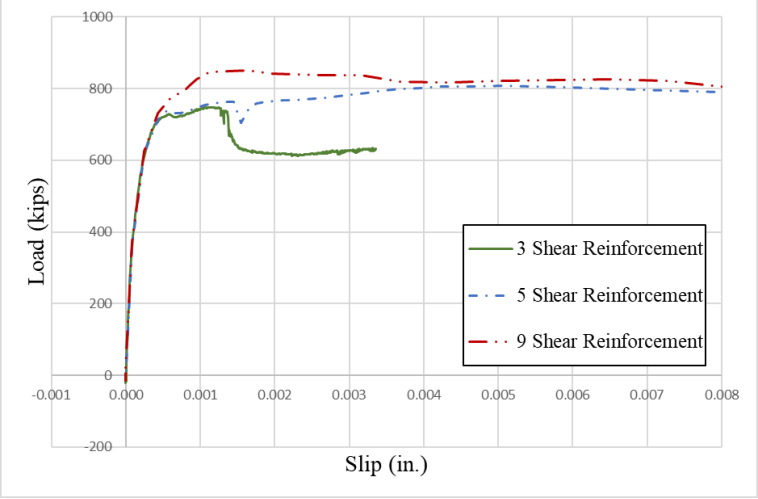

Figure 6.2.1.12 Load versus Slip Variation with No. of Shear Reinforcement (12-in. Haunch with Bars U)

Figure 6.2.1.13 shows load versus slip plots for 6-in. haunch specimens with different amounts of shear reinforcement. The specimens with 5 and 9 bars have similar peak load values. The effect of shear reinforcement is minimal for 6-in. haunch specimens since the failure of the cohesive layer at the simulated PSC girder and haunch interface controlled the specimens' strength.

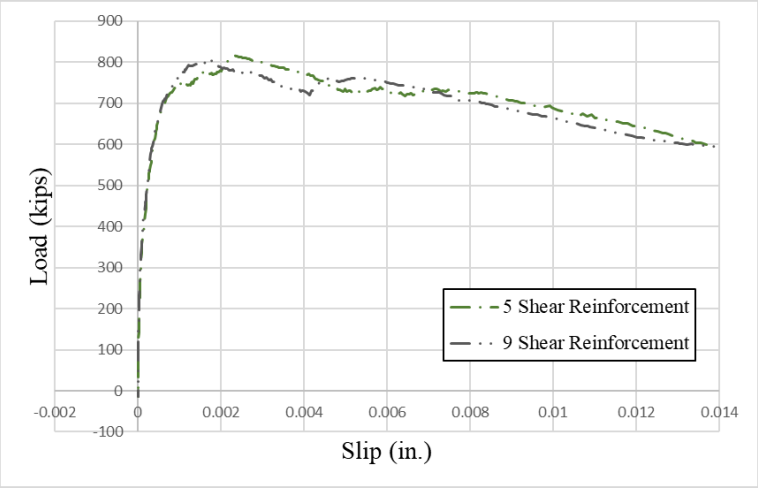

Figure 6.2.1.13 Load versus Slip Variation with No. of Shear Reinforcement (6-in. Haunch)

6.2.1.1.3. Shear Reinforcement Size

The shear reinforcement size tested in all the experiments was #4. The parametric study investigated the effects of increasing the size of bars R and Bars U to #5 and #6. Figure 6.2.1.14 shows the load versus slip plots with variation in shear reinforcement size for 12-in. haunch specimens. As was observed with other parameters, the peak load is mostly dependent on the cohesive layer resistance at the simulated PSC girder-haunch interface and has negligible change with a change in the shear reinforcement size. The peak load values for specimens with #5 and #6 shear reinforcement sizes are lower than the predicted values from the AASHTO LRFD (2020) equation. To ensure that the prediction from the equation remains conservative regardless of the shear reinforcement size, it may be necessary to limit the maximum contribution from shear reinforcement for tall haunches.

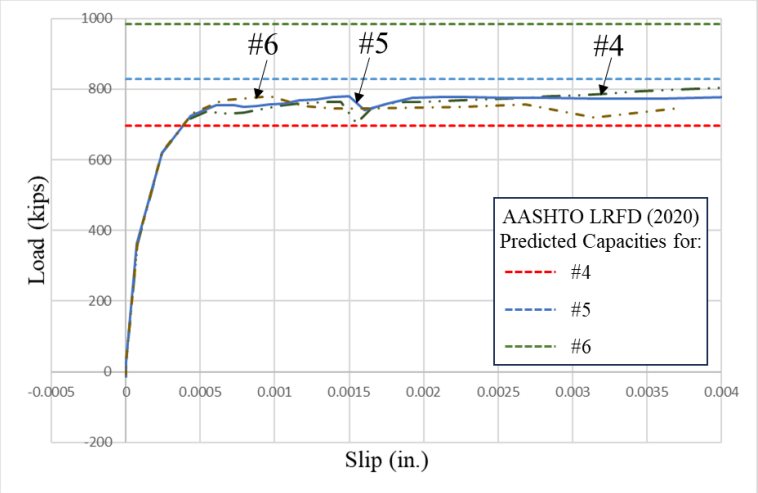

Figure 6.2.1.14 Load versus Slip Variation with Shear Reinforcement Size (12-in. Haunch with Bars U)

6.2.1.1.4. Embedment Depth

TxDOT (2022) does not require haunch reinforcement for haunches ≤ 3.5 in. Figure 6.2.1.15 shows a comparison of load versus slip plots for 2-in. and 3.5-in. haunch specimens. Because the bar R length outside the girder top is fixed to 6 in., the depth of penetration or embedment depth into the CIP deck for 2-in. and 3.5-in. haunch specimens will be 4 in. and 2.5 in., respectively. The figure shows a slight decrease in peak load value with a decrease in embedment depth. Both cases have peak load values higher than the design load (AASHTO LRFD 2020).

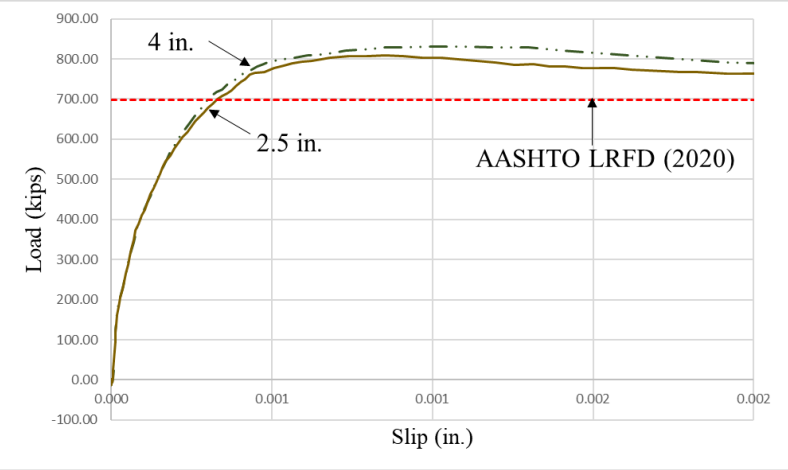

Figure 6.2.1.15 Load versus Slip Variation with Embedment Depth of Bars R

The shear reinforcement Bars U in the PSC girder specimens was tied to the top mat of the slab reinforcement (5.5 in. above the bottom of the deck). The parametric study investigated the effects of tying the shear reinforcement to the bottom mat of the slab reinforcement (1.25 in. above the bottom of the deck). Figure 6.2.1.16 shows that for both cases, specimens have essentially the same response and failure mode for 12-in. haunch specimens.

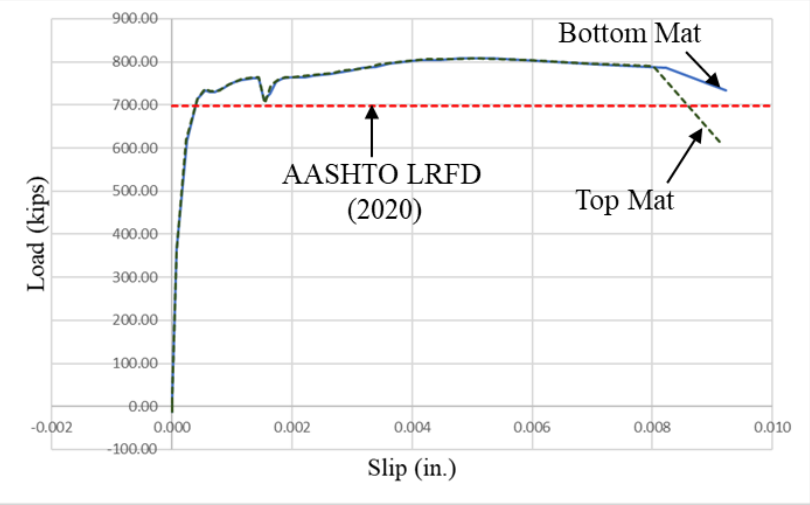

Figure 6.2.1.16 Load versus Slip Variation with Embedment (12-in. Haunch with Bars U)

6.2.1.1.5. Interaction Length

As per the TxDOT (2017) guidelines, bars R extend 6 in. beyond the PSC girder top surface. With a 1.25 in. bottom clear cover for bar U, the interaction length (IL in Figure 6.2.1.17) would be 4.75 in. The researchers investigated the effects of different IL on 12-in. haunch specimens as shown in Figure 6.2.1.18. The peak load decreases slightly with a decrease in IL. The specimen with zero interaction between Bars U and bars R has the peak load almost equal to the AASHTO LRFD (2020) predicted capacity. Based on this result, an IL of at least 3 in. is recommended in Chapter 7.

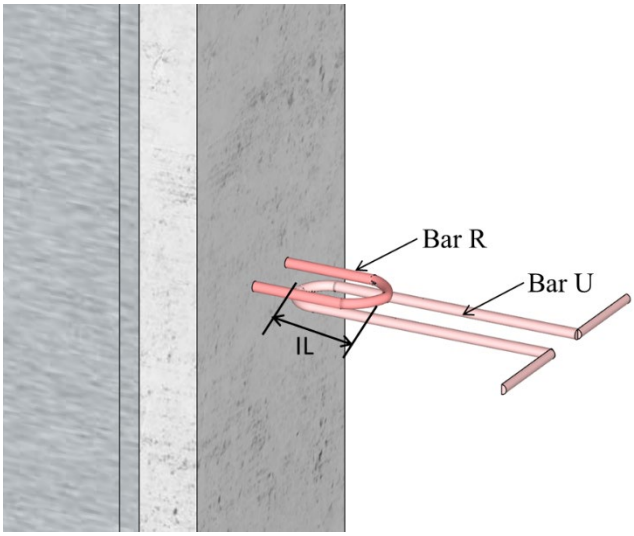

Figure 6.2.1.17 Interaction Length for Haunch Reinforcement

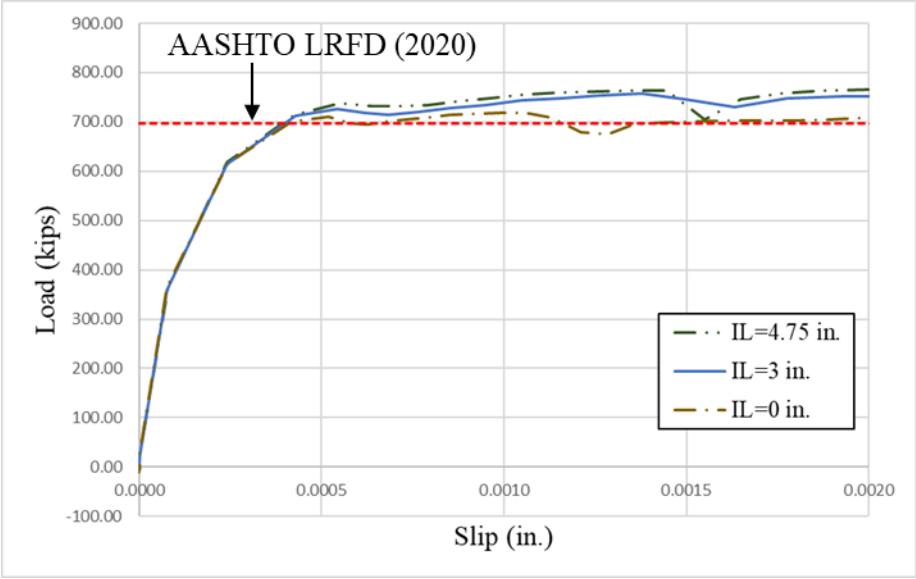

Figure 6.2.1.18 Load versus Slip Variation with Interaction Length (12-in. Haunch with Bars U)

6.2.1.2. CIP Concrete Compressive Strength

This parametric study analyzes 9-in. haunch specimens with varying concrete strengths based on common TxDOT practices. Figure 6.2.1.19 shows load versus slip variation with concrete compressive strength for 9-in. haunch specimens. There is no clear pattern observed in the peak load with variation in the CIP deck and haunch compressive strength. This outcome is due to a change in the failure mode with a change in the relative compressive strength of CIP versus PSC concrete. The slip for the specimens with 3 ksi compressive strength is relatively smaller than the other specimens.

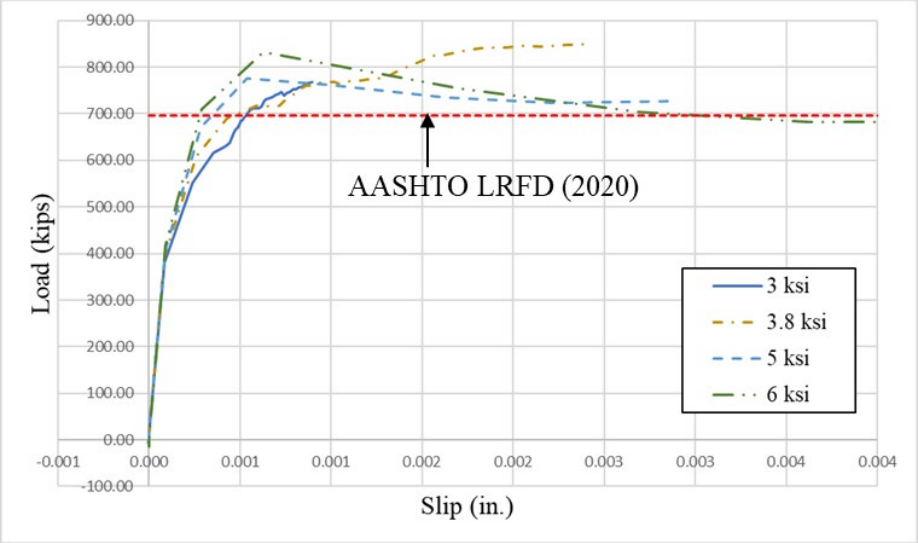

Figure 6.2.1.19 Load versus Slip Variation with CIP Compressive Strength (9-in. Haunch with Vertical Stirrups)

6.2.1.3. Haunch Depth

Specimens with haunch depths of 2 in., 3.5 in., 6 in., 9 in., and 12 in. are investigated, and compared with the AASHTO LRFD (2020) predicted capacity. The haunches with depths ≤ 3.5 in. are provided with bars R only. The haunches with depths ≥ 6 in. are provided with bars R and Bars U in the haunch. Figure 6.2.1.20 illustrates the load-slip behavior of all the specimens. The results from this parametric study indicate that specimens with various haunch depths experience similar strength and ductility of the composite interface. This study did not consider the behavior of specimens with extraordinarily tall haunched decks deeper than 12-in., which may experience different capacities or ductility compared to the specimens examined in this study.

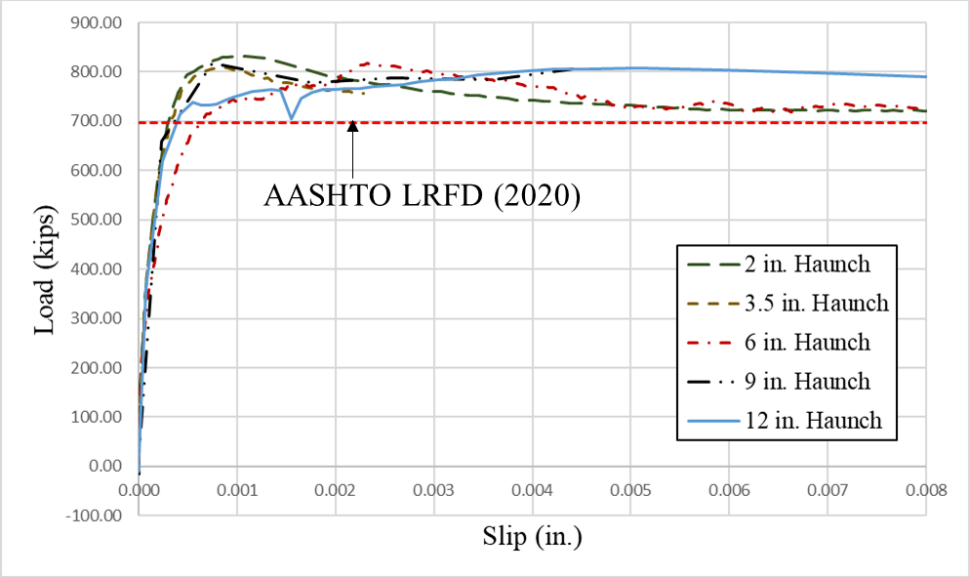

Figure 6.2.1.20 Load versus Slip Variation with Haunch Depth

6.2.1.4. Concluding Remarks

Based on the parametric study performed for shear reinforcement in push-out tests on CIP specimens, the peak load is observed to be mainly affected by the cohesive layer resistance at the simulated PSC girder-haunch interface. Due to a small initial slip, the shear reinforcement participation before the break of the cohesive layer is limited. Thus, the shear reinforcement size and type have limited effects on the peak load, though these details will affect the residual load once the cohesive layer fails and slip becomes more pronounced. The reinforcement layout can affect the failure mode and crack patters that develop in the push-out specimens; however, the effect on peak load is insignificant. The concrete strength and haunch depth also did not affect the peak load significantly.

The reinforcement size, type, layout, minimum concrete strength, and other parameters are recommended for tall haunches in Chapter 7 to allow for minimal cracking in the haunch and to provide sufficient residual capacity. The ease of construction on site is also considered in providing the final guidelines.

6.2.2. PCP Specimens

This section presents the parameters studied for PCP specimens. To keep the load versus slip plots in this section consistent with Section 4.4, the load represents the total load applied on two specimens, and the relative slip is calculated in the same manner as the PSC girder specimen push-out tests. All the load versus slip plots shown in this section are for the PCP-haunch interface since this interface had the maximum relative slip for PCP specimens.

6.2.2.1. Reinforcement Detailing

The researchers investigated the effects of varying reinforcement types, sizes, and spacing in tall haunch specimens. The effect of including longitudinal reinforcement in the specimens is also studied. Additionally, the minimum penetration requirements and interaction length of Bars UP and bars R have been examined.

6.2.2.1.1. Type of Shear Reinforcement

Figures 6.2.2.1–6.2.2.3 show the type of reinforcement studied for the parametric evaluation of PCP specimens. Bars UP and SGD were tested experimentally for haunches ≥ 6 in. (Section 4.4). For specimens with haunch depth ≤ 3.5 in. no additional shear reinforcement is provided other than bars R.

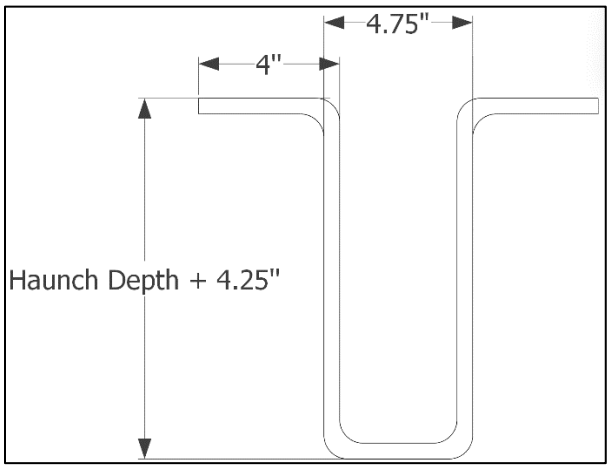

Figure 6.2.2.1 Bar UP Configuration

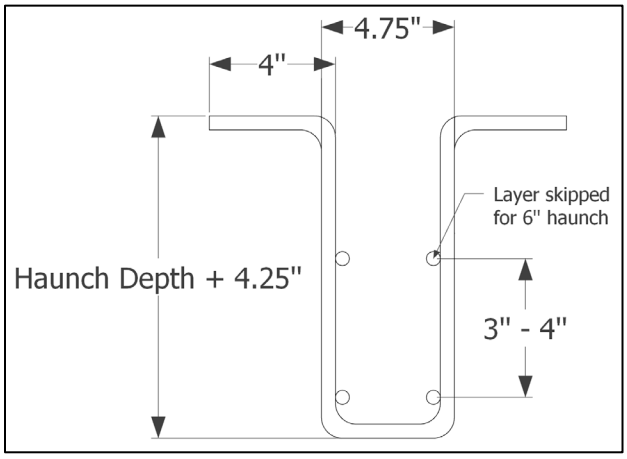

Figure 6.2.2.2 Bars UP with Longitudinal Bars

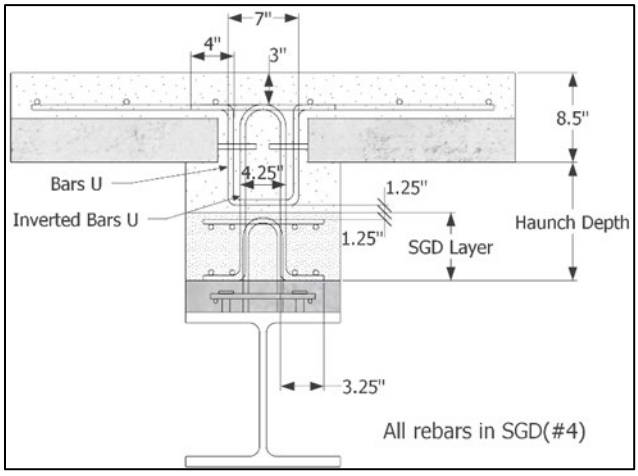

Figure 6.2.2.3 SGD Configuration (Haunches ≥ 6 in.)

Figure 6.2.2.4 shows the load versus slip plots for 2-in. haunch push-out test specimens with five bars R and without bars R. The specimens had a failure at the PCP-haunch interface as observed in the experiment. The cohesive layer strength of the PCP-haunch interface is lower than that of the simulated PSC girder-haunch interface and is lower than the interface shear resistance predicted by AASHTO LRFD (2020). The failure is brittle for the specimens with no bars R since the only resistance mechanism is cohesive strength. For the specimens with five bars R, the load does not drop after the cohesive layer breaks (Figure 6.2.2.4). The slip at the PCP-haunch interface increases the engagement of the shear reinforcement. This mode of response is different from the CIP specimens because the load is applied at the simulated PSC girder-haunch interface and not at the weaker PCP-haunch interface. The load continues to increase until the debonding failure at the simulated PSC girder-haunch interface or steel-yielding failure occurs. It is important to note that if the load was applied at the PCP-haunch interface directly, the specimen would have performed differently. The peak load in that case will be controlled by the cohesive strength at the PCP-haunch interface and can therefore be smaller than the strength predicted by AASHTO LRFD (2020).

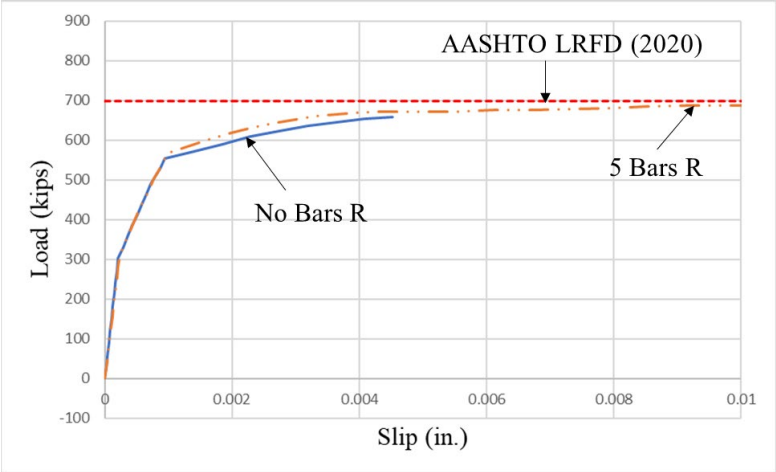

Figure 6.2.2.4 Load versus Slip with and without Bars R (2-in. Haunch)

Figure 6.2.2.5 shows the load versus slip plots for 6-in. haunch push-out test specimens with different detailing strategies. The specimens with no haunch detailing (only bars R as shear reinforcement) failed at the PCP-haunch interface with a smaller peak load value than the other specimens and the AASHTO LRFD (2020) expected value. The specimens with Bars UP detailing have a peak load value higher than the design strength obtained from the AASHTO LRFD (2020). These specimens have a diagonal crack in the haunch combined with a PCP-haunch interface crack at failure. The effect of longitudinal bars is negligible in the specimen. The specimens with SGD have a higher peak load value than all the other specimens as well as the AASHTO LRFD (2020) predicted value. These specimens fail at the simulated PSC girder-haunch interface with minor diagonal cracks in the haunch. These specimens have higher slip values than the other specimens.

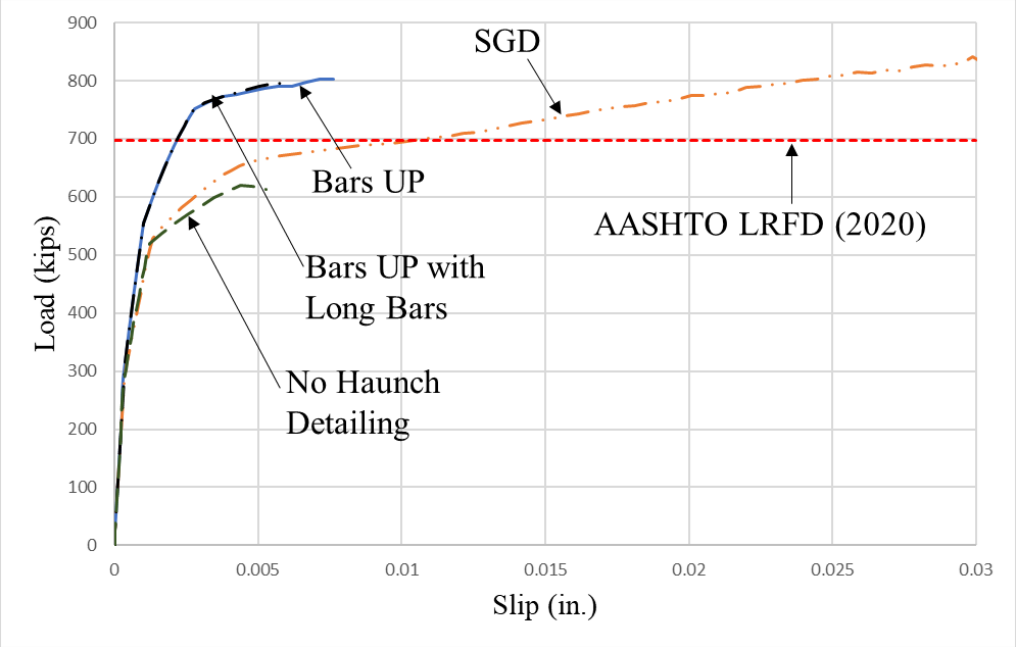

Figure 6.2.2.5 Load versus Slip with Different Haunch Detailing Strategies (6-in. Haunch)

Figure 6.2.2.6 compares the load versus slip plots for 9-in. haunch push-out test specimens. The specimens displayed failure modes similar to the 6-in. haunch specimens with the same detailing. The reinforced haunch specimens examined have peak load values higher than that predicted by AASHTO LRFD (2020).

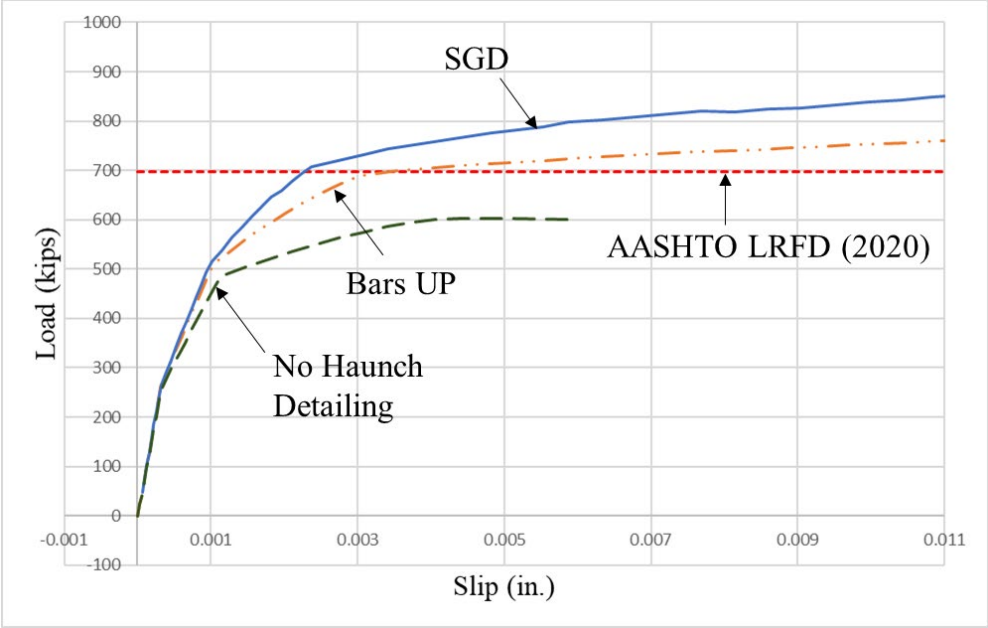

Figure 6.2.2.6 Load versus Slip with Different Haunch Detailing Strategies (9-in. Haunch)

Figure 6.2.2.7 show load versus slip plots for 12-in. haunch specimens. All three detailing practices have similar peak load values, which are higher than the AASHTO LRFD (2020) predicted value. The failure modes observed for SGD and bar UP detailing are similar to that observed in 6-in. and 9-in. haunch specimens. These failure modes agree with the observations from the experiments (Section 4.4)

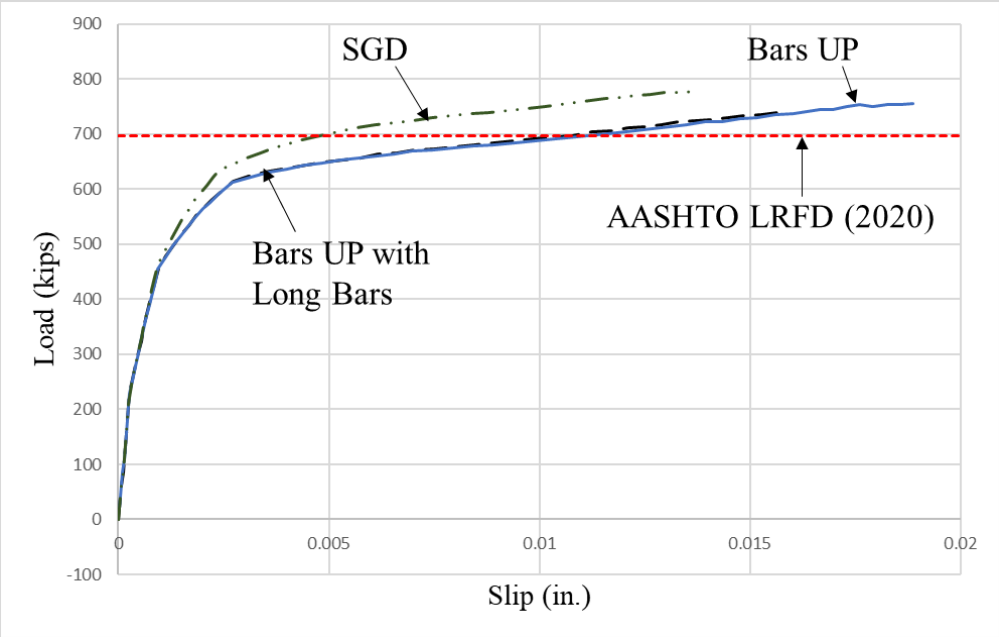

Figure 6.2.2.7 Load versus Slip with Different Haunch Detailing Strategies (12-in. Haunch)

6.2.2.1.2. Shear Reinforcement Layout

Figure 6.2.2.8 shows a 12-in. haunch push-out specimen with three bars R and Bars UP. The spacing between bars R and UP is varied between 12 in. and 24 in. to investigate the effects of shear reinforcement spacing. Figure 6.2.2.9 shows the load versus slip plots for specimens with different spacings. All the specimens have nearly identical peak loads. The failure mode of all the specimens is at the PCP-haunch interface combined with diagonal cracking in the haunch. All specimens have higher peak load values than the predicted value by AASHTO LRFD (2020).

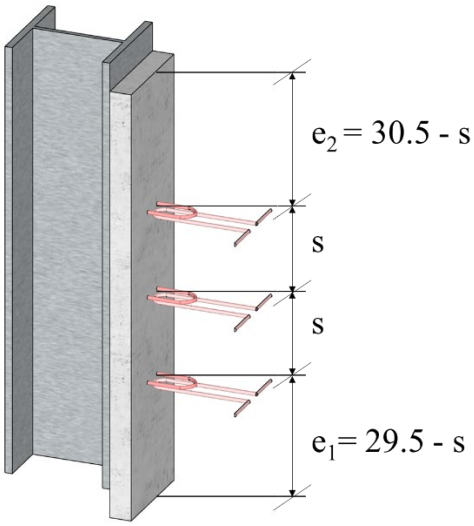

Figure 6.2.2.8 Shear Reinforcement Spacing Variation

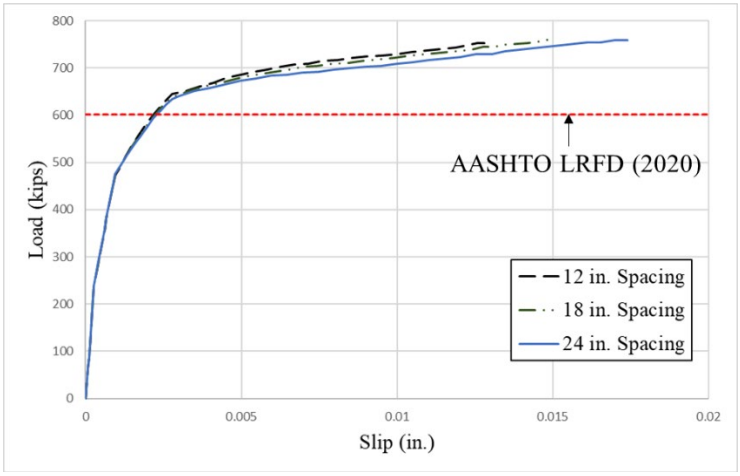

Figure 6.2.2.9 Load versus Slip Variation with Spacing (12-in. Haunch with Bar UP)

The amount of shear reinforcement is varied for 12-in. haunch specimens between 1, 3, and 5 bars (Figures 6.2.2.10). The spacing for all the specimens is 12 in.

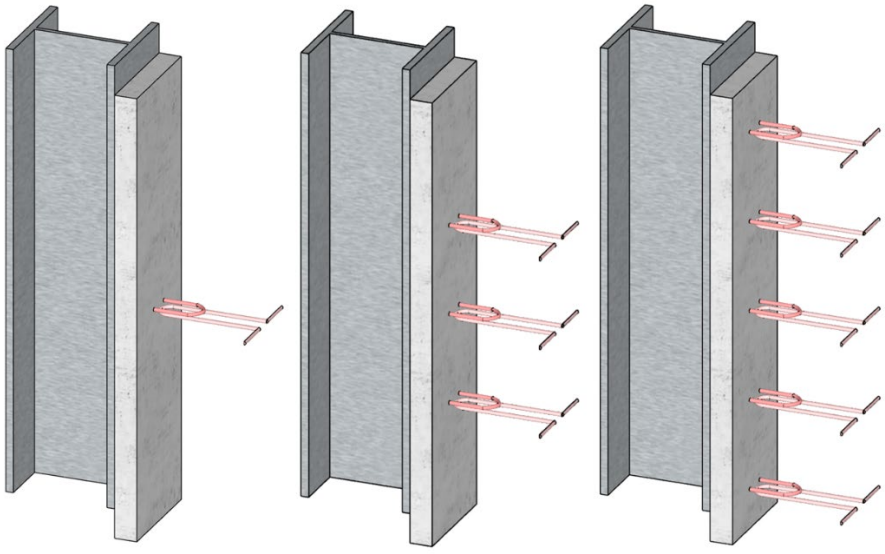

Figure 6.2.2.10 Variation of No. of Shear Reinforcement

Figure 6.2.2.11 shows load versus slip plots for 12-in. haunch specimens with different amounts of shear reinforcement. All specimens have higher capacities than the predicted value from AASHTO LRFD (2020) for five Bars R. The failure mode is as mentioned previously for the other 12-in. haunch specimens with Bars UP. Because the failure mode is controlled by the concrete strut failure (explained in Section 4.4), the amount of shear reinforcement or the spacing did not affect the peak load. The failure mode for 6 in. and 9 in. specimens with Bars UP was the

same as that for 12 in. specimens. Therefore, the shear reinforcement spacing and layout do not affect the results significantly.

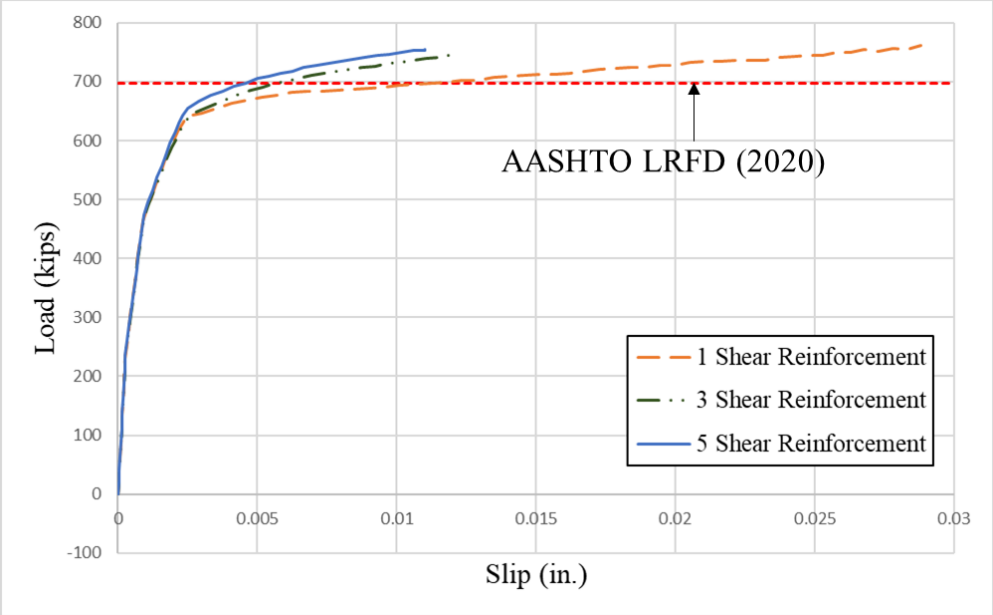

Figure 6.2.2.11 Load versus Slip Variation with No. of Shear Reinforcement (12-in. Haunch with Bars UP)

6.2.2.1.3. Shear Reinforcement Size

The shear reinforcement size tested in all the experiments was #4. The parametric study investigated the effects of increasing the size of bars R and Bars UP to #5 and #6. Figure 6.2.2.12 shows the load versus slip plots with variation in shear reinforcement size for 12-in. haunch specimens. All the specimens have similar peak load values and failure modes. The peak load values for specimens with #5 and #6 shear reinforcement sizes are lower than the predicted values from AASHTO LRFD (2020) equation. Similar to Group I, limiting the maximum contribution from shear reinforcement may be required to ensure conservative results.

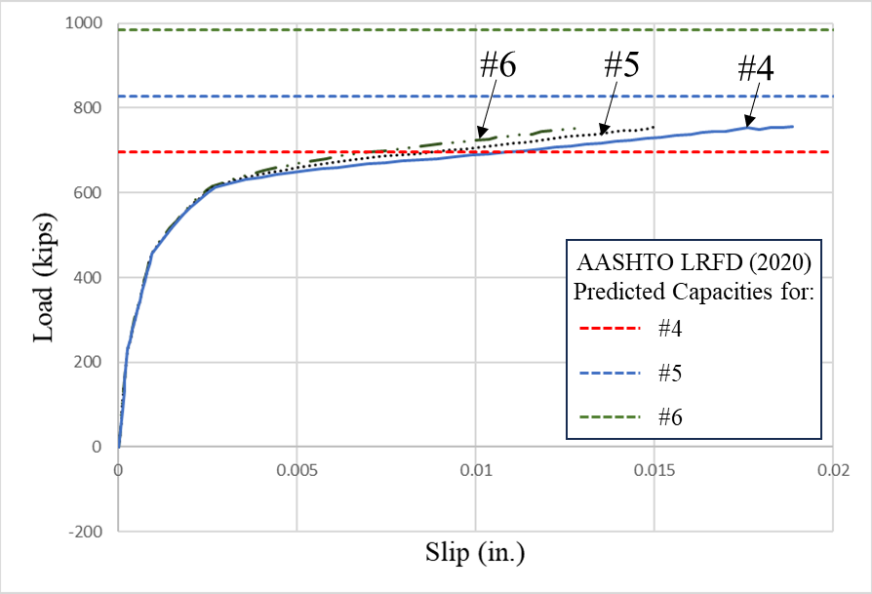

Figure 6.2.2.12 Load versus Slip Variation with Shear Reinforcement Size (12-in. Haunch with Bars UP)

6.2.2.1.4. Embedment Depth

As mentioned previously, TxDOT (2022) does not require haunch reinforcement for haunches ≤ 3.5 in. Figure 6.2.2.13 shows a comparison of load versus slip plots for 2-in. and 3.5-in. haunch specimens. Because the bar R length outside the girder top is fixed to 6 in., the embedment depth into the deck for 2-in. and 3.5-in. haunch specimens will be 4 in. and 2.5 in., respectively. Given that PCPs have a thickness of 4 in., there will be no penetration of bars R into the CIP portion for both the haunch depths considered. The figure shows a slight decrease in peak load value with a decrease in embedment depth. The 2-in. haunch PSC girder specimen had a concrete pull-out failure at the PCP-haunch interface (Section 4.4). The failure mode predicted by the computational model suggests that an embedment depth of even 4 in. into the PCP deck may not be enough to allow shear transfer to occur. The FE model shows a correlation between capacity and embedment depth. Based on these observations, an embedment depth enough to reach the CIP deck may be required to allow for shear transfer.

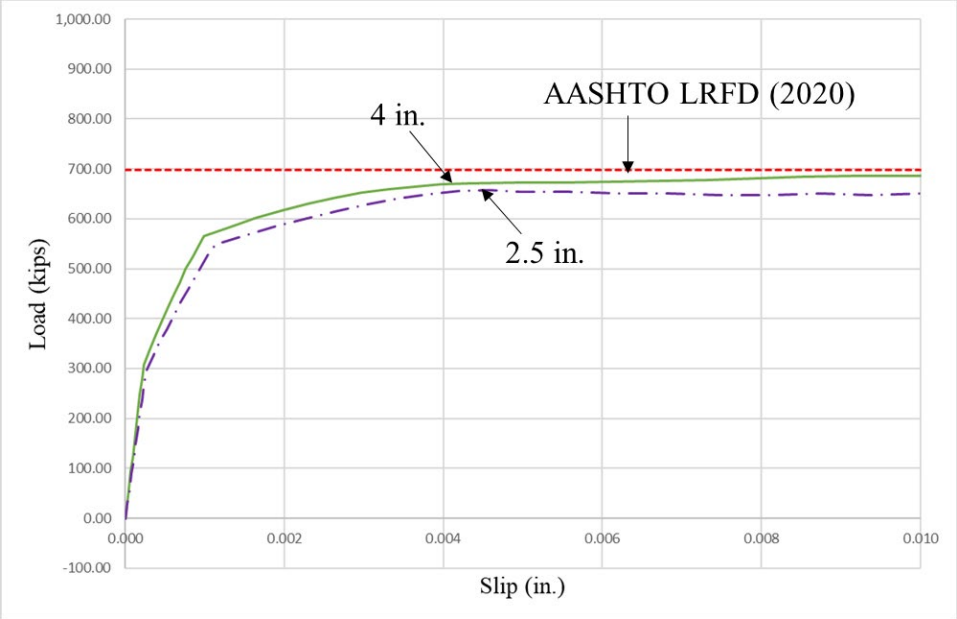

Figure 6.2.2.13 Load versus Slip Variation with Embedment Depth

6.2.2.1.5. Interaction Length (IL)

Based on the results obtained from CIP specimens, a minimum IL of 3 in. is considered. Figure 6.2.2.14 shows the load versus slip plot for 12-in. haunch specimens with Bars UP detailing with an IL of 3 in. and 4.75 in. The load-slip plots for both cases overlap each other suggesting a minimum of 3 in. can work for PCP specimens also.

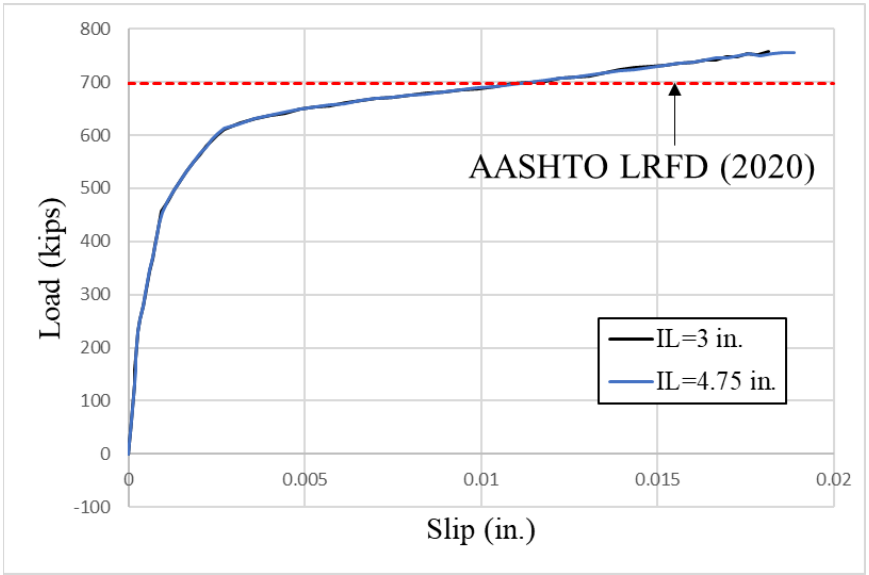

Figure 6.2.2.14 Load versus Slip Variation with Interaction Length (12-in. Haunch with Bars UP)

6.2.2.2. CIP Concrete Compressive Strength

This parametric study analyzes the effect of varying haunch concrete strengths based on common TxDOT practices. Figure 6.2.2.15 shows load versus slip variation with concrete compressive strength for 12-in. haunch specimens with Bars UP. The peak load value increases with an increase in concrete compressive strength. The specimens with a concrete compressive strength of 3.5 ksi have a peak load below the predicted value from AASHTO LRFD (2020).

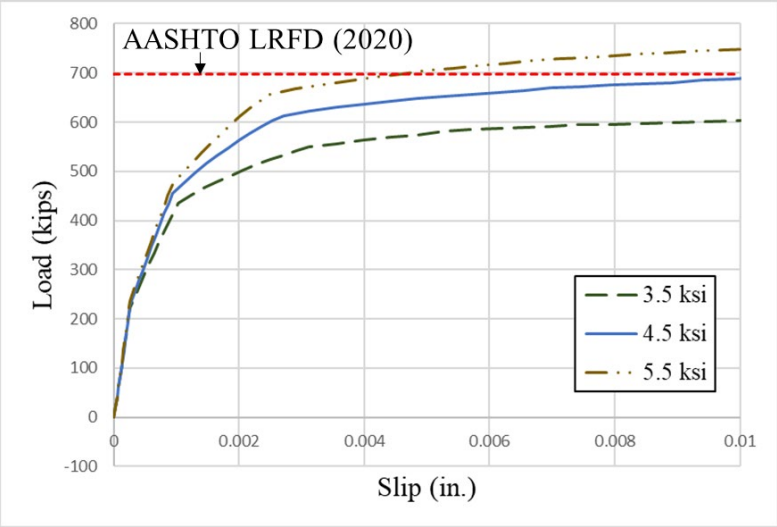

Figure 6.2.2.15 Load versus Slip Variation with CIP Compressive Strength (12-in. Haunch with Bars UP)

6.2.2.3. Haunch Depth

Specimens with haunch depths of 2 in., 3.5 in., 6 in., 9 in., and 12 in. are investigated, and compared with the AASHTO LRFD (2020) predicted capacity. Haunches with depths ≤ 3.5 in. are provided with bars R only. Haunches with depths ≥ 6 in. have bars R and Bars UP in the haunch. Figure 6.2.2.16 illustrates the load-slip behavior of the 2-in., 3.5-in., 6-in., 9-in., and 12-in. haunch specimens. The results suggest that the specimens with 2-in. and 3.5-in. haunch depths may not have sufficient embedment depth of bars R into the CIP portion of the deck, and they have lower peak load values than the predicted strength (AASHTO LRFD 2020). For both the haunch depths, the shear reinforcement does not go above the thickness of PCP (4 in.) in the deck. Because there is no interaction between the CIP deck reinforcement mat and bars R, the pull-out failure of bars R is observed in the experiment and FE model. The 6-in., 9-in., and 12-in. haunch specimens with Bars UP detailing have higher peak load values than the predicted strength from AASHTO LRFD (2020). All three of these specimens have failure at the PCP-haunch interface combined with diagonal cracking in the haunch.

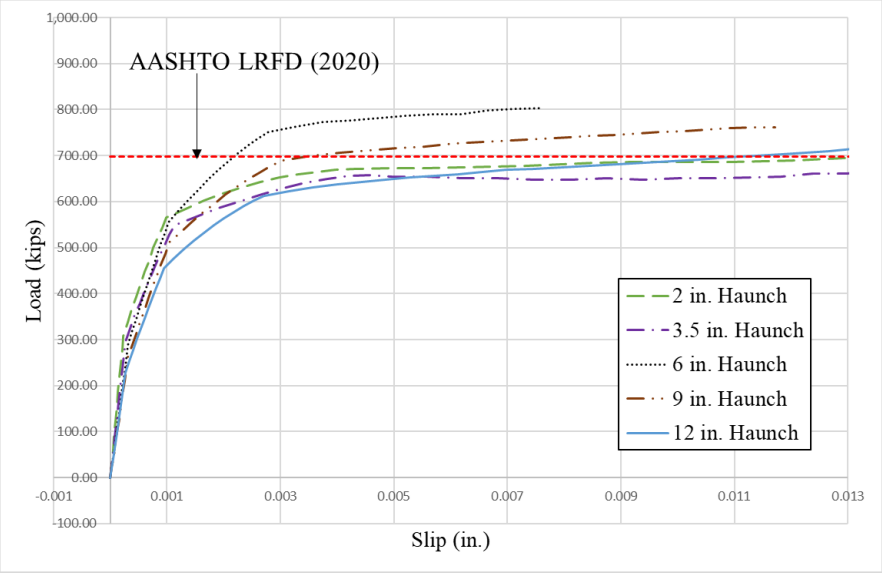

Figure 6.2.2.16 Load versus Slip Variation with Haunch Depth

6.2.2.4. Concluding Remarks

The parametric study for PCP push-out specimens suggests that the peak load value depends on factors such as embedment depth, CIP concrete compressive strength, haunch depth, and the type of shear reinforcement. Since the SGD detailing requires two layers of concrete (Section 4.1), Bars UP detailing will be preferred in terms of ease of construction. Therefore, the parametric study included a detailed evaluation of Bars UP detailing. With sufficient embedment depth and CIP concrete compressive strength, a tall haunch specimen up to 12 in. can have a peak load value higher than predicted by AASHTO LRFD (2020). However, the experimental tests and parametric study performed had load applied at the simulated PSC girder-haunch interface and not at the weaker PCP-haunch interface. As mentioned previously, if the load is applied directly at the PCP-haunch interface, the failure may occur earlier when the cohesive strength is exceeded. Therefore, to consider the possibility of shear load applied at the PCP-haunch interface directly, a revision to current guidelines may be required to consider the cohesive and friction coefficient at the weaker interface.

6.3. Conclusions

A parametric study was performed on steel and PSC girder specimens to identify a broad range of parameters that were not directly evaluated during the experimental program. Based on the study, design recommendations are provided to account for tall haunches in steel and PSC girder bridges, which are presented in the next chapter.

Chapter 7. Conclusions and Design Recommendations

This section provides conclusions from this project based on the experimental and computational results and provides design recommendations for TxDOT.

7.1 Steel Girder

Extreme haunches have occurred in Texas bridges, often as a result of field problems. Haunches 15 in. or larger have occasionally been required in some composite steel and prestressed concrete bridges. Many of the problematic situations necessitating tall haunches require decisions within a relatively short time frame to avoid costly delays. However, design guidelines or specifications are not available for these extreme situations. A search of the available literature did not locate pertinent studies on the behavior or detailing requirements with extreme haunches. To improve the understanding of the behavior of steel and prestressed concrete girders with tall haunches, a research study including both laboratory experiments and computational studies was conducted. The laboratory experiments consisted of a series of push-out tests on specimens reflecting the different variables that were deemed to impact the behavior. The data from the tests were used to validate a computational model used to further understand the impact of a wider range of systems. This report has documented the experiments and computational studies in an effort to develop design guidelines.

In Chapter 2, the review of previous studies and current design specifications and guidelines is discussed. The review summarized possible factors affecting the behavior of the shear connector, as well as the limitations of AASHTO LRFD (2020) and TxDOT bridge standards, including the Bridge Design Guide (2023a), the Bridge Design Manual – LRFD (2023b), the Bridge Detailing Guide (2022), and the standard drawings, related to the shear connectors involving headed shear studs and tall haunches. AASHTO LRFD (2020) and TxDOT bridge standards require minimum deck penetration of 2 in. The Bridge Detailing Guide (2023a) states that a haunch deeper than 3 in. without any shear connectors is required to be transversely reinforced with U-bars at a maximum spacing of 12 in. However, the recommendations do not reflect limitations on the depth of haunch for the detailing method to be valid. Based on the literature review, the factors affecting the shear connectors are stud diameter, stud arrangement, haunch geometry, haunch reinforcement, and concrete strength. A setup for conducting push-out tests to understand the behavior was designed and fabricated as outlined in Chapter 3.

Chapter 3 systematically demonstrates the experimental work of this research project, including the specimen design, the test matrix, the push-out test details, and the discussion of the test results. For steel girder cases, the test matrix covered haunch depth between 0 to 15 in., different haunch reinforcement, and various stud arrangements. Test results showed that stud penetration into the deck plays a significant role in tall haunch behavior. In addition, the stud spacing and haunch reinforcement also impact the resulting failure modes and ultimate capacity.

Chapter 5 and 6 include the numerical analysis for the steel girder tests. A finite element model was developed and validated with the test results, which is provided in Chapter 5. Chapter 6 discusses the parametric study that expanded the research scope and expanded the variables from the experiments. Stud length, stud pitch, and haunch width were considered in the parametric study. The results demonstrate that the ultimate capacity of the shear connectors with tall haunches is positively related to these three variables.

In the next sub-section, the design recommendations are provided for the shear connectors with haunches ranging from 3 in. to 15 in.

7.1.1 Design Recommendations

It is important to clarify that the tall haunch construction practices conducted by TxDOT beyond the current design specifications and guidelines, including stacked shear studs and transverse reinforcement used with longitudinal rebars near haunch bottom, show adequate ultimate capacity. The push-out test results, as shown in Chapter 3, demonstrated that all of the tall haunch designs reached their design capacity. The design recommendations developed in this chapter are to improve tall haunch performances and bring extra redundancy into steel bridge composite girders. The following design guidelines can be used for haunches equal to or deeper than 6 in. For haunches less than 6 in., the current TxDOT design guidelines can be used.

The design recommendations are developed on four aspects, which are 1) deck penetration, 2) stud pitch, 3) haunch reinforcement, and 4) stud clear edge distance. The next four sections specifically demonstrate the strategies to improve the current designs and constructions.

7.1.1.1. Deck Penetration

The strength of composite girders is most impacted by penetration of the shear studs into the deck. Therefore, the shear connectors with tall haunches should ideally have sufficient stud length for deck penetration. AASHTO LRFD (2020) requires a minimum penetration of 2 in. The research in this study reinforced this importance and a penetration of 2 inches or higher is recommended in all composite girder systems (with both standard and tall haunches). Because many of the issues that might require a tall haunch occur as a result of field problems, modifications to the original details are often necessary. Experimental results demonstrated that the use of stacked shear studs provided an effective method to achieve sufficient strength and ductility provided the stacked stud penetrates the deck reinforcing as outlined above.

7.1.1.2. Stud Pitch

Given sufficient longitudinal shear capacity, a minimum stud pitch of 12 in. should be specified in tall haunch regions based on the results from the push-out tests and parametric study. As shown in the standard drawing “Steel Girder Miscellaneous Details” (2015), the minimum pitch required by TxDOT is four times the stud diameter. For tall haunch cases, however, sufficient longitudinal spacing is essentially needed to mitigate the high localized stresses in the concrete close to shear studs. A minimum value of 12 inches seemed sufficient. In addition, the 12 in. pitch matches common practical limits that might be required so that construction personnel can

safely move around the girders during early stages of construction prior to the installation of concrete formwork.

7.1.1.3. Haunch Reinforcement

In tall haunch regions, U-bars or stirrups of #4 Grade 60 can be used with a maximum spacing 12 in. At least two #4 longitudinal rebars should be placed within the transverse reinforcement. Figure 7.1.1.1 illustrates the detailing. The longitudinal rebars serve not only construction but also structural purposes. With concrete failure, the longitudinal rebars improve the ductility of the shear connectors since concrete breakout is prevented and the shear studs may reach sufficient strength and deformation demands.

7.1.1.4. Stud Clear Edge Distance

AASHTO LRFD (2020) allows a minimum clear edge distance of 1 inch for the shear studs. With taller haunches, the edge distance can compromise the strength. Designers should maximize the edge distance whenever possible and larger values are encouraged.

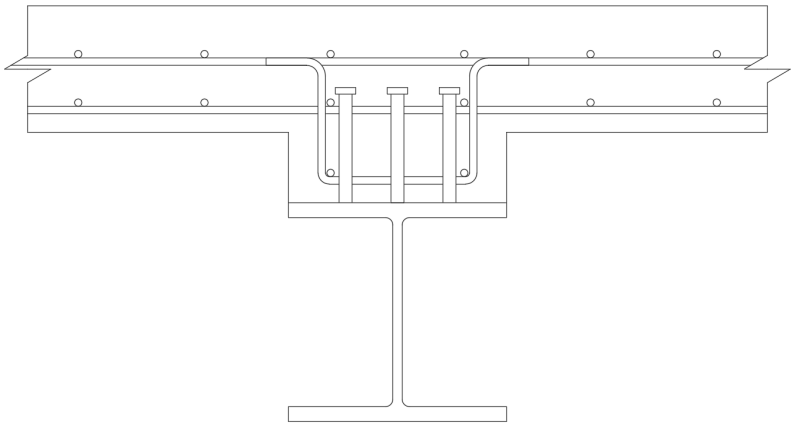

Figure 7.1.1.1 Haunch Reinforcement with Longitudinal Rebars near Haunch Bottom

7.1.2 Research Limitation and Future Recommendations

The experimental research consisted of a wide variety of traditional push out tests to understand the factors impacting the behavior of composite steel and prestressed concrete bridge girders with tall haunches. The tests were the most efficient and practical method to characterize the behavior. While a total of 17 tests on steel girder systems were conducted, additional tests might shed light on other factors impacting the behavior.

In addition to the traditional push-out test that is recognized as an effective and efficient method to investigate composite systems, experiments on composite girder applications might provide additional insight to the behavior. The consideration of tall haunches brings in extra complication. The modified push-out test methods utilized in the studies focus on the critical regions of the structure where compressive forces are at maximum. Additional full-scale beam tests will demonstrate the full impact of a system with an extreme haunch.

7.2. PSC Girder

The objective of the PSC girder specimens shear testing and computational model was to analyze the effects of haunch behavior on the overall response of the bridge. Haunch depths ranging from 0.5 in. to 12 in. are encountered by TxDOT on site. The existing TxDOT (2022) guidelines require haunches > 3.5 in. to be reinforced with Bars U for CIP decks and with Bars UP for PCP decks. The project researchers performed push-out tests to analyze the effectiveness of these and other haunch detailing strategies. The experimental results were complemented with computational models to analyze the effects of specimen parameters that were not analyzed in the test program.

The results from experimental and analytical works (Chapters 4,5, and 6) show that the behavior of haunches in PSC girder specimens depends upon the type of deck used. For PSC girder specimens with CIP deck, the behavior of haunches ≤ 3.5 in. with only bars R as the shear connectors and the behavior of well-detailed (with Bars U or other details shown in Section 6.2.1.1) tall haunches (>3.5 in.) was similar to each other. The specimens with smaller haunches (≤ 3.5 in.) had a clear debonding failure at the simulated PSC girder-haunch interface. The specimens with taller haunches also had debonding at the simulated PSC girder-haunch interface combined with diagonal cracking near the specimen base. The peak loads obtained for all haunch depths from the parametric study were close (Figure 7.2.1). The relative slip at the shear interface was < 0.01 in. for all the specimens and the failure was brittle with a sudden drop at the peak load.

The current AASHTO LRFD (2020) equation used by TxDOT (2022) for interface shear resistance predicts the peak loads for haunches up to 12 in. depth conservatively if the haunches are properly detailed (Figure 7.2.1). Bars U considered by TxDOT (2022) for tall haunches is an acceptable haunch detailing as per the push-out test results. The maximum spacing of Bars U, the rebar size, interaction length with bars R, and other parameters information is currently not provided in the TxDOT (2022) guidelines. Section 7.2.1.1 provides design recommendations that can be considered for tall haunch in PSC girders with CIP decks.

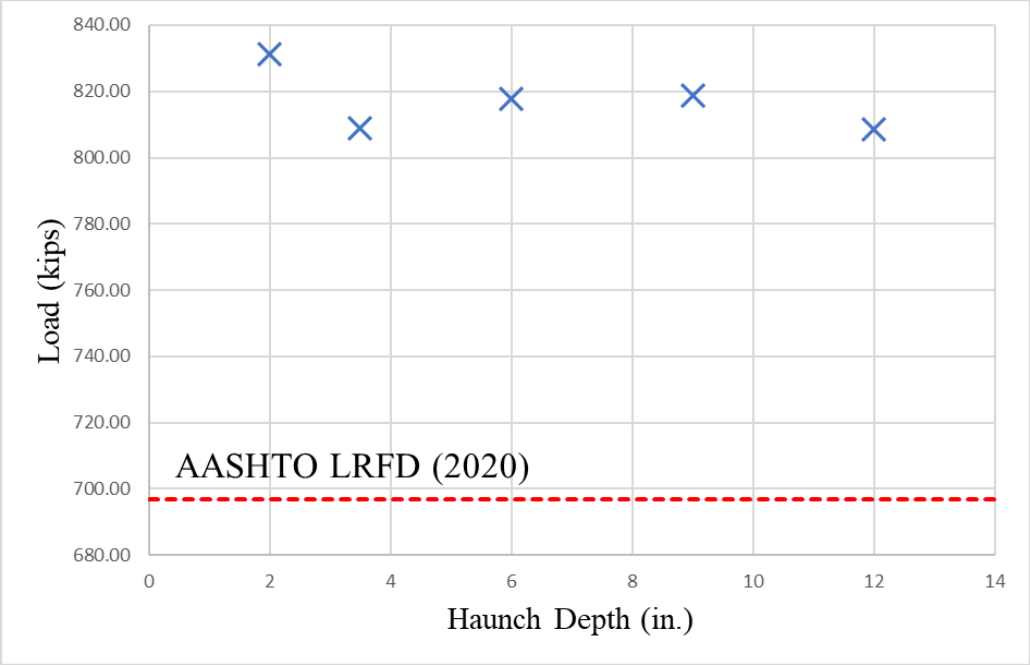

Figure 7.2.1 Peak Loads for CIP Deck Specimens with Varying Haunch Depths

The behavior of PSC girders with PCP decks was also analyzed for haunches ranging from 2 in. to 12 in. The behavior of these specimens was different from the CIP specimens because the controlling or weaker shear interface was not applied with the load directly. The PCP-haunch interface was applied with a combination of shear, transverse, and parallel stresses. Unlike CIP specimens, the peak load does not drop when the cohesive layer at the weaker shear interface (PCP-haunch) breaks. Beyond the break of the cohesive layer, the relative slip at the PCP-haunch interface is increased to engage shear reinforcement until failure occurs. The relative slip obtained for these specimens at the PCP-haunch interface goes up to 0.03 in. which is higher than the relative slip values observed for CIP specimens.

The results of haunch specimens ≤ 3.5 in. suggest that bars R should penetrate the CIP portion of the deck. For 2-in. and 3-in. haunch specimens tested and analyzed, there was no penetration of bars R into the CIP portion of the deck. The failure mode for these specimens was concrete pull-out at the PCP-haunch interface and the peak load measured was lower than the predicted value from AASHTO LRFD (2020) (Figure 7.2.2). In contrast, the tall haunch specimens (> 3.5 in.) reinforced with Bars UP had a debonding failure at the PCP-haunch interface combined with concrete cracking in the haunch. The peak load values for these tall haunch specimens decreased as the haunch depth increased (Figure 7.2.2). The values obtained were higher than the predicted value from AASHTO LRFD (2020) for haunch depths up to 12 in. Because the peak load values were dependent upon the CIP concrete strength (Section 6.2.2), a minimum concrete compressive strength of 4 ksi is required.

Based on the comparison in Figure 7.2.2, Bars UP required by TxDOT (2022) for tall haunches (>3.5 in.) are found an acceptable detailing method. AASHTO LRFD (2022) interface shear design equation can be used to predict the strength of these specimens. TxDOT (2022) detailing guidelines do not provide information about all the parameters affecting tall haunch behavior in PSC girders with PCP decks. Based on the parametric study performed in this project, the design recommendations for Bars UP maximum longitudinal spacing, rebar size, interaction length, and other affecting parameters are provided in Section 7.2.2.1.

It is important to note that if the load in push-out tests was applied at the weaker interface directly (PCP-haunch interface), the failure may have occurred earlier due to the break of the cohesive layer at the PCP-haunch interface. Therefore, a modification to the design equation is suggested for the PSC girder with PCP decks in Section 7.2.2 to consider the weakest interface contact area. The subsequent sections provide details about the development of design recommendations for CIP and PCP decks and proposed design recommendations.

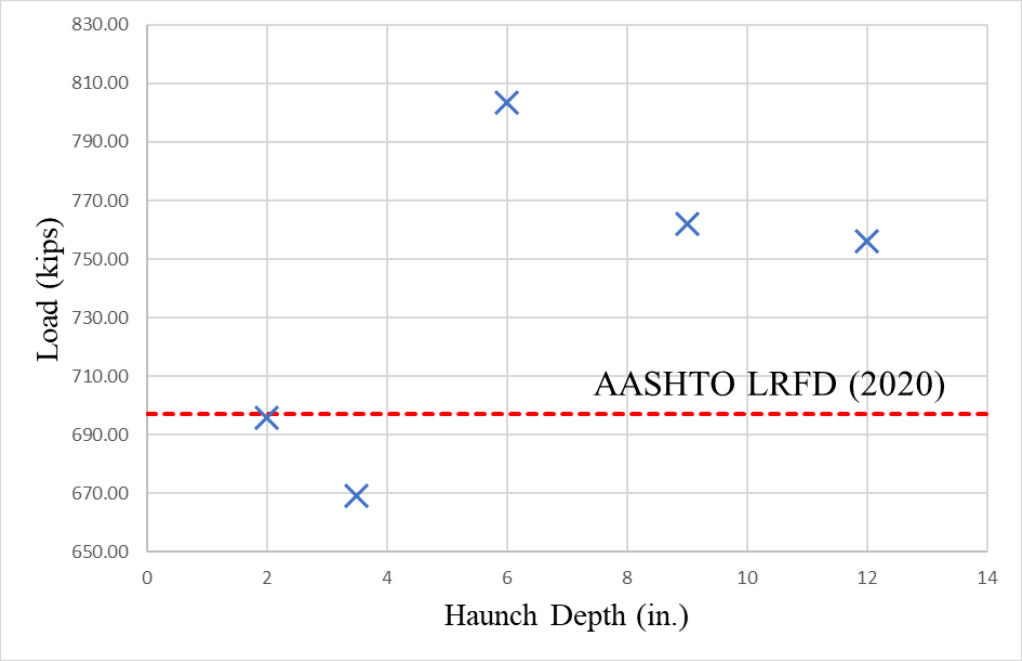

Figure 7.2.2 Peak Loads for PCP Deck Specimens with Varying Haunch Depths

7.2.1. CIP Specimens Design Recommendations Development

The results from Chapter 4 for CIP specimens suggest that the majority of the shear capacity is provided by the cohesive layer at the interface. The shear reinforcement engages only after the cohesive layer breaks at the shear interface to cause a relative slip. The cohesive layer resistance is primarily dependent on the surface roughness and area of contact. The researchers prepared the shear interface for all the push-out test specimens in accordance with TxDOT construction practices. The specimen with no shear reinforcement was able to achieve a higher strength than that predicted by AAHSTO LRFD (2020) (Section A3.2.1). The cohesive layer strength is

therefore higher than predicted. Additionally, the concrete compressive strength and slump test value are observed to affect the cohesive layer resistance in the specimens. The specimens that did not adhere to TxDOT Class S concrete requirements for haunches had a lower bonding strength than the other specimens.

With the presence of a haunch, the shear interface failure is combined with cracking in the haunch. The peak capacity, however, is not affected significantly if the haunch is properly detailed. The maximum haunch depth permitted by TxDOT (2022) without any haunch detailing is 3.5 in. The parametric study showed that haunches up to 3.5 in. provide interface shear resistance adequately with only bars R. For haunch depths greater than 3.5 in., the shear reinforcement detailing tested included Bars U with or without longitudinal bars, vertical stirrups, and SGD rebar detailing. Haunch cracking was reduced for specimens with longitudinal bars or SGD rebar detailing, but the peak load values were not affected significantly. Based on ease of construction, Bars U or vertical stirrups are recommended as a practical detailing strategy.

The results from parametric studies also indicated that the major portion of the peak load is provided by the cohesive layer resistance. The shear reinforcement had minor effects on the peak load and relative slip at the shear interface but can affect the failure mode and residual load of a push-out test specimen. The variation in CIP concrete compressive strength also did not have major effects on the peak load.

A parametric study of haunch depths indicates the minimal influence of this detail on specimen strength and slip if the haunch is properly detailed with either of the details tested. The parametric study did not consider extraordinarily tall haunch depths (beyond 12-in.), focusing only on the range of haunch depths considered experimentally.

The experimental and parametric results also suggest that composite PSC girder bridge decks are prone to brittle debonding failure between the girder and the haunch after the failure of the cohesive layer. All the parameters studied do not significantly improve the slip at the composite interface before failure. Therefore, TxDOT can ensure safety in composite PSC girder bridge decks with haunches by mandating a factor of safety to limit the predicted capacity of these systems, preventing them from reaching their capacity (damage to the cohesive layer at the composite interface), and reducing the likelihood of a brittle failure. Based on all the observations made, design recommendations are provided in the next subsection for interface shear resistance in PSC girders with haunches.

7.2.1.1. Proposed Design Recommendations

- The concrete layer in the haunch should satisfy the requirements for TxDOT Class S.
- The shear interface should be intentionally roughened to have a minimum amplitude of 0.25 in (AASHTO LRFD (2020)).
- Bars U (Figure 6.2.1.1) or vertical stirrups (Figure 6.2.2.2) are suggested haunch detailing strategies for haunches > 3.5 in. Figure 7.2.3 also illustrates the detailing.

- Haunch shear reinforcement can be tied to bars R and the top or bottom mat of the slab reinforcement. A minimum interaction length of 3 in. is suggested between bars R and Bars U (Figure 7.2.3).
- Bars U or vertical stirrups can have a maximum spacing of 24 in.
- Rebar sizes for Bars U or vertical stirrups can range from #4 to #6.
- AASHTO LRFD (2020) equation 5.7.4.3-1 can be used to calculate interface shear resistance for CIP specimens in PSC girders with haunches up to 12-in. deep, with a limit on the contribution from shear reinforcement for tall haunches (> 3.5 in.): $\mu A_{vf} f_y < 50\% \; of \; cA_{cv}$.
- The current TxDOT shear strength reduction factor that limits a bridge deck's shear strength to 90% of its true ultimate capacity should be used in the design.

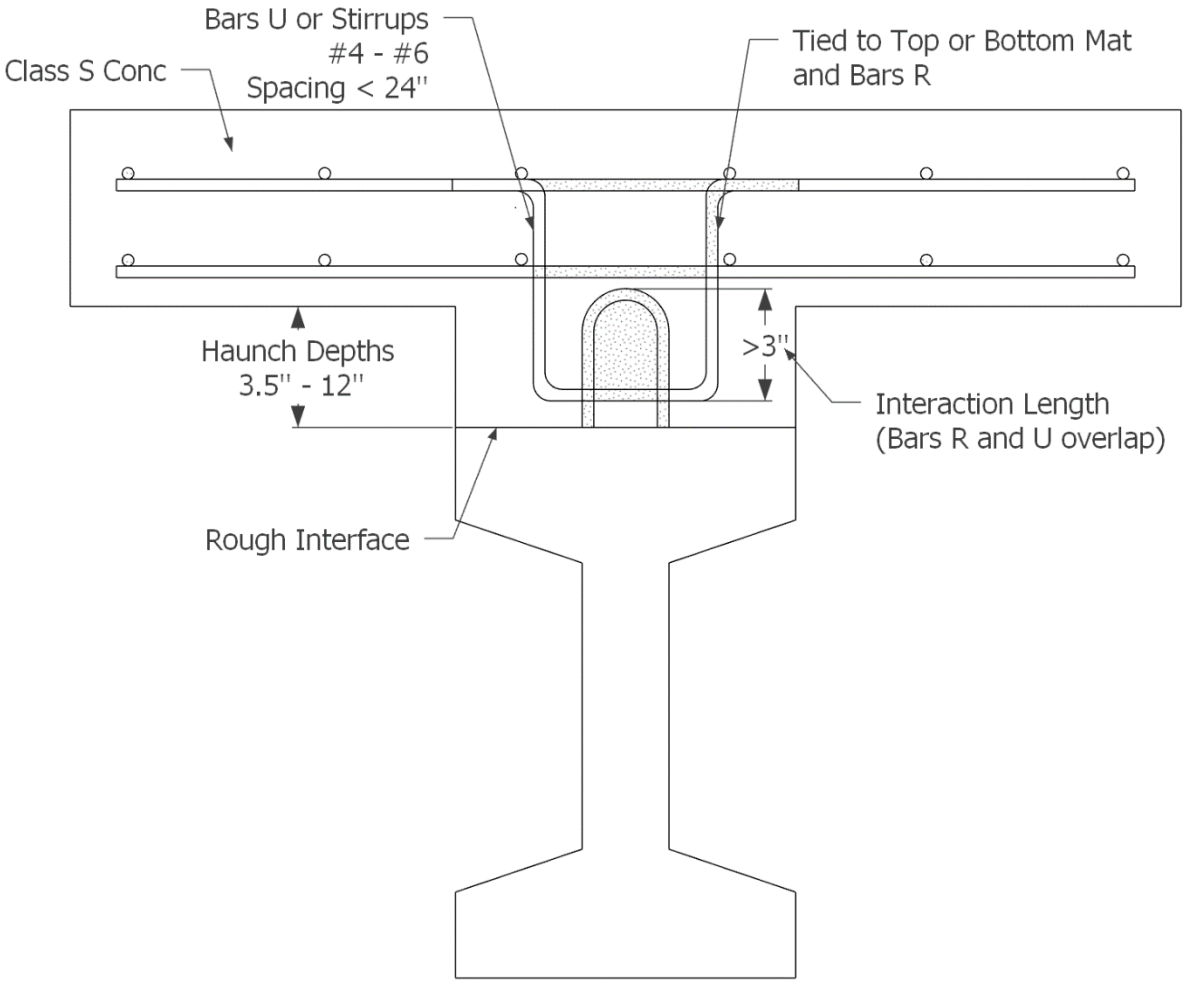

Figure 7.2.3 CIP Haunch Reinforcement Detailing
(for haunch depths ≥ 3.5 in.)

7.2.2. PCP Specimens Design Recommendations Development

The experimental results for PCP specimens suggest that the PCP-haunch interface is weaker compared to the simulated PSC girder-haunch interface. The cohesive layer breaks at the PCP-haunch interface first leading to a relative slip at the interface. This slip engages shear reinforcement to participate in the shear resistance until a debonding failure occurs at the simulated PSC girder-haunch interface or shear reinforcement yields. This failure mode can be preceded by concrete pull-out failure if the embedment depth into the CIP deck is insufficient. The 2-in. haunch specimens have an embedment depth of 4 in., which was equal to the thickness of PCPs in this study. An embedment depth of 5.5 in. is suggested to allow for penetration into the CIP portion of the slab.

The haunch detailing tested for PCP specimens included Bars UP and SGD. Specimen with SGD had comparatively less cracking, and failure occurred due to debonding at the simulated PSC girder-haunch interface. These specimens had higher capacity and ductility than the specimens with Bars UP detailing for haunches ≤ 9 in. Specimens with Bars UP detailing had a failure at the PCP-haunch interface combined with diagonal cracking in the haunch. Both of these details, however, were able to provide a peak load value higher than the predicted strength by AASHTO LRFD (2020) (Section A3.2.1). SGD had an extra layer of concrete cast on top of the simulated PSC girder, which may not be a preferred construction practice.

The results from the parametric study also indicate that the cohesive layer will break at the PCP-haunch interface before the simulated PSC girder-haunch interface. Because the concrete failure mode controls for specimens with Bars UP detailing, the CIP concrete compressive strength affected the peak loads computed. The embedment depth of shear reinforcement into the deck also affected the peak loads. Specimens with no embedment into the CIP concrete had lower peak load values than the other specimens. Finally, the peak load values for tall haunch specimens (≥ 3.5 in.) with Bars UP detailing decreased with an increase in haunch depths.

As mentioned in previous sections, the load was applied at the simulated PSC girder-haunch interface and not at the PCP-haunch interface directly. If a direct load would have been applied at the weaker interface, the load-slip response would have been different. Therefore, in the case of multiple shear planes, the cohesion, friction, and contact area for the weaker interface should be considered in the interface shear resistance equation. Based on all the observations made, design recommendations are provided in the following subsection for interface shear resistance in PSC girders with haunches.

7.2.2.1. Proposed Design Recommendations

- The concrete layer in the haunch should satisfy the requirements for TxDOT Class S.
- The shear interfaces should be intentionally roughened to have a minimum amplitude of 0.25 in (AASHTO LRFD (2020)).
- Bars R should penetrate the CIP portion of the deck. The suggested embedment depth for 8.5-in. thick slab with 4-in. thick PCP layer is 5.5 in. The penetration into the CIP portion of the deck would then be 1.5 in.

- Bars UP (Figure 6.2.2.1) and SGD (Figure 6.2.2.3) are suggested detailing strategies for haunches where the minimum embedment depth criteria is not satisfied. Figure 7.2.4 also illustrates the detailing.
- Haunch shear reinforcement can be tied to bars R. A minimum interaction length of 3 in. is suggested between bars R and Bars UP or SGD.
- Haunch shear reinforcement can have a maximum spacing of 24 in.
- Rebar sizes for haunch shear reinforcement can range from #4 to #6.
- AASHTO LRFD (2020) equation 5.7.4.3-1 can be used to calculate interface shear resistance for PCP specimens in PSC girders with haunches up to 12 in. deep if the cohesion factor, friction factor, and the contact area of the weaker interface are considered. An additional requirement for the equation is the limit on the contribution from shear reinforcement for tall haunches (> 3.5 in.): $\mu A_{vf} f_y < 50\% \, of \, cA_{cv}$.
- The current TxDOT shear strength reduction factor that limits a bridge deck's shear strength to 90% of its true ultimate capacity should be used for design.

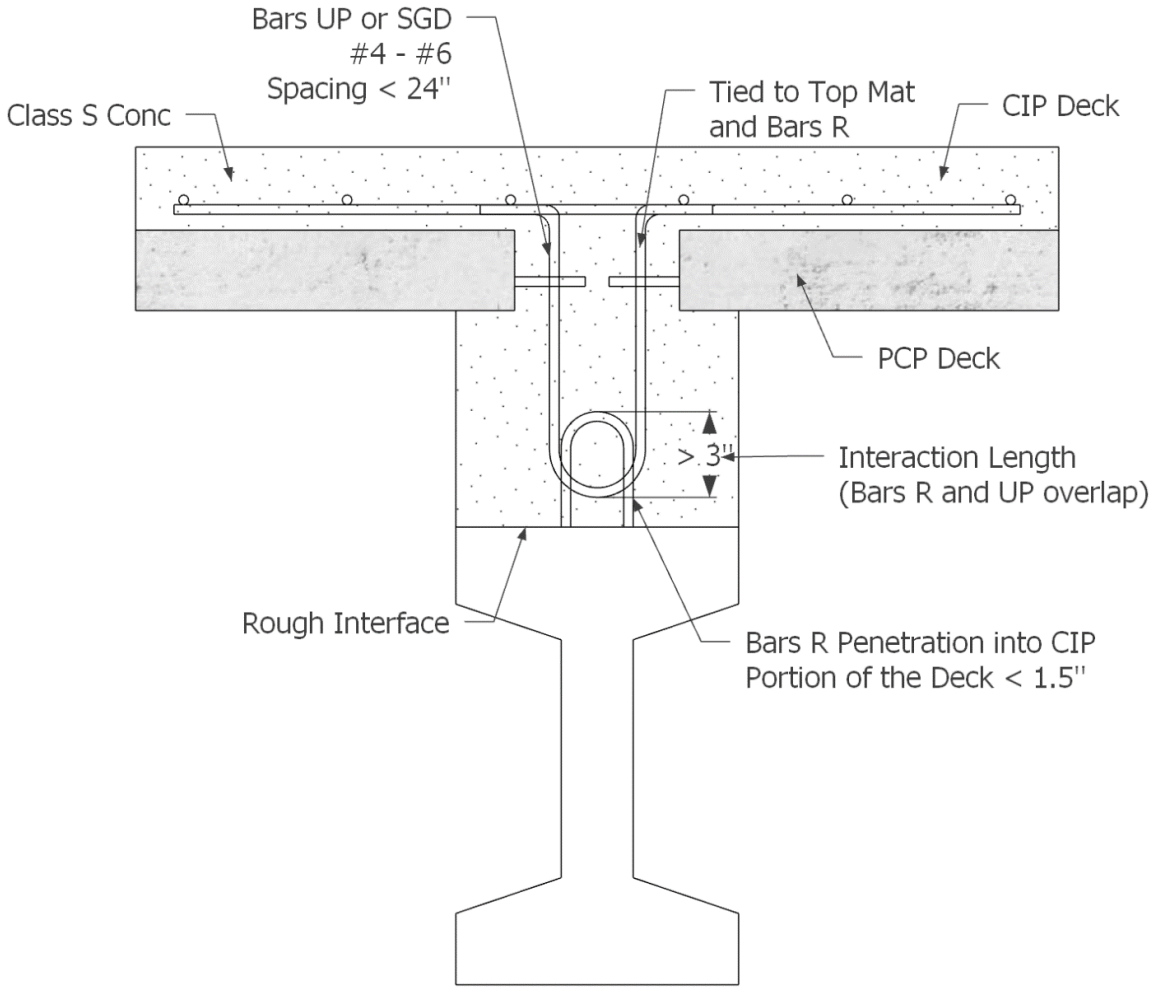

Figure 7.2.4 PCP Haunch Reinforcement Detailing
(when bars R penetration into CIP portion of the deck < 1.5 in.)

7.2.3. Recommendations for Future Research

Results from Chapter 4 prove that the push-out tests performed for tall haunches do not apply pure shear load but have bending effects also present due to eccentricity between the loading and support points. This effect can give slightly higher peak load values than expected for tall haunch specimens. Past research literature shows that no push-out or girder testing has been performed for haunches ≥ 6 in. Aside from the push-out tests completed for the current project, project researchers recommend conducting a large-scale girder test, along with computational simulation, to compare the findings from specimens evaluated with the behavior expected on an actual bridge.

The experimental and parametric results for PSC girder specimens showed that the cohesive and friction properties at the simulated PSC girder-haunch and the PCP-haunch interfaces affect the strength of PSC girder push-out specimens. A literature review demonstrates that surface preparation influences the amount of friction and cohesion between two concrete surfaces. Future research can investigate practical and reliable methods to ensure the preparation of rough and cohesive concrete surfaces in practice. A consistent and reliable method to increase the surface roughness of concrete surfaces at the composite interface can also be investigated to increase the shear capacity of PSC girder bridges.

References

AASHTO. LRFD (2004). *AASHTO LRFD Bridge Design Specifications*, 3rd Ed., American Association of State Highway Transportation Officials, Washington, D.C.

AASHTO LRFD (2020). *AASHTO LRFD Bridge Design Specifications, 9th Ed.*, American Association of State Highway Transportation Officials, Washington, D.C.

ABAQUS. (2006). *Abaqus Analysis User's Guide (Version 6.6)*, https://classes.engineering.wustl.edu/2009/spring/mase5513/abaqus/docs/v6.6/books/usb/default.htm

ABAQUS. (2013). *Abaqus Analysis User's Guide (Version 6.13)*, <http://dsk.ippt.pan.pl/docs/abaqus/v6.13/books/usb/default.htm>.

ACI Committee 318. (2008). *Building Code Requirements for Structural Concrete*, American Concrete Institute, Farmington Hills, Michigan.

ACI 318. (2019). *Building Code Requirements for Structural Concrete*, American Concrete Institute, Farmington Hills, Michigan.

AISC. (1999). *Load and Resistance Factor Design Specification for Structural Steel Buildings*, American Institute of Steel Construction, Chicago, Illinois.

AISC. (2005). *Specification for Structural Steel Buildings*, AISC-360-05, American Institute of Steel Construction, Chicago, Illinois.

AISC. (2016). *Specification for Structural Steel Buildings*, AISC-360-16, American Institute of Steel Construction, Chicago, Illinois.

ASTM A370. (2022). *Standard test methods and definitions for mechanical testing of steel products*, ASTM Standards.

ASTM C39 C39M. (2021). *Compressive strength of cylindrical concrete specimens*, ASTM Standards.

Bridge, R., Ernst, S., Patrick, M., and Wheeler, A. (2006). "The Behavior and Design of Haunches in Composite Beams and their Reinforcement." Included in *Composite Construction in Steel and Concrete V*, 282-292.

BSI. (1990). *Structural Use of Steelwork in Building, Part 3. Design in Composite Construction*, BS 5950.3, British Standards Institution, London.

BSI. (1994). *Eurocode 4: Design of Composite Steel and Concrete Structures, Part 1.1: General Rules and Rules for Buildings (with U.K. National Application Document)*, British Standards Institution, London.

CEN. (2004a). *Eurocode 4: Design of Composite Steel and Concrete Structures, Part 1.1: General Rules and Rules for Buildings*, European Committee for Standardization (CEN).

CEN. (2004b). *Eurocode 2: Design of Concrete Structures, Part 1.1: General Rules and Rules for Buildings*, European Committee for Standardization (CEN).

CEN. (2005a). *Eurocode 4: Design of Composite Steel and Concrete Structures, Part 2: General Rules and Rules for Bridges*, European Committee for Standardization (CEN).

CEN. (2005b). *Eurocode 4: Design of Concrete Structures, Part 2: General Rules and Rules for Bridges*, European Committee for Standardization (CEN).

Chang, G. A. and Mander, J. B. (1994). "Seismic Energy-Based Fatigue Damage Analysis of Bridge Columns: Part 1–Evaluation of Seismic Capacity." *NCEER Technical Rep. No. NCEER-94, 6*.

Chung, C.H., Shim, C.S., Hyun, B.H., and Kim, Y.J. (2010). "Shear Connections in Prestressed Beams with Precast Slabs." *Proceedings of the Institution of Civil Engineers - Structures and Buildings*, 163(5), 317–330. doi: 10.1680/stbu.2010.163.5.317.

Collins, M. P., and Mitchell, D. (1980). "Shear and Torsion Design of Prestressed and Non-Prestressed Concrete Beams." *PCI Journal*, 25(5), 32–100.

Cook, R., Malkus, D., Plesha, M., and Witt, R. (2002). "Concepts and Applications of Finite Element Analysis (fourth edition)". Wiley, New York.

Dassault Systemes (2022). Abaqus FEA (version 2022) [computer software]. https://www.3ds.com/products-services/simulia/products/abaqus/

Deng, X. (2023). "Behavior of Large Diameter Shear Studs in Steel Girder Bridges." Doctoral Dissertation, The University of Texas at Austin.

Ernst, S. (2006). "Factors Affecting the Behavior of the Shear Connection of Steel-Concrete Composite Beams." Dissertation, Western Sydney University, Australia.

Guezouli, S., and Lachal, A. (2012). "Numerical Analysis of Frictional Contact Effects in Push-Out Tests." *Engineering Structures*, 40, 39-50.

Hanson, N. W. (1960). "Precast-prestressed Concrete Bridges: 2. Horizontal Shear Connections." *Skokie, IL, USA: Portland Cement Association*, Research and Development Laboratories.

Hofbeck, J. A., Ibrahim, I. O., and Mattock, A. H. (1969). "Shear Transfer in Reinforced Concrete." *In PCI Journal Proceedings* (Vol. 66, No. 2, pp. 119-128).

Issa, M. A., Salas, J. S., Shabila, H. I., and Alrousan, R. Z. (2006). "Composite Behavior of Precast Concrete Full-depth Panels and Prestressed Girders." *PCI journal*, 51(5), 132.

Jayas, B. S., and Hosain, M. U. (1988). "Behavior of Headed Studs in Composite Beams: Push-Out Tests." *Canadian Journal of Civil Engineering*, 15(2), 240-253.

Johnson, R. (1972). "Design of Composite Beams with Deep Haunches." *Proceedings of the Institution of Civil Engineers*, 51(1), 83–90. doi: 10.1680/iicep.1972.5985.

Kaar, P. H., Kriz, L. B., and Hognestad, E. (1960). "Precast-prestressed Concrete Bridges: 1. Pilot Tests of Continuous Girders." *Portland Cement Association*, Research and Development Laboratories.

Kent, A. H., Gabriel, Z., and Bahram, S., "Toward an Improved Understanding of Shear-Friction Behavior." *ACI Journal*, 109(6): 835-844, 2012.

Kim, B., Wright, H. D., and Cairns, R. (2001). "The Behavior of Through-Deck Welded Shear Connectors: An Experimental and Numerical Study." *Journal of Constructional Steel Research*, 57(12), 1359-1380.

Kozma, A., Odenbreit, C., Braun, M. V., Veljkovic, M., & Nijgh, M. P. (2019). "Push-Out Tests on Demountable Shear Connectors of Steel-Concrete Composite Structures." *Structures*, 21, 45-54.

Lam, D. and El-Lobody, E. (2005). "Behavior of Headed Stud Shear Connectors in Composite Beams." *Journal of Structural Engineering*, 131(1), 96-107.

Liu, Y., Zhang, Q., Bao, Y., and Bu, Y. (2019). "Static and Fatigue Push-Out Tests of Short Headed Shear Studs Embedded in Engineered Cementitious Composites (ECC)." *Engineering Structures*, 182, 29-38.

Loov, R.E. (1978). "Design of Precast Connections". *Seminar Paper at Compa International Pt.*, Ltd. Singapore, 1978, 8p.

LUSAS FE. (2000). *LUSAS Manual, Version 13*, London, Britain.

Mast, R.F. (1968). "Auxiliary Reinforcement In Precast Concrete Connections". *ASCE Structural Journal*, 94(6):1485–504.

Mattock A.H., and Hawkins N.M. (1972). "Shear Transfer in Reinforced Concrete – Recent Research". *Precast Concrete Institute Journal*, 17(2):55–75.

Mattock, A.H., Johal, L., and Chow, H.C. "Shear Transfer in Reinforced Concrete with Moment or Tension Acting Across the Shear Plane," *PCI Journal*, 20(4): 76-93, 1975.

Mefleh, W. and Kovács, N. (2022). "Numerical Analysis for Push-Out Test with Y Type Perfobond Shear Connectors." *CE/Papers*, 5(4), 800-808.

Menkulaski, F. (2002). "Horizontal Shear Connectors for Precast Prestressed Bridge Deck Panels." Doctoral Dissertation, Virginia Tech.

Menkulasi, F., and Roberts-Wollmann, C. L. (2005). "Behavior of Horizontal Shear Connections for Full-depth Precast Concrete Bridge Decks on Prestressed I-girders." *PCI journal*, 50(3), 60-73.

Nguyen, H. T. and Kim, S. E. (2009). "Finite Element Modeling of Push-Out Tests for Large Stud Shear Connectors." *Journal of Constructional Steel Research*, 65(10-11), 1909–1920.

Noel, M., Wahab, N., and Soudki, K. (2016). "Experimental Investigation of Connection Details for Precast Deck Panels on Concrete Girders in Composite Deck Construction." *Engineering Structures*, 106, 15–24. doi: 10.1016/j.engstruct.2015.10.002.

Oehlers, D. J. (1980). "Stud Shear Connectors for Composite Beams." Dissertation, University of Warwick, United Kingdom.

Oehlers, D. J., and Park, S. M. (1994). "Shear Connection in Haunched Composite Beams with Sloping Sides." *Journal of Structural Engineering*, 120(7), 2227–2232. doi: 10.1061/(asce)0733-9445(1994)120:7(2227).

Ollgaard, J. G., Slutter, R. G., and Fisher, J. W. (1971). "Shear Strength of Stud Connectors in Lightweight and Normal Weight Concrete", *AISC Engineering Journal*, April 1971 (71-10).

Pallarés, L., and Hajjar, J. F. (2010). "Headed Steel Stud Anchors in Composite Structures, Part I: Shear." *Journal of Constructional Steel Research*, 66(2), 198-212.

Rambo-Roddenberry, M., Lyons, J. C., Easterling, W. S., and Murray, T. M. (2002). "Performance and Strength of Welded Shear Studs." Included within *Composite Construction in Steel and Concrete IV*. doi:10.1061/40616(281)40.

Roskos, C., Biju-Duval, P., Kintz, J., McCammon, V., Wang, Y., Donahue, S., Helwig, T., Engelhardt, M., Bayrak, O., Clayton, P., and Williamson, E. (2018). "Applications of Partial Depth Precast Concrete Deck Panels on Horizontally Curved Steel and Concrete Bridges." *Report FHWA/TX-18/0-6816-1*, Center for Transportation Research, The University of Texas at Austin, Austin, TX, 489 pp.

Santos, P. M. D., and Júlio, E. N. B. S. (2012). "A State-of-the-art Review on Shear-Friction". *Engineering Structures*, 45, 435–448.

Scholz, D. P., Wallenfelsz, J. A., Lijeron, C., and Roberts-Wollmann, C. L. (2007). "Recommendations for the Connection between Full-depth Precast Bridge Deck Panel Systems and Precast I-beams." *Virginia Center for Transportation Innovation and Research*.

Shim, C.S., Chung, C.H., Hyun, B.H., and Kim, Y.J. (2004). "Experiments on Shear Connections of PSC Girders with Prefabricated Slabs". *Journal of the Korea Concrete Institute*, 16(4), 573–579.

Silva, L. M., Christoforo, A. L., and Carvalho, R. C. (2021). "Calibration Of Concrete Damaged Plasticity Model Parameters For Shear Walls". *Matéria (Rio De Janeiro)*, 26(1). https://doi.org/10.1590/s1517-707620210001.1244

Slutter, R. G., and Driscoll Jr, G. C. (1961). "Research on composite design at Lehigh University." *Proceedings of the AISC National Engineering Conference*, 18-24.

Souza, P. T. D., Kataoka, M. N., and Debs, A. L. H. E. (2017). "Experimental and Numerical Analysis of the Push-Out Test on Shear Studs in Hollow Core Slabs." *Engineering Structures*, 147, 398–409. doi: 10.1016/j.engstruct.2017.05.068.

Stith, J. C. (2010). "Predicting the Behavior of Horizontally Curved I-Girders during Construction." Doctoral Dissertation, The University of Texas at Austin.

Taylor, R., Plum, D., and Papasozomenos, A. (1970). "Investigation of the Use Of Deep Haunches In Composite Construction." *Proceedings of the Institution of Civil Engineers*, 47(1), 43–54. doi: 10.1680/iicep.1970.6691.

Titoum, M., Mazoz, A., Benanane, A. and Ouinas, D. (2016). "Experimental Study and Finite Element Modelling of Push-Out Tests on a New Shear Connector of I-shape." *Advanced Steel Construction*, 12(4), 487-506.

Topkaya, C. (2004). "Behavior of Curved Steel Trapezoidal Box-Girders During Construction." Doctoral Dissertation, The University of Texas at Austin.

Topkaya, C., Williamson, E. B., and Frank, K. H. (2004). "Behavior of Curved Steel Trapezoidal Box-Girders During Construction." *Engineering Structures*, 26(6), 721-733.

TxDOT. (2016). "GIWW Bridge at Sargent Beach at Matagorda." *Prestressed Concrete Panels Deck Details Standard Drawing*, Texas Department of Transportation, Austin, TX.

TxDOT. (2017). *I-Girder Details Standard Drawing*, Texas Department of Transportation, Austin, TX.

TxDOT. (2019a). *Steel Girder Miscellaneous Details Standard Drawing*, Texas Department of Transportation, Austin, TX.

TxDOT. (2019b). *Prestressed Concrete Panels Deck Details Standard Drawing*, Texas Department of Transportation, Austin, TX.

TxDOT. (2019c). *Prestressed Concrete Panel Fabrication Details Standard Drawing*, Texas Department of Transportation, Austin, TX.

TxDOT. (2023a). *Bridge Design Guide*, Texas Department of Transportation, Austin, TX.

TxDOT. (2023b). *Bridge Design Manual*, Texas Department of Transportation, Austin, TX.

TxDOT. (2022). *Bridge Detailing Guide*, Texas Department of Transportation, Austin, TX.

Trejo, D., and Kim, Y. H. (2011). "Development of Precast Bridge Deck Overhang System." *Technical report (No. FHWA/TX-11/0-6100-3)*, Texas Transportation Institute.

Walraven, J., Frénay J., and Pruijssers, A. (1987). "Influence of Concrete Strength and Load History on the Shear Friction Capacity of Concrete Members." *Precast Concrete Institute Journal*, 32(1):66–84.

Waweru, R. N. (2015). "Strength of Horizontal Shear Reinforcement with Limited Development." Doctoral Dissertation, The University of Texas at Arlington.

Zilch, K., and Reinecke, R. (2000). "Capacity of Shear Joints between High-strength Precast Elements and Normal-strength Cast-in-place Decks." *In PCI/FHWA/FIB International Symposium on High Performance Concrete Precast/Prestressed Concrete Institute Federal Highway Administration Federation Internationale du Beton*.

Appendix A1

In Appendix A1, the workshop sketches of the members in the push-out test setup are provided.

A1.1.Top Crossbeam

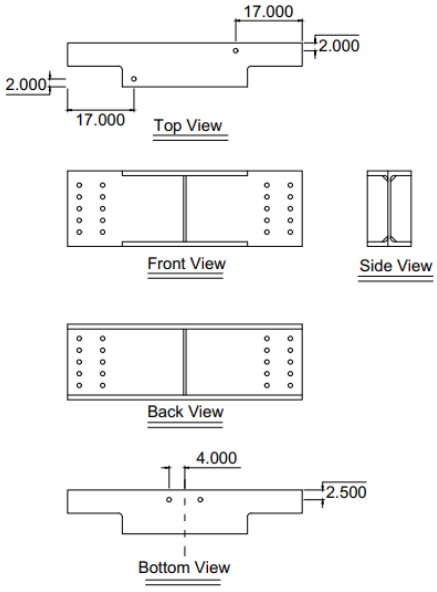

Note:
1. The coping and the bolt holes on the web are identical to the W18x130 beams at the bottom.
2. The geometry of the stiffeners is identical to the one shown in bottom W18x130 sketch.
3. All bolt holes are $1\frac{1}{8}$" except marked in extra.

Unit: inch

A1.2.Bottom Crossbeam

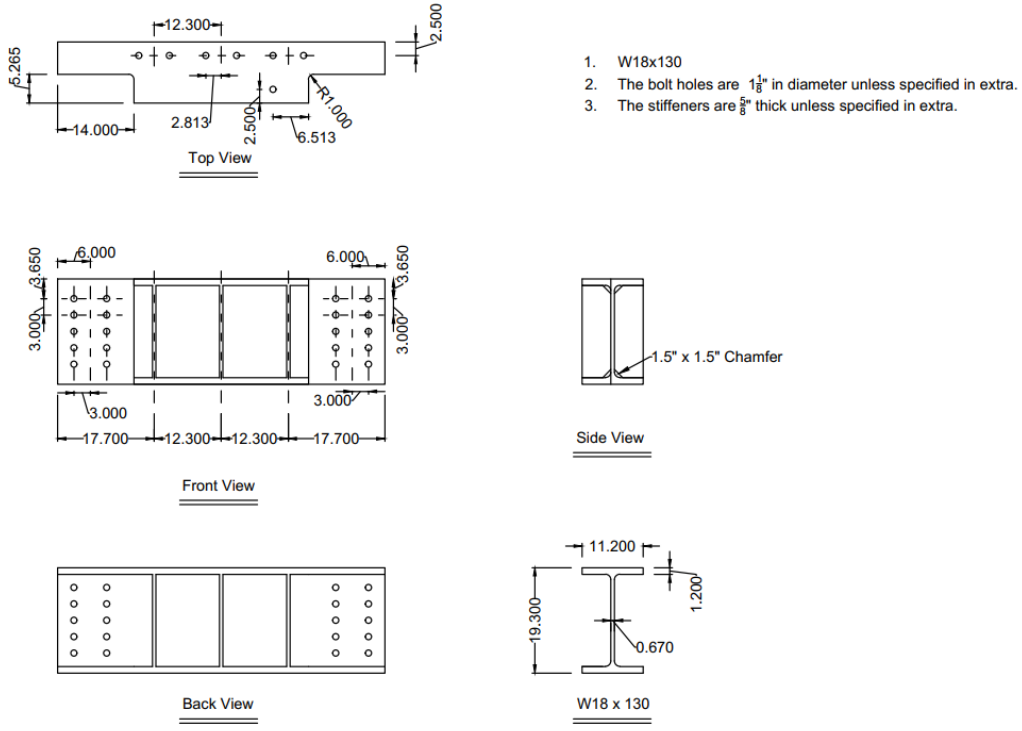

1. W18x130
2. The bolt holes are $1\frac{1}{8}$" in diameter unless specified in extra.
3. The stiffeners are $\frac{5}{8}$" thick unless specified in extra.

A1.3.Load Beam

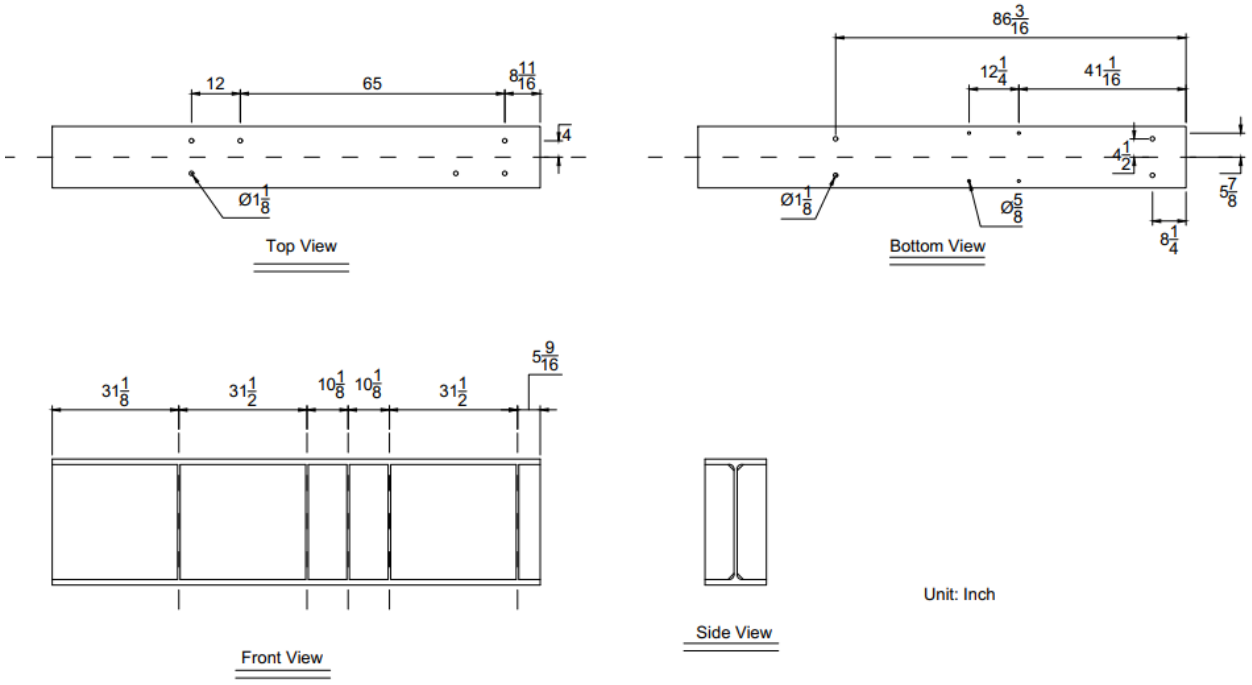

A1.4.Lateral Support

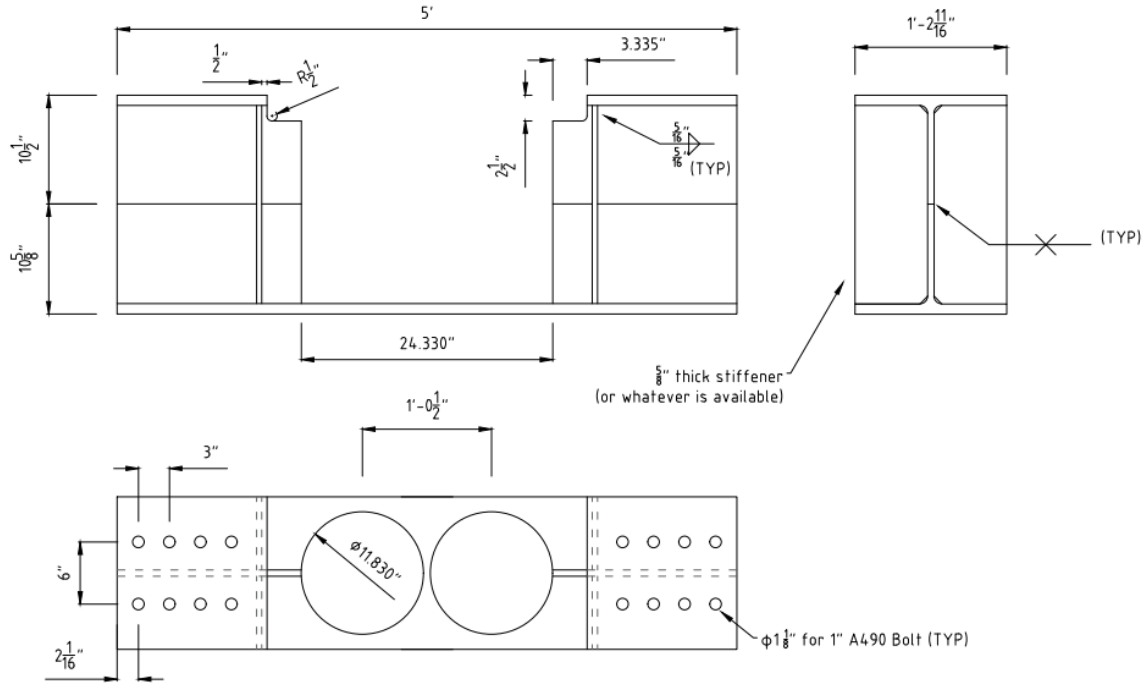

Note:
1) The diameter of the actuators is 10.83".
2) The diameter of the two pockets is 1" larger than the actuators for epoxy.
3) The height of the actuators is 21".
4) The fabricated section is made of two WT sections cut from W14x132s.

A1.5.Actuator Mounting Plate

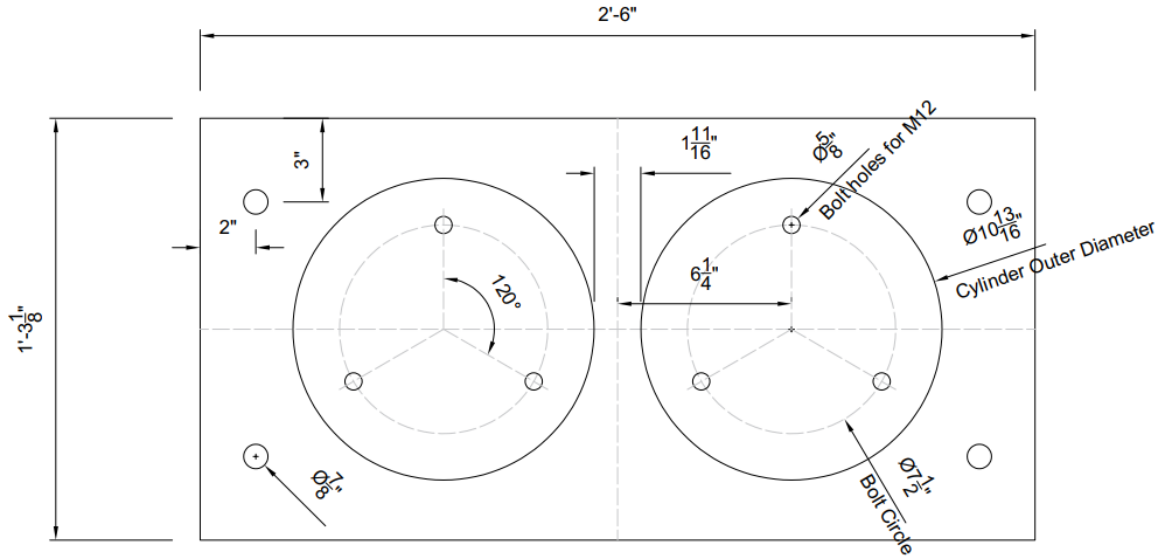

Actuator Diameter: 10.83"

Actuator Mounting Hole Depth: 1.3"
Mounting Plate Thickness: 2"

Mounting Bolts Size: M12 x 1.75mm x 80mm
Countersink Angle: 90-degree
Head Diameter: 24mm (0.94 inch)
Head Depth: 6.5mm (0.26 inch)

A1.6.Load Cell Bearing Plates

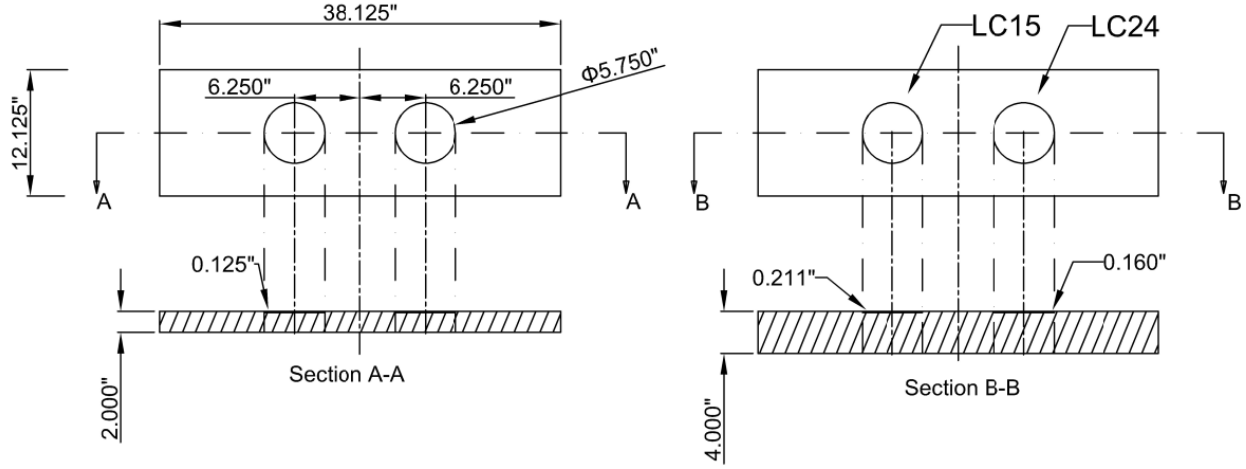

Note:

1) The pockets milled on the plates are designed to locate load cells.
2) The depth of the pockets keeps constant on the 2" plate but varies on the 4" plate due to the height difference of the load cells.
3) Please mark the pockets as indicated in the right-hand-side sketch (LC15/LC24).

A1.7.Foundation Beams

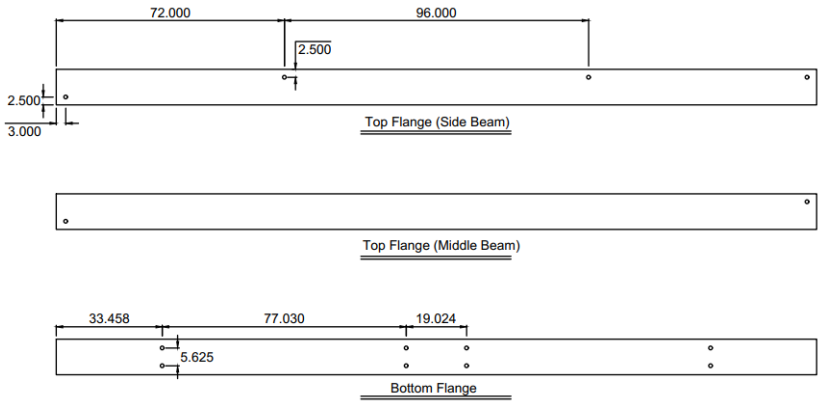

Note:
1. All bolt holes shown in this sketch is $1\frac{1}{8}$" in diameter.
2. Two side beams and one middle beam are needed.
3. Unit: inch

A1.8.Spreader Beam

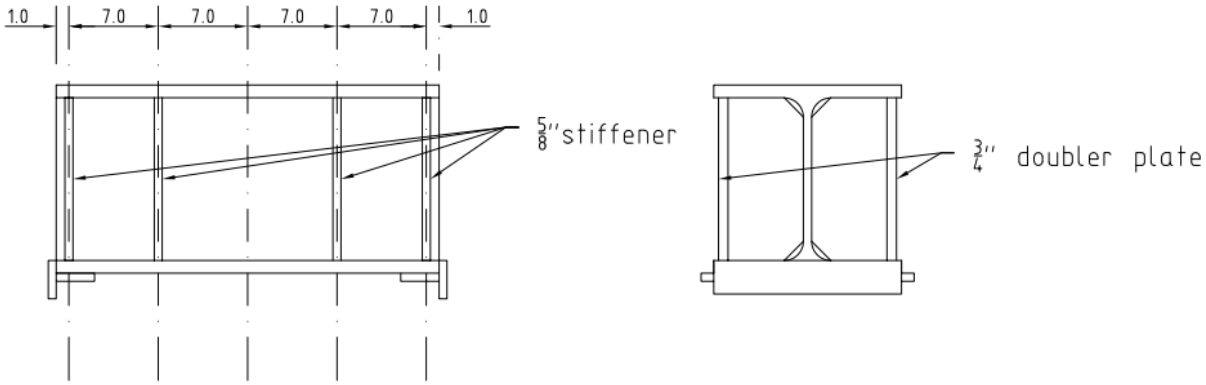

Appendix A2

The details of the steel girder specimens are provided in Appendix A2. Because the specimen designs are similar to each other, the details consistent in all the specimens are not repetitively annotated, such as the deck dimensions, the stud size, the deck rebar mats, and the concrete clear covers. By default, all of the rebars are #4 Grade 60, and the headed shear studs are 7/8 in. in diameter and 6 in. in height.

A2.1. 9 in. Haunch with Stacked Shear Studs

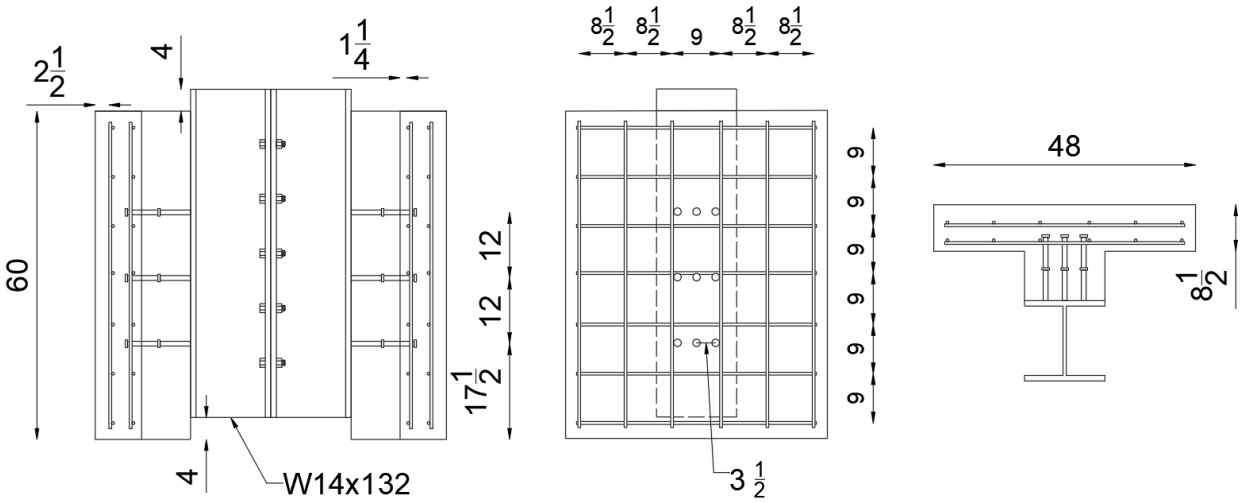

Unit: inch

A2.2. 9 in. Haunch with U-bars

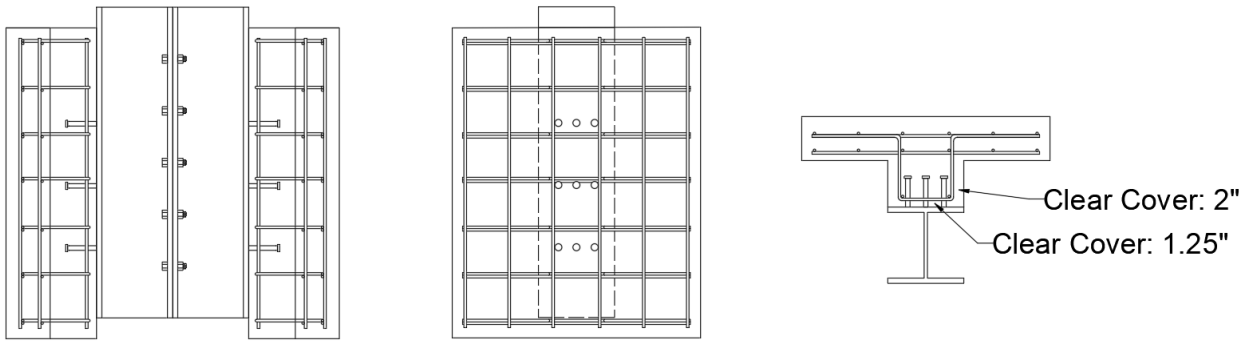

A2.3. 9 in. Haunch with Stirrups

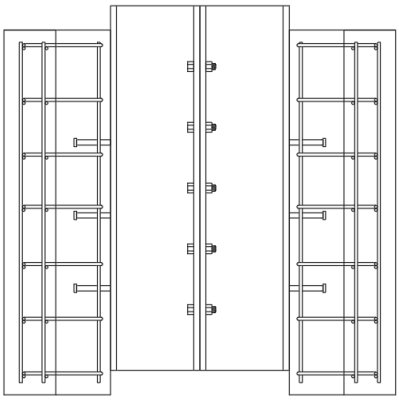

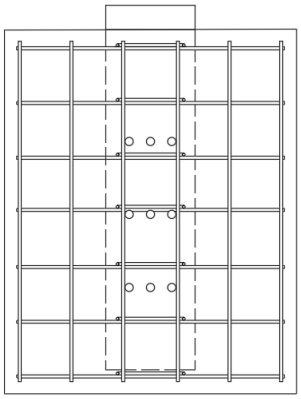

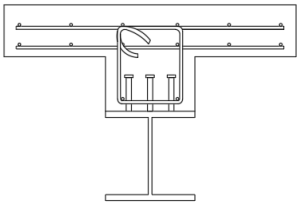

A2.4. 3 in. Haunch

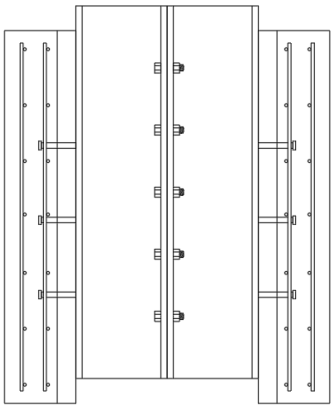

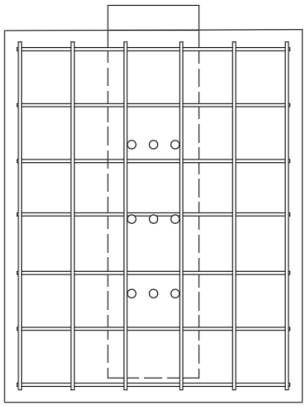

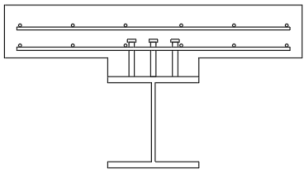

A2.5. Zero-Haunch

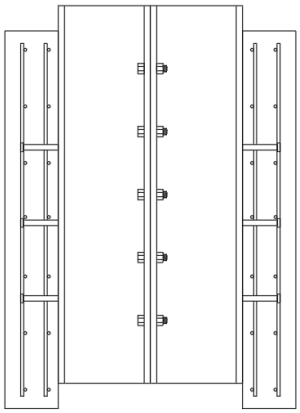

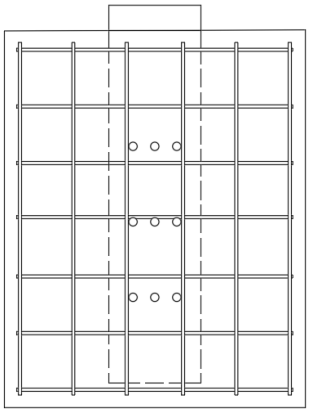

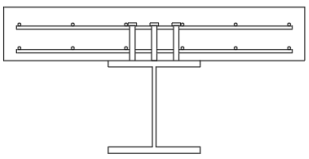

A2.6. 15 in. Haunch with Stacked Shear Studs

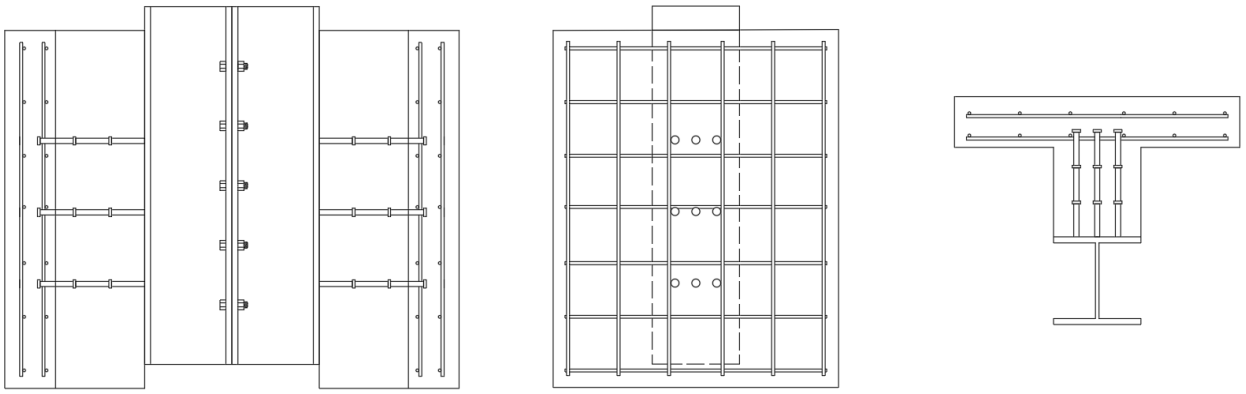

A2.7. 15 in. Haunch with U-bars

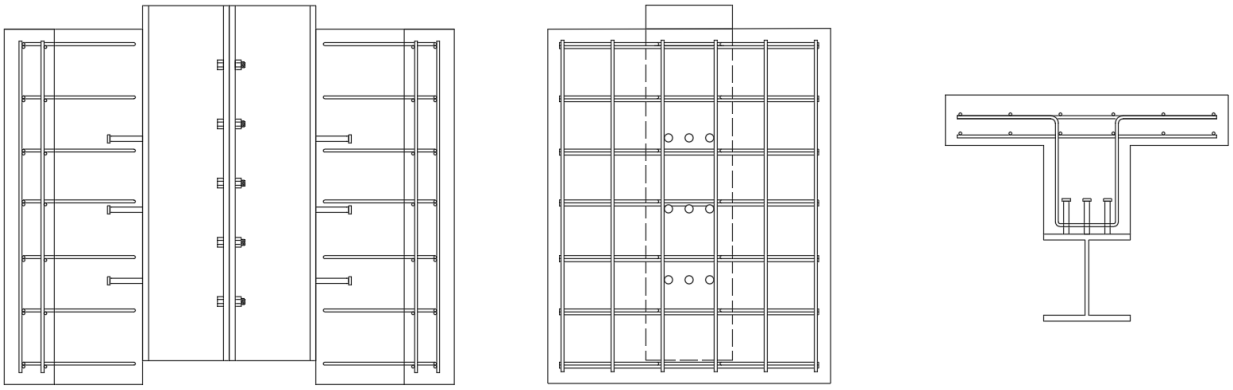

A2.8. 9 in. Haunch

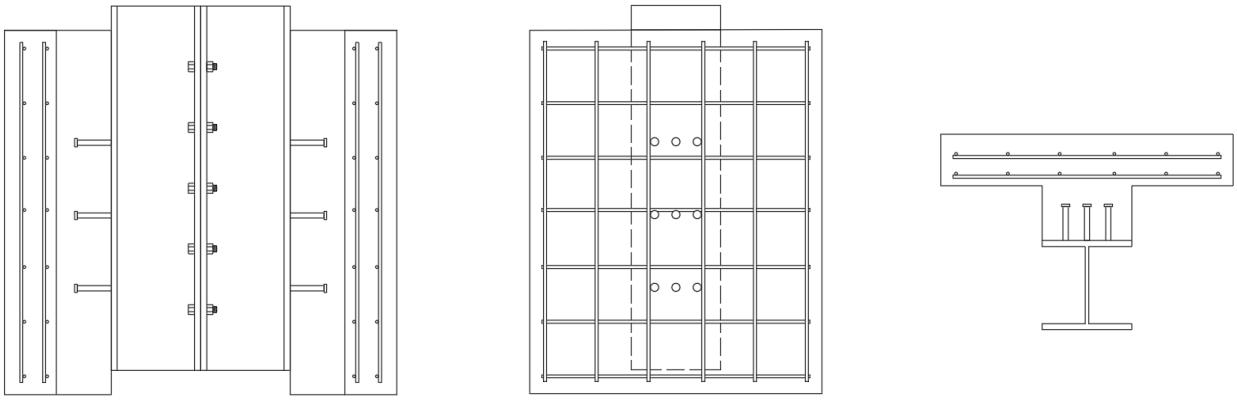

A2.9. 6 in. Haunch with 8 in. Shear Studs

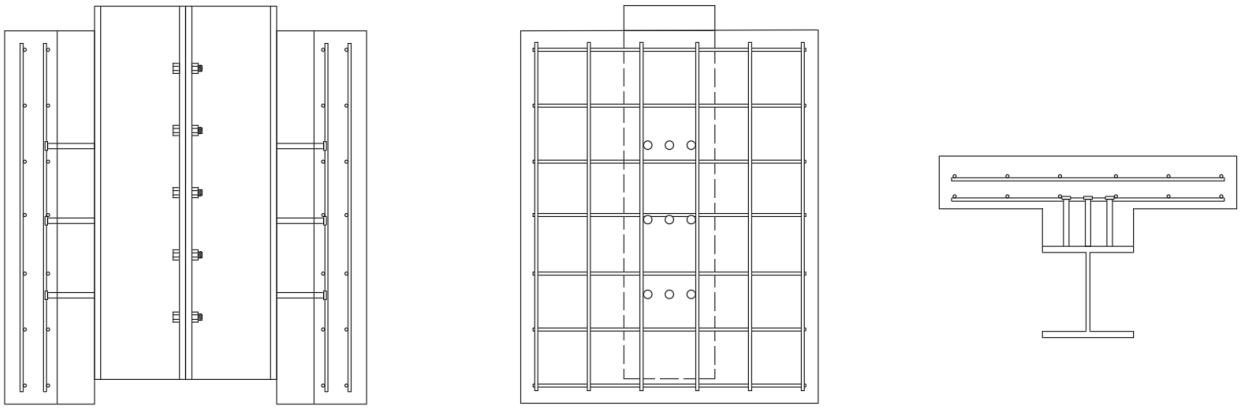

A2.10. 9 in. Haunch with Stacked Shear Studs at 6 in. Pitch

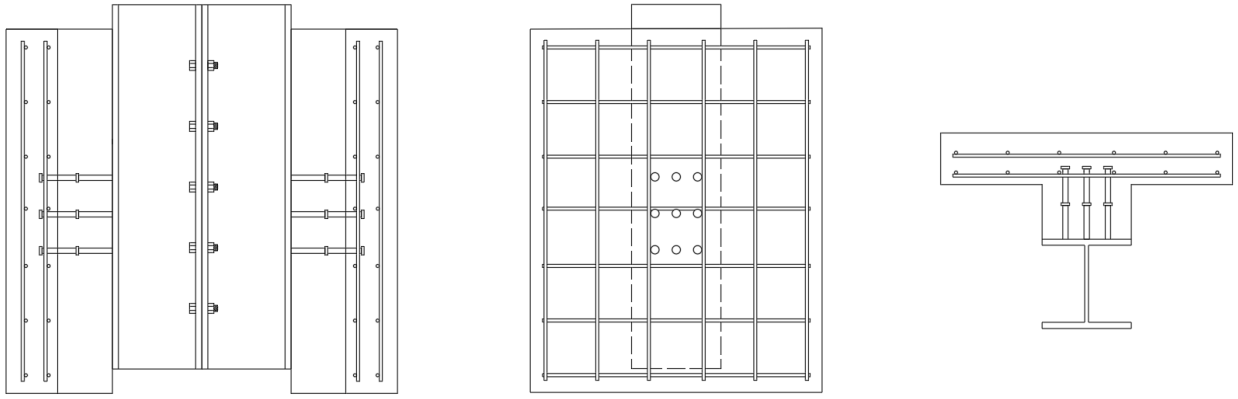

A2.11. 12 in. Haunch with U-bars

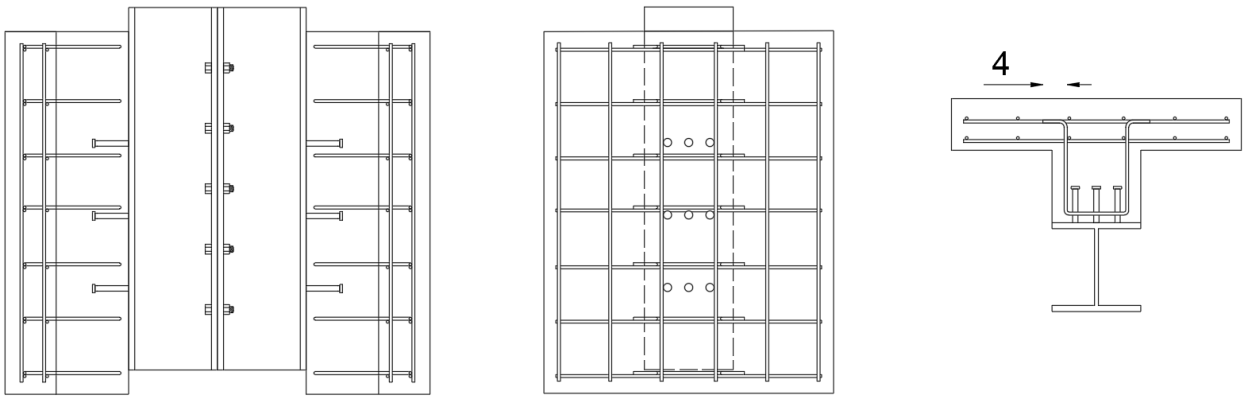

A2.12. 12 in. Haunch with U-bars at Double Spacing

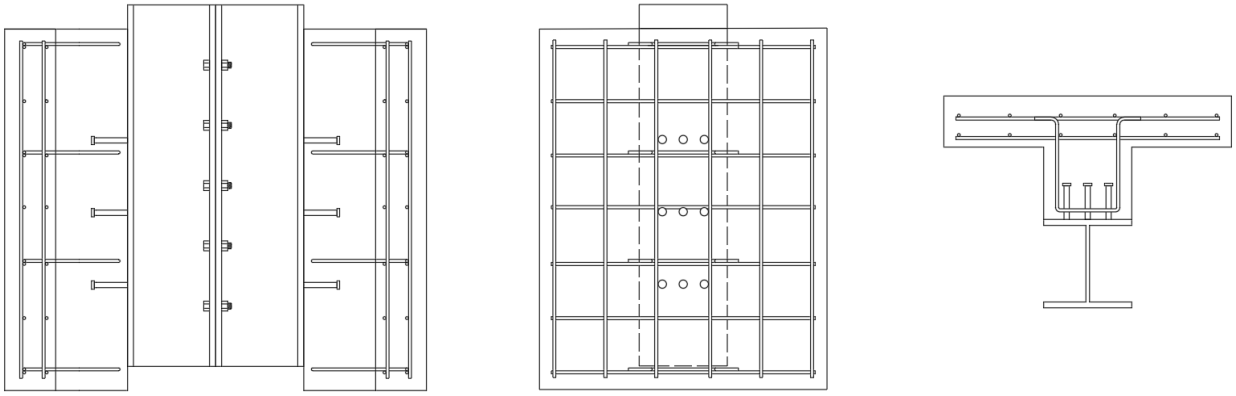

A2.13. 12 in. Haunch with U-bars at Double Spacing (Alternative Positions)

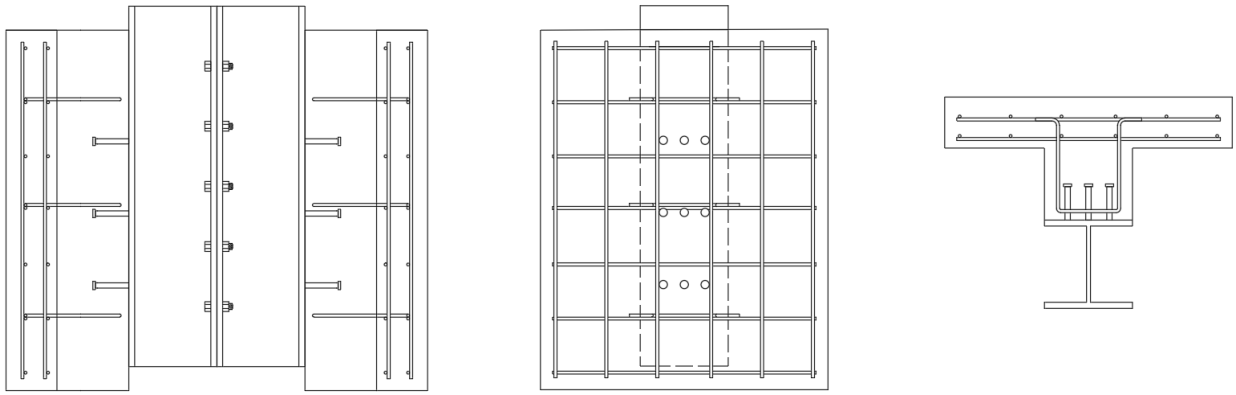

A2.14. 12 in. Haunch with Stirrups

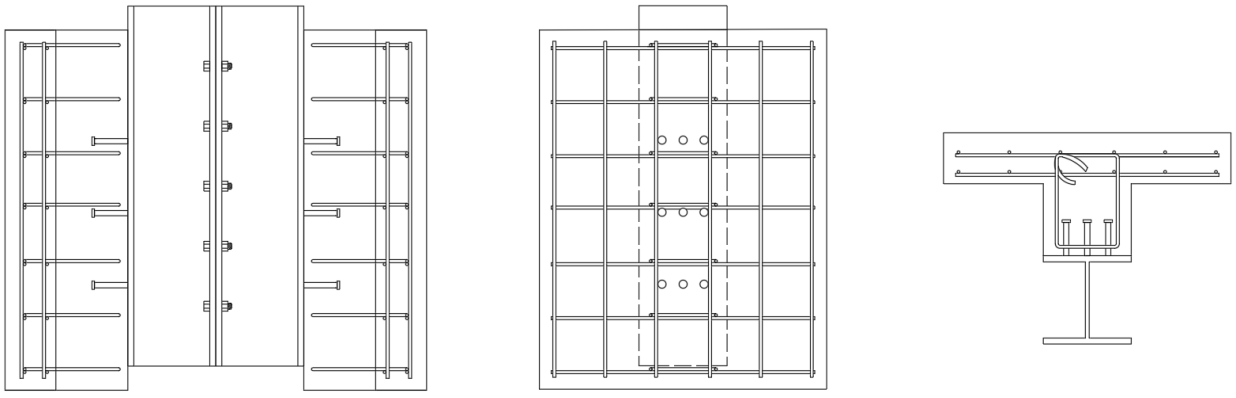

A2.15. 15 in. Haunch with Stirrups and Unconfined Longitudinal Rebars

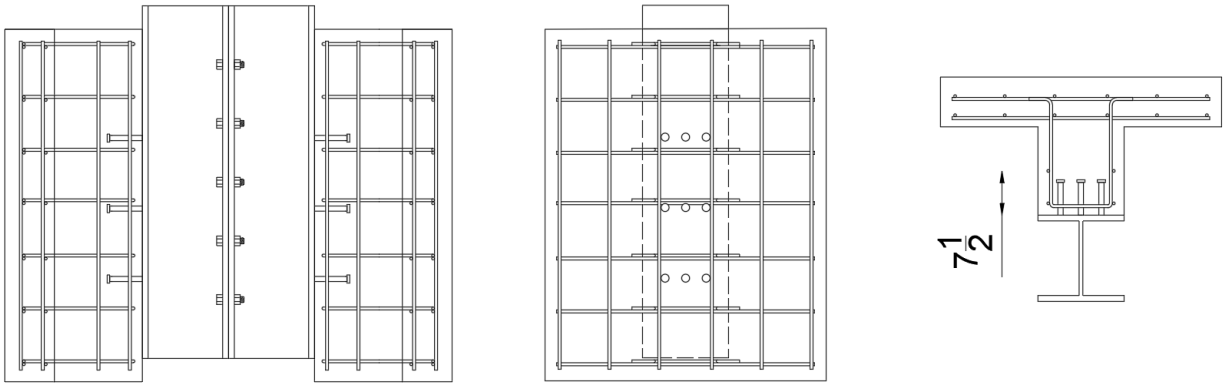

A2.16. 15 in. Haunch with Stirrups and Confined Longitudinal Rebars

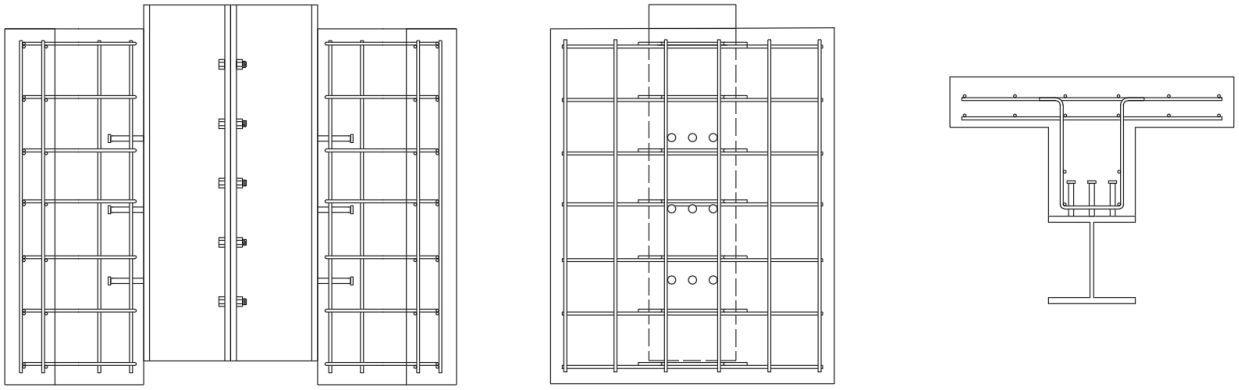

A2.17. 15 in. Haunch with Stirrups and Single Stud per Row

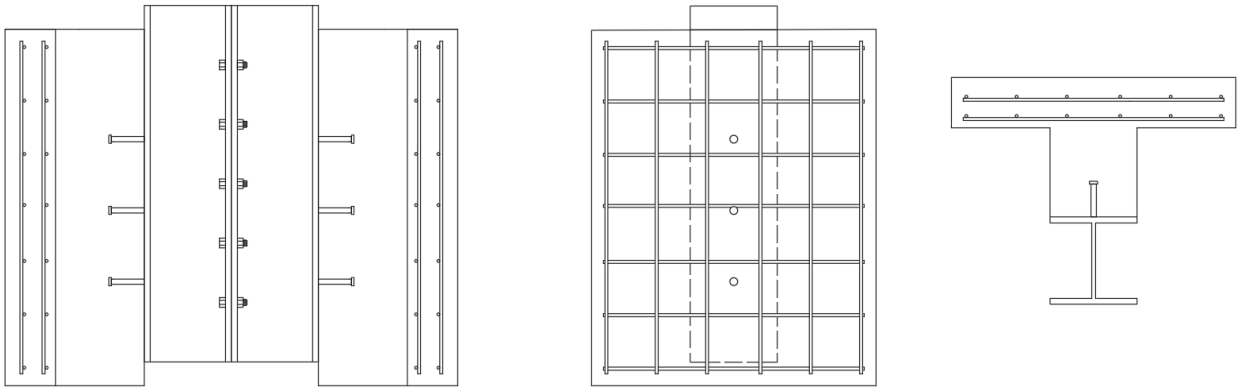

Appendix A3

Section A3.1 presents the specimen drawings. Section A3.2 provides sample calculations for predicted strength using AASHTO LRFD (2020) and some other guidelines (CEN 2004b, ACI 318 2019). Sections A3.3 and A3.4 provide load versus slip and strain versus load plots.

A3.1.Specimen Drawings

Sections A3.1.1 and A3.1.2 show drawings for Specimen Group I and II respectively. The detailed drawings of PCP and the simulated PSC girder are illustrated in Chapter 4. All of the reinforcing bars in the following drawings are #4 by default. The units in these drawings are in inches (in.) unless noted otherwise.

A3.1.1. Specimen Group I

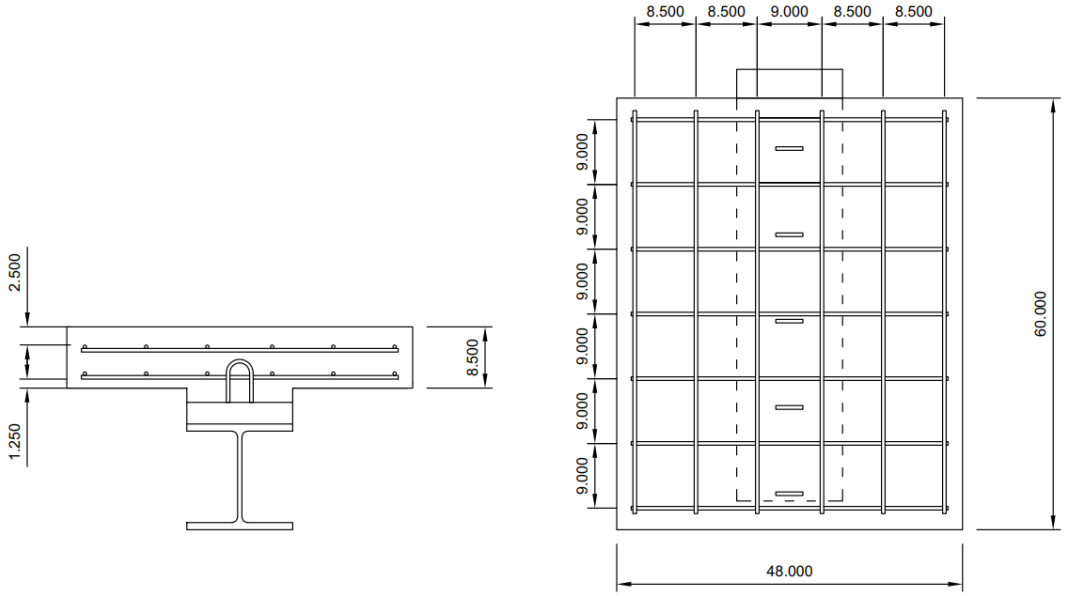

Figure A3.0.1 2-in. CIP Specimen with Bars R

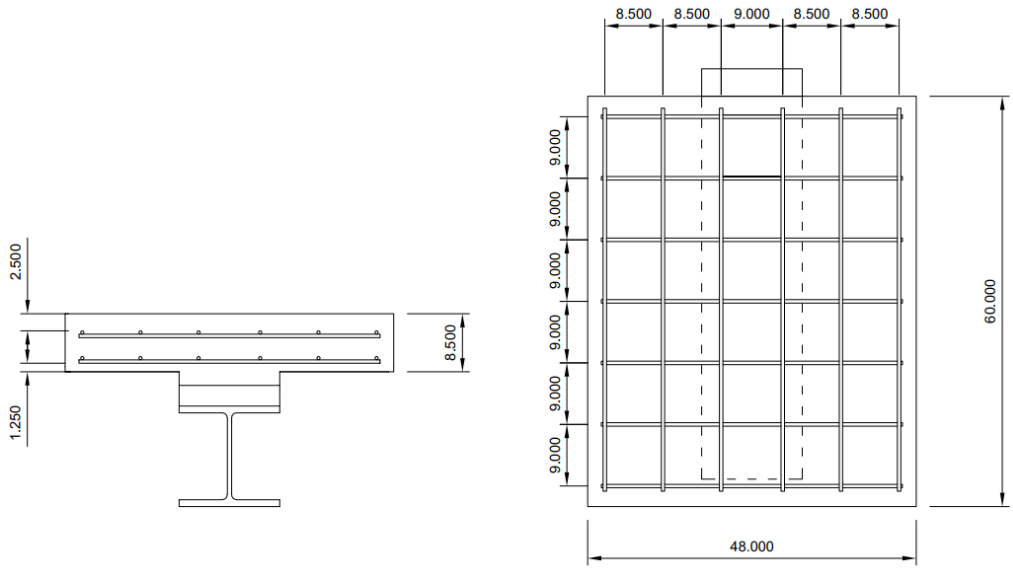

Figure A3.0.2 2-in. CIP Specimen with no Bars R

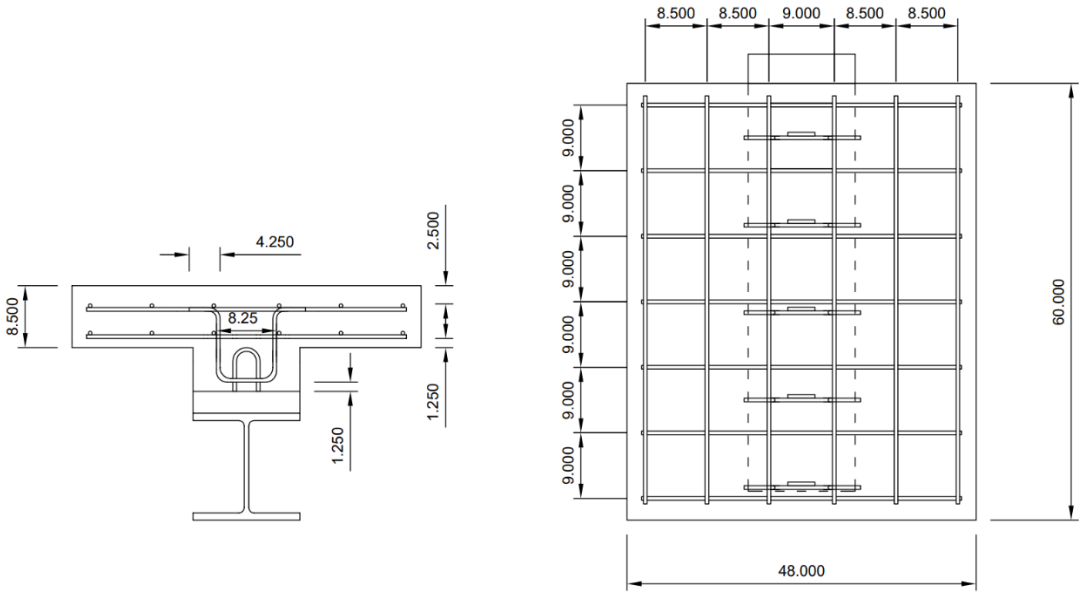

Figure A3.0.3 6-in. CIP Specimen with Bars U

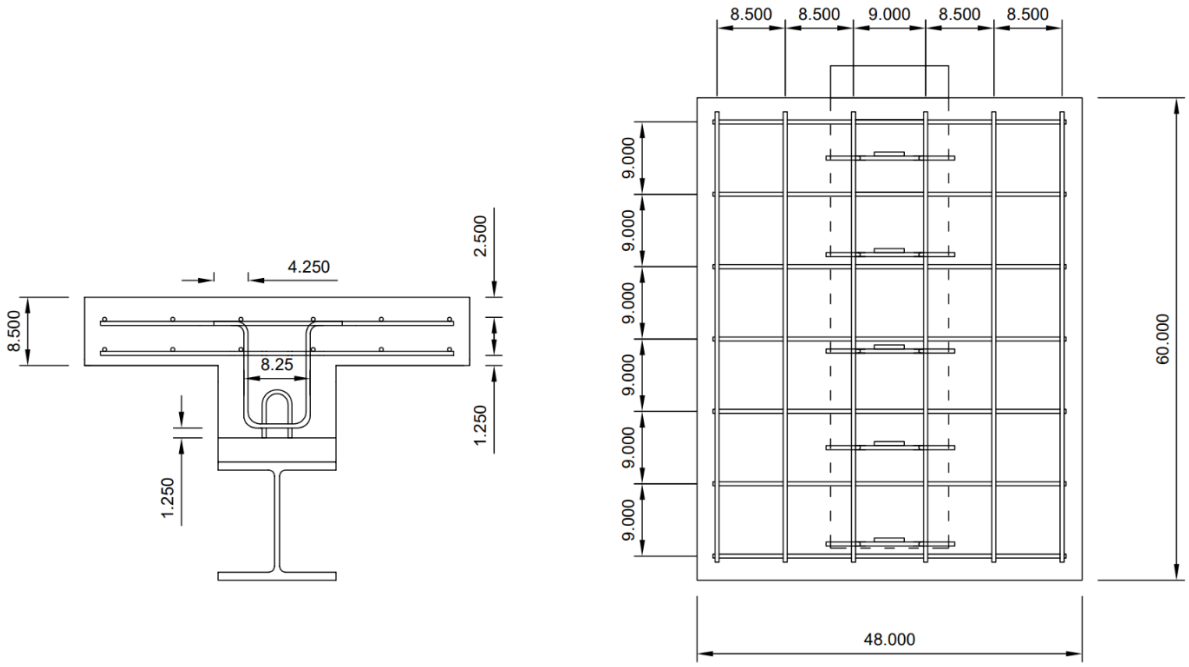

Figure A3.0.4 9-in. CIP Specimen with Bars U

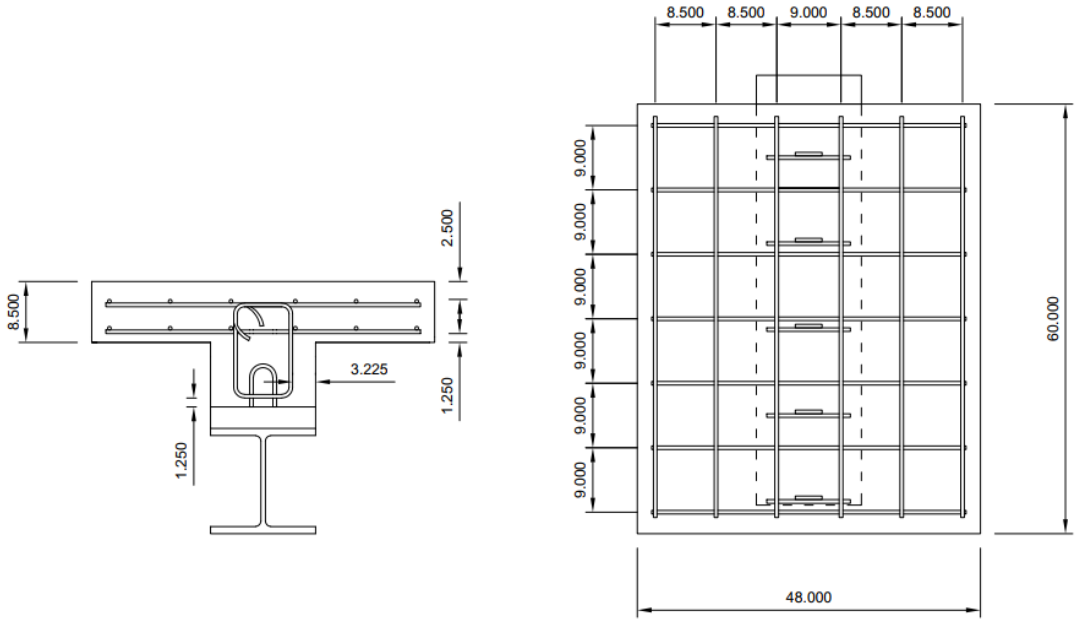

Figure A3.0.5 9-in. CIP Specimen with Vertical Stirrups

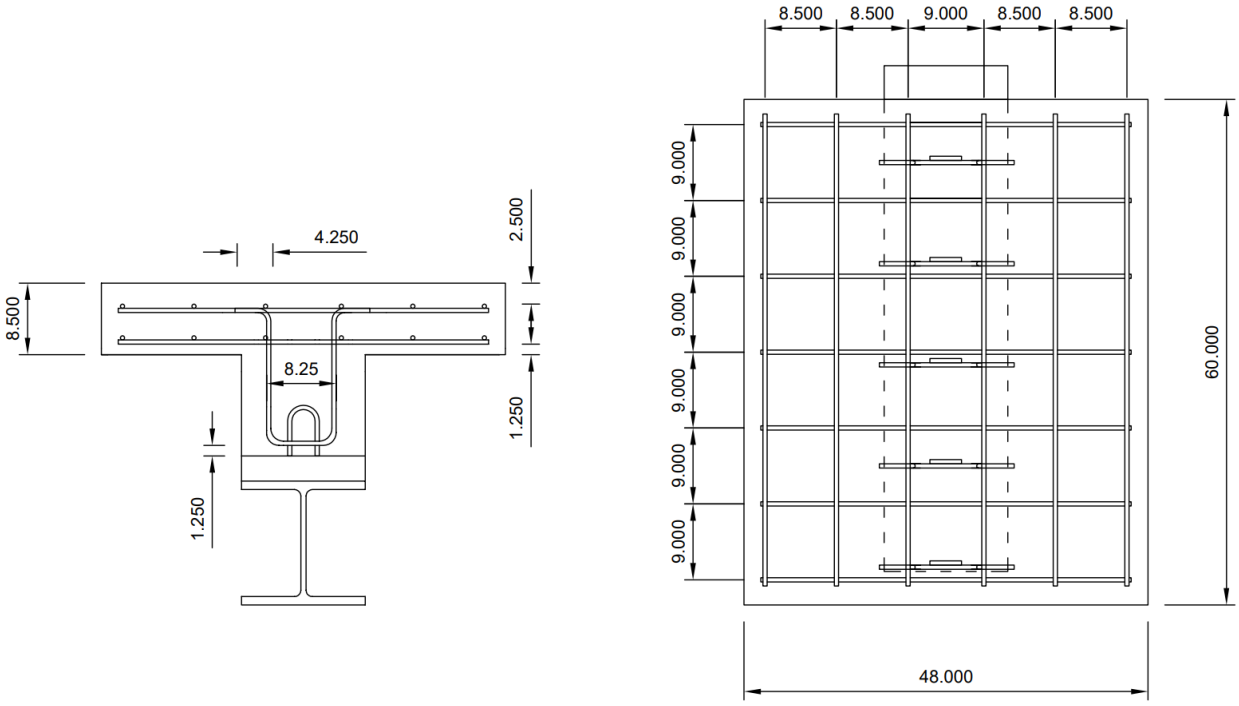

Figure A3.0.6 12-in. CIP Specimen with Bars U

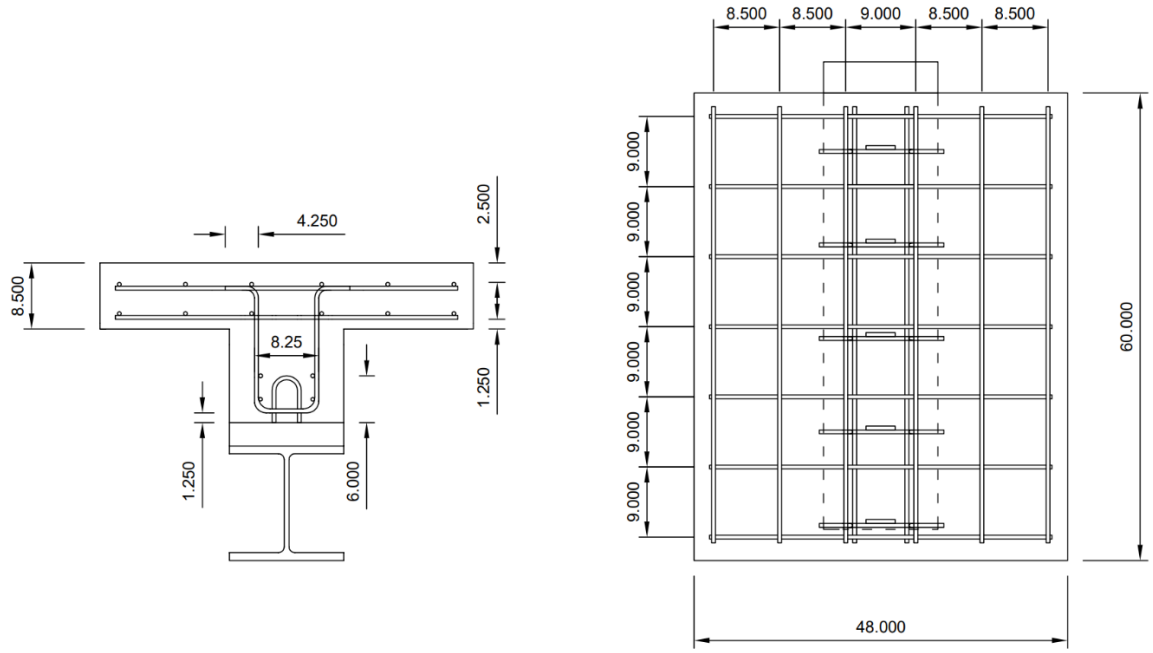

Figure A3.0.7 12-in. CIP Specimen with Bars U and Longitudinal Rebars

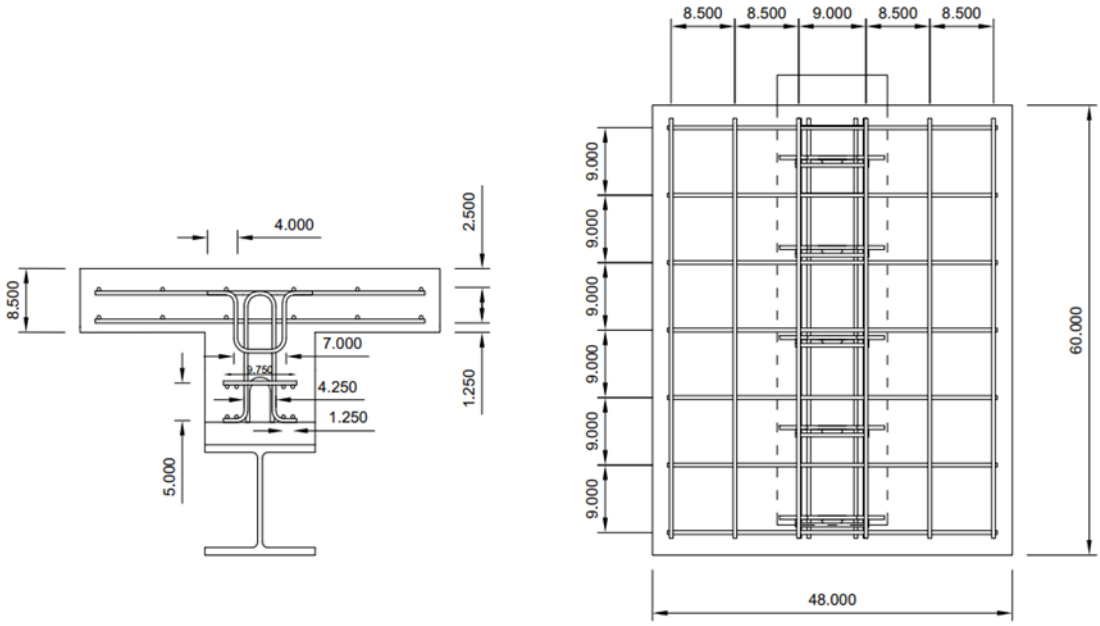

Figure A3.0.8 12-in. CIP Specimen with SGD Rebar Cage

A3.1.2. Specimen Group II

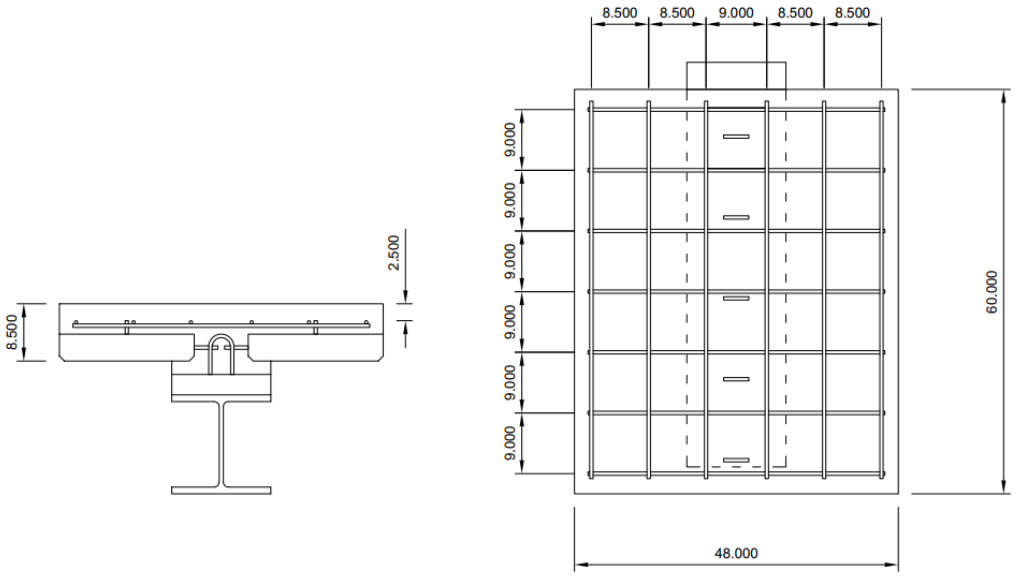

Figure A3.0.1 2-in. PCP Specimen

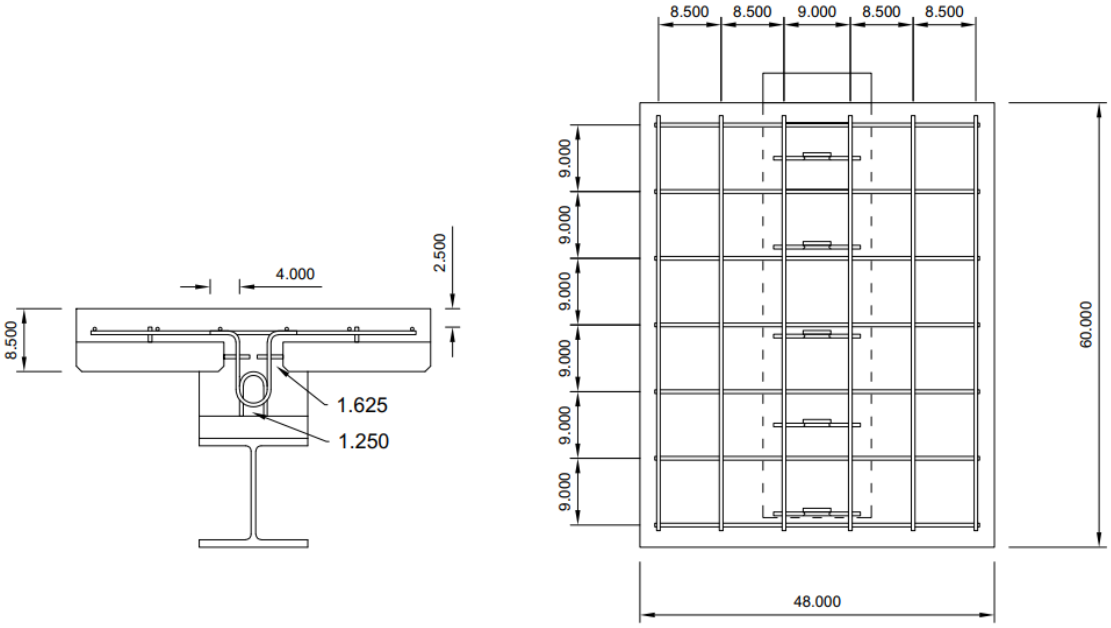

Figure A3.0.2 6-in. PCP Specimen with Bars UP

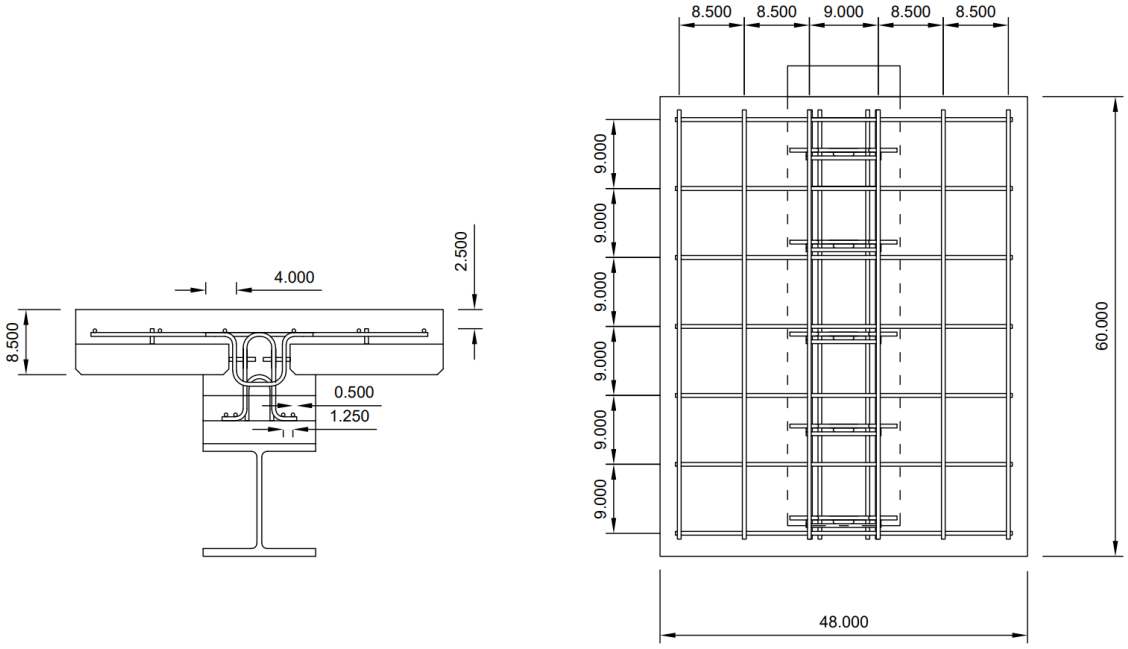

Figure A3.0.3 6-in. PCP Specimen with SGD

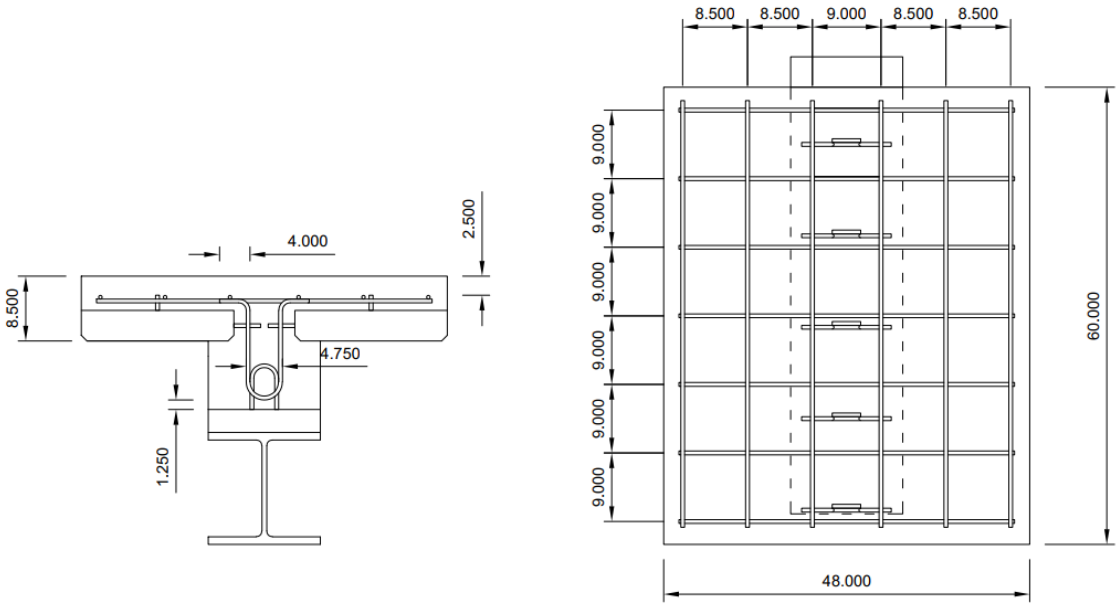

Figure A3.0.4 9-in. PCP Specimen with Bars UP

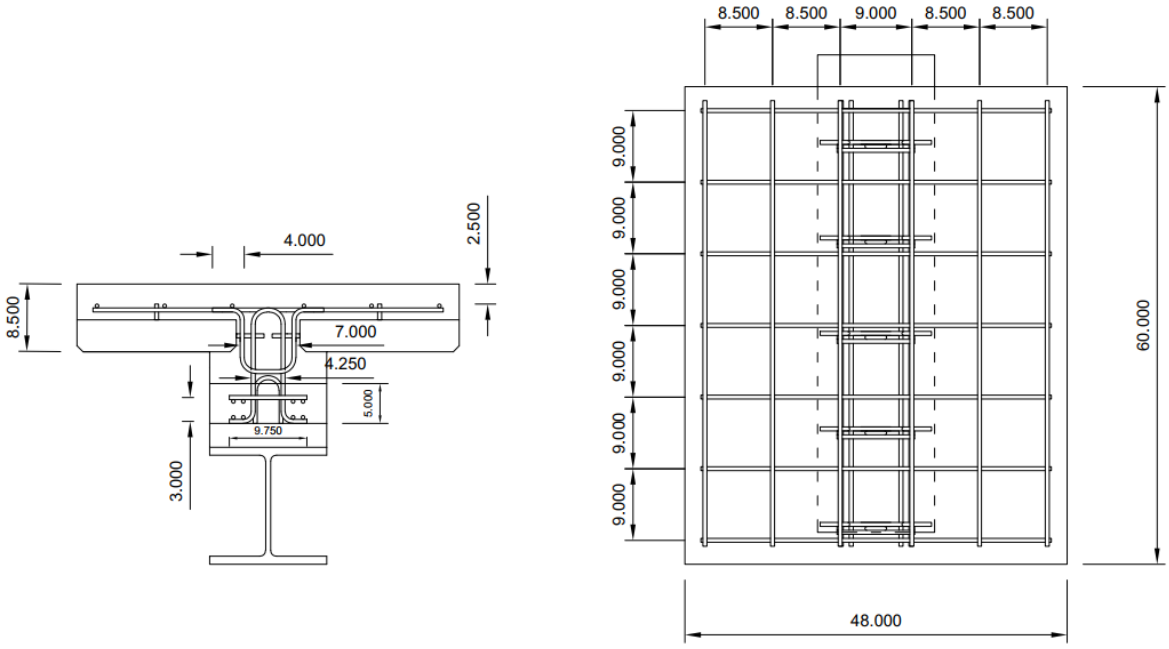

Figure A3.0.5 9-in. PCP Specimen with SGD

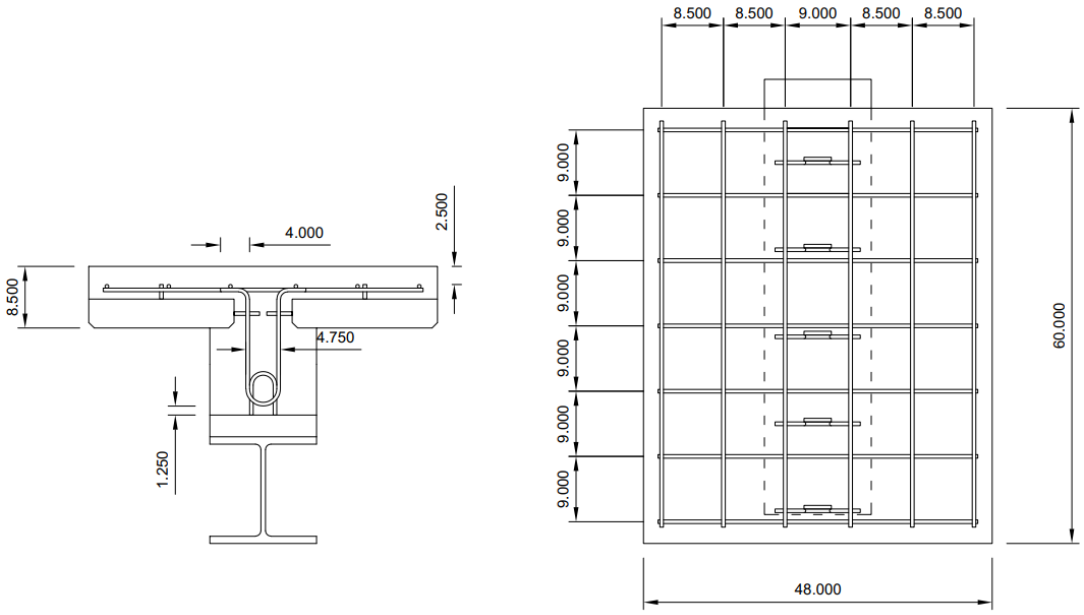

Figure A3.0.6 12-in. PCP Specimen with Bars UP

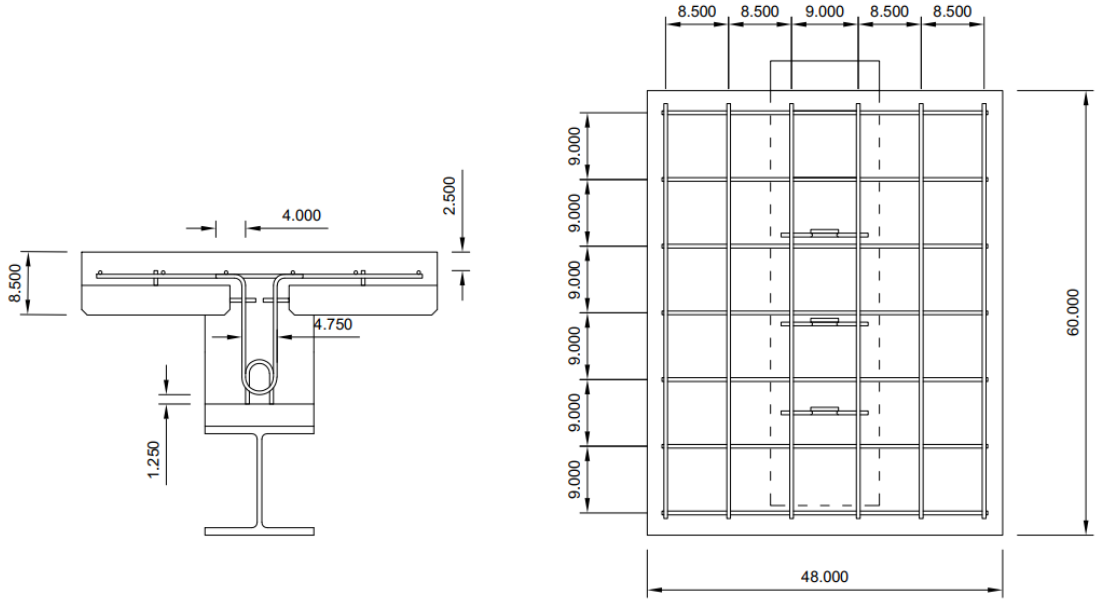

Figure A3.0.7 12-in. PCP Specimen with Reduced Bars R and Bars UP

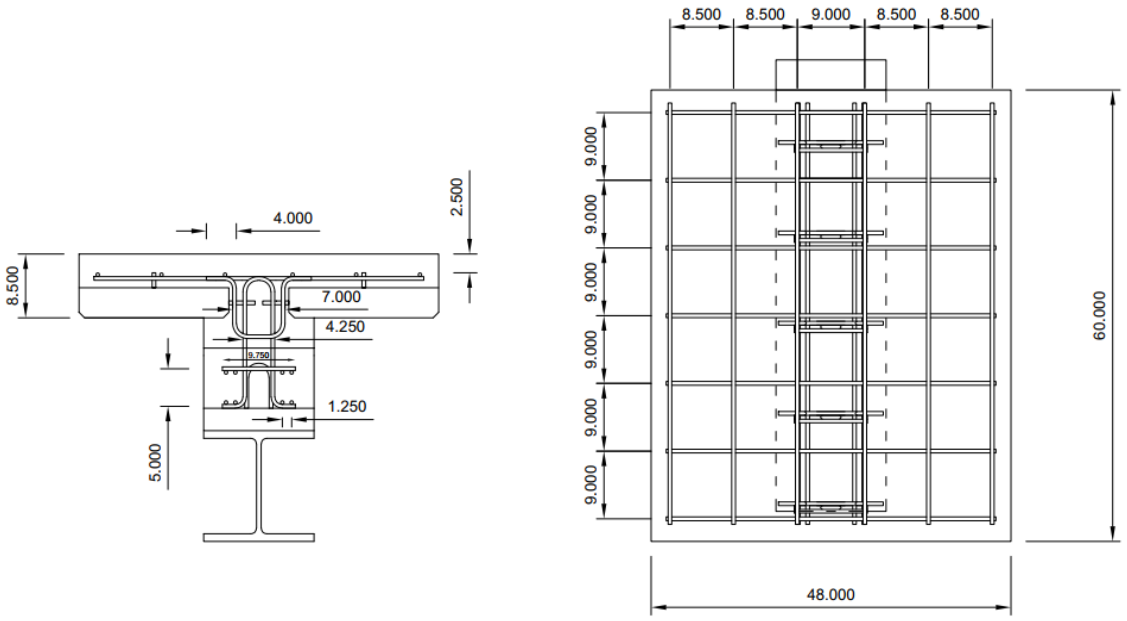

Figure A3.0.8 12-in. PCP Specimen with SGD

A3.2.Strength Prediction from Codes

This section presents sample calculations for the interface shear resistance calculated using AASHTO LRFD (2020), CEN (2004b), and ACI 318 (2019).

A3.2.1. AASHTO LRFD (2020) Design Equation

As per AASHTO LRFD (2020) Article 5.7.4.3, the factored interface shear resistance (in kips) shall be taken as:

$$V_{ri} = \phi V_{ni} \qquad \text{Equation A3.0.1}$$

where ϕ = resistance factor for shear specified in AASHTO LRFD (2020) Article 5.5.4.2 (considered 0.90 for shear in prestressed concrete sections with CIP closures having bonded strands)

V_{ni} = nominal interface shear resistance (kips)

$$V_{ni} = cA_{cv} + \mu\,(A_{vf} f_y + P_c) \qquad \text{Equation A3.0.2}$$

where $A_{cv} = b_{vi} L_{vi}$

c = cohesion factor, considered 0.28 (as per TxDOT (2023b))

b_{vi} = interface width engaged in shear transfer, (14.7 in. (width of W14×132 section))

L_{vi} = interface length engaged in shear transfer, (60 in. (Figures in Section A3.1))

μ = friction factor, considered 1.0 (as per TxDOT (2023b))

A_{vf} = area of interface shear reinforcement, here considered twice the area of 5-#4 rebars

f_y = yield strength of reinforcement (66.5 ksi from material testing)

P_C = permanent compressive force normal to the shear plane (7 kips – see following)

The following assumptions are made:

spacing between girders = 10 ft.

girder length = 60 in. (in this study)

slab thickness = 8.5 in. (in this study and TxDOT (2023b)

haunch depth = 12 in. (maximum for this study)

haunch width = 14.7 in. (in this study)

total applied permanent load = 6.3 kips (concrete weight = 150 lb/ft^3)

additional 10% increase (for permanent coatings and other dead loads on a bridge)

Also,

$$V_{ni} \leq K_1 f'_c A_{cv} \quad \text{Equation A3.0.3}$$

$$V_{ni} \leq K_2 A_{cv} \quad \text{Equation A3.0.4}$$

where K_1 = fraction of concrete strength available to resist interface shear, considered 0.3 (as per TxDOT (2023b))

K_2 = limiting interface shear resistance, considered 1.8 (as per TxDOT (2023b))

f'_c = design concrete compressive strength of the weaker concrete on either side of the interface in ksi, considered 4 ksi minimum for the CIP concrete in the haunch

Therefore, based on Equations A3.2.1.2, A3.2.1.3, and A3.2.1.4,

$$V_{ni} = 385\ kips\ \leq \min(1058,1588)$$

In each test, two specimens are loaded simultaneously. Thus, twice the interface nominal shear resistance gives

$$V_{ni} = 774\ kips \quad \text{Equation A3.0.5}$$

From Equations A3.2.1.1 and A3.2.1.5,

$$V_{ri} = 697\ kips \quad \text{Equation A3.0.6}$$

Therefore, the maximum capacity considered for each test as per AASHTO LRFD (2020) is 697 kips.

A3.2.2. CEN (2004b) Design Equation

As per CEN (2004b) Article 6.2.5, the design shear resistance (in MPa) at the interface shall be taken as:

$$v_{Rdi} = c f_{ctd} + \mu\sigma_n + \rho f_{yd}(\mu \sin\alpha + \cos\alpha) \leq 0.5\, \nu\, f_{cd} \quad \text{Equation A3.0.1}$$

where c = factor depending on interface, considered 0.4 (for rough interface)

f_{ctd} = design tensile strength,

$$f_{ctd} = \frac{\alpha_{ct} f_{ctk}}{\gamma_c} \quad \text{Equation A3.0.2}$$

α_{ct} = coefficient taking account of long-term effects on the tensile strength and of unfavorable effects, resulting from the way load is applied (recommended value = 1.0)

γ_c = partial factor for concrete (recommended value = 1.5)

f_{ctk} = characteristic axial tensile strength of concrete,

$$f_{ctk} = 0.21 f_{ck}^{2/3} \quad \text{Equation A3.0.3}$$

f_{ck} = characteristic compressive cylinder strength of concrete in MPa (=27.6 MPa for 4 ksi)

μ = factor depending on interface, considered 0.7 (for rough interface)

σ_n = stress per unit area caused by normal force (0.055 MPa, calculations as shown in Section 4.4.1)

$\rho = A_s/A_i$

A_s = area of interface shear reinforcement, here twice the area of 5-#4 rebars

A_i = area of joint, here 60 in. x 14.7 in.

f_{yd} = design yield strength of reinforcement,

$$f_{yd} = \frac{f_{yk}}{\gamma_s} \qquad \text{Equation A3.0.4}$$

f_{yk} = characteristic yield strength of reinforcement in MPa (459 MPa for 66.5 ksi)

γ_s = partial factor for steel (recommended value = 1.15)

α = angle of shear reinforcement (90 degrees)

ν = strength reduction factor,

$$\nu = 0.6\,[1 - \frac{f_{ck}}{250}] \qquad \text{Equation A3.0.5}$$

f_{cd} = design compressive strength,

$$f_{cd} = \frac{\alpha_{cc} f_{ck}}{\gamma_c} \qquad \text{Equation A3.0.6}$$

α_{cc} = coefficient taking account of long-term effects on the compressive strength and of unfavorable effects, resulting from the way load is applied (recommended value = 1.0)

Based on Equations A3.2.2.1-A3.2.2.6, the design shear resistance at the interface

$$v_{Rdi} = 0.17\ ksi < 0.71\ ksi$$

The longitudinal shear force that each test can resist is,

$$V_{Rdi} = 2 v_{Rdi}\, A_i = 302.5\ kips$$

Therefore, the maximum capacity considered for each test as per CEN (2004b) is 302.5 kips.

A3.2.3. ACI 318 (2019) Design Equation

As per ACI 318 (2019) Article 16.4.4 and 16.4.5, if applied longitudinal shear force (in lbs),

$$V_{uh} \leq \phi 500 A_c \qquad \text{Equation A3.0.1}$$

where ϕ = shear strength reduction factor, 0.75

A_c = area of joint, here 60 in. x 14.7 in.

the nominal horizontal shear strength (in lbs) for roughened concrete surface shall be taken as:

$$V_{nh1} = \min\left(260 + \frac{0.6A_v f_y}{\mathrm{b}_v s}, 500\right) A_c \qquad \text{Equation A3.0.2}$$

where A_v = area of shear reinforcement withing spacing s,

f_y = yield strength for transverse reinforcement in psi (66500 psi)

b_v = interface width engaged in shear transfer, (14.7 in.)

s = spacing of transverse reinforcement (here 12 in. for most specimens),

If applied longitudinal shear force (in lbs),

$$V_{uh} > \phi 500 \mathrm{A}_c \qquad \text{Equation A3.0.3}$$

the nominal horizontal shear strength (in lbs) for roughened concrete surface shall be taken as:

$$V_{nh2} = \min\left(\mu A_v f_y, 0.2f'_c A_c, 1600 A_c, (480 + 0.08f'_c) A_c\right) \qquad \text{Equation A3.0.4}$$

μ = coefficients of friction, 1 (for rough interface)

f'_c = specified compressive strength of concrete, 4000 psi

Based on Equations A3.2.3.1-A3.2.3.4, the nominal shear strength for each test shall be

$$V_{nh1} = 459\ kips$$

$$V_{nh2} = 266\ kips$$

Therefore, the maximum capacity considered for each test as per ACI 318 (2019) is 459 kips.

A3.3.Specimens Load-Slip Plots

This section presents the load versus slip plots for Specimen Groups I and II. The locations for LPs are given in Figures 4.4.10 for Specimen Group I and Figures 4.4.43 and 4.4.44 for Specimen Group II.

A3.3.1. Specimen Group I

A.3.3.1.1. PSC Girder-Haunch Interface

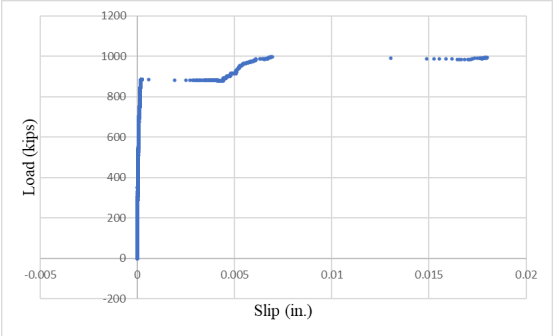

Figure A3.0.1 2-in. Specimen (SB_P)

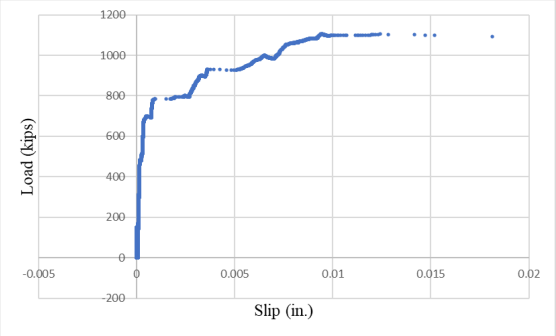

Figure A3.0.2 2-in. Specimen (SB_S)

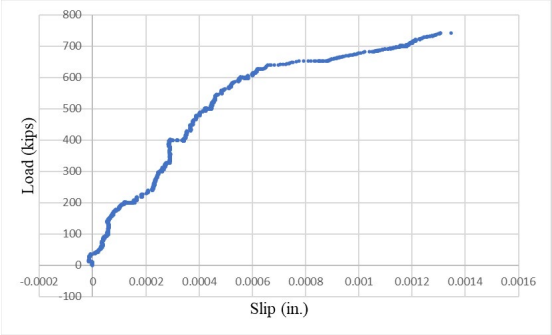

Figure A3.0.3 2-in. Specimen w/o Bars R

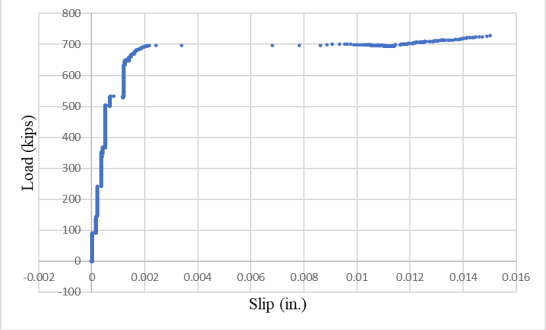

Figure A3.0.4 6-in. Specimen w/ Bars U (SB_P)

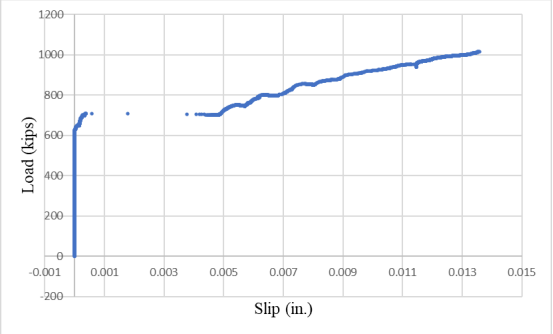

Figure A3.0.5 9-in. Specimen w/ Bars U (SB_S)

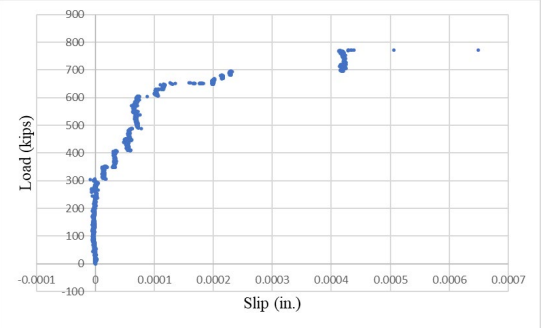

Figure A3.0.6 9-in. Specimen w/ Stirrups (SB_P)

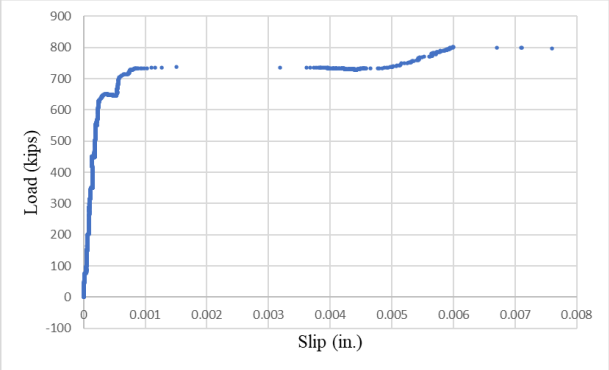

Figure A3.0.7 12-in. Specimen w/ Bars U (SB_P)

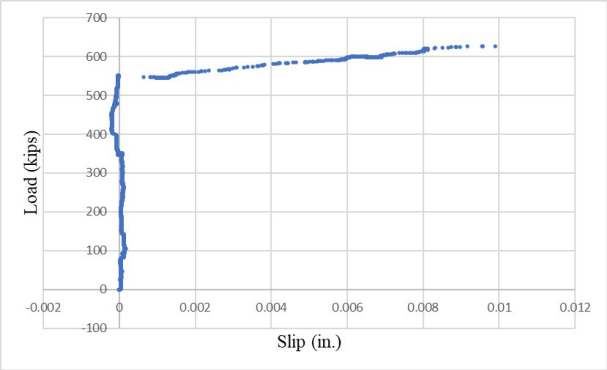

Figure A3.0.8 12-in. Specimen w/ Bars U and Long. Bars (SB_P)

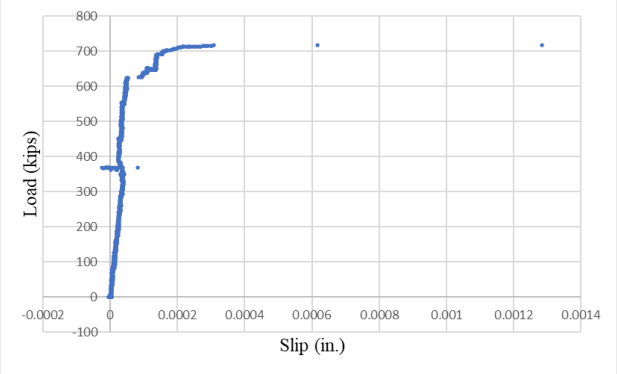

Figure A3.0.9 12-in. Specimen w/ SGD Rebar Detailing (SB_P)

A3.3.1.2. Steel Girder-PSC Girder Interface

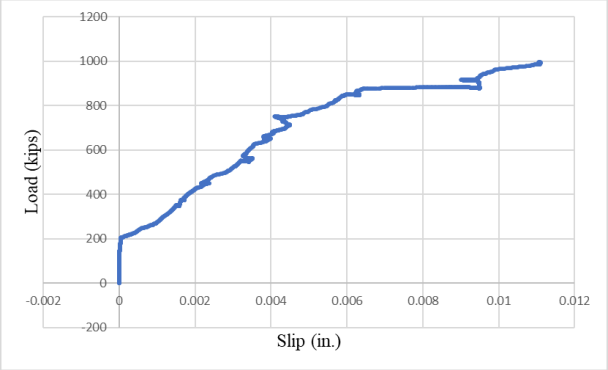

Figure A3.0.10 2-in. Specimen (SB_P)

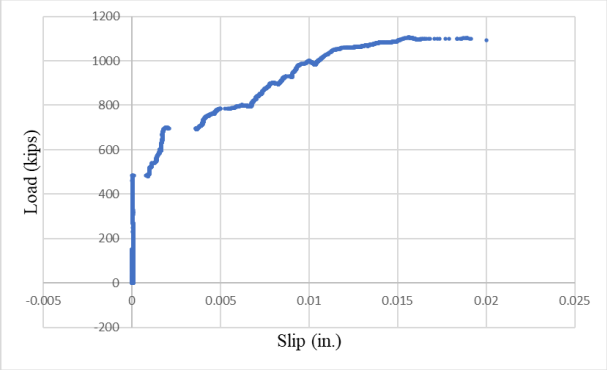

Figure A3.0.11 2-in. Specimen (SB_S)

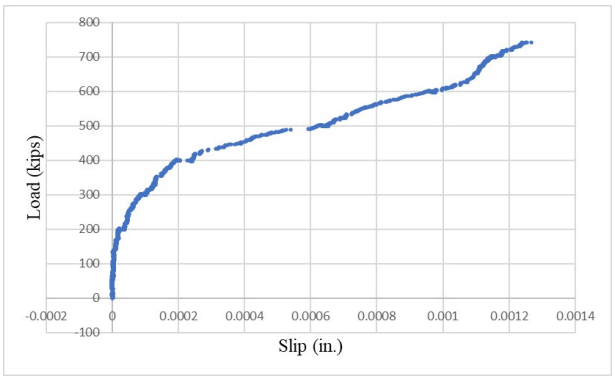

Figure A3.0.12 2-in. Specimen w/o Bars R (SB_P)

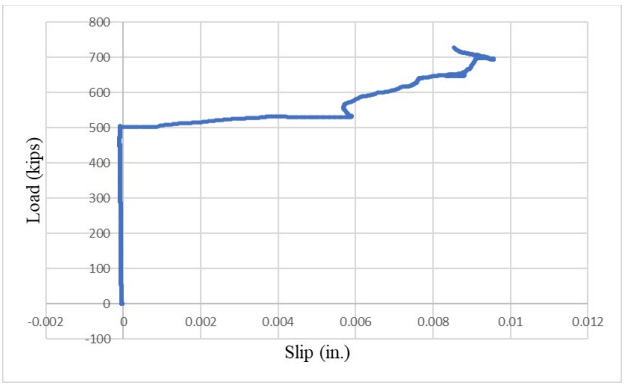

Figure A3.0.13 6-in. Specimen w/ Bars U (SB_P)

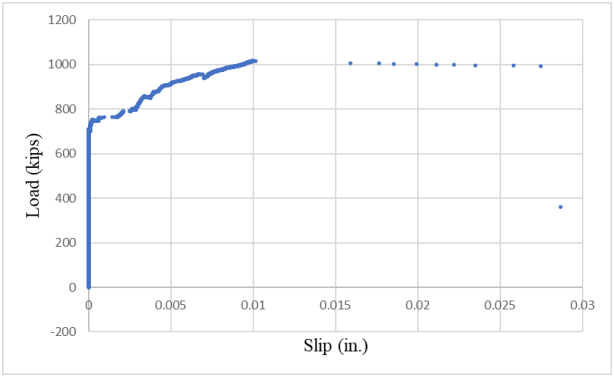

Figure A3.0.14 9-in. Specimen w/ Bars U (SB_S)

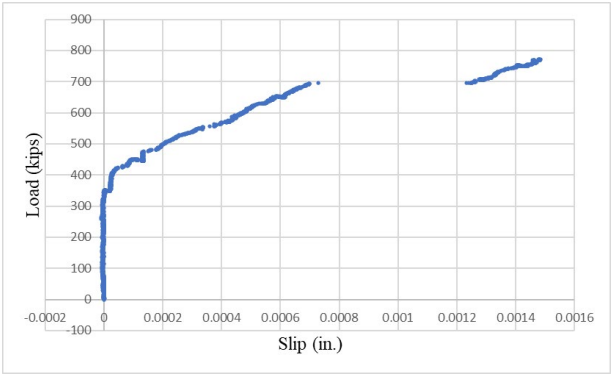

Figure A3.0.15 9-in. Specimen w/ Stirrups (SB_P)

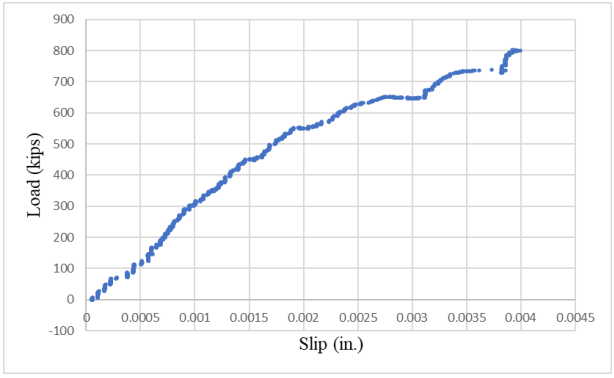

Figure A3.0.16 12-in. Specimen w/ Bars U (SB_P)

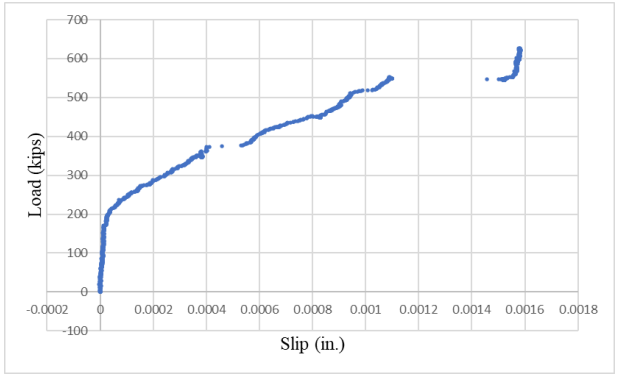

Figure A3.0.17 12-in. Specimen w/ Bars U and Long. Bars (SB_P)

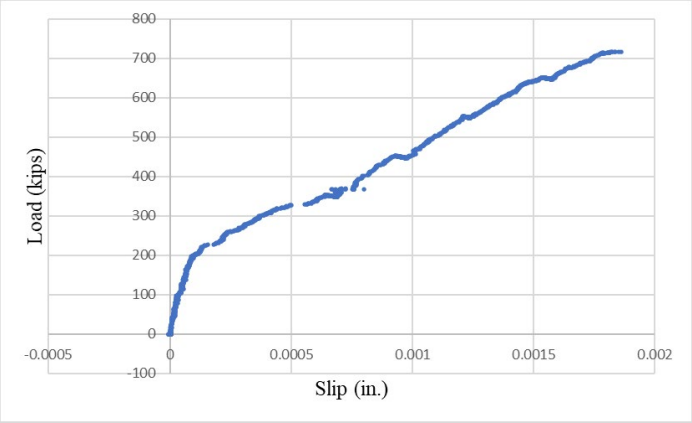

Figure A3.0.18 12-in. Specimen w/ SGD Rebar Detailing (SB_P)

A3.3.2. Specimen Group II

A3.3.2.1. PSC Girder-Haunch Interface

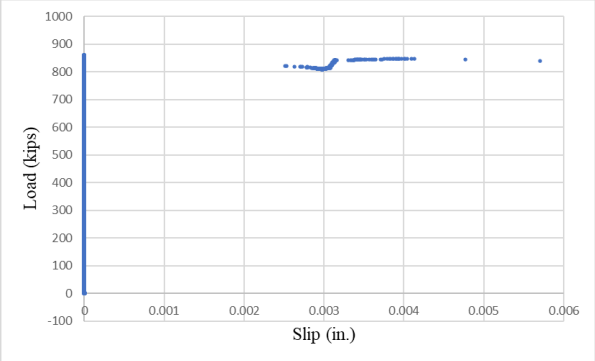

Figure A3.0.1 2-in. Specimen

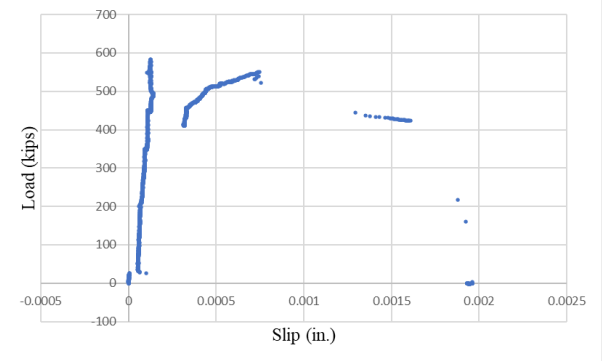

Figure A3.0.2 2-in. Specimen

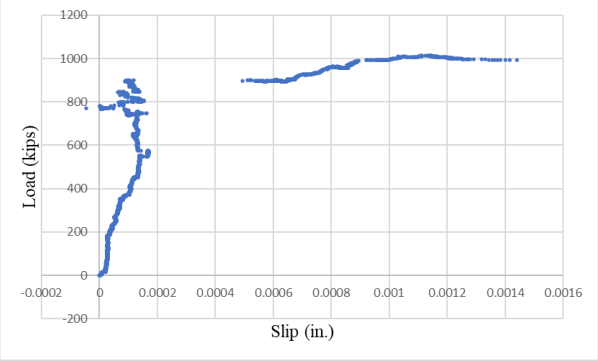

Figure A3.0.3 6-in. Specimen w/ Bar UP (SB_P)

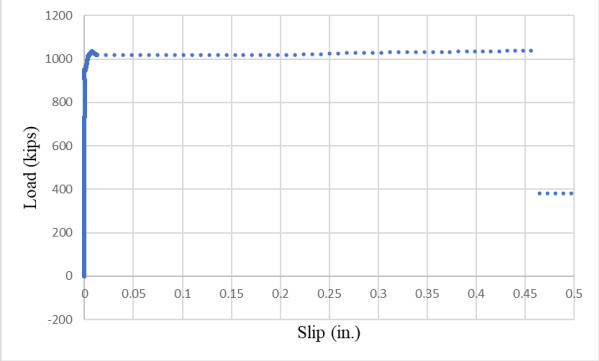

Figure A3.0.4 6-in. Specimen w/ SGD (SB_P)

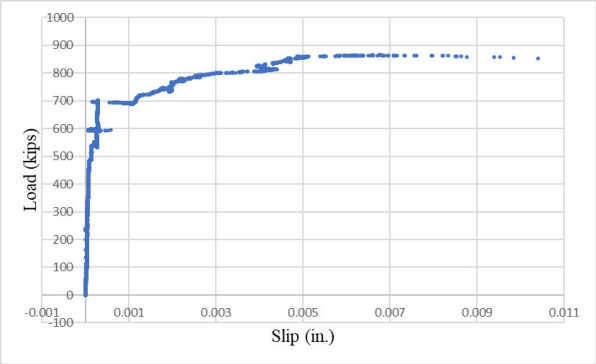

Figure A3.0.5 9-in. Specimen w/ Bar UP (SB_S)

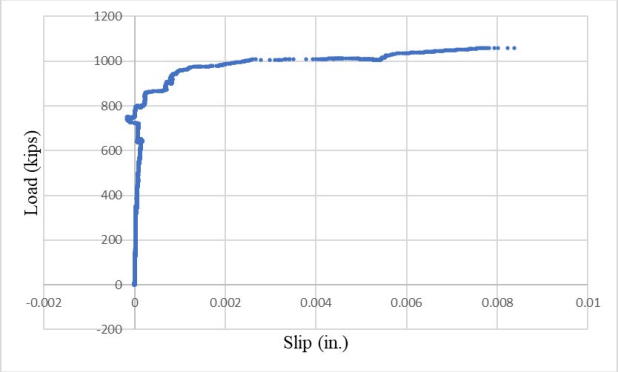

Figure A3.0.6 9-in. Specimen w/ SGD (SB_P)

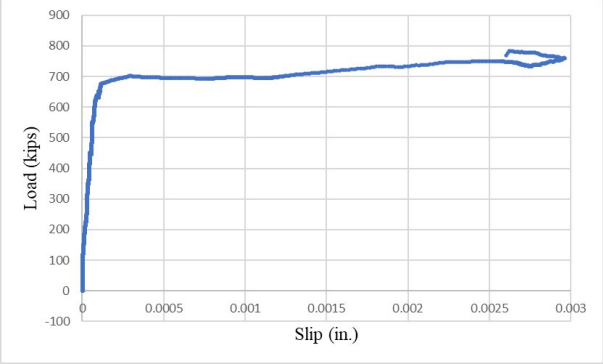

Figure A3.0.7 12-in. Specimen w/ Bar UP (SB_P)

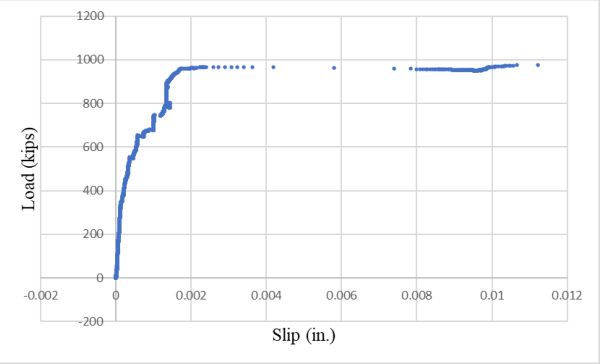

Figure A3.0.8 12-in. Specimen w/ Reduced Bars (SB_P)

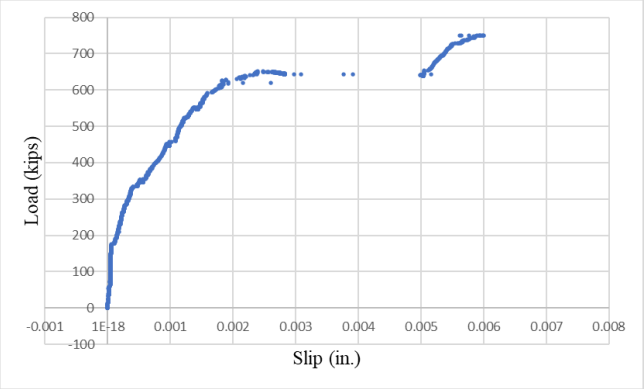

Figure A3.0.9 12-in. Specimen w/ SGD (SB_P)

A3.3.2.2. Steel Girder-PSC Girder Interface

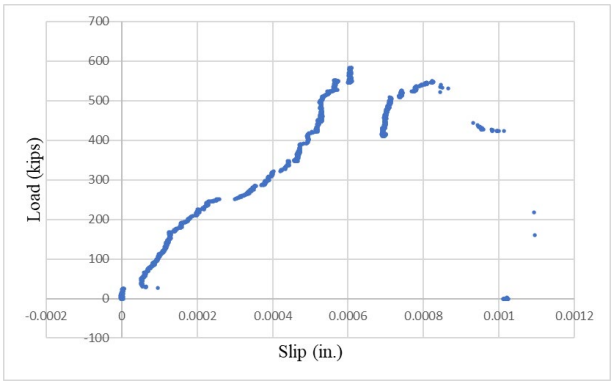

Figure A3.0.10 2-in. Specimen

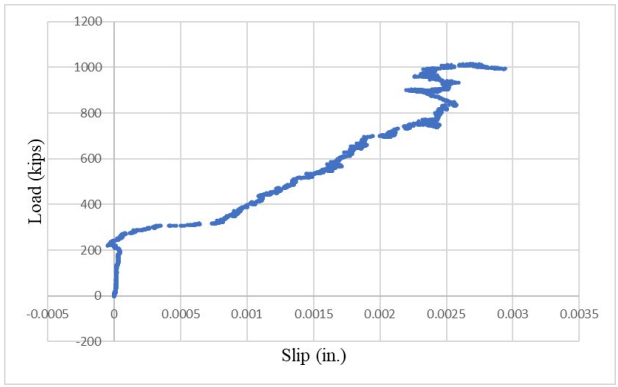

Figure A3.0.11 6-in. Specimen w/ Bar UP (SB_P)

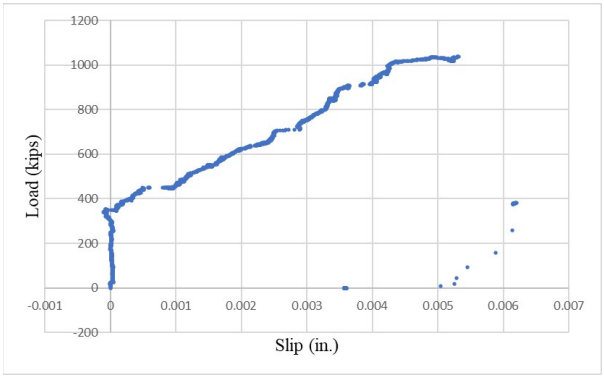

Figure A3.0.12 6-in. Specimen w/ SGD (SB_P)

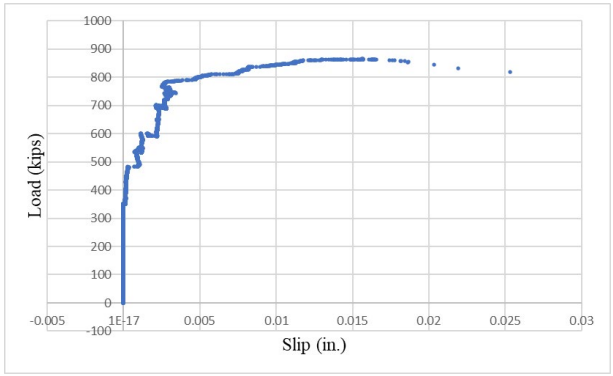

Figure A3.0.13 9-in. Specimen w/ Bar UP (SB_S)

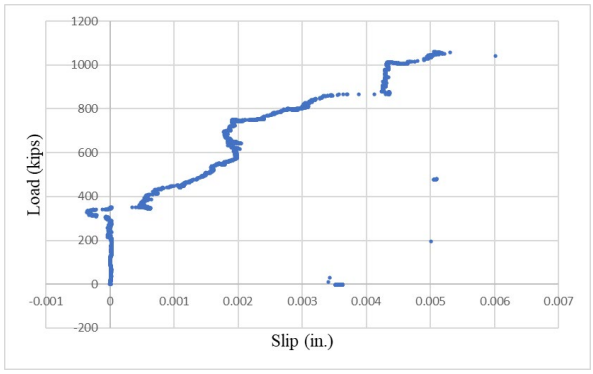

Figure A3.0.14 9-in. Specimen w/ SGD (SB_P)

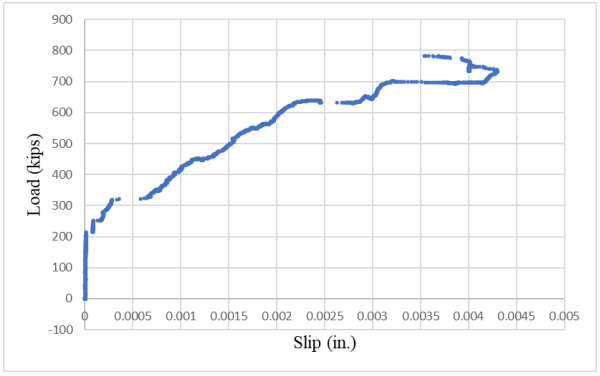

Figure A3.0.15 12-in. Specimen w/ Bar UP (SB_P)

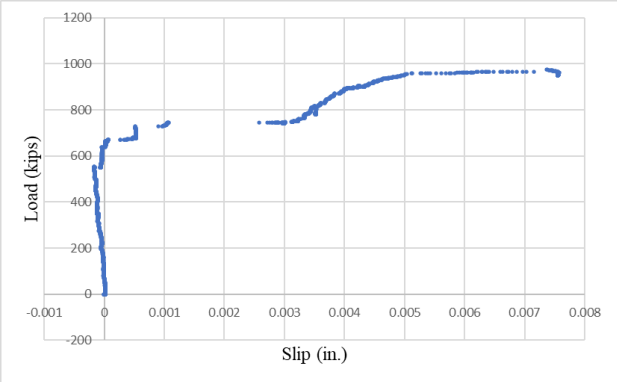

Figure A3.0.16 12-in. Specimen w/ Reduced Bars (SB_P)

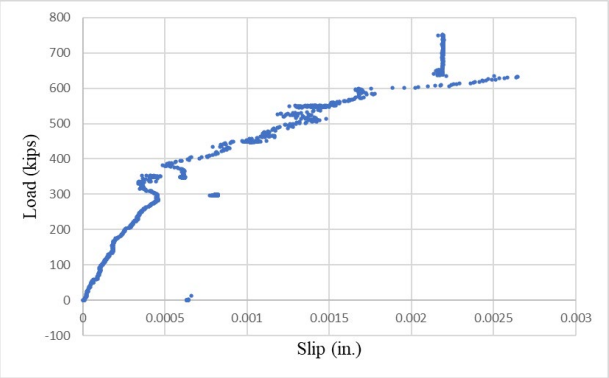

Figure A3.0.17 12-in. Specimen w/ SGD (SB_P)

A3.3.2.3. PCP-Haunch Interface

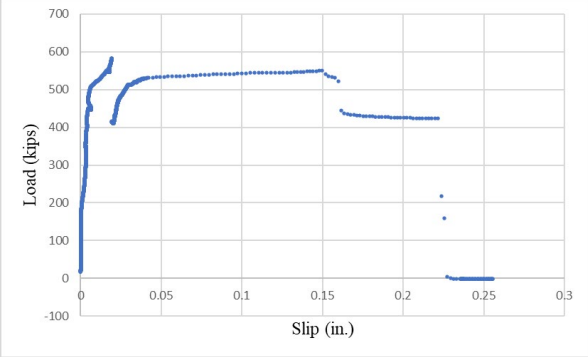

Figure A3.0.18 2-in. Specimen

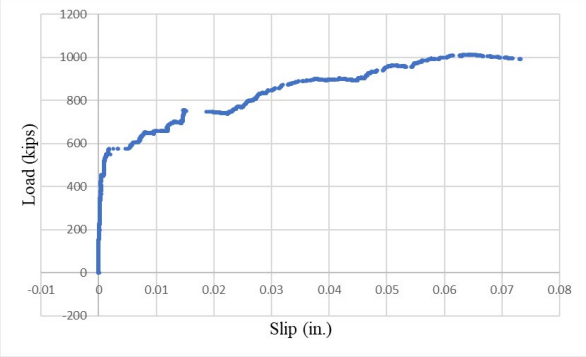

Figure A3.0.19 6-in. Specimen w/ Bar UP (SB_P)

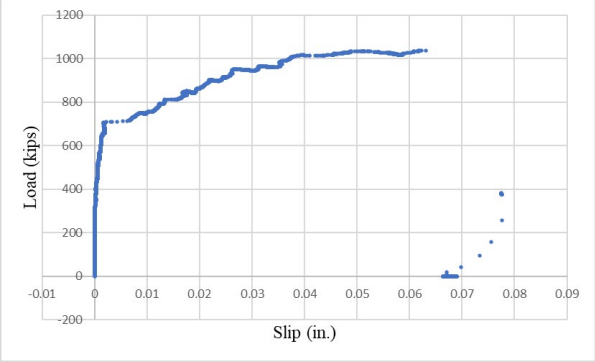

Figure A3.0.20 6-in. Specimen w/ SGD (SB_P)

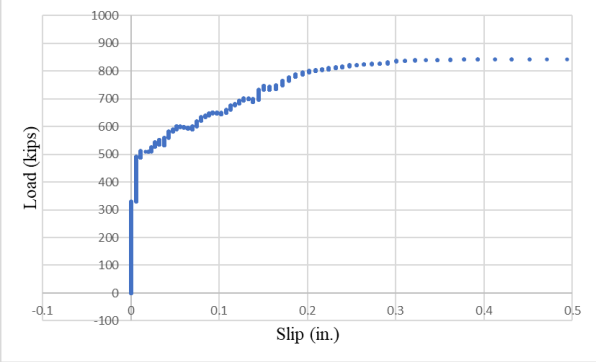

Figure A3.0.21 9-in. Specimen w/ Bar UP (SB_S)

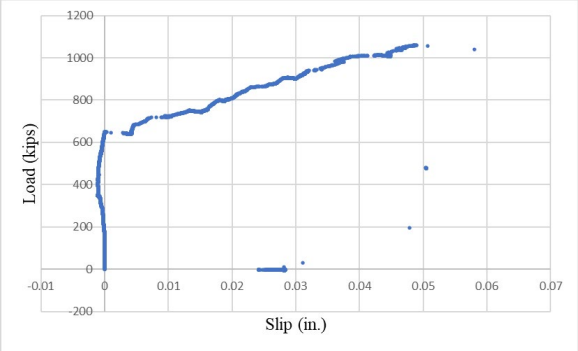

Figure A3.0.22 9-in. Specimen w/ SGD (SB_P)

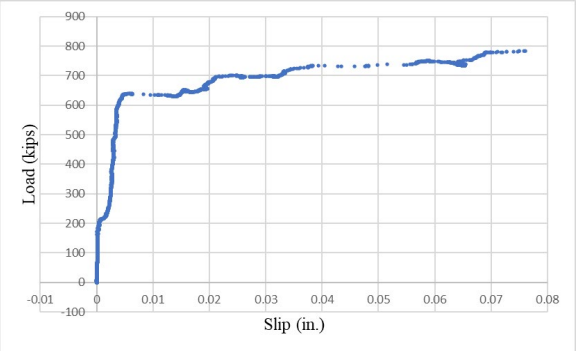

Figure A3.0.23 12-in. Specimen w/ Bar UP (SB_P)

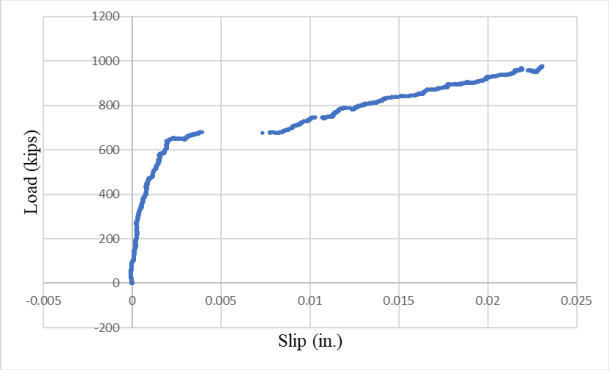

Figure A3.0.24 12-in. Specimen w/ Reduced Bars (SB_P)

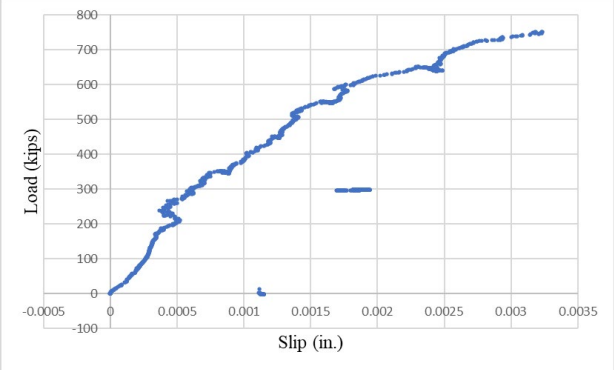

Figure A3.0.25 12-in. Specimen w/ SGD (SB_P)

A3.3.2.4. SGD-Haunch Interface

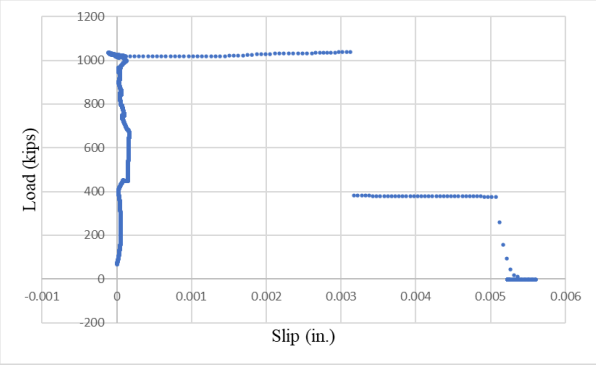

Figure A3.0.26 6-in. Specimen w/ SGD (SB_P)

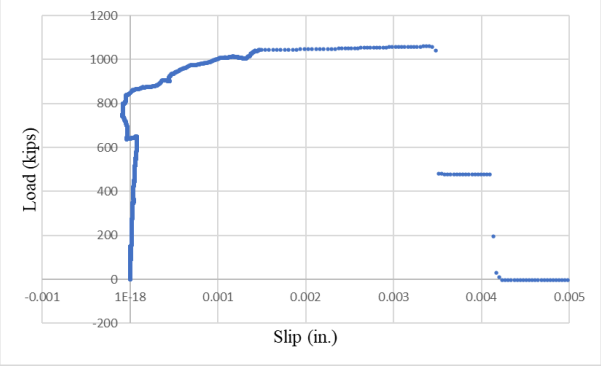

Figure A3.0.27 9-in. Specimen w/ SGD (SB_P)

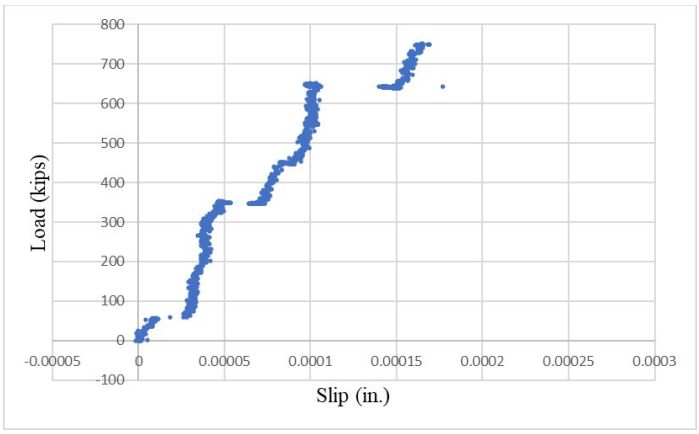

Figure A3.0.28 12-in. Specimen w/ SGD (SB_P)

A3.4.Specimens Strain-Load Plots

Sections 4.4.1.2 and 4.4.2.2 provide strain versus load plots for gauges provided on the steel web most of the specimens in Group I and II. The plots for remaining specimens are shown here. The location of strain gauges are shown in Figure 4.4.15.

A3.4.1. Specimen Group I

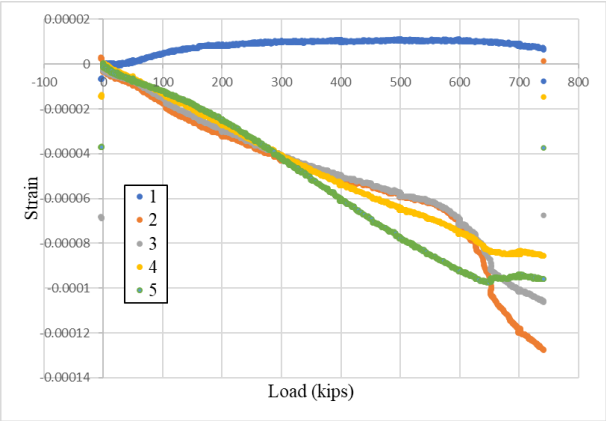

Figure A3.0.1 Strain versus Load for Test 1

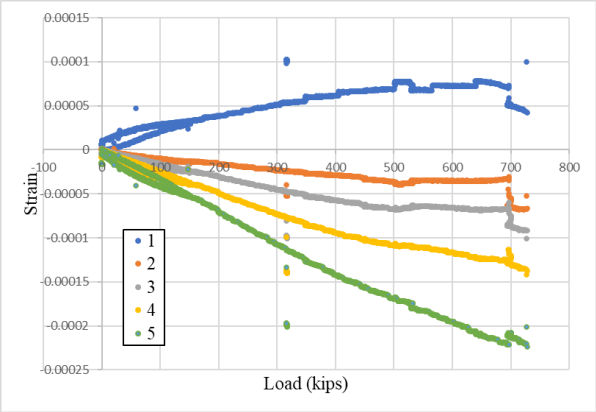

Figure A3.0.2 Strain versus Load for Test 4

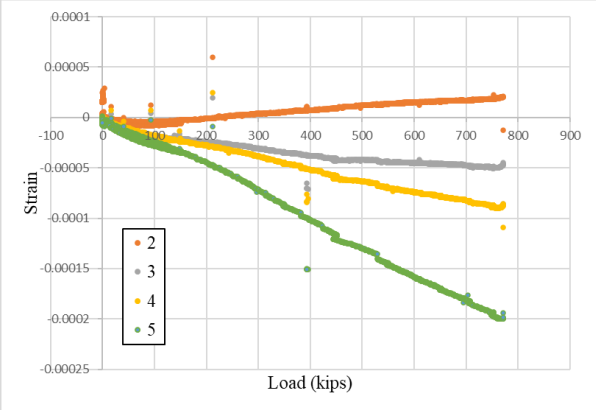

Figure A3.0.3 Strain versus Load for Test 6 (1 Damaged)

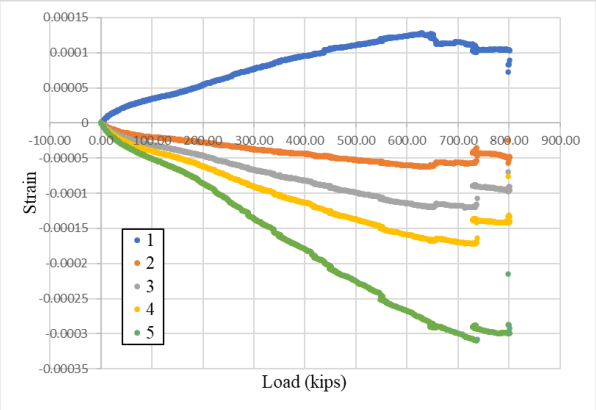

Figure A3.0.4 Strain versus Load for Test 7

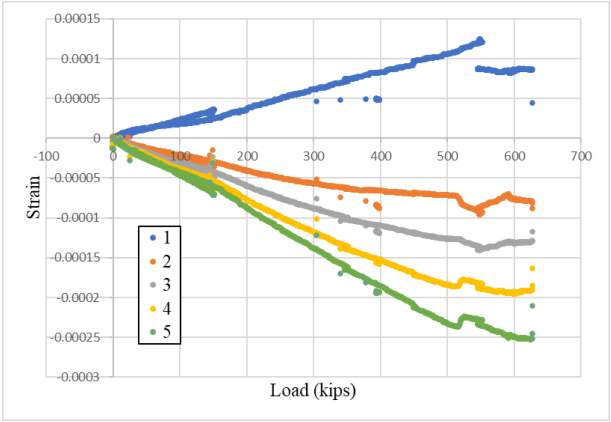

Figure A3.0.5 Strain versus Load for Test 8

A3.4.2. Specimen Group II

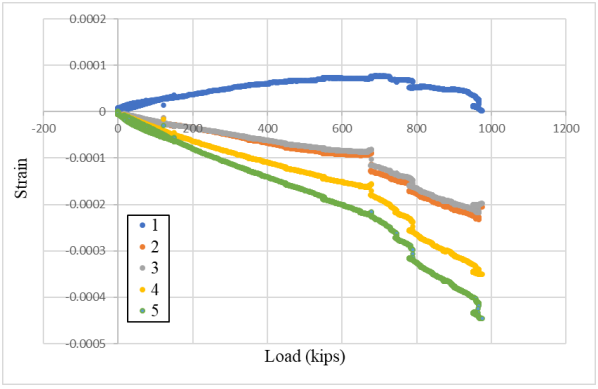

Figure A3.0.1 Strain versus Load for Test 17

Chapter 8. APPENDIX B - Value of Research

B. Value of Research - Overview

The haunch region over the tops of the girders improves the constructability of steel and concrete girder bridges by providing a valuable means of adjusting the slab elevation relative to the girder at various locations along the length of the bridge. The haunch allows designers the ability to vary the flange thickness or account for other important features such efficiently accounting for small changes in cross-slope on a bridge. For the contractor, the haunch allows field adjustments that account for variations in the geometry, differential camber, and other issues. However, when extreme problems occur in the field, relatively extreme haunches are sometimes necessary. In many instances, decisions need to be made relatively quickly related to detailing of shear connectors and deck/haunch reinforcement to avoid costly delays in the construction schedule. In these cases, construction and design personnel need to have confidence that field changes provide a bridge that has adequate strength without compromising the long-term behavior of the bridge system. This research study is one of the first investigations to consider the behavior of tall haunches. There are a number of contributions from this research that have long term advantages for both construction schedules and economy. Table B. 1 provides a summary of the advantages of this research.

Table B. 1: The project value of research (VoR).

Benefit Area	QUAL	ECON	Both	TxDOT	State	Both
Level of Knowledge	x			x		
Management and Policy	x			x		
System Reliability		x		x		
Increased Service Life		x		x		
Reduced Construction, Operations, and Maintenance Cost		x			x	
Infrastructure Condition		x				x
Engineering Design Development/Improvement			x			x

Note:

- QUAL: qualitative.
- ECON: economic.
- State: State of Texas.

B.1 Qualitative Value

B.1.1 Level of Knowledge

There have been several instances over the past several decades when tall to extreme haunches have been necessary to account for problems in the field. This study was one of the first investigations to consider various details that have been utilized in the past on steel and concrete girder systems and the resulting impact on the shear transfer between the girders and the concrete slab. This bridge therefore provides valuable insight into the shear-transfer behavior of girders with tall haunches and also instills confidence in past details that have been used. In addition, the research has contributed with recommendations on detailing of shear connectors and the reinforcing details so that designers and construction personnel have confidence in field changes that often have to be made relatively quickly to avoid delays in the construction schedule that can impact construction operations on Texas bridges and also impact the travelling public with longer construction schedules on busy thoroughfares.

B.1.2 Management and Policy

As noted above, when field problems occur, decisions need to be made relatively quickly. Delays that may occur from oversights in design can result in difficulties between TxDOT and the contractors. The research documented from this study provide a means to quickly evaluate the best options to account for field problems and minimize any delays.

B.2 Economic Value

B.2.1 System Reliability

Details have been used in the past for shear connectors and deck reinforcement that were not well understood with respect to behavior from both a strength and durability perspective. The research outlined in this study provides clear guidance on the various methods of strengthening tall haunches leading to reliable predictions in the ultimate strength of the girder systems. The recommended details can avoid unforeseen problems or failure modes and avoid costly failures.

B.2.2 Increased Service Life

Corrosion or excessive cracking in concrete deck elements is one of the most costly problems with steel and concrete girder systems. The proposed details in this study provide improvements in the predictability of the behavior of the concrete deck and haunch region. The details not only improve the strength of the composite girders, but also will lead to improved crack control. Therefore, the service life of the decks in cases with tall haunches should be improved using the recommended details from the research investigation.

B.2.3 Reduced Construction, Operations, and Maintenance Cost

The recommendations from the study can be implemented into standard details for use in steel and concrete girder bridges with tall haunches. Because many cases with tall or extreme haunches arise as a result of unforeseen problems during bridge construction, the ability to make quick decisions that can be implemented efficiently in the field are extremely important. Because these decisions can be made quickly and implemented into as-built bridge, excessive delays can be avoided, therefore improving the economy and efficiency of construction, maintenance, and operations.

B.2.4 Infrastructure Condition

The recommended details from the research will lead to improved structural performance ins systems with tall haunches, thereby avoiding undesirable crack sizes or spacing that can compromise the long-term behavior of the deck system.

B.2.5 Engineering Design Improvement

The research conducted in this investigation provides valuable insight into the design and behavior of both standard and tall haunch systems. The design recommendations summarized in the research provide valuable/ insight into the behavior of the haunch sections. Therefore, designers can have confidence in detailing for haunches of various sizes to provide good solutions for a variety of planned and unplanned conditions in the field.